



Fakultät: Geowissenschaften, Geotechnik und Bergbau

Studiengang: Advanced Mineral Resources Development

THEMA DER MASTERARBEIT:

Differentiation of the artificial rocks in mechanical cutting based on the acoustic emission signals


bearbeitet von: **Abdallah, Ahmed Sobhi Mohamed**


zur Erlangung des akademischen Grades: **Master of Science**

1. Prüfer/Gutachter:
Stellungnahme: **Prof. Dr. Carsten Drebenstedt
Dr. Serdar Yasar**

Übergabetermin des Themas: **26.05.2021**

Abgabetermin der Masterarbeit: **26.11.2021**


.....
Vorsitzender des Prüfungsausschusses


.....
Prüfer

Declaration of Authorship

I hereby confirm that I have written the accompanying thesis by myself, without contributions from any sources other than those cited in the text and acknowledgements.

This applies also to all figures, drawings, maps and images included in the thesis.

I give consent of publishing in the library and online.

Place/Date _____ Signature _____

Acknowledgement

I acknowledge the great help and support of Dr. Serdar Yasar and Dr. Taras Shepel. I would like to thank them a lot, I am full of gratitude to them and also to Prof. Dr. Carsten Drebenstedt and Dr. Nils Hoth. This study was completed within the frame of RockFeel Project (Support Code: 03EFPSN172) which is funded by Federal Ministry of Economic Affairs and Energy (BMWi) through PTJ Jülich, thanks to them. The thanking is delivered as well to my parents for supporting me by all means to achieve success. I thank Allah for allowing me to get this great opportunity studying at the eminent institutes of TU Bergakademie Freiberg and MU Leoben and getting the outstanding knowledge from the professors, doctors and all the teaching staff in the universities, I thank all of them along with the administrative and student services staff. My thank is delivered as well to all colleagues and friends and family members who supported me.

Table of Contents

| | |
|--|----|
| Introduction..... | 1 |
| 1 Literature Survey..... | 1 |
| 1.1 Mechanical Excavation..... | 1 |
| 1.1.1 Advantages of Mechanical Excavation Over Drilling and Blasting | 1 |
| 1.1.2 Cutting Tools | 1 |
| 1.1.3 Characteristics of Conical Picks | 5 |
| 1.1.4 Excavation Machines | 13 |
| 1.2 Selective Mining | 18 |
| 1.2.1 Selective Mining Applications..... | 19 |
| 1.3 Acoustic Emission..... | 20 |
| 1.3.1 Aim of Adding AE Sensors to Rock Cutting..... | 20 |
| 1.3.2 AE in Rocks and Rock Cutting..... | 21 |
| 1.3.3 AE Studies in Rock Cutting..... | 21 |
| 1.3.4 AE Measuring Units..... | 23 |
| 1.3.5 FFT and Signal Analysis | 25 |
| 2 Materials and Methods | 26 |
| 2.1 The Cutting Test..... | 26 |
| 2.1.1 Linear cutting machine "HSX 1000-50" | 26 |
| 2.1.2 Concrete Blocks | 27 |
| 2.1.3 AE Measuring System..... | 28 |
| 2.1.4 Force Sensors | 29 |
| 2.1.5 Data Acquisition System | 30 |
| 2.2 Experimental Procedures | 30 |
| 2.2.1 Preparing and Conditioning..... | 31 |
| 2.2.2 Cutting and Measuring | 34 |
| 2.2.3 Data Processing..... | 36 |

| | | |
|-------|---|-----|
| 2.3 | Processing of AE Data..... | 36 |
| 2.3.1 | Preparing audio Files for Processing..... | 36 |
| 2.3.2 | Processing and Analysis..... | 37 |
| 2.4 | Force Data Processing..... | 39 |
| 2.4.1 | Force signal analysis..... | 39 |
| 3 | Results and Discussions..... | 42 |
| 3.1 | AE signal analysis..... | 42 |
| 3.1.1 | Block AC..... | 42 |
| 3.1.2 | Block CB..... | 50 |
| 3.2 | FFT Analysis..... | 57 |
| 3.3 | Analysis of “Moving Average” and “Interquartile Range”..... | 70 |
| 3.4 | Optimization of AE Signal Quality..... | 74 |
| 3.4.1 | Adjusting the Gain Level..... | 74 |
| 3.4.2 | Adjusting Proximity of The Cutting to The Microphone..... | 79 |
| 4 | Conclusion..... | 83 |
| 5 | Future Recommendation..... | 84 |
| 6 | References..... | 85 |
| 7 | Appendices..... | 92 |
| 7.1 | Appendices AE Data..... | 92 |
| 7.1.1 | AE Signals Analysis..... | 92 |
| 7.1.2 | FFT Analysis of AE Signals..... | 109 |
| 7.2 | Appendices Force Data..... | 121 |
| 7.2.1 | Force Data Processing Graphs:..... | 121 |
| 7.2.2 | Summary Force Data Relieved..... | 122 |
| 7.2.3 | Summary Force Data Unrelieved..... | 124 |
| 7.2.4 | Summary Concrete ‘A’..... | 125 |
| 7.2.5 | Summary Concrete ‘B’..... | 129 |

LIST OF FIGURES

| | |
|---|----|
| Figure 1. Drag tools mounted on shearer drum (Sifferlinger, 2018)..... | 2 |
| Figure 2. Conical pick (left), radial pick (middle), forward attack pick (right) (Yasar & Yilmaz, 2018)..... | 4 |
| Figure 3 : Chisel Picks: simple shaped (left), complex shaped (right) (Yasar & Yilmaz, 2018). | 5 |
| Figure 4. Conical picks components (Sifferlinger, 2018)..... | 6 |
| Figure 5. Angles that affect the pick’s performance (Yasar, 2020). | 9 |
| Figure 6. Variations in pick forces with rake angles (Fowell, et al., 1987)..... | 9 |
| Figure 7. Variations in pick forces with back-clearance angle (Fowell, et al., 1987)..... | 9 |
| Figure 8. Different diameters of conical picks (Prakash, et al., 2020)..... | 10 |
| Figure 9. Spacing between tools: (a) wide, (b) very close, (c) optimum (Fowell, 1993)..... | 11 |
| Figure 10. Force components acting on conical pick (Copur, et al., 2017)..... | 12 |
| Figure 11. Cutting force diagram (Fowell, 1993). | 12 |
| Figure 12 . Transversal Roadheader (Sifferlinger, 2018)..... | 15 |
| Figure 13. Axial Roadheader (Bilgin, et al., 2014). | 15 |
| Figure 14. Continuous miner (Fowell, 1993)..... | 16 |
| Figure 15. Drum shearer excavation machine (Bilgin, et al., 2014)). | 17 |
| Figure 16. Coal plough (Fowell, 1993). | 18 |
| Figure 17. Room and pillar underground mining method (Atlas Copco, 2007)..... | 19 |
| Figure 18. Example of FFT analysis graph..... | 25 |
| Figure 19. Linear cutting machine: (a) moving table (left), (b) conical pick (top right), (c) control Panel (bottom right)..... | 27 |
| Figure 20. Artificial concrete blocks: (a) block AC (left), (b) block CB (right)..... | 28 |
| Figure 21. Concrete blocks dimensions..... | 28 |
| Figure 22. Acoustic signal capture and recording equipment..... | 29 |
| Figure 23. Force sensors (Piezoelectric sensors). | 30 |
| Figure 24. Dewetron (data acquisition system): (a) DAQ Computer, (b) Cables connected to the LCM: HSX 1000-50, (c) Dewesoft DAQ software. | 30 |
| Figure 25. Cubic samples for UCS determination of concrete. | 31 |
| Figure 26. Conditioned concrete surface. | 32 |
| Figure 27. Gain settings tested for optimization of acoustic signal: Very High (left), medium (middle), and Very Low (Right). | 33 |
| Figure 28. Gain settings used in the test: High Gain (left), and Low Gain (right). | 33 |

| | |
|---|----|
| Figure 29. Various distances of acoustic sensor from cutting position. | 34 |
| Figure 30. acoustic signal graph: by Excel 2019 (above), by Audacity 3.03 (below). | 37 |
| Figure 31. "Interquartile range" graph (bottom), Acoustic signal graph (top). | 38 |
| Figure32 . "Moving Average" graph (bottom), and the +ve value of the acoustic signal (top). | 38 |
| Figure 33. comparison FFT frequency spectrum: (1) Audacity 3.03 (left), and (2) DewesoftX 2021.03 (right)..... | 39 |
| Figure 34. Cutting force for "concrete block CB" (separated): block C (top), block B (bottom). | 40 |
| Figure 35. Normal force for "concrete block CB" (separated): block C (top), block B (bottom). | 40 |
| Figure 36. Side force for "concrete block CB" (separated): block C (top), block B (bottom). | 41 |
| Figure37 . AE signal during cutting Block "AC" at a depth of 2 mm and a speed of 0.5 m/s. | 43 |
| Figure38 AE signal during cutting Block "AC" at a depth of 2 mm and a speed of 1.0 m/s. | 43 |
| Figure39 . AE signal during cutting Block "AC" at a depth of 2 mm and a speed of 1.5 m/s. | 44 |
| Figure 40. AE signal during cutting Block "AC" at a depth of 5 mm and a speed of 0.5 m/s. | 44 |
| Figure41 . AE signal during cutting Block "AC" at a depth of 5 mm and a speed of 1.0 m/s. | 45 |
| Figure 42. AE signal during cutting Block "AC" at a depth of 5 mm and a speed of 1.5 m/s. | 45 |
| Figure 43. AE signal during cutting Block "AC" at a depth of 10 mm and a speed of 0.5 m/s. | 46 |
| Figure 44. AE signal during cutting Block "AC" at a depth of 10 mm and a speed of 1.0 m/s. | 47 |
| Figure 45. AE signal during cutting Block "AC" at a depth of 15 mm and a speed of 0.5 m/s. | 48 |
| Figure 46. AE signal during cutting Block "AC" at a depth of 15 mm and a speed of 1.0 m/s. | 48 |
| Figure 47. AE signal during cutting Block "AC" at a depth of 15 mm and a speed of 1.5 m/s. | 49 |
| Figure 48. AE signal during cutting Block "CB" at a depth of 2 mm and a speed of 0.5 m/s. | 50 |
| Figure 49. AE signal during cutting Block "CB" at a depth of 2 mm and a speed of 1.0 m/s. | 51 |
| Figure 50. AE signal during cutting Block "CB" at a depth of 2 mm and a speed of 1.5 m/s. | 51 |
| Figure 51. AE signal during cutting Block "CB" at a depth of 5 mm and a speed of 0.5 m/s. | 52 |
| Figure 52. AE signal during cutting Block "CB" at a depth of 5 mm and a speed of 1.0 m/s. | 52 |
| Figure 53. AE signal during cutting Block "CB" at a depth of 5 mm and a speed of 1.5 m/s. | 53 |

| | |
|--|----|
| Figure 54. AE signal during cutting Block “CB” at a depth of 10 mm and a speed of 0.5 m/s. | 53 |
| Figure 55. AE signal during cutting Block “CB” at a depth of 10 mm and a speed of 1.0 m/s. | 54 |
| Figure 56. AE signal during cutting Block “CB” at a depth of 10 mm and a speed of 1.5 m/s. | 55 |
| Figure 57. AE signal during cutting Block “CB” at a depth of 15 mm and a speed of 0.5 m/s. | 56 |
| Figure 58. AE signal during cutting Block “CB” at a depth of 15 mm and a speed of 1.0 m/s. | 56 |
| Figure 59. AE signal during cutting Block “CB” at a depth of 15 mm and a speed of 1.5 m/s. | 57 |
| Figure 60. FFT of AE signal during cutting Block “CB” at a depth of 2 mm and a speed of 0.5 m/s. | 58 |
| Figure 61. FFT of AE signal during cutting Block “CB” at a depth of 2 mm and a speed of 1.0 m/s. | 59 |
| Figure 62. FFT of AE signal during cutting Block “CB” at a depth of 2 mm and a speed of 1.5 m/s. | 60 |
| Figure 63. FFT of AE signal during cutting Block “CB” at a depth of 5 mm and a speed of 0.5 m/s. | 61 |
| Figure 64. FFT of AE signal during cutting Block “CB” at a depth of 5 mm and a speed of 1.0 m/s. | 62 |
| Figure 65 . FFT of AE signal during cutting Block “CB” at a depth of 5 mm and a speed of 1.5 m/s..... | 63 |
| Figure 66. FFT of AE signal during cutting Block “CB” at a depth of 10 mm and a speed of 0.5 m/s..... | 64 |
| Figure 67. FFT of AE signal during cutting Block “CB” at a depth of 10 mm and a speed of 1.0 m/s..... | 65 |
| Figure 68. FFT of AE signal during cutting Block “CB” at a depth of 10 mm and a speed of 1.5 m/s..... | 66 |
| Figure 69. FFT of AE signal during cutting Block “CB” at a depth of 15 mm and a speed of 0.5 m/s..... | 67 |
| Figure 70. FFT of AE signal during cutting Block “CB” at a depth of 15 mm and a speed of 1.0 m/s..... | 68 |

| | |
|--|----|
| Figure 71. FFT of AE signal during cutting Block “CB” at a depth of 15 mm and a speed of 1.5 m/s..... | 68 |
| Figure 72 . AE signal positive values (top), Moving Average (middle) and Interquartile Range (bottom) during cutting Block “AC” at a depth of 2 mm and a speed of 0.5 m/s..... | 71 |
| Figure 73. AE signal positive values (top), Moving Average (middle) and Interquartile Range (bottom) during cutting Block “AC” at a depth of 2 mm and a speed of 1.0 m/s..... | 72 |
| Figure 74. Positive values (top), Moving Average (middle) and Interquartile Range (bottom) of AE signal during cutting Block “CB” at a depth of 2 mm and a speed of 0.5 m/s..... | 73 |
| Figure 75. Positive values (top), Moving Average (middle) and Interquartile Range (bottom) of AE signal during cutting Block “CB” at a depth of 2 mm and a speed of 1.0 m/s..... | 74 |
| Figure 76. AE signal during cutting at a depth of 5 mm and a speed of 0.5 m/s, (a) Low gain settings (top), (b) High gain settings (bottom). | 75 |
| Figure77 . AE signal during cutting at a depth of 5 mm and a speed of 1.0 m/s, (a) Low gain settings (top), (b) High gain settings (bottom). | 76 |
| Figure 78 . AE signal during cutting at a depth of 5 mm and a speed of 1.5 m/s, (a) Low gain settings (top), (b) High gain settings (bottom). | 77 |
| Figure 79. AE signal during cutting at a depth of 10 mm and a speed of 0.5 m/s, (a) Low gain settings (top), (b) High gain settings (bottom). | 78 |
| Figure 80. AE signal during cutting at a depth of 10 mm and a speed of 1.0 m/s, (a) Low gain settings (top), (b) High gain settings (bottom). | 79 |
| Figure81 . AE signal for cutting test of close distance from the microphone. | 80 |
| Figure 82. AE signal for cutting test of medium distance from the microphone. | 80 |
| Figure83 . AE signal for cutting test of far distance from the microphone. | 81 |
| Figure 84. AE differentiation system based on FFT frequency Spectrum | 84 |

List of Tables

| | |
|--|----|
| Table 1. Results of the uniaxial compressive strength tests. | 31 |
| Table 2. List of Unrelieved Cutting Tests..... | 35 |
| Table 3. List of relieved cutting tests. | 36 |
| Table 4. Summary of numerical results of AE signal analysis of block “AC” | 49 |
| Table 5. Summary of numerical results of AE signal analysis of block “CB”. | 57 |
| Table 6. Average peaks and maximum peaks in FFT analysis of AE signals recorded during cutting block CB..... | 69 |
| Table 7. Highest four MDFs in FFT analysis of AE signals for block AC cutting..... | 70 |
| Table 8. Number of clipping occurrences at high and low gain settings (comparison results). | 79 |
| Table 9. Comparison results of microphone proximity to the cutting position, and the effect on AE signal intensity | 82 |

List of Abbreviations

d : Cutting depth (mm)

v : Cutting speed (m/s)

S : spacing between cuts (mm)

F_c : Cutting force (N)

F_n : Normal force (N)

F_s : Side force (N)

α : Rake angle ($^\circ$)

β : Back-clearance angle ($^\circ$)

θ : Half-cone angle ($^\circ$)

γ : Attack angle ($^\circ$)

ξ : Tilt angle ($^\circ$)

λ : Skew angle ($^\circ$)

AE: Acoustic emission

MDF: Major dominant frequency

FFT: Fast Fourier transform

IQR: Interquartile range

MA: Moving average

SI: Sound intensity level (dB)

LCM: Linear cutting machine

Introduction

In 2050, global raw material consumption is estimated to reach 184 billion tons (European Commission, 2018). Sustainable, economic, responsible, and ecologically friendly mining requires efficient production methods such as selective mining. Rock excavation machines such as roadheaders, surface miners, and hydraulic excavators with cutting head components are used to do selective mining. Different approaches have been developed to identify variations in the excavated material towards selective mining and to keep real-time data while changing the cutting activity into autonomous excavation instead of using human vision with these equipment. In a roadheader cutting operation, (Orteu, et al., 1992) employed computer vision to differentiate between the rocks on the excavation face during the cutting process. Sandvik patented this form for use on partial-face cutting machines after developing a prototype to detect tool forces for conical picks. (Kargl, et al., 2011). Gamma ray sensors are utilized by continuous miners in high-wall mining operations to distinguish coal from other rock/soil layers. (Luo, 2014). In open-pit mining, Wirtgen Company is employing camera vision on surface miner to distinguish between coal/ore and gangue material layers. (Volk, 2016). Research to estimate the tool forces encountered by conical picks on roadheaders was completed by researchers from Silesian University of Technology and Famur Machinery Company. The forces were measured using piezo-electric load sensors. (Cheluska, 2019).

Even if the mining machinery sector has numerous solutions with industry applications, there is still a need for a technical solution for selective mining or material differentiation, as all of these solutions have limitations. For example, under subterranean situations when the atmosphere is dark and dusty and vision is exceedingly limited, traditional cameras are impractical. On the other hand, because there is a clear link between tool forces and cutting depth, solutions based on force estimate require adjustment according to the cutting depth. The scientific community has taken notice of acoustic emission (AE) signals as an alternate strategy (Bartnitzki & Vraetz, 2018; Liu, et al., 2021), despite the fact that AE in material differentiation has been the subject of multiple patents (John F. Bryan, 1992; Marston et al., 1997).

It was proposed in this thesis to identify changes in material properties, such as uniaxial compressive strength, in mechanical cutting in order to achieve selective mining. On this basis, three different concretes having different uniaxial compressive strengths were casted in two blocks. Following that, these two blocks were cut in a full-scale rock cutting test to

Introduction

acquire tool forces, and AE measurements were taken using an industrial microphone at the same time. Then, using various approaches such as frequency analysis and amplitude analysis, the experimental results were displayed and discussed. There are five chapters in the thesis. The topics of mechanical excavation, selective mining, and AE will be covered in depth in the first chapter. Afterwards, the experimental procedure, which includes sample preparation, uniaxial compression tests on concrete cube samples, rock cutting tests with the HXS 1000-50 full-scale linear rock cutting machine, and AE measurements during the cutting tests, will be reported in the second chapter. And then, the results of the experimental investigations will be discussed in depth within the research and in relation to the current literature in the third chapter. In the fourth chapter, and as a conclusion, the results and outcomes of this investigation will be reported. Finally, future proposals on the issue of AE for material differentiation will be provided in the fifth chapter.

1 Literature Survey

1.1 Mechanical Excavation

Mechanical excavation is becoming more popular, especially for softer rocks, because it is a cost-effective way to produce huge volumes of material while keeping the environment safe. The major goal of modern mechanical excavation systems is to boost productivity and automation in soft ground excavation (Bilgin, et al., 2014). Mechanical Excavation is defined as cutting the rock or rock mass of the earth crust through the mechanical transfer of energy from the cutter to the rock to break the rock, and fragment it. While in the other method, the drilling and blasting method, the energy is transferred to the rock not through mechanical means (Bilgin, et al., 2014).

1.1.1 Advantages of Mechanical Excavation Over Drilling and Blasting

The advantages of mechanical excavation aren't only improving safety and reducing risks for workers and environment, as it produces fewer toxic gases, but it also saves ventilation costs. And not only eliminating the disturbance and vibrations in downtown and near old buildings, but it has many other advantages, economically, as it allows easy transporting of the excavated rock by conveyors, which boost the continuity of the operation, as there is no need for loaders and hauling trucks, which save time also. It has greater accuracy with regard to final excavation dimensions, it maintains excavation walls from damage, has less overbreak, and require less scaling work, minimizing accidents, improving safety and saving money, and it has great ease with regard to mechanization and Automation. Moreover, it minimizes the cost of processing ore as it mine the soft ore separately from the hard rock, reducing ore dilution, and increasing the recovery, and separate excavation of rock layers, which make excavation easier. it also requires less support work, as it keeps the pillars in good condition (Sifferlinger, et al., 2017; Sifferlinger, 2018; Bilgin, et al., 2014).

1.1.2 Cutting Tools

Cutting tools are used to transfer energy from the excavation machine to the rock (Fowell, 1993). Cutting tools are two main types: firstly, drag cutters, which called picks or sliding tools, and secondly, rotary cutters, which called discs, or rolling tools. The drag tools are used to cut medium and soft rocks, while disc cutters are used to cut hard rocks (Bilgin, et al.,

2014). Drag tools are the focus in this study, the conical pick in particular, but an overview of all the drag tools is going to be briefly displayed.

1.1.2.1 Drag Cutting Tools

The drag cutting tools are mounted on the cutting head or drum (Figure 1), which rotate to cut the rock. Many Drag cutting tools are installed on one cutting head/drum, so they cut the rock in sequence, one drag tool after the other, in a rotational motion. The cutting head/drum move forward, while rotating to allow the cutting tools to cut the rocks. The drag tools are mounted on partial-face cutting machines (Sifferlinger, 2018). The specific information about the drag tools is following: regarding the energy consumption they are efficient, and regarding the rock they can cut they are limited, as they can cut rocks of medium and low strength and non-abrasive rocks (Fowell, 1993). when they cannot excavate the rocks economically, because they are hard rocks then the disk cutters are used (Sifferlinger, 2018). The drag cutting tool are classified according to their geometry into four main types: conical picks, forward attack picks, radial picks, and chisel-shaped picks.

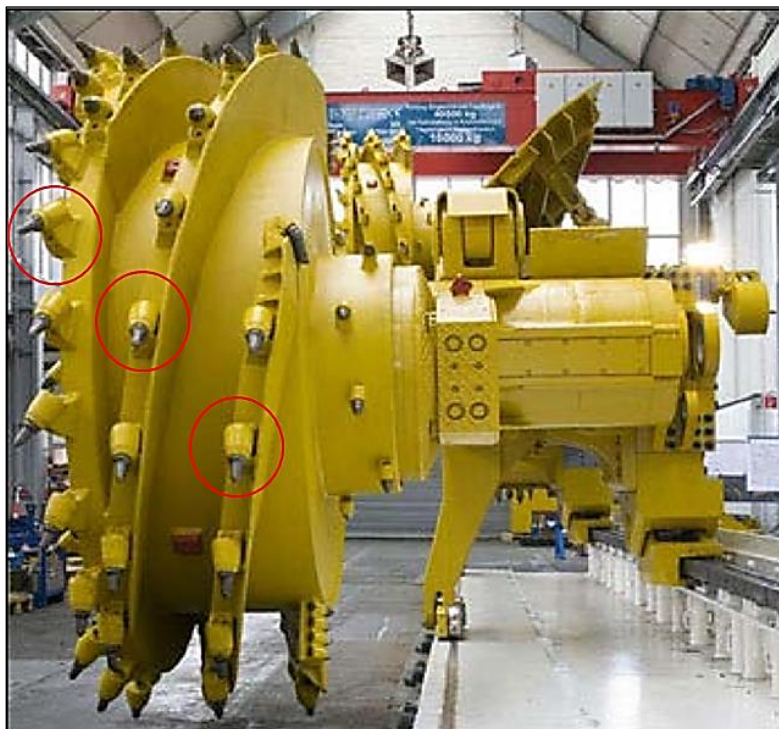


Figure 1. Drag tools mounted on shearer drum (Sifferlinger, 2018).

1.1.2.1.1 Conical Picks

Conical picks (Figure 2) are the focus of this study among all cutting tools. Conical Picks are classified as drag-cutting tools. They are called “point attack cutting tools”, They have the shape of a pencil, therefore they are called also “pencil picks” (Fowell, et al., 1987). They

have a conical tip, and not the wedge tip of the radial pick, but otherwise they look the same (Hurt & MacAndrew, 1985). They have cylindrical body (Fowell, et al., 1987). One of the common names of them is “tangential pick” because of the orientation of their axis, which is in-line with the conical tip (Fowell, et al., 1987). Dewangan & Chattopadhyaya (2016) stated that most of the excavation machines are using the conical picks. Conical pick currently is no more preferred in coal cutting, even though it was used to cut it a lot in the past (Fowell, et al., 1987), because they generate more dust than other cutting tools. However, Dewangan & Chattopadhyaya (2016) stated that conical picks are still in use today in coal mining, and they have many advantages too, and they are preferred in high production of coal. Nonetheless, Evans (1984) stated that the conical picks are less widespread in coal mining than previously. Medium and solid rock are increasingly being cut with the conical picks, they are now very important tools in roadheaders and the most used. The conical pick hones itself as it swirls in the holder, which is what gives it a longer service life, it wears evenly from all sides (Fowell, et al., 1987). If the conical picks are sharp, they are stronger and better and have longer service-life, and if they become blunt, their strength decrease dramatically (Fowell, et al., 1987). The sharper they are, the longer life, and therefore the continuity of excavation, no maintenance interruptions, no need of changing the pick, thus the more efficient is the excavation process (Fowell, et al., 1987).

1.1.2.1.2 Radial Picks

The radial pick (Figure 2) is called prism-shaped pick (Sifferlinger, 2018). It is an important type of the drag cutting tools. The radial line of the cutting head is parallel to the axis of the pick shank (Fowell, et al., 1987). Moreover, Hekimoglu, (1995) draw the axis of the pick parallel to the radial line of the cutting head. The tip of a radial pick is wedge-shaped (Bao, et al., 2011). The shanks of radial picks are oriented perpendicular to the cutting direction (Hurt & MacAndrew, 1985; Bao, et al., 2011). The cutting mechanism by radial pick can be explained in 2D model (Bao, et al., 2011). Only the tungsten carbide tip of a radial type pick should be in cutting contact with the rock; no other parts of the pick should be actively involved in cutting (Hekimoglu, 1995). Radial picks can be found on partial-face excavation machines, for example roadheaders, shearers and coal plough and continuous miners (Yasar & Yilmaz, 2017). On the drum of the roadheader radial picks with a short gauge are often used, whereas those with a large-gauge are typically used on the shearer drums (Fowell, et al., 1987). Soft rocks are being cut by the radial tools as well as the coal (Wang, et al., 2017), as

well as medium-strength rocks (Fowell, et al., 1987). The specific Energy to cut rocks for radial picks is lower than specific energy to cut rock for conical picks, but that is in severe conditions (Bilgin, et al., 2014).

1.1.2.1.3 Forward Attack Picks

Forward attack picks (Figure 2) are called “tangential picks” (Fowell, et al., 1987). They are among drag cutting tools. The tip geometry is the same like radial pick. The tip of a forward-attack pick is wedged, and the shank is slanted rearward from the cutting direction, generally at 45 degrees (Hurt and Evans 1981 cited in Bao, et al., 2011; Hurt & MacAndrew, 1985). The pick force is approximately parallel to the tool axis, which give it very good resistance to the breakage of the shank, and also the wear of the tool holder (Fowell, et al., 1987). Forward attack picks can be seen on partial-face excavation machines, such as the cutting head of roadheaders, and on coal plough and continuous miners (Yasar & Yilmaz, 2017), and on drums of shearers (Fowell, et al., 1987; Yasar & Yilmaz, 2017). Forward attack picks are used to cut coal in United Kingdom, they are also employed on cutting machines (Hurt & MacAndrew, 1985). They have the following advantages: They need energy not that much comparing to conical picks which require high energy, and they have very good chipping characteristics (Fowell, et al., 1987).

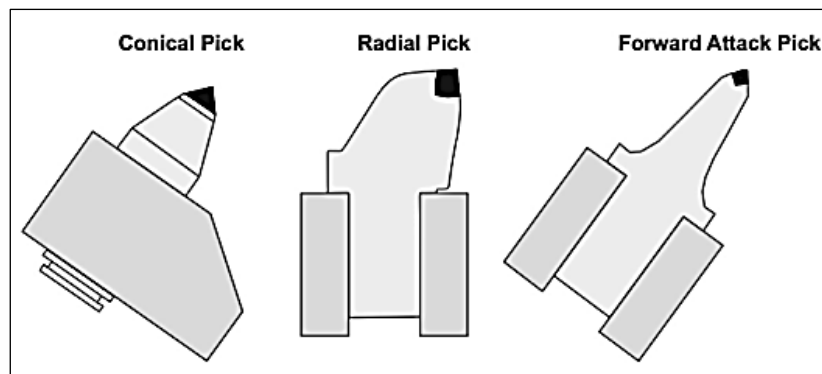


Figure 2. Conical pick (left), radial pick (middle), forward attack pick (right) (Yasar & Yilmaz, 2018).

1.1.2.1.4 Chisel Pick

Chisel picks (Figure 3) are among drag cutting tools. They have the shape of the wedge; therefore, they are called the wedge cutting tools (Copur, et al., 2017). They are famous and old types of the drag cutting tools. Simple chisel picks are being produced and used in cutting before radial or complex-shaped picks (Bilgin, et al., 2014). When excavation machines were firstly invented, chisel pick were utilized as cutting tools on them (Yasar & Yilmaz, 2017). And then the picks shapes evolved by days to the other strong shapes of drag tools (Copur, et

al., 1998). Simple chisel picks are rarely today to be seen on excavation machines, they are scarcely used or employed in rock cutting (Mohammadi, et al., 2020; Yasar & Yilmaz, 2017). However, complex-shaped chisel picks are used in tunnel boring machines together with the disc cutters if the face has a variety of conditions, and it may be used singly to cut low/medium strength rocks (Bilgin et al. 2012 cited in Yasar & Yilmaz, 2017). There are two shapes of chisel picks: simple shaped and complex shape. By comparing Simple chisel pick to complex chisel pick, it turns out that the first is more efficient than the second (Bilgin, et al., 2014). The geometry of the chisel tools is really efficient (Hartman, 1992; Fowell, et al., 1987) yet drag tools with complicated geometries are more favored and find more applications in rock cutting, due to their very high endurance and ability to last, as they have longer service-life (Fowell, et al., 1987). The specific Energy to cut rocks for chisel picks is lower than that for conical picks, and that is in harsh conditions (Bilgin, et al., 2014).

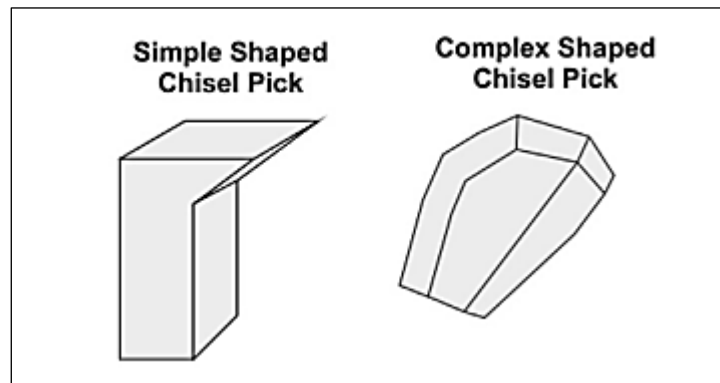


Figure 3 : Chisel Picks: simple shaped (left), complex shaped (right) (Yasar & Yilmaz, 2018).

1.1.3 Characteristics of Conical Picks

1.1.3.1 Components of Conical Picks

The cutting pick generally comprises of two main components: a forged steel body and a tip of another hard material, e.g. tungsten carbide (Fowell, et al., 1987). The detailed analysis of conical pick shows that it comprises of four components: a tungsten carbide tip (inserted or a cap), a cone, a shaft, and a retainer (clip ring), and the pick is mounted in a pick box (Figure 4) (Sifferlinger, 2018).

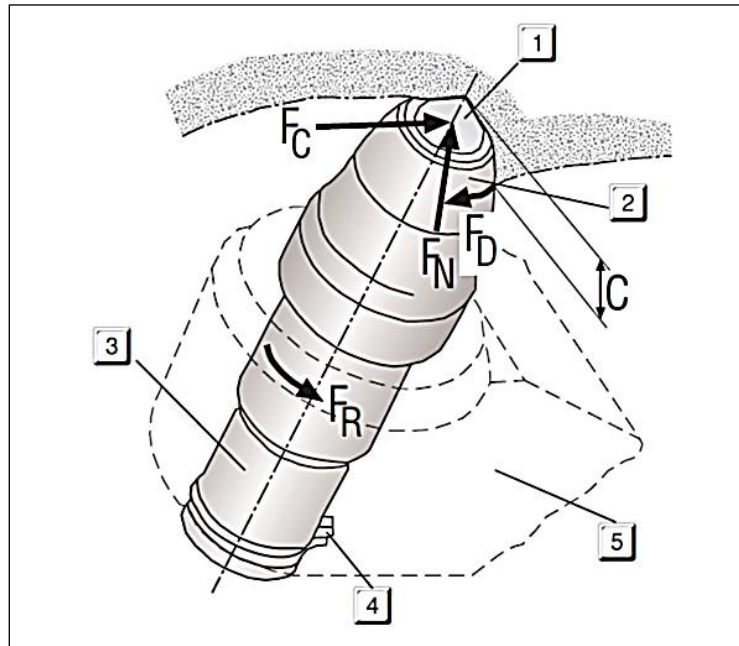


Figure 4. Conical picks components (Sifferlinger, 2018).

1.1.3.2 Tip Materials

The tip of the cutting tool is the very front part of it that face the rock. In conical picks, the tip has the shape of a cone, in other tools geometries it can have other shapes, such as the wedge. In conical picks, the tip is proportionately installed in the steel body so that it may be in-line with the pick axis, and that's done via brazing (Dewangan, et al., 2015). Drag tools tips are made of either tungsten carbide or polycrystalline diamond (PCD) (Bao, et al., 2011). however, several other materials have been attempted as substitutes. Synthetic diamond inserts are being researched in the last years (Sifferlinger, et al., 2017); yet, they cannot compete with tungsten carbide due to their high cost. According to Sifferlinger, et al. (2017), Researches on cemented wolfram carbide in the last years made only small improvements. Dewangan et al (2016) stated that several researches in cemented carbide helped improving its quality and decreased the wear of cutting tool. Tough cobalt (Co) is cemented together with fine particles of very hard tungsten carbide (WC), and named cemented carbide "WC-CO" (Fowell et al 1987). Cemented carbide – Cobalt combination is famous of its high hardness, high modulus of elasticity and high compressive strengths (Fowell et al 1987). However, Fowell et al (1987) stated that increasing the cobalt content results in reduction of hardness of the composition.

1.1.3.3 Tip Geometry

The tip geometry affects the cutting performance and the tool in a great degree. The angles that affect the cutting performance and the cutting tool are: rake angle, back-clearance angle,

cone angle, attack angle, skew angle, and tilt angle (Figure 5) (Sarwary and Hagan 2016; Wang et al. 2018 cited in Yasar 2020). Wang et al. (2018) stated that the attack and cone angles are the most important parameters that affect the conical pick performance depending on the condition. Li et al (2020) stated that rake angle is an important parameter affecting the forces of the pick.

1.1.3.3.1 Attack Angle

The attack angle (Figure 5) is the angle between the cutting route and the pick axis. This angle is one of the parameters that affects the performance of point attack pick. Failure to choose this angle correctly significantly changes the effective geometry (Fowell, et al., 1987). The optimum attack angle lies around 50 degrees at the point attack pick, because at this value the cutting forces are lower, but that if the cone angle is 75° (Hurt and Evans 1981, cited in Fowell et al. 1987), and if the back-clearance angle is 12° (Bilgin, et al, 2006). but if the cone angle is 90° then the optimum cone angle would be 55° (Fowell, et al., 1987). Increasing this angle increases the forces acting on the conical pick (Sarwary and Hagan 2016; Wang et al. 2018, cited in Yasar 2020). Anyway, Hurt (1980) stated that attack angle between 40° and 55° can be chosen (Hurt 1980 cited in Yasar & Yilmaz 2018).

1.1.3.3.2 Rake Angle

Rake angle is the angle between the high tip of the pick and the line perpendicular to the cutting line (Figure 5). Rake angle is very important parameter that affect the conical pick performance by affecting the forces acting against the pick. Fowell et al. (1987) suggested to increase the positive rake angle value to decrease the forces acting on a cutting pick (Figure 6), but avoiding high values in hard rocks, because it makes the pick more likely to failure, except for cutting soft rocks and coal. Ouyang et al (2018) also discovered the same result, that increasing the rake angle to a positive value decreases the forces (Ouyang et al 2018 cited in Li, 2020). Fowell, et al., (1987) stated that negative rake angle cause the highest forces acting against a cutting pick. Hood & Roxborough (1992) stated that the pick achieved the optimum performance at +20° rake angle. Parakash et al. (2020) stated that a rake angle larger than +20° shall be avoided. However, Fowell et al. (1987) stated that when cutting soft rocks and coal, a rake angle between +20 and +30 can be used. Goktan (1990) stated that negative rake angle must be used when cutting rocks of high strength, because it is more probable then to damage of pick.

1.1.3.3.3 Back Clearance Angle

The back-clearance angle (Figure 5) is the angle between the lower tip of pick and the course of cutting. Fowell, et al., (1987) stated that the optimum clearance angle is near 10° degrees for conical pick, because lower angle will increase the forces acting on the cutting tool, and if lower than 5° , forces will increase dramatically, while higher clearance angle than 10° has no effect on the forces (Figure 7). However, Bilgin et al. (2006) stated that the optimum back-clearance angle is 12° for the conical pick when cone angle is 75° . Nonetheless, Wang et al. (2018) confirmed what Fowell (1987) by his statement that clearance angle above 10° has no more effect on the forces, while clearance angle of 0° increase the forces significantly, yet, clearance angle of 5° cause more forces than 10° . Though, Prakash et al (2020) stated that the optimum clearance angle is below 10° and above 5° .

1.1.3.3.4 Cone Angle

Cone angle (Figure 5) is specific only to conical picks, it corresponds to the wedge angle in the simple chisel pick. It is the angle between the higher tip and the lower tip of the conical pick (the angle of the tip). Stronger rock requires a larger tip angle. However, Fowell et al. (1987) stated the optimum cone angle lies between 70° to 80° , since the forces acting against the pick are optimum between these two values. He stated that the most optimum cone angle is 75° , he said that the lowest of forces was at this angle. According to Prakash et al. (2020), higher cone angle than 80° is not advised, as increasing the cone angle lead to a linear increase of the forces acting against the pick. Gollick (1999) discovered that the conical pick of 80° cone angle exposed to double the force as the one with 76° cone angle. Prakash et al. (2020) stated that for cutting strong rocks, a cone angle between 70° - 80° is preferred. Nonetheless, Wang et al. (2018) stated that a cone angle above 80 can be chosen in case of hard and abrasive rock, as a smaller angle may be used for medium-hard rocks and coal.

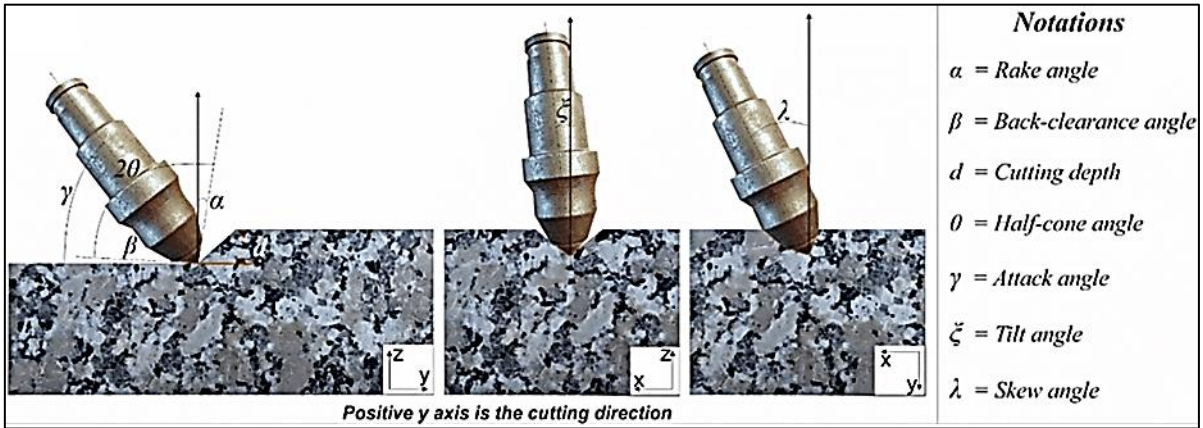


Figure 5. Angles that affect the pick's performance (Yasar, 2020).

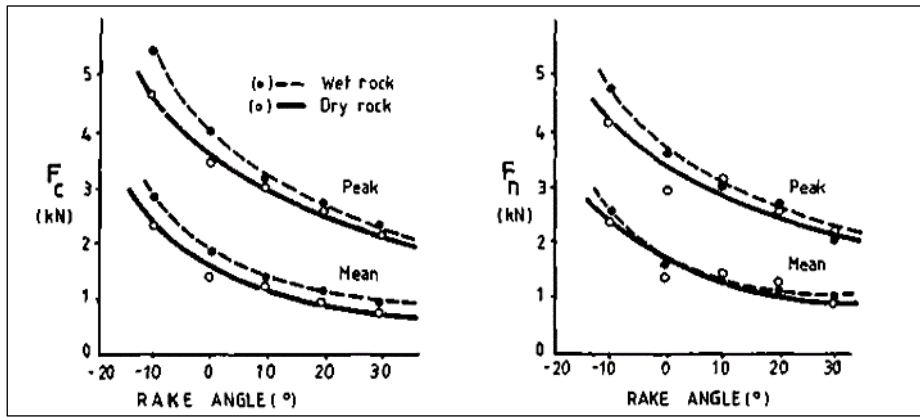


Figure 6. Variations in pick forces with rake angles (Fowell, et al., 1987).

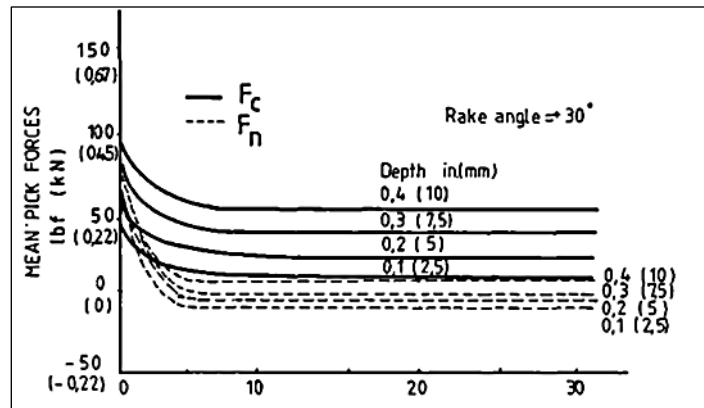


Figure 7. Variations in pick forces with back-clearance angle (Fowell, et al., 1987).

1.1.3.4 Diameter of the Conical Pick

Diameter of the pick is an important aspect that affects the cutting performance. Picks with a larger diameter are more efficient than those with a smaller diameter (Figure 8). They can keep up with the cutting force and, more importantly, the cutting force variations that

excavation machine can handle. Stronger rocks may be cut with a larger diameter conical pick, while soft rocks are cut with slim version (Sifferlinger, 2018; Prakash, et al., 2020).

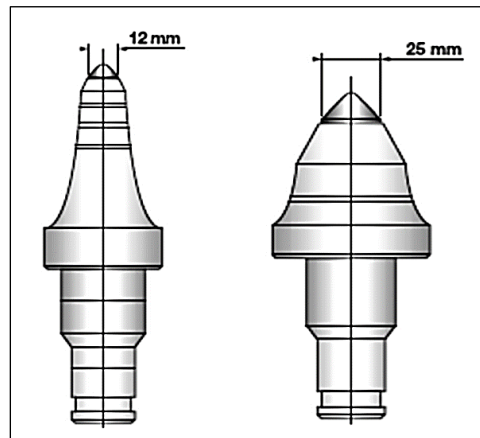


Figure 8. Different diameters of conical picks (Prakash, et al., 2020).

1.1.3.5 Spacing Between Picks

Spacing between picks on the drum or the cutting head is a very important aspect that affects the performance of cutting. The cutting tools which are installed on a cutting head are organized to cut in sequence. The tool that comes first prepare the rock (condition the rock) and reduce the forces for the next pick in a sequence, and thus the next tool does the same for the tool next to it. So, always the first tool to cut is subjected to higher forces than the next tools in sequence (Fowell, 1993). For a particular cut depth, there are three spacing options: wide spacing, very close spacing, and optimum spacing (Figure 9). In the wide spacing mode, the tools do unrelieved cutting producing very high forces. In the close spacing mode, the tools cuts inefficiently and specific energy is high. The optimum spacing is the most efficient (Fowell, 1993).

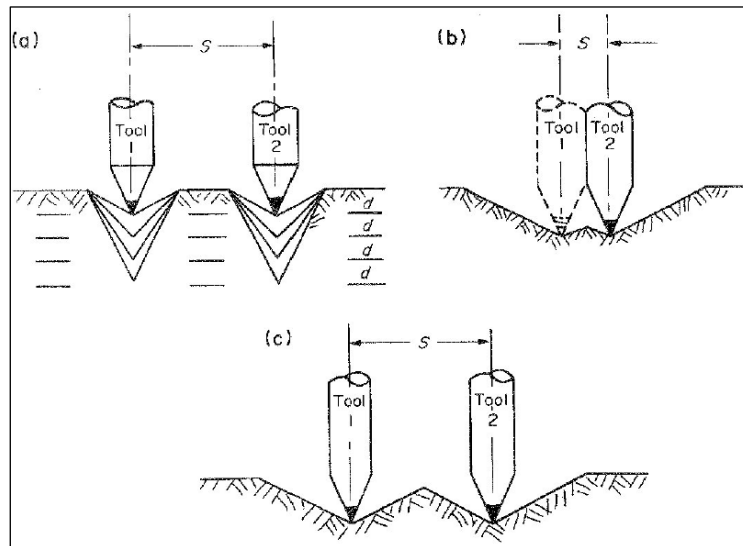


Figure 9. Spacing between tools: (a) wide, (b) very close, (c) optimum (Fowell, 1993).

1.1.3.6 Cutting speed

For the rotating cutterhead/drum, the cutting speed of conical pick and drag tools is determined by two factors: the speed of the slewing movement of the cutting head/drum and the diameter of the cutting tool's course. Fowell (1993) found that cutting speed has no influence on the magnitude of the force levels recorded, but wear rate increases with speed when cutting abrasive materials.

1.1.3.7 Wear of Picks

Wear of the pick is an important parameter that affects the performance of cutting. Conical picks and drag tools, like any other mechanical tool, they may wear. Wear reduces the efficiency of picks to a very large degree, because it changes the characteristics of the picks (Fowell, et al., 1987), it changes the tip geometry, the angles...etc.

1.1.3.8 Forces Acting on Conical Pick

Forces acting on drag cutting tools during the cutting process are three perpendicular forces: cutting, normal, and side forces (Figure 10). The cutting force (F_c) is acting in the path of cutting and opposite to the pick direction. The normal force (F_n) is perpendicular to the route of cutting and opposite to the pick direction. The lateral force (F_s) is perpendicular to the plane on which cutting and normal forces lie, and it act against the cutting tool from both lateral sides. Generally, the forces acting on a tool vary dramatically as the tool shape changes. Moreover, due to the nature of rock breakage, which take the shape of several chips, and is called “chipping”, but it does not take the shape of a nonstop chip, therefore forces oscillate repetitively (Figure 11) (Fowell, et al., 1987).

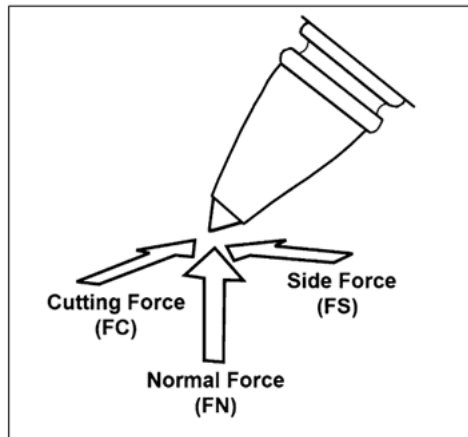


Figure 10. Force components acting on conical pick (Copur, et al., 2017).

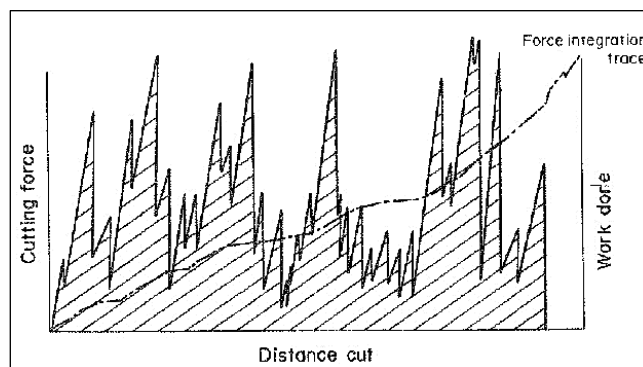


Figure 11. Cutting force diagram (Fowell, 1993).

1.1.3.9 Mechanism and of Rock Cutting by Conical Pick

The rotary cutterhead/drum on which several conical picks are placed start revolving, and with each rotation the picks affect the surface and eject the rock, and this action leads to transitional changes in stress levels within the rock, leading to fragmentation and the formation of separate rock chips. As the tool continues to move there is a constant rise and fall in pressure levels within the rock as the chips are broken away from the surface (Williams & Hagan, 2006). The nature of rock breakage has the shape of several chips, and this mechanism is called “chipping”, but it does not take the shape of a nonstop chip like metal cutting (Fowell, et al., 1987). According to Sifferlinger (2018), the cutting start with rock penetration by the pick, followed by crack imitation, and then propagation of the crack, afterwards large chips rupture, and finally stress release and removal of fragments from cutting groove. Sifferlinger (2018) also stated that the penetration force on the contact area between pick and rock has to overcome the strength of the rock. If the force is not enough, no chips will be formed, but rock grinding will occur. According to Yasar & Yilmaz (2018), Conical Pick move along the rock surface parallelly, and cut the rock by dragging its pieces in

front of its face. Due to that, the horizontal force component is more prominent (Serdar, 2020).

1.1.4 Excavation Machines

Excavation machines are classified based on many parameters, such as the type of the cutting tools installed on them whether drag tools or disc tools, and the degree of compressive strength of the rock whether hard rock or soft rock, and on the space consumed of the cutting face by the machine, whether the full face (full-face cutting machine) or only a part of the face (partial-face cutting machine). In general, the excavation machines that employ drag cutters are partial-face machines for cutting soft and medium strength rocks, but the excavation machines that use disc cutters are full-face, hard rock cutting machines. The focus in this study will be on the drag tools-based excavation machines. Excavation machines are classified also according to mining method, e.g. coal plough, sharer, trepanner are all sorted to one category, they are all used in longwall mining.

1.1.4.1 Drag Tools Based Excavation machines

Drag tools-based excavation machines are the excavation machines that employ the drag cutting tool. Machines that use the Drag cutting tool are used to cut soft and medium hard rocks. These machines are of limited use to hard and abrasive rocks. Those machines are: Roadheader (transverse and axial), Continuous miner (Pickmat and Hardhead), and longwall mining machines (Shearer, Coal plough, and Trepanner) (Fowell, 1993). Drag tools excavation machines are used frequently for mechanized coal production in longwall, and room and pillar mining methods.

1.1.4.1.1 Roadheader

Roadheaders are boom-type, partial-face tunneling machines (Figure 12). They are suitable for cutting rocks of low and medium strength, they are limited in case of hard rocks cutting, they possess a great degree of selectivity, as well as they have high amount of mobility and flexibility, as they may be moved from a working place to another (Sifferlinger, 2018; Copur, et al., 1998). Deshmukh, et al., (2020); and Sifferlinger, et al., (2017) stated that Roadheader can cut rocks with strength that reach 160 MPa uniaxial compressive strength. Sifferlinger, et al., (2017) stated that they can cut rocks with abrasivity index up to 3.5 CAI. They are of great importance among all the excavation machines. Cheluszka (2020) stated that roadheaders are extensively used in underground mines and in civil engineering for excavating roadways.

roadheader consist of: revolving cutterhead with cutter tools attached on it, extendable hydraulic boom, rotatable turret, loading apron, chain conveyor, crawler track, driver cabin, and the main frame. Two types of cutting heads are available and interchangeable: transversal-cutting head, and inline-cutting head (axial cutterhead) (Figure 13). The transversal type rotates perpendicular to the boom axis, but the inline type rotates parallel to the boom axis. The transversal type has four kinematic degrees of freedom: rotation of the cutterhead, horizontal and vertical slewing, and longitudinal movement of the hydraulic boom (Sifferlinger, 2018). The invention of roadheaders were at the end of 1940s for mechanical excavation of coal (Bilgin, et al., 2014). Nowadays they are a good excavation machine for selective mining purposes (Bilgin, et al., 2014; Asadi, et al., 2017). The cutting tools that are being employed on Roadheader cutting heads are short-gauge radial picks (Fowell, et al., 1987) and conical picks (Cheluszka, 2020). According to Restner & Plinnenger (2015), the net cutting rate (NCR) and specific pick consumption are important parameters for assessing the roadheader performance. They have high cutting rate when cutting soft layers, therefore the capacity must be high to fit the condition, and in case of low capacity, a reduction in the advance will be the outcome. The cutting sequences are sumping, cutting, and profiling (Sifferlinger, 2018). The number of cutting tools attached to one cutting head vary according to the strength of the rock, in case of softer rock, the number of cutting tools will be decreased and vice versa (Sifferlinger, 2018).

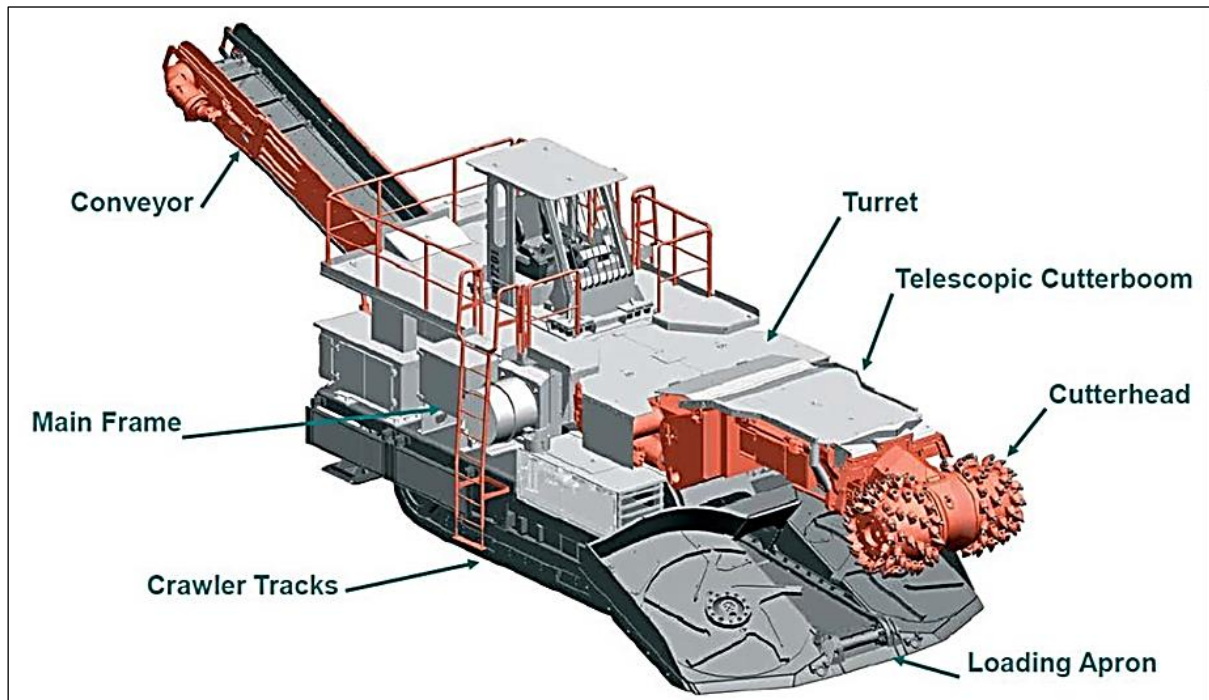


Figure 12 . Transversal Roadheader (Sifferlinger, 2018).



Figure 13. Axial Roadheader (Bilgin, et al., 2014).

1.1.4.1.2 Continuous Miner

Continuous miner (Figure 14) is an excavation machine which employ drag cutting tools. It was invented in the early 1940s in the US (Deliac, 1993) and was introduced in the 1950s (Khair, et al., 1989). They are used in room and pillar underground mining method (Fowell, 1993). Continuous miners are very popular in coal mining (Roxborough, et al., 1981; Demou, et al., 1983). They count for more than half of the coal production (Fowell, 1993). Continuous miner consists of horizontal cylindrical drum, transversely placed, with many cutting picks of

drag-type mounted on it (Fowell, 1993), and usually it comes with a boom, extensible or non-extensible (Mezyk, et al., 2019) on which the head is mounted. Among its components also a loading apron to collect the cut material, chain conveyor to convey the cut material, crawler track, and the main frame. They may have one drum or two drums (Deliac, 1993). It has two types: former one which is called “Hardhead”, and the other type is called “Pickmat”, The first is capable of cutting harder material than the second (Fowell, 1993). It moves forward by either the crawler or the boom. The drum can increase its width using extensible parts on the sides (Mezyk, et al., 2019). The aim of continuous miners is to increase productivity, but also, they produce a lot of dust (Khair, et al., 1989). The mechanism of cutting is that the drum rotates and being pushed forward while in motion to allow the picks to fragment the coal or mineral. Continuous miners are manufactured by many companies, for example: Joy, Caterpillar, Sandvik, Jeffrey, Eickhoff (Mezyk, et al., 2019).

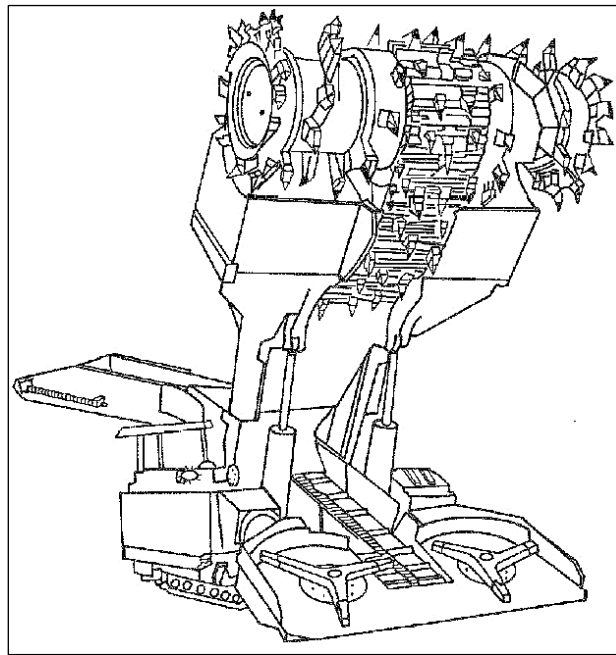


Figure 14. Continuous miner (Fowell, 1993).

1.1.4.1.3 Longwall Shearer

Longwall Shearer (Figure 15), which is called also “Coalface shearer”, is used in longwall mining method, and using drag cutting tools (Fowell, et al., 1987; Fowell, 1993). It has cylindrical drum with drag cutting tools mounted on it. It can have one or two cylindrical drums (Fowell, 1993). The two drum shearer is used when the coal seam is high, so the second drum cut the higher parts. The two drums are parallel to each other, and there is a distance between them, one is higher to cut the higher part, and the other is lower to cut the lower part. the first drum is called “leading drum”, and the drum in the back is called “trailing

drum” (Reid, et al., 2006). The drag tools that are usually employed on shearer drums are radial, forward attack, and point attack picks (Fowell, et al., 1987). The Radial picks that employed on shearer are often those with long reach (long gauge) (Fowell, et al., 1987). Drum Shearer was invented in the beginning of 1950s in United Kingdom (Deliac, 1993). The length of the shearer can reach 15m, and the weight can reach 90 tons (Reid, et al., 2006), it can be used in coal seams of thickness between 1.5 meters and up to 7 meters (Bilgin, et al., 2014). Shearers can be used in hard and soft coal layers (Bilgin, et al., 2014). The mechanism of working of the machine: the drums rotate and the coal is fragmented and falls on armoured face conveyor (AFC) (Bilgin, et al., 2014), to be transported from the work area to another place.

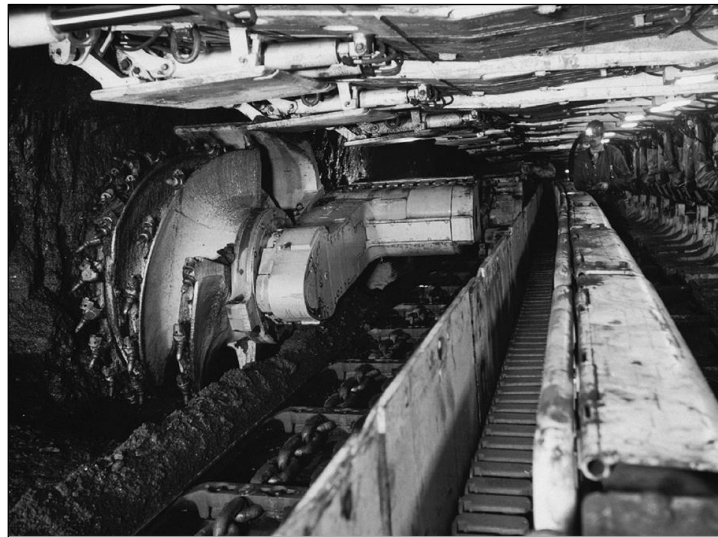


Figure 15. Drum shearer excavation machine (Bilgin, et al., 2014).

1.1.4.1.4 Coal Plough

The coal plough (Figure 16) consists of a series of drag tools, the plough moves along the coal face while pushing forward, this removes coal slices off the face of coal into a face conveyor (Bilgin, et al., 2014). Coal Plough was invented in Germany in the 1950s (Deliac, 1993). It is used for production of coal in hard coal mines in Poland (Bołoz, 2013). Ploughs were used much in Germany between 1950 and 1990 (Bilgin, et al., 2014). Ploughs can be used in coal seams of thickness between 0.6 – 2.3 m (Bilgin, et al., 2014). the coal strength to be cut by the plough is medium strength (Bilgin, et al., 2014).

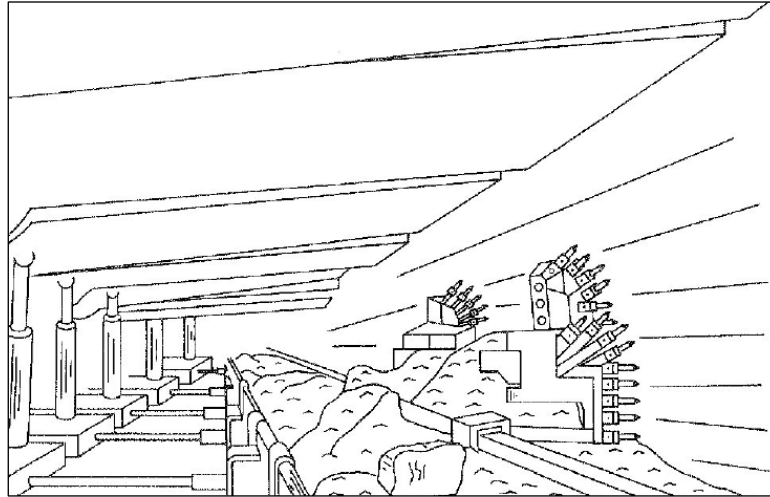


Figure 16. Coal plough (Fowell, 1993).

1.2 Selective Mining

Selective mining is defined as the process of selectively excavating rocks according to the degree of their strengths, the weak rock is excavated separately from the strong rock to ease excavation process (Bilgin, et al., 2014, p. 125). In the field of mining, it is defined as the process of extracting the profitable mineral, and leaving the unprofitable waste, it can also be defined by avoiding mixing the valuable materials with the unvaluable overburden during excavation (Heiniö, 1999; Krige, 1962).

Selective mining is used in deposits such as lodes, veins, seams, lenses, and stratiform orebodies (Villaescusa, 1998), and in thin seam of rich ore (Heiniö, 1999). It is used if the orebodies are disconnected or in case of strongly faulted environment or if there are strong variations in the ore grade distribution (Villaescusa, 1998; Dunbar, 2012). The ore body may contain high-grade and low-grade parts, and is surrounded by waste rocks. In order to achieve profit and avoid losses, extraction of low-grade ore or waste rocks must be avoided. low-grade ore and waste rocks extraction and mixing with the high-grade ore leads to ore dilution and must be avoided, to keep the mineral content high in the extracted ore, so the ore may be processed easily and the ore recovery may be increased. avoidance of extracting, processing and transporting of low-grade ore and surrounding rocks leads to high amount of cost reduction and hence increasing the profits (Copur, et al., 1998). Selective mining machines are partial-face machines; therefore, the cutters can be easily examined and replaced because the face is open. Grafe, et al., (2019) stated that applying sensors to excavation machines facilitate selective mining, as the machine recognize the condition of the cut material.

1.2.1 Selective Mining Applications

Open pit mining has been considered as bulk and non-selective mining method, as all high- and low-grade areas of the orebody has to be excavated (Dunbar, 2012). Underground mining in general has higher degree of selectivity than open pit mining, But the used mining method also may limit the amount of selectivity. Not only the mining method but also the rock and deposit characteristics, and the geometry of deposit. Examples of elective methods are Cut and fill mining method where the tabular deposit is steeply dipping and rock mass is stable (Dunbar, 2012). Another example also is Narrow vein mining which is used in very narrow ore bodies, a very selective method, the waste rocks are left in the footwall and hanging wall (Dunbar, 2012). Also, Overhand stoping, bench stoping, and Room and pillar (Villaescusa, 1998) (Figure 17) are all examples of selective mining method. Examples of non-selective methods are Block caving, open stoping (Moser, 2018). Generally, high-grade deposits might be mined with a selective method, to avoid mining of low-grade ore or waste (Dunbar, 2012), but low-grade, massive, deposits require “mass mining methods” (Moser, et al., 2018). Selective mining methods such as room and pillar, cut and fill, and bench stoping can completely recover the high-grade zone in a deposit.

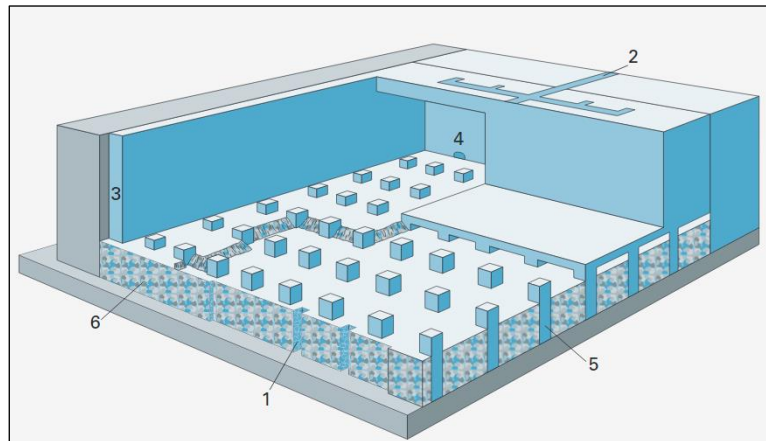


Figure 17. Room and pillar underground mining method (Atlas Copco, 2007).

Roadheader is used in selective mining operations (Bilgin, et al., 2014), and it has number of benefits over other underground excavation machines. It has great amount of selectivity, beside its mobility and flexibility. Also surface miner (Prakash, et al., 2020), highwall miner...etc.

1.3 Acoustic Emission

“**Acoustic emission (AE)** is the fast release of strain energy during fracture propagation, plastic deformation, or phase change that produces high frequency elastic waves in a material under stress. These waves make their way to the surface, where they may be heard (detected)” (Hussein, 1996).

“**Acoustic emissions** are mechanical vibrations that spread through solids, liquid or gases” (Hardy cited in Crosland, et al., 2009).

1.3.1 Aim of Adding AE Sensors to Rock Cutting

The aim of the development of the AE control system is the possibility of detecting changes in rock cutting conditions (Crosland, et al., 2009), and distinguishing between different rocks: hard rocks and soft rocks. The significance of this is the development of a real-time monitoring system to be installed on rock excavation machines (Crosland, et al., 2009), which can automatically modify the performance of the cutting machine to suit each rock and its strength. This will greatly improve the performance of rock cutting machines and increase their efficiency, such as longwall shearers, roadheaders and others. (Crosland, et al., 2009).

The features of the variation in AE energy may be utilized as preparatory information for the maximum cutting force, which is critical for intelligent mining machinery control and intelligent mining (Liu, et al., 2021). There is a link between cutting force and AE, and cutting force is an essential signal for smart mining and cutting machinery management.

Understanding the force change process may assist enhance machine rock cutting. (Liu, et al., 2021). It is very attractive for rock cutting equipment manufacturers and operators alike, as there is an increasing amount of excavation required in harsh and abrasive underground environments (Crosland, et al., 2009), developing a semi-autonomous operating system for the excavation machine will make the most of the machine and maximize its production capacity, maintaining it from damage and unnecessary change of tools and saving maintenance costs (Crosland, et al., 2009). Automated control system with acoustic sensors and others better than traditional system through auditory and visual observations of a skilled operator and saves time and money and maintains operator safety. In order to increase safety and efficiency through automation, online detection of rock properties during underground drilling allows for better control, improves drilling machine run, torque, reduces bit wear, etc. (Jung, et al., 1994). Intelligent real-time sensing of cutting process variables aids the intelligent control of rock-cutting and mining machinery (Liu, et al., 2021). Tool wear can

reduce the efficiency of rock cutting, and the monitoring of this wear may be done visually, which is unsafe and lead to pausing the cutting machine, but the online inspection system to detect wear issues in right time and will decrease the premature pausing of the machine (Crosland, et al., 2009). Saving money by avoiding premature replacing the cutting tool will save also energy and will increase safety (Crosland, et al., 2009).

1.3.2 AE in Rocks and Rock Cutting

AE in rocks is a deep-rooted phenomenon that is being attempted to be exploited in the field of rock cutting and was exploited in geomechanics (Williams & Hagan, 2006). Solids are known to release low-level acoustic emission or seismic signals when they experience variations in induced stress or deformation (Kaiser cited in Crosland, et al., 2009). The focus on measuring AE during cutting was limited to the metal machining industry, but there was area for application in rock cutting (Crosland, et al., 2009). In cutting process the AE signal vary clearly from rock to another, and also the AE signal characteristics (Liu, et al., 2021). The rate of AE energy was used to investigate microscopic activity in rocks under strain, and it was discovered that there is a direct link between the released energy and the strength of the rocks (Jung, et al. 1994). The first record of using AE in rock cutting was in the 1960s as a part of automated control system to control the excavation machine, but technology limitation hindered more examination (Williams & Hagan, 2006). Many researchers used AE to study rock fracture in drilling-related applications (Jung, et al., 1994).

1.3.3 AE Studies in Rock Cutting

Brown and Sing (1960) inspected AE while rock cutting, and discovered that the amount of AE energy radiated and the strength of rocks with same grain sizes had a direct relationship. (Brown J. and Sing M., cited in Jung, et al., 1994).

Nakamura (1977) stated that counting the number of AE events needed more advanced processing of AE signals (Nakamura, Y., 1977, cited in Jung, et al., 1994).

Pollok (1977) stated that the primary factor for measuring AE data should be AE energy. (Pollok, A., 1977, cited in Jung, et al., 1994).

Jung, et al. (1994) inspected AE while rock cutting, and discovered that AE energy increase when the hardness of rock increases.

Jung, et al., (1994) stated that the usual measurement parameters for determining the AE intensity are the AE rate and the number of events.

Shen and Hardy (1996), investigated the frequency domain of the AE signal, and noticed the existence of major dominant frequencies (MDFs) (Crosland, et al., 2009).

Ma and Zhang (1996) founded that AE waveforms and spectra are sensitive to different conditions in cutting, with various rocks, and having different AE frequencies (Ma and Zhang, 1996, cited in Liu, et al., 2021)

Williams and Hagan (2006) monitored AE on rock cutting and found that changes in rock cutting circumstances changed the character of the AE signal.

Crosland et, al (2009) found that AE were sensitive to changes in rock cutting configurations.

Crosland et, al. (2009) also inspected frequency domain and discovered change occurrence in the MDFs as he changed the configuration of cutting, he also plotted the amplitude of AE signal against time as another way of analysis.

Liu, et al. (2021) monitored AE during rock cutting and used FFT and power spectrum density (PSD) to investigate the AE. He found that AE signal has clear characteristics in energy magnitude, and PSD index. He found also that AE energy can represent the phases of the cutting process. He stated also that the AE waveform for the similar types of coal has equal MDFs. He investigated the relation between the AE to the force of cutting and he found that AE energy could be used for preliminary identifying the peak cutting force, and the AE can mirror the development stages of cutting force. Therefore, the AE can correlate the cutting force very well. He founded that AE waveform at the peak cutting force has some in common: MDF, PSD frequency spectrum and PSD area value.

1.3.3.1 Crosland, et al., 2009 Experiment

Crosland et, al (2009) used AE transducer of 50-200 Khz frequency range connected to a preamplifier, using gain settings of 20, 40, and 60 dB. The equipment allowed sampling rate of maximum 250,000 samples per second, but the used sampling rate was 200,000 Sample/sec. He set the gain of preamplifier on maximum sensitivity. Crosland et, al (2009) used different rocks in the experiment: sandstone, gypsum plaster, and coal blocks. The sandstone block was of 395 mm length and 265 mm width and a UCS of 40 MPa. He used “Dasylab” as a data acquisition software to store the data of tests. He conducted the cutting tests using Linear cutting machine, and recorded the AE signals using AE equipment. He

connected the AE transducer directly on the rock block using super glue, and then he tried with the beeswax, to inspect the effect on the AE signal by different attachment methods. He tried two different location of AE transducer: first on the cutting tool holder, and second on the surface of rock block. Crosland et, al (2009) experimented many depths of cutting and speed of cutting to inspect the effect on AE signal. He experimented many sampling rates as well to also investigate the effect on AE signal. He depended on the examination of the frequency content in the AE signal based on FFT, he also plotted the amplitude of AE signal against time as another way of analysis.

The result of his experiments: Crosland et, al (2009) found that AE magnitude / time graphs reflected the changes in force on the cutting tool with time, and identified changes in cutting condition. He found that MDFs became clear only at sampling rates above 100,000 samples per second. He found the best AE signal was when connecting AE transducer on the cutting tool using glue. He found little insignificant differences when he changed the speed of cutting regarding the MDFs of FFT. He found very little difference in MDFs, when he changed the depth of cutting. He also found little difference in MDFs when he changed method of attaching AE transducer to the rock block. He found substantial difference on the frequency response when he changed the location of AE transducer have, as well as he found a change in the level of noise in the AE signal, so it became hard to describe the MDFs. He found significant differences in the

of the AE signals and the MDFs when he changed the rock type. He stated that the most common MDFs were 50, 56 kHz for sandstone; 50, 54 kHz for Coal; and 56, and 57 kHz for Gypsum plaster.

1.3.4 AE Measuring Units

The acoustic emission (or sound level, or loudness) is measured using either logarithmic scale, which is called decibel, or the linear scale. The decibel scale is used for measuring sound intensity (Steven, 1955). The decibel (dB) is a logarithmic unit for sound intensity level measurement. In other words, it is a logarithmic means of defining a ratio. The ratio might be based on power, sound pressure, voltage, intensity, or others (UNSW, Wolfe, J., et al., 1991). The decibel is a relative measurement rather than an absolute measurement. All dB measures are comparisons (i.e., ratios) of a given level to a reference level, which is usually the hearing threshold. They are not absolute intensity or pressure readings (Truax, 1984). The relationship between loudness and decibel is nonlinear (Steven, 1955).

According to Audacity application manual (2021), “Linear is a simple, directly proportional, one-to-one, "straight-line" relationship. This term is used to contrast with exponential, logarithmic, or other complex relationships”. Audacity (2021) stated that the linear scale is the amplitude scale, that runs linearly from +1 at the top (the maximum allowed loudness without distortion when the signal is positive) to -1 at the bottom (the maximum when signal is negative)”. Audacity (2021) stated that the linear scale is very convenient for editing audio in the application, but the linear waveform does not correspond to the way the ears function, they sense quiet sounds more effectively. Audacity (2021) stated that halving the volume on the linear scale from +/- 1.0 to +/- 0.5 will require only -6dB to achieve, and that does not sound much quieter. A reduction of -18 dB is needed by Human hearing to make audio "appear to sound" half as loud (Audacity , 2021).

1.3.4.1 Calculating of The Decibel

A deci-bell is one tenth of a bell, it can be defined as:

$$SI = 10 \log \left(\frac{I}{I_0} \right)$$

Where SI is the sound intensity Level in dB (Roberts, 1984).

(I) is the sound intensity (or the magnitude of sound) in W/m^2 it is the sound energy transmitted per unit time through a unit area (Roberts, 1984).

I_0 is a reference sound intensity. At the threshold of hearing at 1000 Hz the reference sound magnitude equates to $10^{-12} W/m^2$ (Roberts, 1984).

1.3.4.2 Sound Intensity Representation in The Decibel Scale

Intensity of sound is measured in watt per squared metre (W/m^2). It is defined as the power carried by sound waves per unit area in a direction perpendicular to that area (Truax, B., cited in SFU, 1999). A sound Intensity of $1 \times 10^{-12} W/m^2$ is attributed to the hearing threshold; this sound corresponds to a sound Intensity level of 0 dB (Truax, B., cited in SFU, 1999). A sound level of 10 dB is attributed to a sound that is 10 times more powerful ($1 \times 10^{-11} W/m^2$). A sound intensity equates to 1 watt/ m^2 is designated to the threshold of pain (Truax, B., cited in SFU, 1999).

By using the previous decibel measuring law, the difference between two sound sources in dB would be as following: if the second generates twice, 10 times, or million times as much

power as the first, the difference in sound intensity between the two will be 3 dB, 10 dB, or 60 dB respectively. (UNSW, Wolfe, J., et al., 1991).

1.3.5 FFT and Signal Analysis

According to Oberst (2007) “[Fast Fourier transforms (FFTs)] are low-complexity algorithms that compute the discrete Fourier transform (DFT)”. According to Heckbert (1995) “[The FFT] is a fast algorithm for computing the DFT”. According to Elliott (1987), “[the FFT] computes the DFT with a significantly lower number of arithmetic operations”. According to Oshana (2006), “[The FFT] removes practically all of these unnecessary calculations, saving a substantial amount of time and making it far more realistic to utilize in many applications today”. According to Cooley & Tukey (1965) “[The FFT] results in a procedure requiring a number of operations proportional to $N \log N$ rather than N^2 ”. The approach is efficient because it removes redundancies (Elliott, 1987).

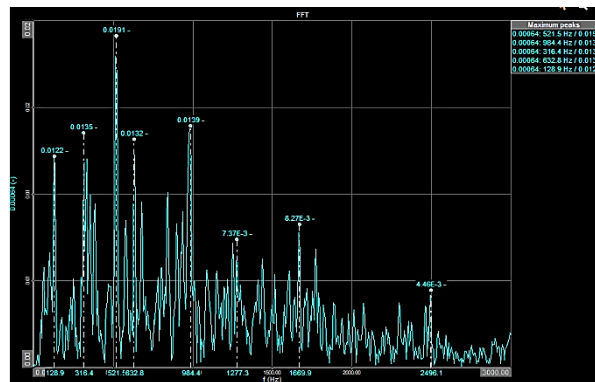


Figure 18. Example of FFT analysis graph.

1.3.5.1 Usage and Importance of FFT

For signal analysis, the DFT and its particular version, the FFT, are commonly utilized. (Heß, 2010). The FFT is one of the most helpful techniques in signal processing and is frequently utilized (Zhu, et al., 2014). FFT and the power spectrum are powerful tools for analyzing and measuring signals from plug-in data acquisition (DAQ) devices (Harvey & Audrey, 2000). The topic of Fourier transform has been at the center of digital signal processing since its beginning (Burrus, et al., 2012). Zoom FFT analysis may give high frequency domain resolution and detailed signal analysis for a specific frequency range (Zhu, et al., 2014). They are among the most significant algorithms in applied and engineering mathematics as well as computer science, with applications in one- and multidimensional systems theory and signal processing in particular (Oberst, 2007).

2 Materials and Methods

The experiment was undertaken at the rock cutting laboratory at ‘TU Bergakademie Freiberg’, The Technical Mining University in Freiberg, at the institute of mining and special civil engineering. Differentiation between different concrete blocks during concrete cutting using acoustic emission is the purpose of this study, in order to improve the mechanical excavation industry, and the selective mining operations. Instead of traditional methods via the ears of a skilled operator, the using of AE sensors is thought to evolve rock cutting operation. When the rock is cut, AE from the Cutting is released, which varies from rock to rock and from cut to cut depending on many parameters. These parameters are going to be studies, including the characteristics of the rock, depth of cutting, and speed of cutting.

2.1 The Cutting Test

The components of the test are the linear cutting machine, concrete blocks, acoustic equipment, force sensors, and data acquisition system.

2.1.1 Linear cutting machine "HSX 1000-50"

The full-scale linear rock cutting machine (LCM) "HSX 1000-50" (Figure 19) is manufactured by the company “ASW” GmbH (Automation, Sonder- und Werkzeugmaschinen GmbH). It was made specially for the university TU Bergakademie Freiberg; to carry out full-scale cutting tests on rock blocks. The machine allows maximum speed of 1.7 m/s, and it provide maximum power of 60KW, and allow rock samples of relatively large sizes up to 60*120*50 cm.

2.1.1.1 Components of the " HSX 1000-50"

The machine consists of (a) a cutting rig containing a table moving in the X axis to enable cutting in the direction of the table movement, moving at different speeds, for the possibility of changing the cutting speed, (b) a conical pick moving in the direction of Y and Z to enable cutting in different positions and at different depths, and (c) a control panel “steering board” to steer the pick and the table movement (see Figure 19).

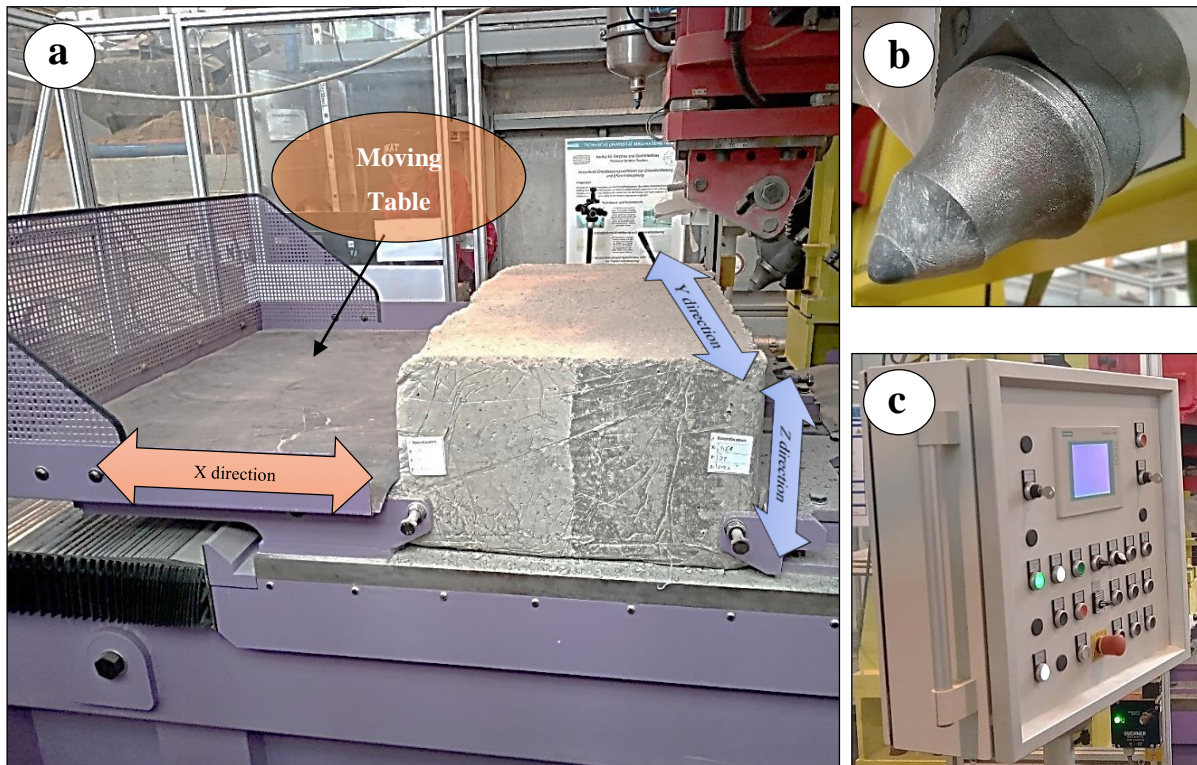


Figure 19. Linear cutting machine: (a) moving table (left), (b) conical pick (top right), (c) control Panel (bottom right).

2.1.2 Concrete Blocks

Concrete was used instead of rock samples in order to control the uniaxial compressive strength of the test sample without changing other properties such as particle size. Two concrete blocks were used: “block AC” which consists of two blocks: block ‘A’ and block ‘C’ joined together. “block CB”, which consists of two blocks: block ‘C’, and block ‘B’ joined together (Figure 20). The concrete blocks were joined together; to be cut for differentiation between them.



Figure 20. Artificial concrete blocks: (a) block AC (left), (b) block CB (right).

2.1.2.1 Concrete Blocks Dimensions

The dimension of the two joined block -whether “AC” or “BC”- is (58 x 106 x 37 cm), each single block “A”, “B”, or “C” has half of this dimension (29 x 106 x 37 cm) (see Figure 21).

2.1.2.2 Concrete blocks Materials and Characteristics

Both blocks “AC”, and “CB” are made of concrete. The concrete blocks have the following characteristics: block A (C8/10) has 8 MPa cylinder strength and 10 MPa cube strength, block B (C20/25) has 20 MPa cylinder strength and 25 MPa cube strength, and block C (C35/45) has 35 MPa cylinder strength and 45 MPa cube strength. The maximum particle size of all concretes is 8 mm.

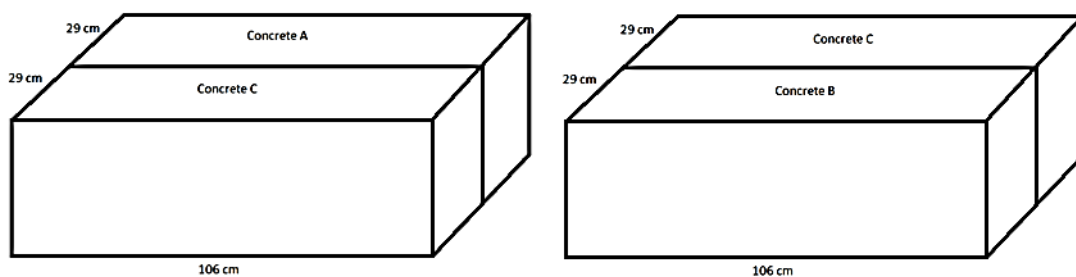


Figure 21. Concrete blocks dimensions.

2.1.3 AE Measuring System

AE measuring equipment are used for capturing and storing the AE coming from the rock cutting operation. The AE system consist of: (a) omni directional Microphone M30, manufactured by Earthworks company in USA, it picks up sound from all directions equally, it captures the acoustic signal, and send it to the next device (b) Preamplifier, named “TUBE

ULTRAGAIN MIC 100”, manufactured by Behringer company in Germany, it receives the acoustic signal from the acoustic sensor and adjust the, input and output gain, and then send it to the recorder device, as well as it provide 48v phantom power to the microphone. (c) PCR recorder for DSLR (the commercial name: Tascam DR-60D MK II), manufactured by Tascam company, it picks up the acoustic signal from the preamplifier and stores it on a storage device, It also allows adjustment of the input gain. It works on Battery. (d) Storage device (SD card), to store acoustic data. (e) connecting cables, to connect the different acoustic equipment together. (F) Tripod; to carry the acoustic sensor, which is mounted on it (see Figure 22).



Figure 22. Acoustic signal capture and recording equipment.

2.1.4 Force Sensors

The force sensors are called “Piezoelectric sensors”. They are used to capture all force signals (to measure forces): cutting, normal, and side forces. It was manufactured by “Kistler” company. it can measure forces up to 75 KN for cutting, and normal forces; and 50 KN for side force (see Figure 23).

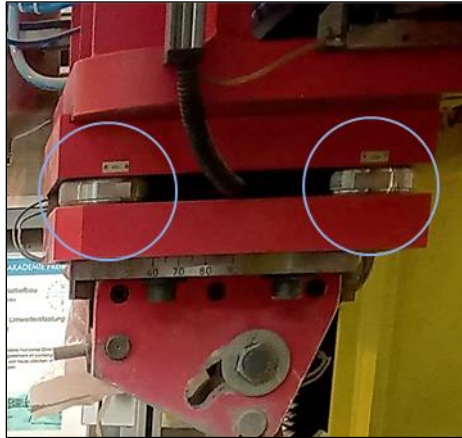


Figure 23. Force sensors (Piezoelectric sensors).

2.1.5 Data Acquisition System

Dewetron is the used data acquisition system. It consists of: (a) DAQ computer, (b) Cables connected to the HSX 1000-50, (c) Dewesoft DAQ software. It receives the force signals from the force sensors and store them (see Figure 24).

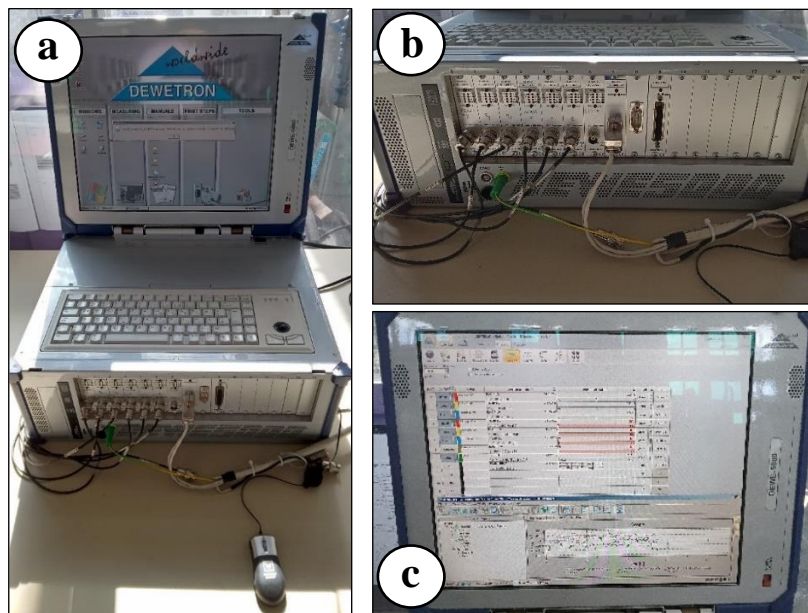


Figure 24. Dewetron (data acquisition system): (a) DAQ Computer, (b) Cables connected to the LCM: HSX 1000-50, (c) Dewesoft DAQ software.

2.2 Experimental Procedures

The experimental procedures included preparing and conditioning, optimization of acoustic signal quality, cutting and measuring: acoustic measurement (to obtain acoustic data), force measurement (to obtain force data), and finally processing of the data: acoustic data processing, and force data processing.

2.2.1 Preparing and Conditioning

Concrete blocks were poured (casted) within the context of RockFeel project. New concrete was obtained from Schwenk Concrete Company in Freiberg. concrete casting studies were carried out with specially produced casting forms (see Figure 25). cubic samples with a size of 150 x 150 x 150 mm³ were prepared to determine the uniaxial compressive strength (UCS) of concrete. Five or more cubic samples were casted for each concrete type. UCS tests were carried out 28 days after concrete was casted. The tests were carried out using a hydraulic press with a loading capacity of 1000 KN. (The results of the compression tests are presented in Table 1).



Figure 25. Cubic samples for UCS determination of concrete.

Table 1. Results of the uniaxial compressive strength tests.

| Sample | UCS (MPa) | Standard Deviation (MPa) | Coefficient of Variation (%) |
|--------------------|-----------|--------------------------|------------------------------|
| Concrete A- C8/10 | 14.68 | 0.42 | 2.85 |
| Concrete B- C20/25 | 22.29 | 0.67 | 2.99 |
| Concrete C- C35/45 | 40.48 | 1.24 | 3.08 |

2.2.1.1 Levelling of the concrete surface and installing the sensors

The concrete samples then were brought to the rock cutting testing facility of TU Freiberg. The rock sample was placed above the test table of the LCM, and was tightened using screw bolts fitted on the table. The appropriate pick (conical pick) was installed over the holder. The Force sensors (Piezo sensors) are installed in place above the cutting pick. The rock block was conditioned (levelled) to make it symmetrically flat to be ready for the test, by making dozens

of parallel small cuts (low-depth cuts) on the surface of the rock (about 300 cuts) (see Figure 26). Force sensors (Piezo sensors) were connected to the data acquisition system (Dewetron) that is connected to a power source and it was operated. AE measuring equipment were installed, connected to a power source, turned on and prepared for recording the audio signal.



Figure 26. Conditioned concrete surface.

2.2.1.2 Optimization of Acoustic Signal Quality

Different modes (different settings) were tested in order to optimize the acoustic signal quality. That was done by: adjusting the gain, and adjusting acoustic sensor location.

2.2.1.2.1 Adjusting the Gain Level

2.2.1.2.1.1 Preliminary Trials

Different gain settings (sound level settings) were tested for optimization of the acoustic signal quality. Three different settings tested at first: very high gain, very low gain, and medium gain (see Figure 27). The result, the proper gain was around the middle, since at high gain settings clipping issue was faced, and the quality of the acoustic signal was very bad. The acoustic signal, and FFT frequency spectrum were plotted for each gain setting, a comparison between the results was made.

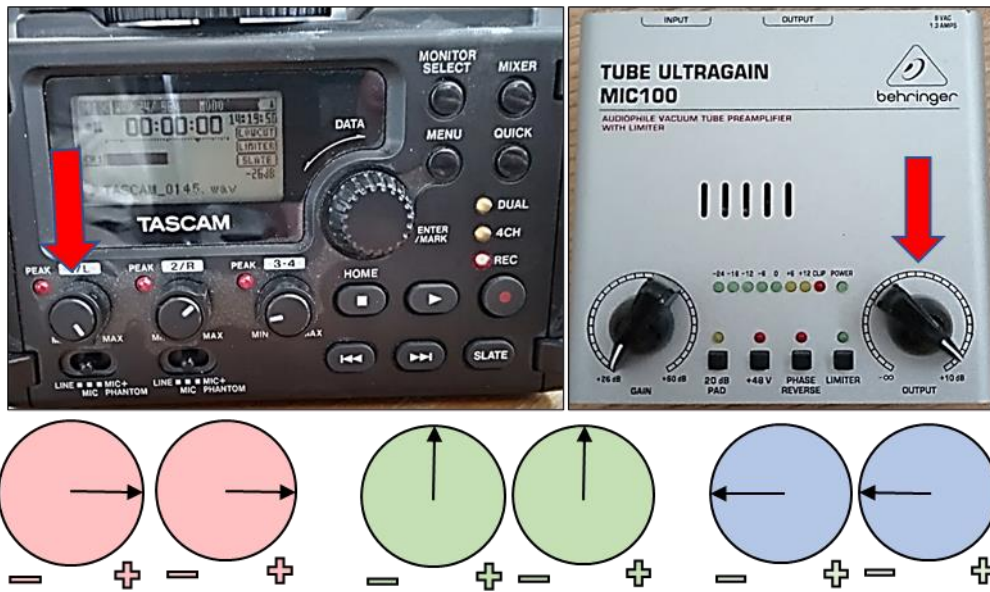


Figure 27. Gain settings tested for optimization of acoustic signal: Very High (left), medium (middle), and Very Low (Right).

2.2.1.2.1.2 Applied Gain Settings

Two more gain settings (input sound levels) were tested: Low Gain Settings, and High Gain Settings, both were considered and applied during the rock cutting test. Some of the acoustic records of rock cutting were made using the low gain settings, and some are made according to the high gain settings. A comparison between the results of each gain setting was made. The results of this comparison are presented in chapter 4: Results and Discussions.

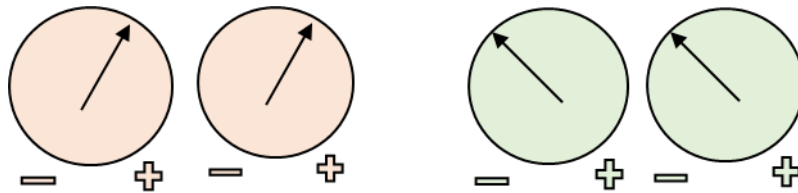


Figure 28. Gain settings used in the test: High Gain (left), and Low Gain (right).

2.2.1.2.2 Adjusting the distance of the cut from the acoustic sensor

Three distances of the acoustic sensor from the cutting position were tested for the optimization of the acoustic signal quality: far, middle, and close distances (see Figure 29). The results of this comparison are presented in chapter 4: Results and Discussions.

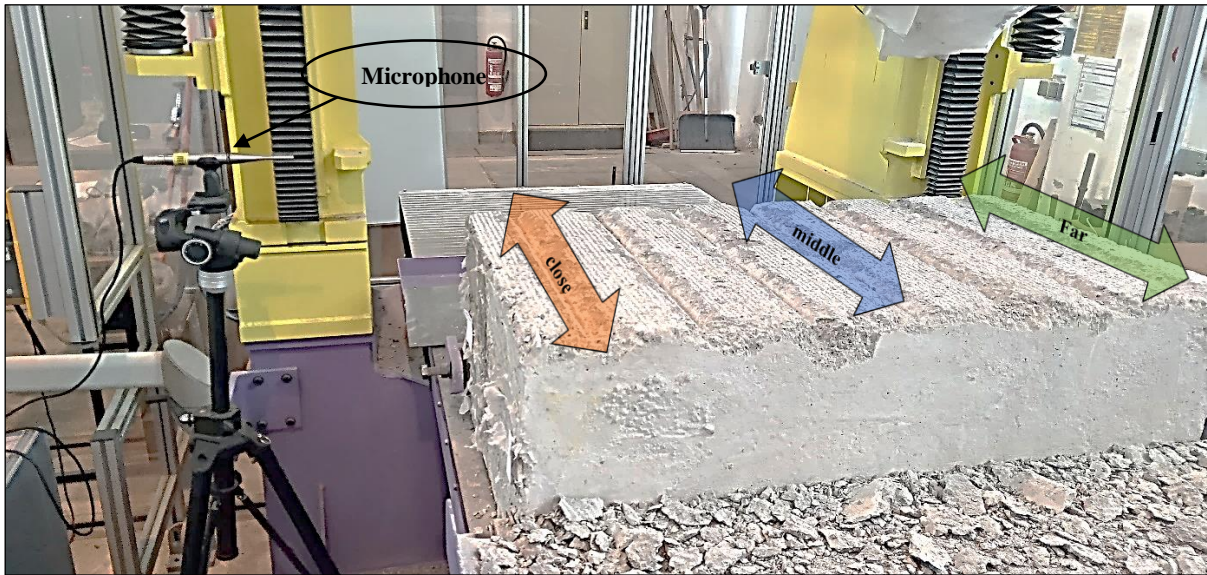


Figure 29. Various distances of acoustic sensor from cutting position.

2.2.2 Cutting and Measuring

Using conical pick, cuttings were implemented. Measurements were done Simultaneously with the cutting, forces were measured using Dewesoft, and AE were measured using acoustic equipment.

2.2.2.1 Cutting parameters

Different parameters of cutting were used: different speeds, different depths, different spacings between cuts. The reason is to optimize the cutting operation. The more parameters to try, the better results of experiments to acquire (a list of all cutting tests is shown in Table 2, and Table 3).

2.2.2.2 Cutting plans

Cutting plan was made possible by using the control panel of the LCM machine, that can do both: steer the cutting pick to control its position using coordinate system, as well as moving the table and controlling its speed, different plans of cutting were implemented, different parameters were applied. Generally, two modes of cutting were used: unrelieved cutting, and relieved cutting modes. 117 cutting tests were implemented for each concrete block: 36 unrelieved, and 81 relieved (234 for the whole test for the two concrete blocks). Within this number, each set of parameters: speeds, and depths were repeated multiple times, according to plan, for optimization of the quality of the test. (A list of all cutting tests is shown in Table 2, and Table 3).

2.2.2.2.1 Unrelieved Cutting Plan

The unrelieved cutting mode was performed with different parameters that were applied for each cut: three speeds of cutting: 0.5, 1.0 , and 1.5 m/s, as well as four cutting depths: 2, 5, 10 , and 15 mm. the spacing between cuts was ten times the depth of the cut (10 x d). 36 unrelieved cutting test were performed for each block; 12 cuttings of a certain depth and cutting speed, each was repeated three times (12 cuts x 3 trials). (A list of the unrelieved cuttings is shown in Table 2).

Table 2. List of Unrelieved Cutting Tests.

| Concrete block | Test Number | Trial | Depth | Speed | Concrete block | Test Number | Trial | Depth | Speed | | | | |
|----------------|-------------|-------|--------|---------|----------------|-------------|-------|--------|---------|-----|--|--|--|
| | | | d (mm) | v (m/s) | | | | d (mm) | v (m/s) | | | | |
| AC | 1 | . | 2 | 0.5 | CB | 1 | . | 2 | 0.5 | | | | |
| | . | | | 1.0 | | . | | | 1.0 | | | | |
| | | | | 1.5 | | | | | . | 1.5 | | | |
| | . | | 5 | 0.5 | | . | | 5 | | 0.5 | | | |
| | | | | 1.0 | | | | | 1 | 1.0 | | | |
| | | | | 1.5 | | | | | | 1.5 | | | |
| | . | | 10 | 0.5 | | . | | 10 | 0.5 | | | | |
| | | | | 1.0 | | | | | 3 | 1.0 | | | |
| | | | | 1.5 | | | | | | 1.5 | | | |
| | . | | 15 | 0.5 | | . | | 15 | 0.5 | | | | |
| | | | | 1.0 | | | | | . | 1.0 | | | |
| | | | | 1.5 | | | | | | 1.5 | | | |
| | 36 | | | | | | | | 36 | | | | |

2.2.2.2.2 Relieved Cutting Plan

The relieved cutting mode (plan) was performed also with different cutting parameters, using 3 different depths (5, 10, 15mm) and 3 different speeds of cutting (0.5, 1.0, 1.5 m/s). Two layers of cutting were used for each set of parameters. The spacing between cuts was 35mm, The first cut of each group of a depth has to be a “dummy cut”. 81 relieved cutting tests were performed for each block: 9 cuttings of certain depth and speed were repeated 9 times: 5 times for the first layer, and 4 times for the second layer. (A List of relieved cuttings is shown in Table 3).

Table 3. List of relieved cutting tests.

| Concrete block | Test Number | Layer | Spacing | d | v | Concrete block | Test Number | Layer | Spacing | d | v | | |
|----------------|-------------|-------|---------|----|-----|----------------|-------------|-------|---------|---|-----|----|-----|
| | | | s | mm | mm | | | | m/s | s | mm | mm | m/s |
| AC | 1 | 1 | 35 | 5 | 0.5 | CB | 1 | 1 | 35 | 5 | 0.5 | | |
| | . | | | | 1.0 | | 1.0 | | | | | | |
| | | | | | 1.5 | | 1.5 | | | | | | |
| | | . | 2 | 35 | 5 | | 0.5 | 0.5 | | | | | |
| | | | | | | | 1.0 | 1.0 | | | | | |
| | | | | | | | 1.5 | 1.5 | | | | | |
| | | . | 1 | 35 | 10 | | 0.5 | 0.5 | | | | | |
| | | | | | | | 1.0 | 1.0 | | | | | |
| | | | | | | | 1.5 | 1.5 | | | | | |
| | | . | 2 | 35 | 10 | | 0.5 | 0.5 | | | | | |
| | | | | | | | 1.0 | 1.0 | | | | | |
| | | | | | | | 1.5 | 1.5 | | | | | |
| | | . | 1 | 35 | 15 | | 0.5 | 0.5 | | | | | |
| | | | | | | | 1.0 | 1.0 | | | | | |
| | | | | | | | 1.5 | 1.5 | | | | | |
| | | . | 2 | 35 | 15 | | 0.5 | 0.5 | | | | | |
| | | | | | | | 1.0 | 1.0 | | | | | |
| | | | | | | | 1.5 | 1.5 | | | | | |
| | | 81 | | | | | | | 81 | | | | |

2.2.3 Data Processing

Two types of rock cutting data were received from measurement by sensors from each cut: AE data from acoustic sensor's measurements, and force data from force sensor's measurements. Both of the data were put under processing steps to be ready for the final results of rocks differentiation. Both are further discussed, each in a separate section.

2.3 Processing of AE Data.

The acoustic data (audio recordings of rock cutting tests) has been processed to differentiate between different rocks.

2.3.1 Preparing audio Files for Processing.

Audacity 3.03 was used to trim the audio files, to be ready for processing. The software was also used to export files in txt format, for the possibility of processing them later on other programs.

2.3.2 Processing and Analysis.

The analysis of the acoustic data was based on: the analysis of the AE signal itself, and also on three functions: moving average, Interquartile range, and FFT frequency spectrum.

2.3.2.1 Acoustic signal analysis

“Excel office 2019” and “Audacity 3.03” program were tested to obtain an illustration graph of the acoustic signal, in which the difference between the two different artificial rock blocks was clear: concrete A and concrete C for block “AC”, as well as concrete C and concrete B for “block CB”. (See Figure 30). Finally, Excel 2019 was used to plot AE signal graphs of all cutting tests; for it has wide range of functions and calculation possibilities. Part of the results is presented and discussed in Chapter 4: Results and Discussion, the rest are presented in the last chapter: The Appendices.

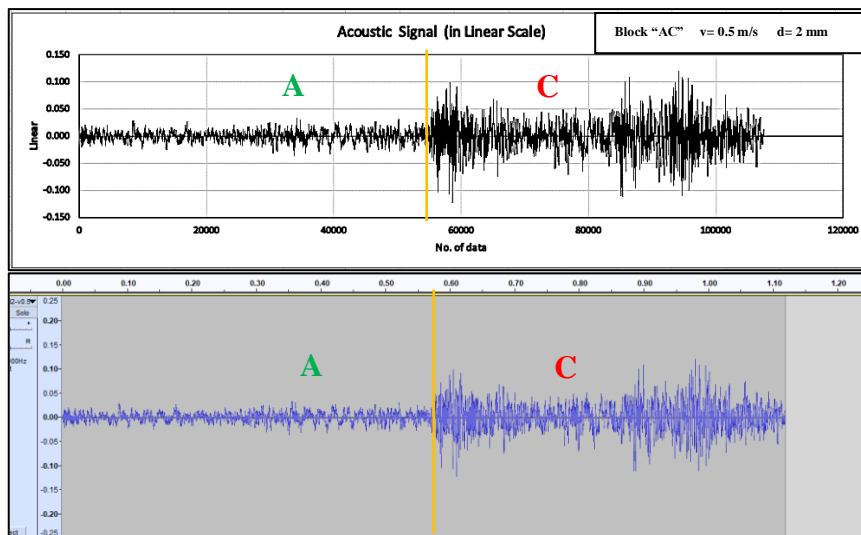


Figure 30. acoustic signal graph: by Excel 2019 (above), by Audacity 3.03 (below).

2.3.2.2 “Moving Average” and “Interquartile Range”

The A.E signal was further analyzed and processed, for trying of finding more methods of differentiation between different rocks depending on the A.E., The “Interquartile Range” and “Moving Average” graphs were plotted (see Figure 31 & Figure32). Excel Office 2019 was used to get and plot these functions. For the possibility of obtaining the moving average function, it was needed to use only positive values from the acoustic signal. Part of the results are presented and discussed in Chapter 4: Results and Discussion. The rest is presented in the last chapter: the Appendices.

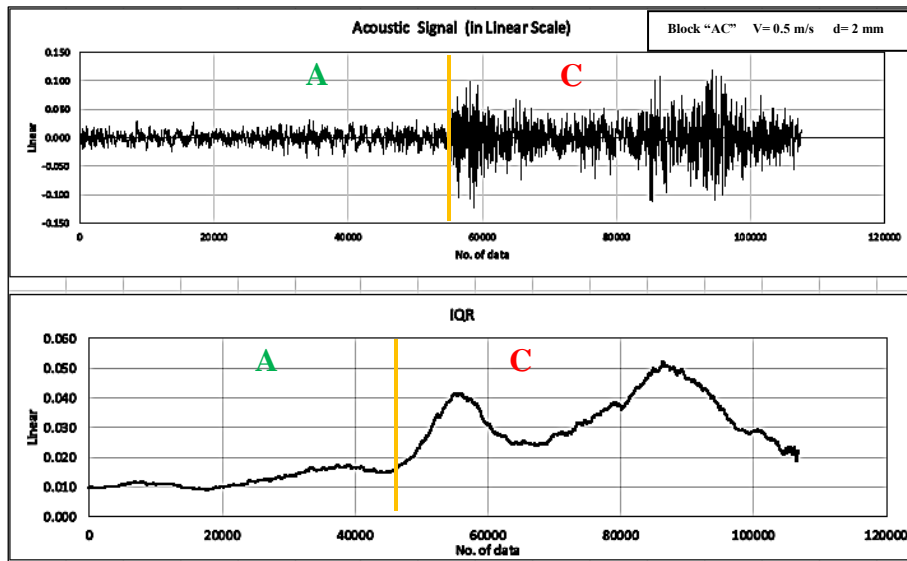


Figure 31. "Interquartile range" graph (bottom), Acoustic signal graph (top).

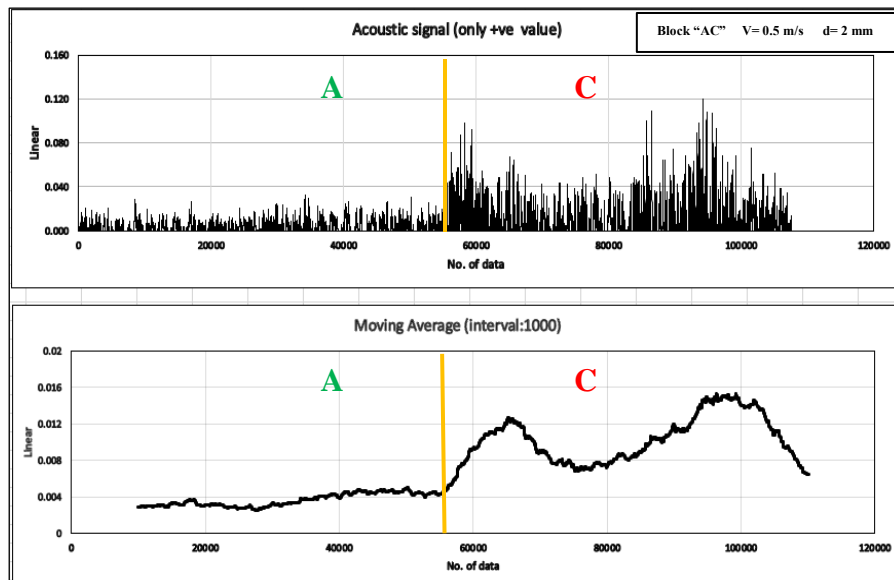


Figure 32. "Moving Average" graph (bottom), and the +ve value of the acoustic signal (top).

2.3.2.3 FFT Analysis

More attempts have been made to search for methods to differentiate different rocks during cutting depending on the AE signals. FFT frequency spectrum therefore was plotted. Two programs were tested: Audacity 3.03, and DewesoftX 2021. After comparison of the results, it was decided to use "Dewesoft X 2021" since it gives a more realistic frequency resolution (See Figure 33).

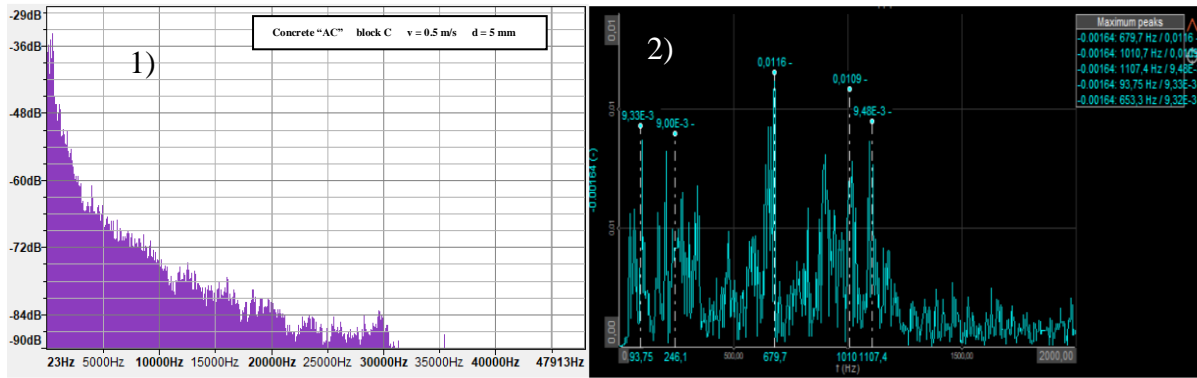


Figure 33. comparison FFT frequency spectrum: (1) Audacity 3.03 (left), and (2) DewesoftX 2021.03 (right).

FFT frequency spectrum were drawn for all AE signals from rock cutting tests, using DewesoftX 2021.03. They were compared to different rock blocks, to study the possibility of using them for differentiation of different rock types. Part of the results are presented and discussed in chapter 4: results and discussion, the rest is presented in the appendices part, the last chapter.

2.4 Force Data Processing

For material characterisation, the force data was processed in two parts: analysis of forces (cutting, normal, and lateral forces) for each block separately, and analysis of FFT frequency spectrum for each block separately.

2.4.1 Force signal analysis

To differentiate between the cut rock blocks, two procedures were applied to the strength signal: 1- Data were calculated for each rock block separately, 2- Illustrations Graphs were Plotted for each block separately as well. The result: the difference was clear through the numerical data and also through the illustration graphs.

2.4.1.1 Data Calculation

Calculation was performed for each block separately, A, B and C, for all forces, cutting, normal, and lateral forces. Following data were calculated: maximum force, minimum force, average peak force, average force, average maximum force divided by the depth, average force divided by the depth, average peak force divided by the average force. The average force was calculated by taking the average of all forces. The average peak force was calculated by taking the average of the ten highest peaks.

2.4.1.2 Graphs Plotting

Cutting, normal, and lateral forces (in newton measuring unit) were drawn against time (in seconds measuring unit) for each block separately, to differentiate between different concrete blocks (see Figure 34, Figure 35, and Figure 36).

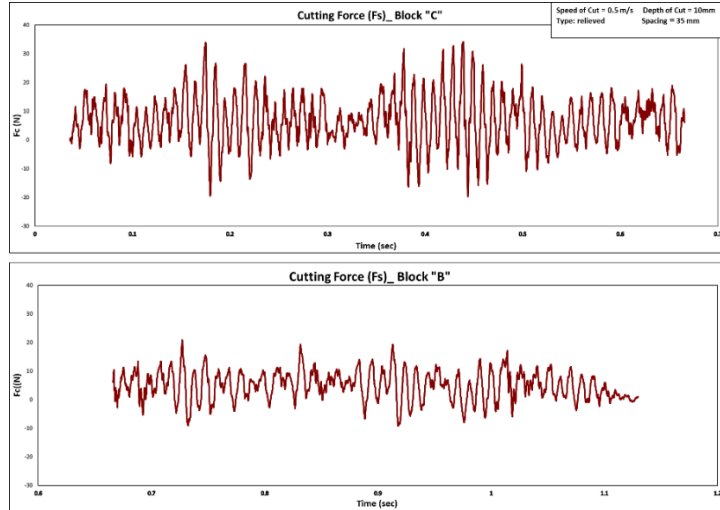


Figure 34. Cutting force for “concrete block CB” (separated): block C (top), block B (bottom).

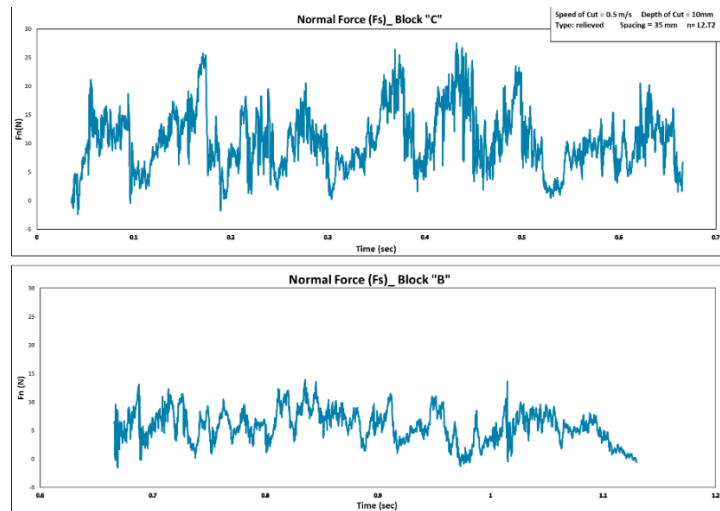


Figure 35. Normal force for “concrete block CB” (separated): block C (top), block B (bottom).

Chapter 2: Materials and Methods

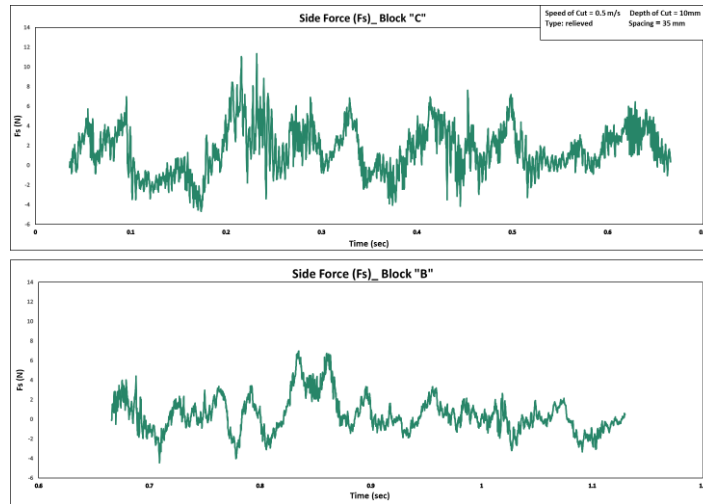


Figure 36. Side force for “concrete block CB” (separated): block C (top), block B (bottom).

3 Results and Discussions

3.1 AE signal analysis

Twenty-four AE signals recorded with low gain settings (which were mentioned in the previous section) during cutting tests on concrete blocks AC and CB with different cutting parameters: different depths and different speeds were selected for analysis, discussion and presentation.

3.1.1 Block AC

Twelve AE signals recorded with low gain settings (which were mentioned earlier in the previous chapter) during cutting tests on concrete block AC, with different cutting criteria: different depths and different speeds, were selected, for analysis, discussion and presentation.

By looking at the AE signal resulted from cutting of “block AC” with a cutting depth 2 mm and a cutting speed 0.5 m/s (Figure37), it is possible to differentiate between block A and block C by visual observation, as the AE signal of block C has higher peaks than block A. But through the numbers, it is possible to accurately differentiate between block A and block C, by analyzing the AE signal numerically by the computer, it is found that the average value of peaks of block A is 0.0190422, while the average peak value of block C is 0.058696531, which is higher than A, and the maximum peak of block A is 0.03265, while the maximum peak For Block C 0.11951, which is also higher than that of block A. Those calculation were made based on 100 peak per cut. This difference is due to the fact that the higher strength concrete block when cut emits a more intense AE signal than the lower strength concrete block, and vice versa.

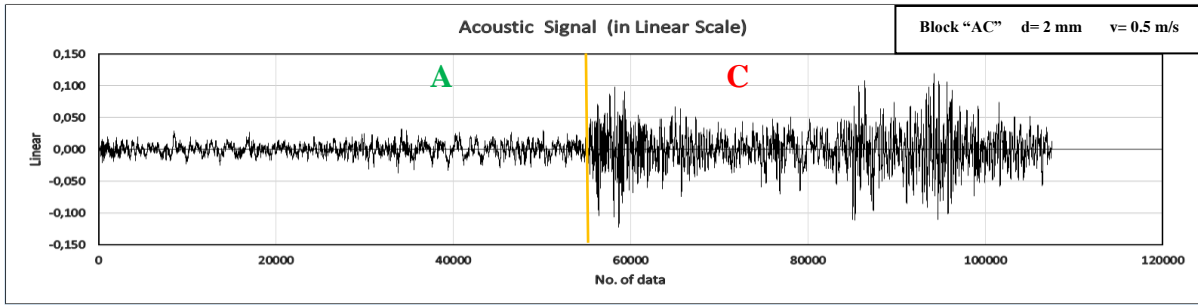


Figure 37. AE signal during cutting Block “AC” at a depth of 2 mm and a speed of 0.5 m/s.

The speed of cutting was increased from 0.5 m/s to 1.0 m/s for the same cutting depth (Figure 38), and the difference between block A and block C is still observable, both by visual observation and numerical representation, as the average peak for block A is 0.025968235 and the maximum peak is 0.06763, while the average of the peaks for block C is 0.079749792, and the maximum peak is 0.17264, which are higher than those of block A. Another thing was observed, the intensity of the AE signal also increased by increasing speed of cutting, as the maximum peak value of block C increased from 0.11951 to 0.17264 and the average peak value of block C increased from 0.058696531 to 0.079749792, and the same for block A, the maximum peak value increased from 0.03265 to 0.06763 and the average peak value increased from 0.0190422 to 0.025968235.

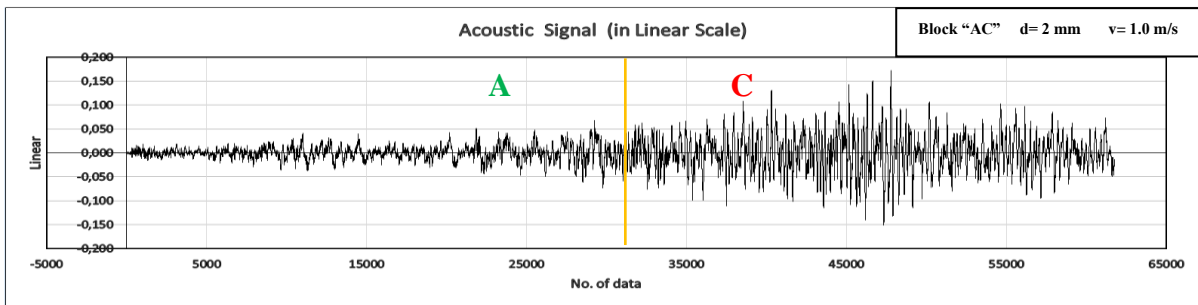


Figure 38 AE signal during cutting Block “AC” at a depth of 2 mm and a speed of 1.0 m/s.

The cutting speed was further increased from 1.0 m/s to 1.5 m/s for the same cutting depth (Figure 39), and the difference between block A and block C is still visible, both visually and numerically, as the average peak for block A is 0.030336731 and the maximum peak is 0.0639, while the average peak for block C is 0.082851702, and the maximum peak is 0.16234. And it was again observed that the intensity of the AE signal increased cutting speed was increased, as the average peak value of block C increased from 0.079749792 to 0.082851702, but the maximum peak value decreased from 0.17264 to 0.16234, For block A, the average peak value also increased from 0.025968235 to 0.03033673, and the maximum

peak value also decreased from 0.06763 to 0.0639. The issue of decreasing the maximum peaks when cutting speed is increased could be considered as an irregularity, since the average of the peaks always increases by raising the cutting speed.

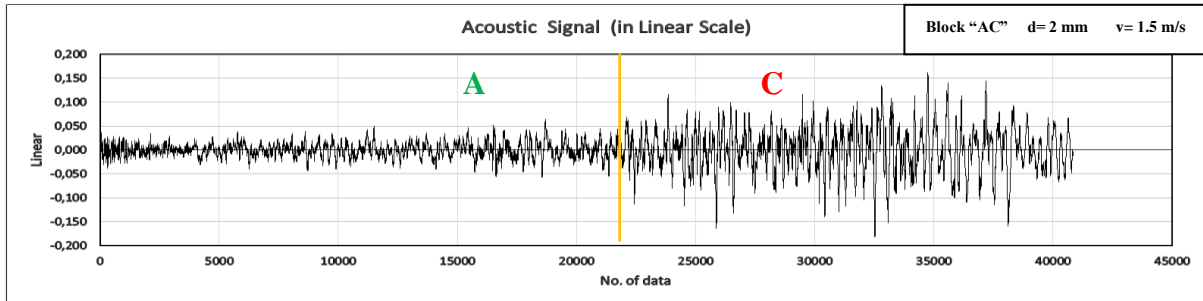


Figure 39. AE signal during cutting Block “AC” at a depth of 2 mm and a speed of 1.5 m/s.

The depth of cutting was increased from 2 mm to 5 mm for the cutting speed 0.5 m/s (Figure 40), and the difference between block A and block C still noticeable, both visually and numerically, as the average peak for block A is 0.02989283 and the maximum peak is 0.06287, while the average peak for block C is 0.095334565, and the maximum peak is 0.18568, which are higher than those of block A. And an increase in the intensity of AE was observed when cutting depth was increased, as the maximum peak value of block C increased from 0.11951 to 0.18568 and the average peak of block C increased from 0.058696531 to 0.095334565, and the same for block A, the maximum peak value increased from 0.03265 to 0.06287 and the average peak value increased from 0.0190422 to 0.02989283.

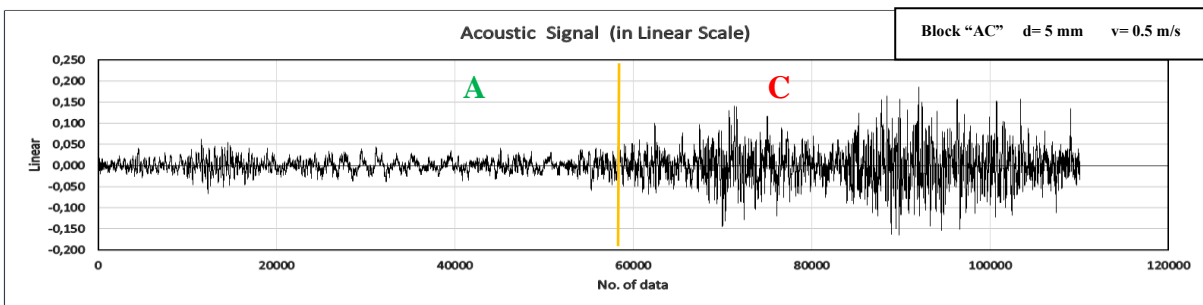


Figure 40. AE signal during cutting Block “AC” at a depth of 5 mm and a speed of 0.5 m/s.

The speed of cutting was increased from 0.5 m/s to 1.0 m/s for the same cutting depth (Figure 41), and the difference between block A and block C remains visible, visually and numerically, as the average peak for block A is 0.033489787 and the maximum peak is 0.0723, while the average of the peaks for block C is 0.157554231, and the maximum peak is 0.29607, which are higher than those of block A. And an increase in the intensity of AE was once more observed, as the maximum peak of block C increased from 0.18568 to 0.29607,

and the average peak value of block C increased from 0.095334565 to 0.157554231, and the same for block A, the average peak value increased from 0.0294467 to 0.03349 and the maximum peak value increased from 0.06287 to 0.0723, which confirm the previous results that the intensity of AE increases with increasing cutting speed.

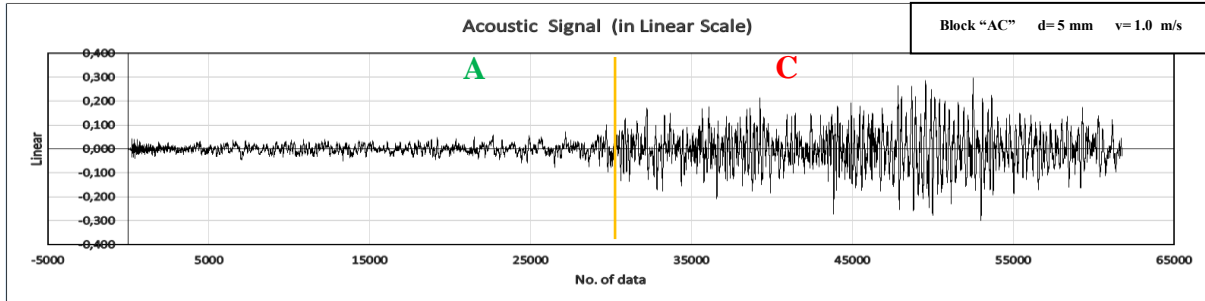


Figure 41. AE signal during cutting Block “AC” at a depth of 5 mm and a speed of 1.0 m/s.

The speed of cutting was increased from 1.0 m/s to 1.5 m/s for the same cutting depth (Figure 42), and the difference between block A and block C still observable, visually and numerically, as the average peak for block A is 0.070790392 and the maximum peak is 0.13018, while the average of the peaks for block C is 0.19152875, and the maximum peak is 0.3906, which are higher. And an increase in the intensity of the AE was again observed, as the highest peak value of block C increased from 0.29607 to 0.3906 and the average peak of block C increased from 0.157554231 to 0.19152875, and the same for block A, the average peak value increased from 0.03349 to 0.0707904 and the maximum peak value increased from 0.0723 to 0.13018, which prove the previous results that the intensity of AE increases by increasing the speed of cutting.

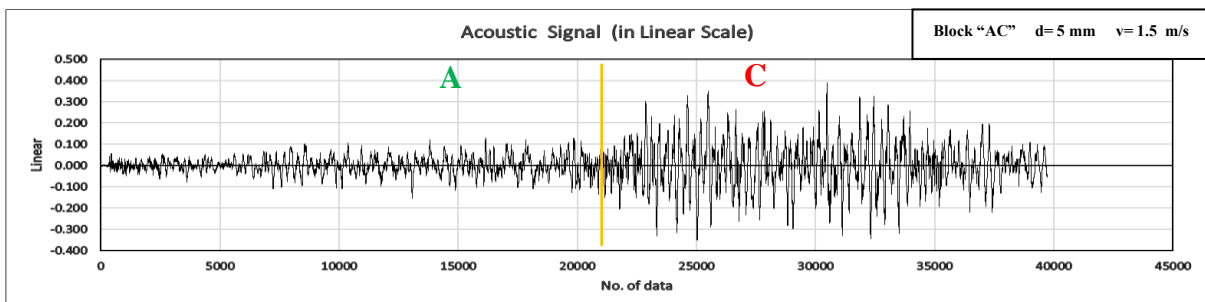


Figure 42. AE signal during cutting Block “AC” at a depth of 5 mm and a speed of 1.5 m/s.

The depth of cutting was increased from 5 mm to 10 mm for the cutting speed 0.5 m/s (Figure 43), and the difference between block A and block C remains visible, visually and numerically, as the average peak for block A is 0.054681538 and the maximum peak is 0.10284, while the average peak for block C is 0.167440851 and the maximum peak is

0.38795, which are higher. And again, an increase in the intensity of the AE was observed, as the average peak value of block C increased from 0.095334565 to 0.167440851, and the maximum peak value increased from 0.18568 to 0.38795, and the same for block A, the average peak value increased from 0.0294467 to 0.054682 and the maximum peak value increased from 0.06287 to 0.10284, which prove the same previous results, that the AE intensity increases by increasing the depth of cutting.

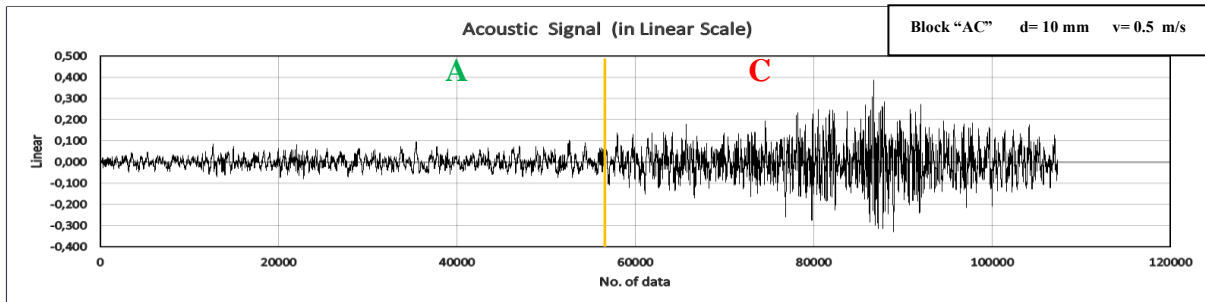


Figure 43. AE signal during cutting Block “AC” at a depth of 10 mm and a speed of 0.5 m/s.

The speed of cutting was increased from 0.5 m/s to 1.0 m/s for the same cutting depth (Figure 44), and the difference between block A and block C remains visible, visually and numerically, as the average peak for block A is 0.0878525 and the maximum peak is 0.1843, while the average of the peaks for block C is 0.225753617 and the maximum peak is 0.4225, which are higher. And again an increase in the intensity of the AE was observed when the cutting speed was increased, as the average peak value of block C increased from 0.167440851 to 0.225753617, and the maximum peak value increased from 0.38795 to 0.4225, and the same for block A, the average peak value increased from 0.054682 to 0.0878525 and the maximum peak value increased from 0.10284 to 0.1843, which demonstrate the earlier results that the intensity of AE increases with increasing the speed of cutting.

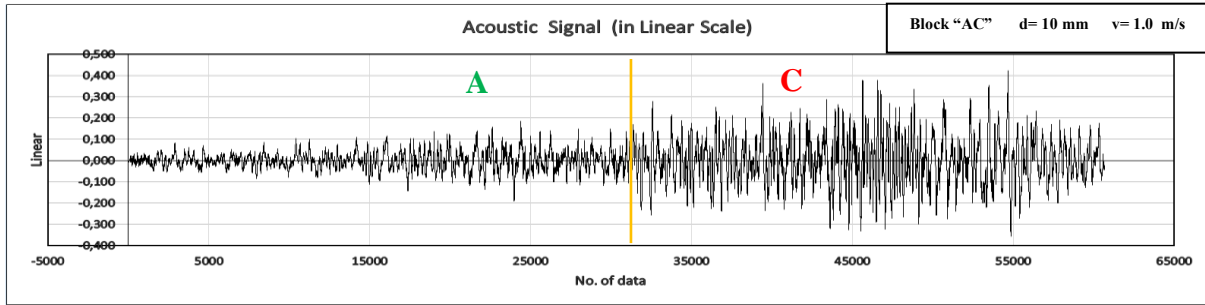


Figure 44. AE signal during cutting Block "AC" at a depth of 10 mm and a speed of 1.0 m/s.

The depth of cutting was increased from 10 mm to 15 mm for the cutting speed 0.5 m/s (Figure 45), and the difference between block A and block C remains visible, visually and numerically, as the average peak for block A is 0.054843 and the maximum peak is 0.12677, while the average peak for block C is 0.209256 and the maximum peak is 0.40102, which are higher.

It must be mentioned that it shows the opposite of the previous tests results, the AE decreased, so another trial was selected "Trial 3" and again, an increase in the intensity of the AE was noticed, as the average peak of block C increased from 0.167440851 to 0.20925551 and the maximum peak increased from 0.38795 to 0.40102, and the same for block A, the average peak value increased from 0.054682 to 0.054843 and the maximum peak value increased from 0.10284 to 0.12677, which validate the previous results, that the AE intensity increases by increasing the depth of cutting.

There is a noticeable matter, which is that the AE signal of block A (the block that is cut first) has a longer duration than that of block C (the block that is cut second), and that's more evident when the depth of cut is large, and this is due to the fact that the last part of block C did not succeed in the cutting process, as this part was completely cut off, and it flew as a large piece of concrete (see Figure 45).

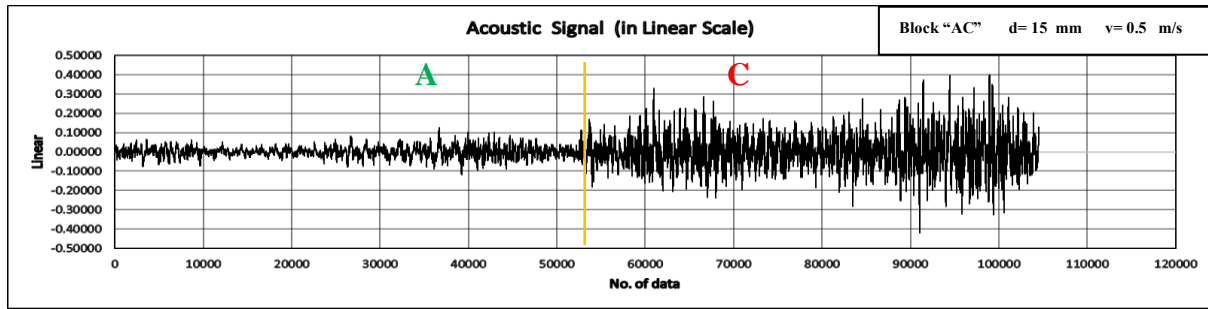


Figure 45. AE signal during cutting Block “AC” at a depth of 15 mm and a speed of 0.5 m/s.

The speed of cutting was increased from 0.5 m/s to 1.0 m/s for the same cutting depth (Figure 46), and the difference between block A and block C remains visible, visually and numerically, as the average peak for block A is 0.070814 and the maximum peak is 0.1354, while the average of the peaks for block C is 0.243057 and the maximum peak is 0.44084, which are higher than those of block A.

It must be mentioned that it shows the opposite of the previous tests results, so another trial was selected “Trial 2”, and again, an increase in the intensity of AE was observed, as the average peak value in block C increased from 0.20925551 to 0.243057, but the highest peak decreased from 0.40102 to 0.44084, and the same for block A, the average peak value increased from 0.054843 to 0.070814 and the maximum peak value increased from 0.12677 to 0.1354, which demonstrate the earlier results that the intensity of AE increases by increasing the speed of cutting.

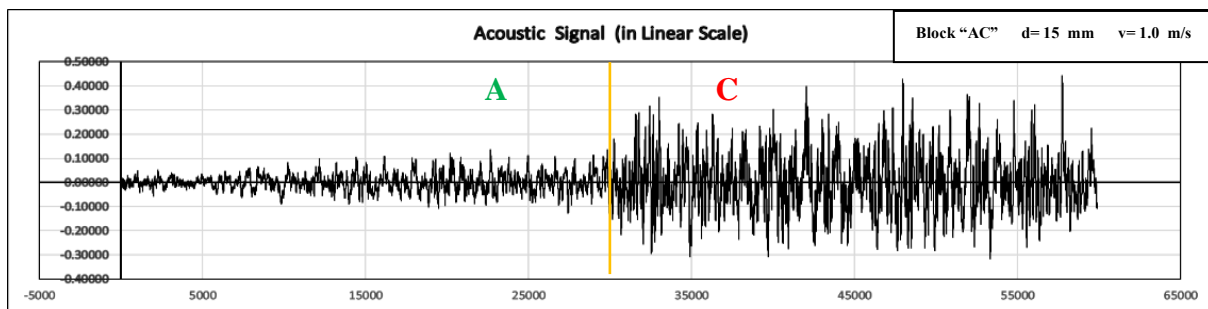


Figure 46. AE signal during cutting Block “AC” at a depth of 15 mm and a speed of 1.0 m/s.

The speed of cutting was increased from 1.0 m/s to 1.5 m/s for the same cutting depth (Figure 47), and the difference between block A and block C remains visible, visually and numerically, as the average peak for block A is 0.1044529 and the maximum peak is 0.27116, while the average peak for Block C is 0.25552, and the maximum peak is 0.50148, which are higher. The intensity of the AE increased again, as the average peak value in block C increased from 0.211593125 to 0.25552, and the maximum peak value increased from

0.37494 to 0.50148, and the same for block A, the average peak value increased from 0.070814 to 0.1044529 and the maximum peak value increased from 0.1354 to 0.27116, which again confirm the prior results that the intensity of AE increases by increasing the speed of cutting.

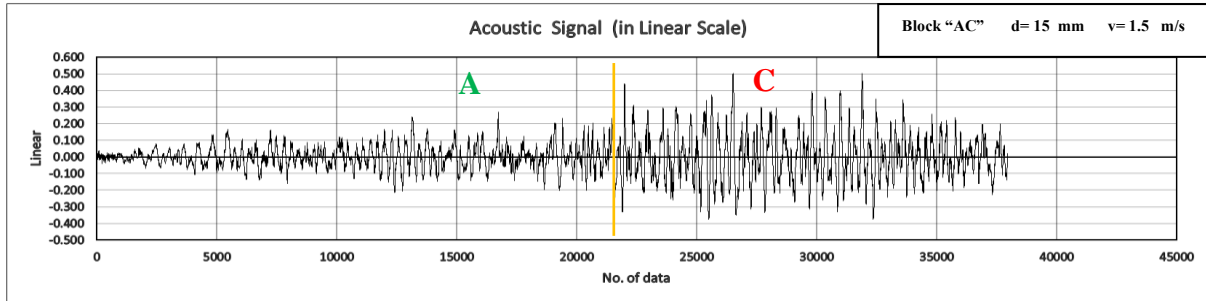


Figure 47. AE signal during cutting Block “AC” at a depth of 15 mm and a speed of 1.5 m/s.

A summary table of the numerical analysis results of AE signals of block “AC” cutting process is presented in (Table 4). For the tests which are in **Bold** font, they showed opposite results, so, other trials were chosen, and then they showed the previously stated results. The reason of that is unknown, maybe due to close proximity to microphone, since it was changeable.

Table 4. Summary of numerical results of AE signal analysis of block “AC”

| Depth (mm) | Speed (m/s) | Average Peak (A) | Maximum Peak (A) | Average Peak (C) | Maximum Peak (C) |
|------------|-------------|------------------|------------------|------------------|------------------|
| 2 | 0.5 | 0.0190422 | 0.03265 | 0.058696531 | 0.11951 |
| 2 | 1.0 | 0.025586 | 0.06763 | 0.07975 | 0.17264 |
| 2 | 1.5 | 0.0301872 | 0.0639 | 0.0828517 | 0.16234 |
| 5 | 0.5 | 0.0294467 | 0.06287 | 0.0953346 | 0.18568 |
| 5 | 1.0 | 0.03349 | 0.0723 | 0.157554 | 0.29607 |
| 5 | 1.5 | 0.0707904 | 0.13018 | 0.1915288 | 0.3906 |
| 10 | 0.5 | 0.054682 | 0.10284 | 0.167441 | 0.38795 |
| 10 | 1.0 | 0.0878525 | 0.1843 | 0.2257536 | 0.4225 |
| 15 | 0.5 | 0.054843 | 0.12677 | 0.209256 | 0.40102 |
| 15 | 1.0 | 0.070814 | 0.1354 | 0.243057 | 0.44084 |
| 15 | 1.5 | 0.1044529 | 0.27116 | 0.25552 | 0.50148 |

3.1.2 Block CB

By looking at the AE signal resulted from cutting of “block CB” (Figure 48), it is possible to differentiate between block C and block B by visual observation, as the AE signal of block B has lower peaks than block C. but numerical analyses has been implemented to precisely differentiate between block C and block B, and it was found that the average value of peaks of block C is 0.0514228, while the average peak value of block B is 0.03391898, which is lower than that of block C, and the maximum peak of block C is 0.0994, while the maximum peak For block B 0.0786, which is also lower than that of block C, Those calculation were made based on 100 peak per cutting test. This prove the previous results for block “AC” that this difference is due to the fact that the higher strength concrete block when cut emits a AE signal of higher intensity than the lower strength concrete block, and vice versa.

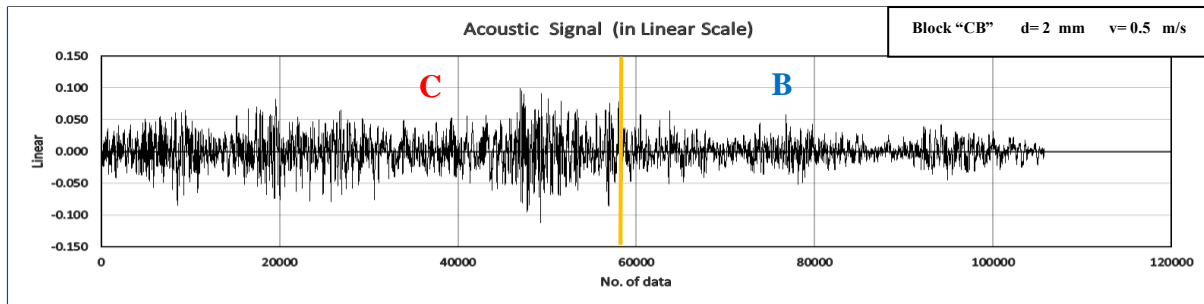


Figure 48. AE signal during cutting Block “CB” at a depth of 2 mm and a speed of 0.5 m/s.

The speed of cutting was increased from 0.5 m/s to 1.0 m/s for the same cutting depth (Figure 49), and the difference between block C and block B is still observable, both by visual observation and Numerical representation, as the average peak for Block C is 0.0820686 and the maximum peak is 0.1887, while the average of the peaks for Block B is 0.038467959, and the maximum peak is 0.09675. Another thing was observed, the intensity of the AE signal also increased by increasing the speed of cutting, as the average peak value of block C increased from 0.0514228 to 0.0820686 and the maximum peak value of block C increased from 0.0994 to 0.1887, and the same for block B, the average peak value increased from 0.03391898 to 0.038467959 and the maximum peak value increased from 0.0786 to 0.09675.

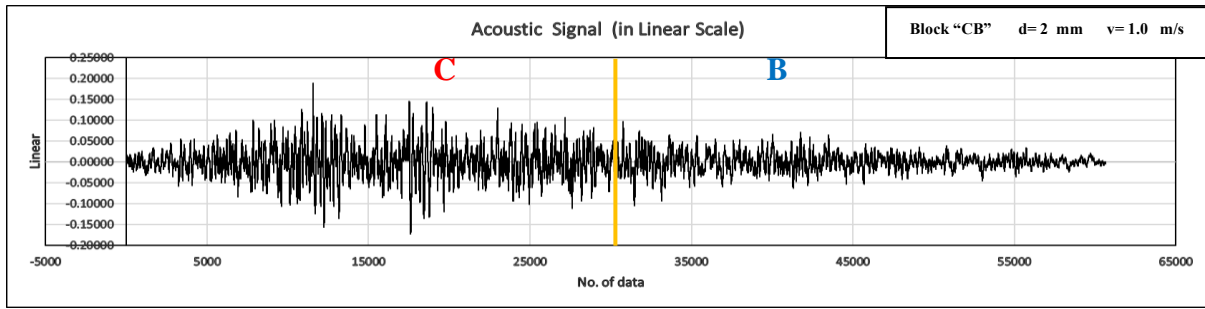


Figure 49. AE signal during cutting Block "CB" at a depth of 2 mm and a speed of 1.0 m/s.

The speed of cutting was increased from 1.0 m/s to 1.5 m/s for the same cutting depth (Figure 50), and the difference between block C and block B is still observable, visually and numerically, as the average peak for block C is 0.088994231 and the maximum peak is 0.16901, while the average peak value for block B is 0.052289149, and the maximum peak is 0.10028, which are lower than those of C. And again, the intensity of the AE signal increased by increasing speed of cutting, as the average peak value of block C increased from 0.0820686 to 0.088994231 but the maximum peak value decreased from 0.1887 to 0.16901, and the same for block B, the average peak value increased from 0.038467959 to 0.052289149 but the maximum peak value increased from 0.09675 to 0.10028.

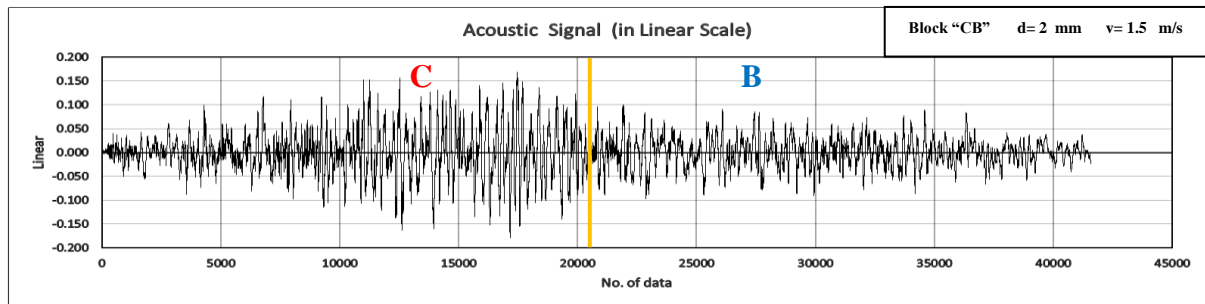


Figure 50. AE signal during cutting Block "CB" at a depth of 2 mm and a speed of 1.5 m/s.

The depth of cutting was increased from 2 mm to 5 mm for the cutting speed 0.5 m/s (Figure 51), and the difference between block C and block B remains visible, visually and numerically, as the average peak for block C is 0.107274706 and the maximum peak is 0.20793, while the average peak for block B is 0.055621042, and the maximum peak is 0.14232, which are lower than those of block C. And an increase in the intensity of the AE was observed when the cutting depth was increased, as the average peak value of block C increased from 0.0514228 to 0.107274706p, and the maximum peak value increased from 0.0994 to 0.20793, and the same for block B, the average peak value increased from 0.03391898 to 0.055621042 and the maximum peak value increased from 0.0786 to 0.14232,

which prove the same previous results, that the AE intensity increases by increasing the depth of cutting.

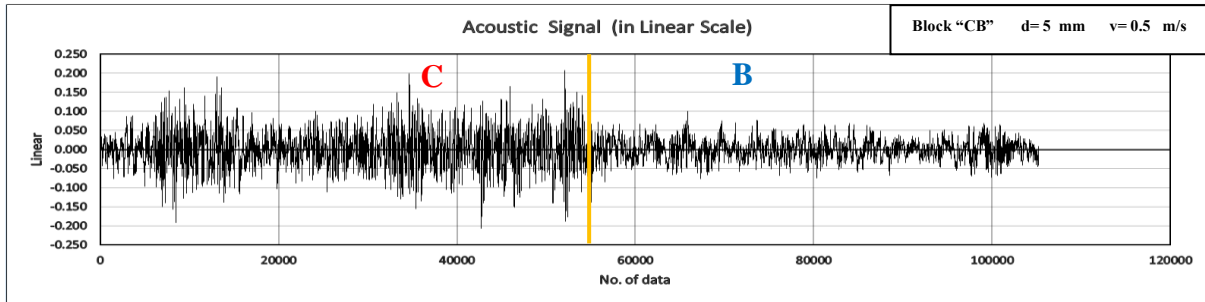


Figure 51. AE signal during cutting Block “CB” at a depth of 5 mm and a speed of 0.5 m/s.

The speed of cutting was increased from 0.5 m/s to 1.0 m/s for the same cutting depth (Figure 52), and the difference between block C and block B is still observable, both by visual observation and Numerical representation, as the average peak value of block C is 0.133614615 and the maximum peak is 0.22567, while the average of the peaks of block B is 0.07252617, and the maximum peak is 0.15816, which are lower than those of block C. And an increase in the AE intensity was once more noticed when speed of cutting was increased, as the average peak value of block C increased from 0.107274706 to 0.133614615 and the maximum peak increased from 0.20793 to 0.22567, and the same for block B, the average peak increased from 0.055621042 to 0.07252617 and the maximum peak value increased from 0.14232 to 0.15816.

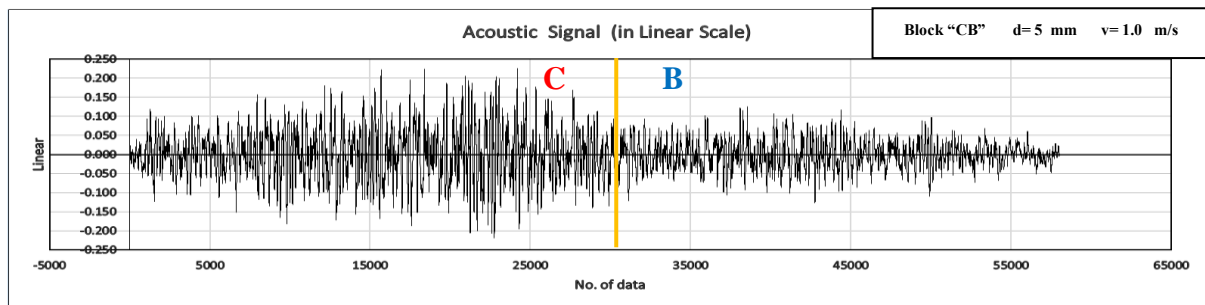


Figure 52. AE signal during cutting Block “CB” at a depth of 5 mm and a speed of 1.0 m/s.

The speed of cutting was increased from 1.0 m/s to 1.5 m/s for the same cutting depth (Figure 53), and the difference between block C and block B remains noticeable, visually and numerically, as the average peak for block C is 0.158372885 and the maximum peak is 0.29138, while the average of the peaks for block B is 0.107299792, and the maximum peak is 0.18996, which are lower than those of block C. And again, the intensity of the AE signal increased by increasing speed of cutting, as the average peak value of block C increased from

0.133614615 to 0.158372885 and the maximum peak value of block C increased from 0.22567 to 0.29138, and the same for block B, the average peak value increased from 0.07252617 to 0.107299792 and the maximum peak value increased from 0.15816 to 0.18996, which demonstrate the previous results that the AE intensity increases by increasing speed of cutting.

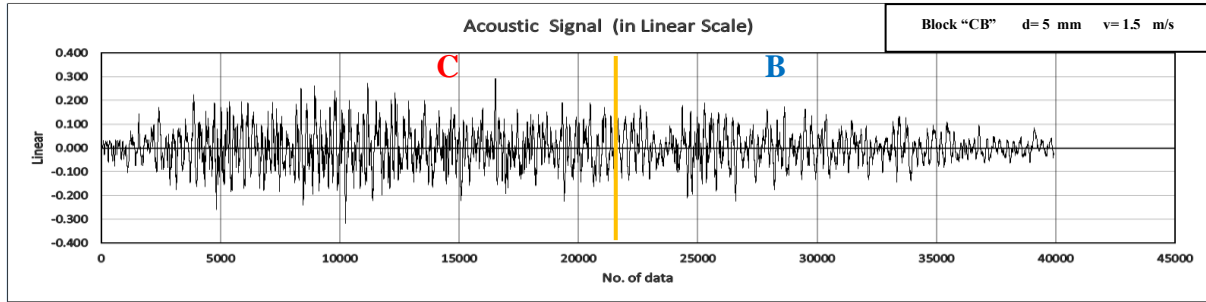


Figure 53. AE signal during cutting Block “CB” at a depth of 5 mm and a speed of 1.5 m/s.

The depth of cutting was increased from 5 mm to 10 mm for the cutting speed 0.5 m/s (Figure 54), and the difference between Block C and block B remains noticeable, both by visually and numerically, as the average peak for block C is 0.123439 and the maximum peak is 0.30039, while the average peak for block B is 0.0867978, and the maximum peak is 0.16593. And again, an increase in the intensity of the AE was noticed when the cutting depth was increased, as the average peak value of block C increased from 0.107274706 to 0.123439, and the maximum peak value increased from 0.20793 to 0.30039, and the same for block B, the average peak value increased from 0.055621042 to 0.0867978 and the maximum peak value increased from 0.14232 to 0.16593, which prove the previous results, that the AE intensity increases by increasing the depth of cutting.

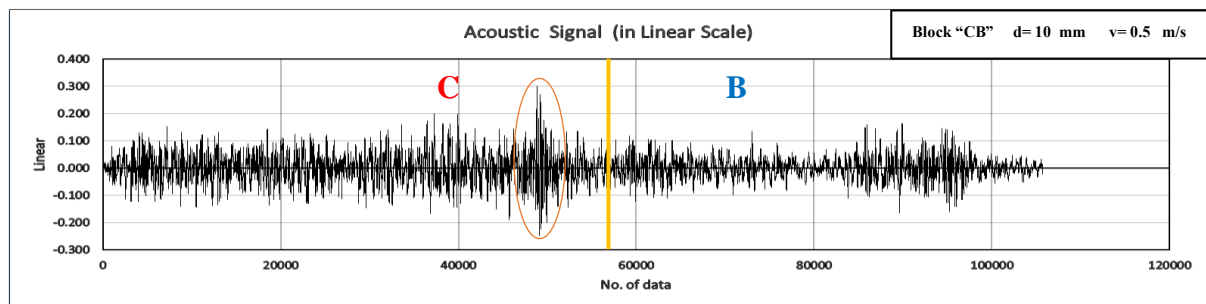


Figure 54. AE signal during cutting Block “CB” at a depth of 10 mm and a speed of 0.5 m/s.

The speed of cutting was increased from 0.5 m/s to 1.0 m/s for the same cutting depth (Figure 55), and the difference between block C and block B remains observable, visually and numerically, as the average peak for block C is 0.129769808 and the maximum peak is

0.23272, while the average of the peaks for block B is 0.107446667, and the maximum peak is 0.20608. And an increase in the AE intensity was once more noticed when speed of cutting was increased, as the average peak value of block C increased from 0.123439 to 0.129769808, but the maximum peak value decreased from 0.30039 to 0.23272; due to an irregular peak visible in the previous Cut, but for block B, the average peak value increased from 0.0867978 to 0.107446667 and the maximum peak value increased from 0.16593 to 0.20608, which confirm the earlier results that the AE intensity increases by increasing speed of cutting.

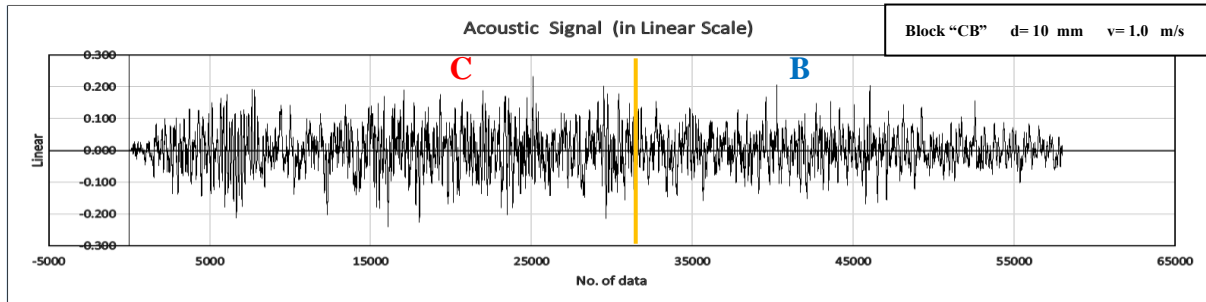


Figure 55. AE signal during cutting Block "CB" at a depth of 10 mm and a speed of 1.0 m/s.

The speed of cutting was increased from 1.0 m/s to 1.5 m/s for the same cutting depth (Figure 56), and the difference between block C and block B remains noticeable, visually and numerically, as the average peak for block C is 0.193634231 and the maximum peak is 0.32471, while the average of the peaks for block B is 0.137952083, and the maximum peak is 0.27627, which are lower than those of block C. It must be mentioned that it shows the opposite of the previous tests results, so another trial was selected, and again, the intensity of the AE signal increased by increasing speed of cutting, as the average peak value of block C increased from 0.129769808 to 0.193634231, and the maximum peak value increased from 0.23272 to 0.32471, and the same for block B, the average peak value increased from 0.107446667 to 0.137952083 and the maximum peak value increased from 0.20608 to 0.27627, which confirm the earlier results that the intensity of AE increases by increasing the cutting speed (Figure 56).

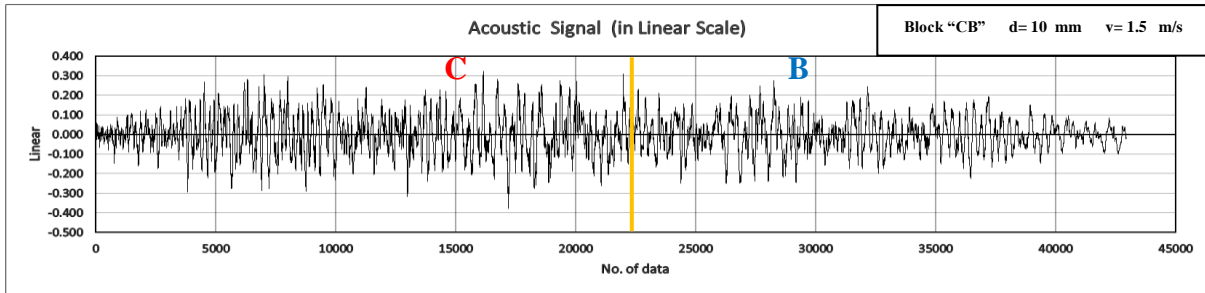


Figure 56. AE signal during cutting Block "CB" at a depth of 10 mm and a speed of 1.5 m/s.

The depth of cutting was increased from 10 mm to 15 mm for the cutting speed 0.5 m/s (Figure 57), and the difference between block C and block B remains visible, both visually and numerically, as the average peak for block C is 0.226955962 and the maximum peak is 0.35889, while the average peak for block B is 0.125261875, and the maximum peak is 0.26285, which are lower than those of block C. And an increase in the intensity of the AE was once more observed when the cutting depth was increased, as the average peak value of block C increased from 0.123439 to 0.226955962, and the maximum peak value increased from 0.30039 to 0.35889 although there is an irregular high peak for the first. For block B, the average peak value also increased from 0.0867978 to 0.125261875 and the maximum peak value increased from 0.16593 to 0.26285, which prove the previous results, that the AE intensity increases by increasing the depth of cutting.

As in block AC, it was noticed again in block CB, that the AE signal of block C (the block that is cut first) has a longer duration than that of block B (the block that is cut second), this is noticeable visually and numerically, as the number of data for block C is 57000 but the number of data for block B is 50525, which is lower. This is more visible when the depth of cut is large. This is due to the fact that the last part of block B the cutting process was unsuccessful, as the part was completely cut off, and it flew as a large fragment (see Figure 57).

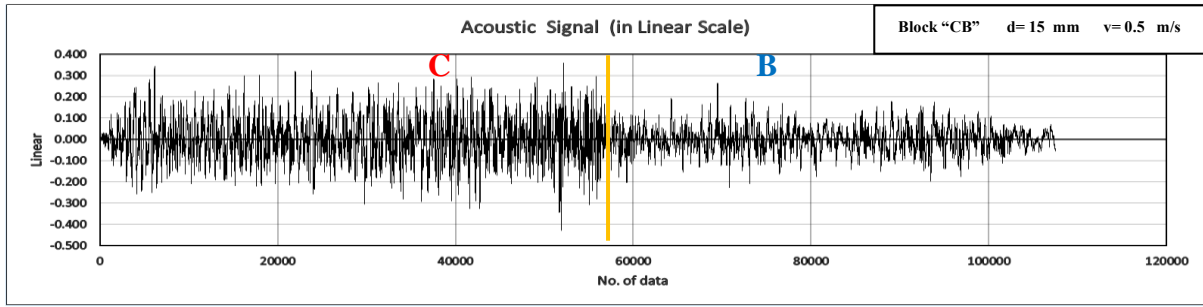


Figure 57. AE signal during cutting Block “CB” at a depth of 15 mm and a speed of 0.5 m/s.

The speed of cutting was increased from 0.5 m/s to 1.0 m/s for the same cutting depth (Figure 58), and the difference between block C and block B remains observable, visually and numerically, as the average peak for block C is 0.241865098 and the maximum peak is 0.50233, while the average peak for block B is 0.141610408 and the maximum peak is 0.27529, which are lower than those of block C. And an increase in the AE intensity was again noticed when speed of cutting was increased, as the average peak value of block C increased from 0.226955962 to 0.241865098, and the maximum peak value increased from 0.35889 to 0.50233, and the same for block B, the average peak value increased from 0.125261875 to 0.141610408 and the maximum peak value increased from 0.26285 to 0.27529.

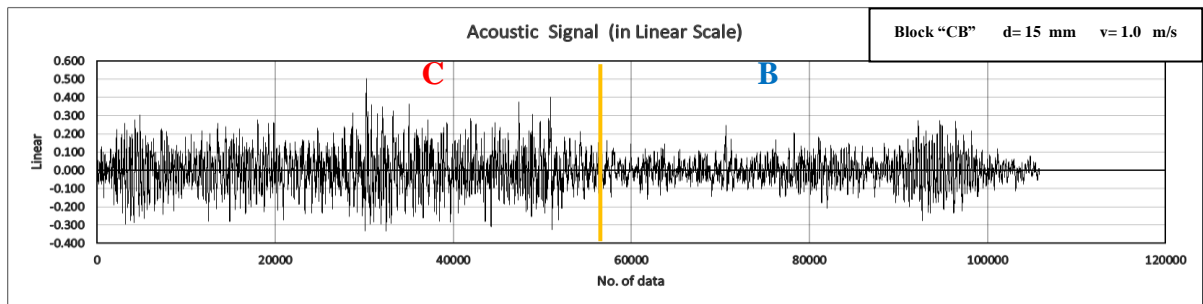


Figure 58. AE signal during cutting Block “CB” at a depth of 15 mm and a speed of 1.0 m/s.

The speed of cutting was increased from 1.0 m/s to 1.5 m/s for the same cutting depth (Figure 59), and the difference between block C and block B remains noticeable, visually and numerically, as the average peak for block C is 0.314985686 and the maximum peak is 0.70411, while the average peak for block B is 0.246665102, and the maximum peak is 0.4764. And again, the intensity of the AE signal increased when speed of cutting was increased, as the average peak value of block C increased from 0.241865098 to 0.314985686, and the maximum peak value increased from 0.50233 to 0.70411, and the same for block B, the average peak value increased from 0.141610408 to 0.246665102 and the maximum peak value increased from 0.27529 to 0.4764.

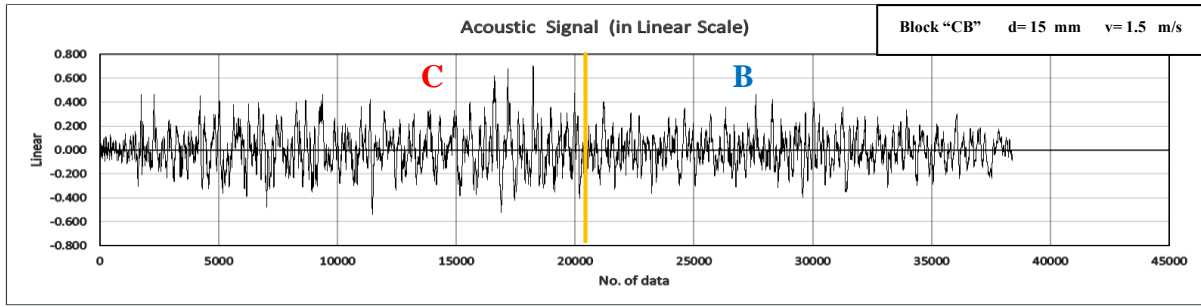


Figure 59. AE signal during cutting Block “CB” at a depth of 15 mm and a speed of 1.5 m/s.

A summary table of the numerical analysis results of AE signals of block “CB” cutting process is presented (Table 5). For the test which is in **Bold** font, it showed opposite result, so, other trial was chosen, and then it showed the previously stated results. The reason of that is unknown, maybe due to proximity to microphone, since it was changeable.

Table 5. Summary of numerical results of AE signal analysis of block “CB”.

| Depth (mm) | Speed (m/s) | Average Peak (C) | Maximum Peak (C) | Average Peak (B) | Maximum Peak (B) |
|------------|-------------|--------------------|------------------|--------------------|------------------|
| 2 | 0.5 | 0.0514228 | 0.0994 | 0.03391898 | 0.0786 |
| 2 | 1.0 | 0.0820686 | 0.1887 | 0.038467959 | 0.09675 |
| 2 | 1.5 | 0.088994231 | 0.16901 | 0.052289149 | 0.10028 |
| 5 | 0.5 | 0.107274706 | 0.20793 | 0.055621042 | 0.14232 |
| 5 | 1.0 | 0.133614615 | 0.22567 | 0.07252617 | 0.15816 |
| 5 | 1.5 | 0.158372885 | 0.29138 | 0.107299792 | 0.18996 |
| 10 | 0.5 | 0.123439 | 0.30039 | 0.0867978 | 0.16593 |
| 10 | 1.0 | 0.129769808 | 0.23272 | 0.107446667 | 0.20608 |
| 10 | 1.5 | 0.193634231 | 0.32471 | 0.137952083 | 0.27627 |
| 15 | 0.5 | 0.226955962 | 0.35889 | 0.125261875 | 0.26285 |
| 15 | 1.0 | 0.241865098 | 0.50233 | 0.141610408 | 0.27529 |
| 15 | 1.5 | 0.314985686 | 0.70411 | 0.246665102 | 0.4764 |

3.2 FFT Analysis

Twelve FFT frequency spectrums of AE signals recorded at low gain settings (which were mentioned earlier in the previous section) during cutting tests on concrete block CB, with

different cutting parameters: different depths and different speeds, were selected for analysis, discussion and presentation.

Looking at the FFT frequency spectrum of the AE signal recorded while cutting at a depth of 2 mm and a speed of 0.5 m/s (Figure 60), it is possible to differentiate between Block C and Block B, as the highest peak of Block C is 0.00915, while the highest peak of Block B is 0.00472, which is lower than that of block C, and the average of highest peaks of block C is approximately 0.00492, while the high peaks average of block B is approximately 0.00303, which is lower than that of block C. This average is an approximation and is calculated based on the ten highest peaks of each block.

Following the footsteps of (Crosland, et al., 2009; Williams & Hagan, 2006), the major dominant frequencies (MDFs) were analyzed and the results were assessed. The highest four MDFs for block C are 102.5, 234.4, 480.5, 887.7, which are the highest four peaks, and the highest peak is located at the second position at 234.4 Hz. The highest ten MDFs lie between approximately 100-1100 Hz. As for the block B, the Highest four MDFs are 331.1, 785.2, 793.9, 881.8, and the highest peak is located at the second position at 785.2 Hz. The highest ten MDFs lie between approximately 20-1100 Hz,

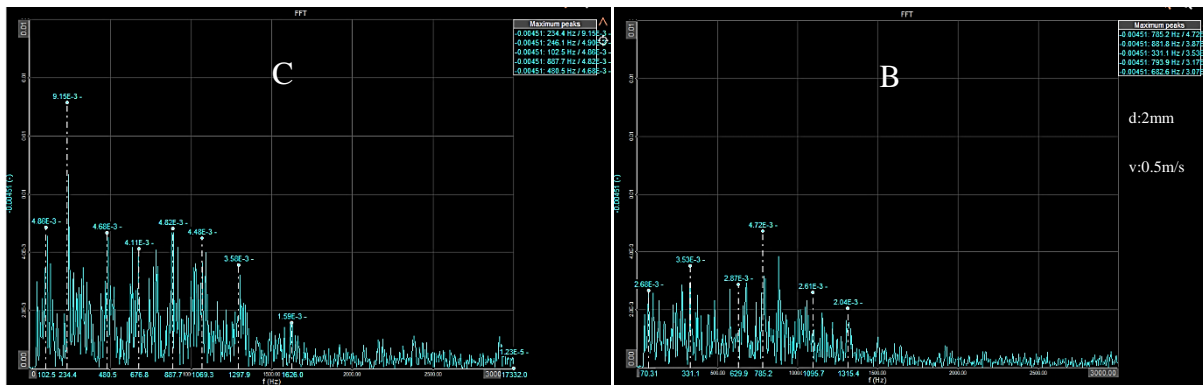


Figure 60. FFT of AE signal during cutting Block “CB” at a depth of 2 mm and a speed of 0.5 m/s.

The cutting speed was increased to 1.0 m/s for the same cutting depth (Figure 61), and it is still possible to differentiate between block C and block B, as the highest peak of block C has a value of 0.0191, while the highest peak of block B has a value of 0.0113, which is less than that of block C, and the average of high peaks of block C is about 0.01215, while the average of high peaks of block B is about 0.0071, which is lower than that of block C. These averages are approximate and are calculated based on the ten highest peaks of each block.

An increase in the magnitude of FFT was observed when the cutting speed increased, as the average of high peaks of block C increased from 0.00492 to 0.01215 and the highest peak increased from 0.00915 to 0.0191, as for block B, the average of the high peaks increased from 0.00303 to 0.0071 and the highest peak increased from 0.00472 to 0.0113.

The highest four MDFs for block C, are 316.4, 521.5, 632.8, 984.4, 650.4, and the highest peak is the second at 521.5 Hz. The highest ten MDFs lie between approximately 100-1000 Hz. As for the block B, the Highest four MDFs are 650.4, 767.6, 978.5, 996.1, and the highest peak is the fourth at 996.1 Hz. The highest ten MDFs lie between approximately 20-1300 Hz.

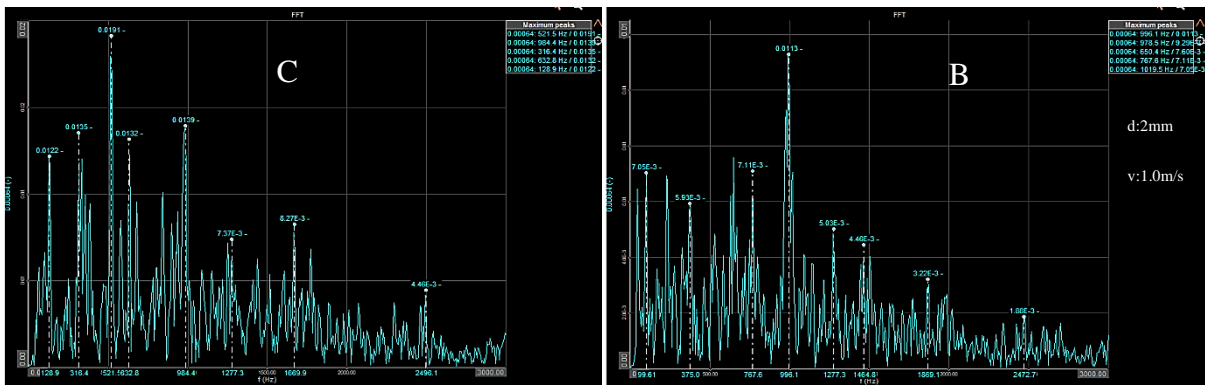


Figure 61. FFT of AE signal during cutting Block “CB” at a depth of 2 mm and a speed of 1.0 m/s.

The cutting speed was increased to 1.5 m/s for the same cutting depth (Figure 62), and it is still possible to differentiate between block C and block B, as the average of high peaks of block C has a value of 0.01408 approximately, and the highest peak is 0.0231, while the average of high peaks of block B is 0.00955 approximately and the highest peak is 0.0141, which are lower than those of block C. These averages are approximations and are calculated based on the ten highest peaks of each block.

An increase in the magnitude of FFT was observed when the cutting speed was increased, as the average of high peaks of block C increased from 0.01215 to 0.01408 and the highest peak increased from 0.0191 to 0.0231, as for block B, the average of the high peaks increased from 0.0071 to 0.00955 and the highest peak increased from 0.0113 to 0.0141.

The highest four MDFs for block C are 580.1, 632.8, 861.3, 884.8, and the highest peak is the second at 632,8 Hz. The highest ten MDFs lie between approximately 200-1100 Hz. As for

the block B, the Highest four MDFs are 580.1, 638.7, 650.4, 873.0, and the highest peak is the second at 638,7 Hz. The highest ten MDFs lie between approximately 50-1150 Hz.

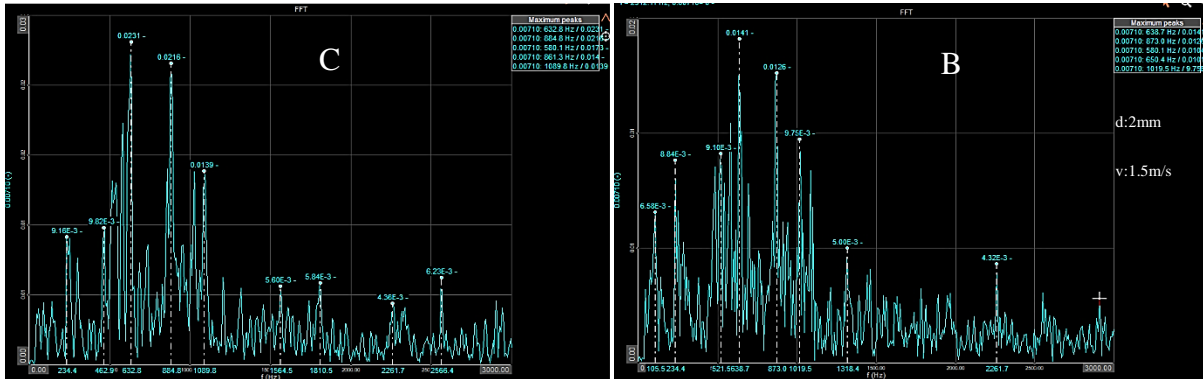


Figure 62. FFT of AE signal during cutting Block “CB” at a depth of 2 mm and a speed of 1.5 m/s.

The cutting depth was increased to 5 mm for a cutting speed of 0.5 m/s (Figure 63), and it is still possible to differentiate between block C and block B, as the average of high peaks of block C has a value of 0.01112 approximately, and the highest peak is 0.0169, while the average of high peaks of block B is 0.00585 approximately and the highest peak is 0.0105, which are lower than that of block C. These averages are approximations and are calculated based on the ten highest peaks of each block.

An increase in the magnitude of FFT was observed when the cutting speed increased, as the average of high peaks of block C increased from 0.00492 to 0.01112 and the highest peak increased from 0.00915 to 0.0169, as for block B, the average of the high peaks increased from 0.00303 to 0.00585 and the highest peak increased from 0.00472 to 0.0105.

The highest four MDFs for block C are 331.1, 629.9, 997.8, 1092.8, and the highest peak is the fourth at 1092.8 Hz. The highest ten MDFs lie between approximately 20-1200 Hz. As for

the block B, the Highest four MDFs are 45.88, 272.5, 334.0, 1018.6, and the highest peak is the first at 45.88 Hz. The highest ten MDFs lie between approximately 20-1050 Hz.

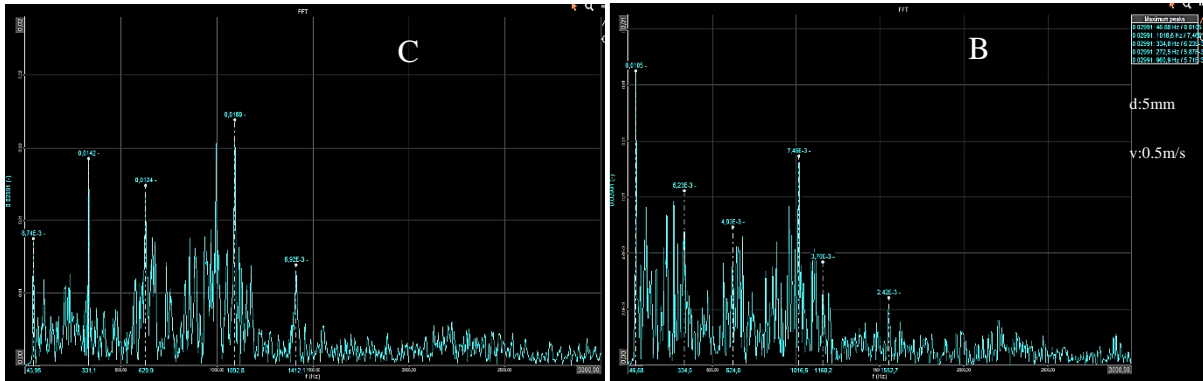


Figure 63. FFT of AE signal during cutting Block “CB” at a depth of 5 mm and a speed of 0.5 m/s.

The cutting speed was increased to 1.0 m/s for the same cutting depth (Figure 64), and it is still possible to differentiate between block C and block B, as the average of high peaks of block C has a value of 00 approximately, and the highest peak is 00, while the average of high peaks of block B is 00 approximately and the highest peak is 00, which are lower than those of block C. These averages are approximations and are calculated based on the ten highest peaks of each block.

An increase in the magnitude of FFT was observed when the cutting speed was increased, as the average of high peaks of block C increased from 0.01112 to 0.0208 and the highest peak increased from 0.0169 to 0.0316, as for block B, the average of the high peaks increased from 0.00585 to 0.0101 and the highest peak increased from 0.0105 to 0.0169.

The highest four MDFs for block C are 582.5, 656.3, 990.2, and 1066.4, and the highest peak is the third at 990.2 Hz. The highest ten MDFs lie between approximately 300-1200 Hz. As for the block B, the Highest four MDFs are 345.7, 638.7, 1019.5, and 1113.3, and the highest

peak is the second at 638.7 Hz. The highest ten MDFs lie between approximately 200-1200 Hz.

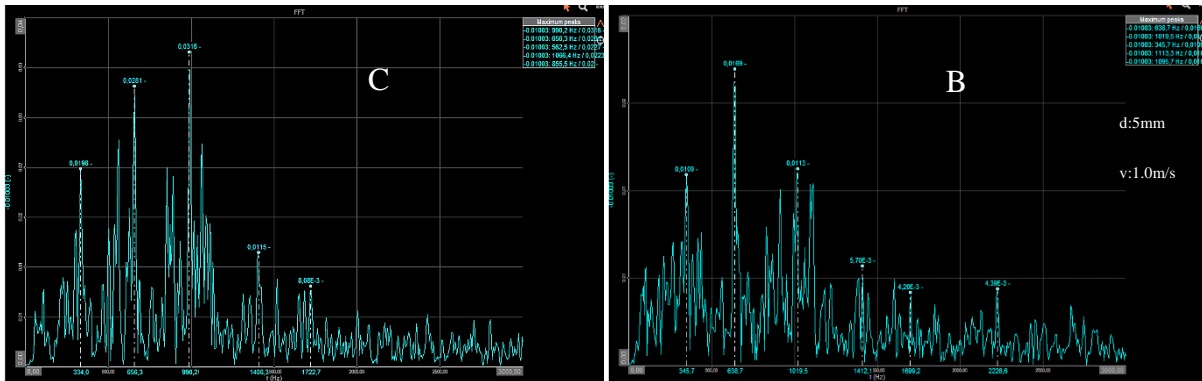


Figure 64. FFT of AE signal during cutting Block “CB” at a depth of 5 mm and a speed of 1.0 m/s.

The cutting speed was increased to 1.5 m/s for the same cutting depth (Figure 65), and it is still possible to differentiate between block C and block B, as the average of high peaks of block C has a value of 0.0256 approximately, and the highest peak is 0.0518, while the average of high peaks of block B is 0.0184 approximately and the highest peak is 0.0445, which are lower than those of block C. These averages are approximations and are calculated based on the ten highest peaks of each block.

An increase in the magnitude of FFT was observed when the cutting speed was increased, as the average of high peaks of block C increased from 0.0208 to 0.0256 and the highest peak increased from 0.0316 to 0.0518, as for block B, the average of the high peaks increased from 0.0101 to 0.0184 and the highest peak increased from 0.0169 to 0.0445.

The highest four MDFs for block C are 527.3, 679.7, 937.5, and 1160.2, and the highest peak is the second at 679.7 Hz. The highest ten MDFs lie between 200-2200 Hz. As for the block

B, the Highest four MDFs are 328.1, 632.8, 679.7, and 972.7, and the highest peak is the third at 679.7 Hz. The highest ten MDFs lie between 100-1000 Hz.

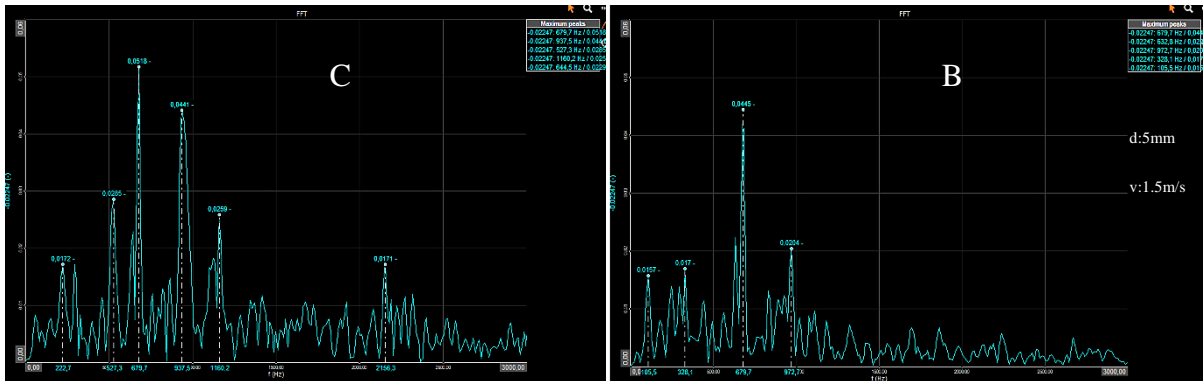


Figure 65 . FFT of AE signal during cutting Block “CB” at a depth of 5 mm and a speed of 1.5 m/s.

The cutting depth was increased to 10 mm for the cutting speed 0.5 m/s (Figure 66), and it is still possible to differentiate between block C and block B, as the average of high peaks of block C has a value of 0.01343 approximately, and the highest peak is 0.0175, while the average of high peaks of block B is 0.00794 approximately and the highest peak is 0.0121, which are lower than those of block C. These averages are approximations and are calculated based on the ten highest peaks of each block.

An increase in the magnitude of FFT was observed when the cutting speed was increased, as the average of high peaks of block C increased from 0.01112 to 0.01343 and the highest peak increased from 0.0169 to 0.0175, as for block B, the average of the high peaks increased from 0.00585 to 0.00794 and the highest peak increased from 0.0105 to 0.0121.

The highest four MDFs for block C are 208.0, 219.7, 237.3, and 632.8, and the highest peak is the first at 208.0 Hz. The highest ten MDFs lie between approximately 200-1100 Hz. As for

the block B, the Highest four MDFs are 213.9, 331.1, 1013.7, and 1028.3, and the highest peak is the first at 213.9 Hz. The highest ten MDFs lie between approximately 40-1100 Hz.

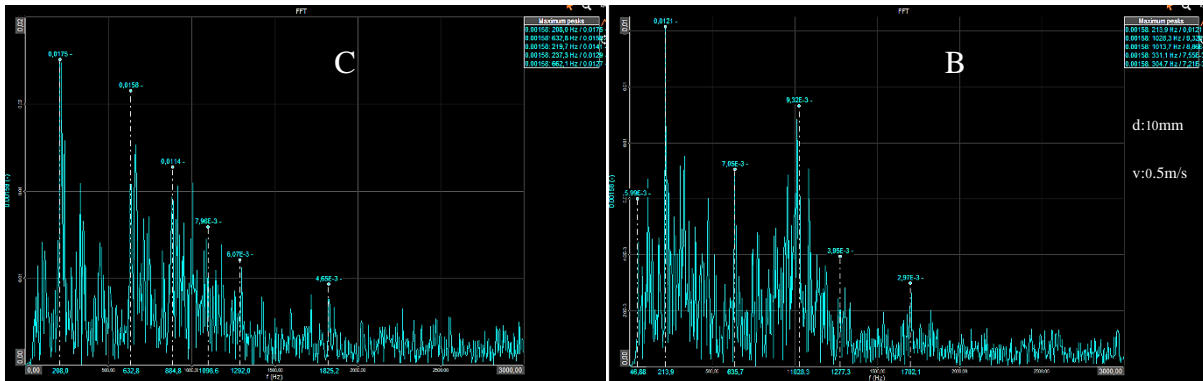


Figure 66. FFT of AE signal during cutting Block “CB” at a depth of 10 mm and a speed of 0.5 m/s.

The cutting speed was increased to 1.0 m/s for the same cutting depth (Figure 67), and it is still possible to differentiate between block C and block B, as the average of high peaks of block C has a value of 0.01801 approximately, and the highest peak is 0.0233, while the average of high peaks of block B is 0.01388 approximately and the highest peak is 0.0197, which are lower than those of block C. These averages are approximations and are calculated based on the ten highest peaks of each block.

An increase in the magnitude of FFT was observed when the cutting speed was increased, as the average of high peaks of block C increased from 0.01343 to 0.01801 and the highest peak increased from 0.0175 to 0.0233, as for block B, the average of the high peaks increased from 0.00794 to 0.01388 and the highest peak increased from 0.0121 to 0.0197.

The highest four MDFs for block C are 99.61, 582.5, 996.1, and 1084.0, and the highest peak is the first at 99.61 Hz. The highest ten MDFs lie between 50-1150 Hz. As for the block B, the

Highest four MDFs are 234.4, 638.7, 1025.4, and 1101.8, and the highest peak is the second at 638.7 Hz. The highest ten MDFs lie between approximately 150-1150 Hz.

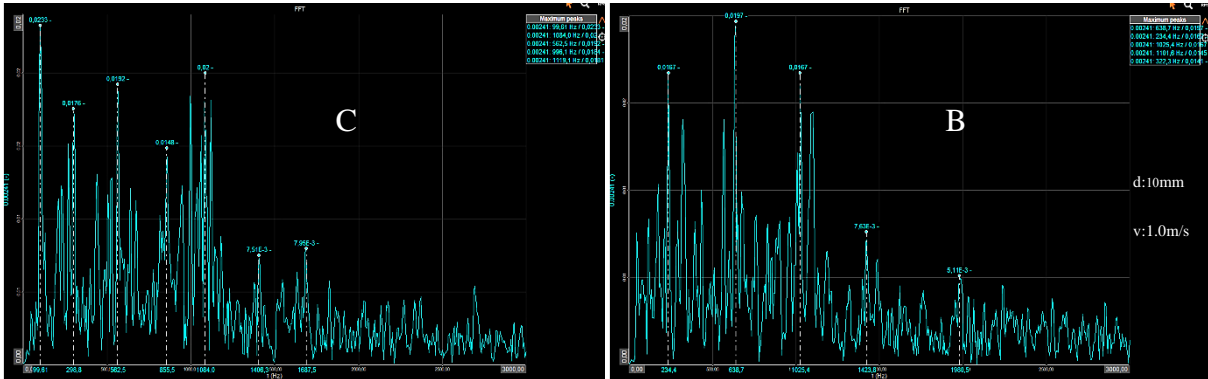


Figure 67. FFT of AE signal during cutting Block “CB” at a depth of 10 mm and a speed of 1.0 m/s.

The cutting speed was increased to 1.5 m/s for the same cutting depth (Figure 68), and it is still possible to differentiate between block C and block B, as the average of high peaks of block C has a value of 0.02804 approximately, and the highest peak is 0.0506, while the average of high peaks of block B is 0.01907 approximately and the highest peak is 0.0394, which are lower than those of block C.

An increase in the magnitude of FFT was observed when the cutting speed was increased, as the average of high peaks of block C increased from 0.01801 to 0.02804 and the highest peak increased from 0.0233 to 0.0506, as for block B, the average of the high peaks increased from 0.01388 to 0.01907 and the highest peak increased from 0.0197 to 0.0394.

The highest four MDFs for block C are 328.1, 691.4, 925.8, and 984.4, and the highest peak is the second at 691.4 Hz. The highest ten MDFs lie between 20-1150 Hz. As for the block B,

the Highest four MDFs are 46.88, 632.8, 668.0, and 972.7, and the highest peak is the second at 632.8 Hz. The highest ten MDFs lie between 300-1100 Hz.

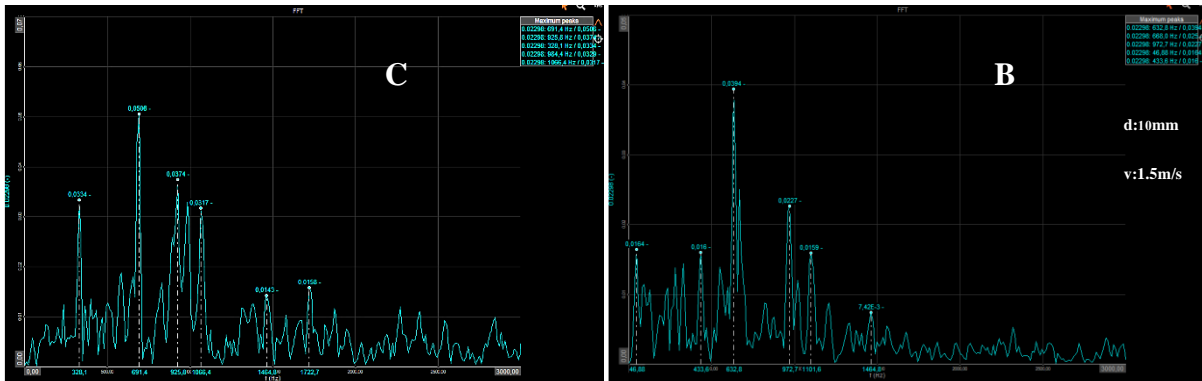


Figure 68. FFT of AE signal during cutting Block “CB” at a depth of 10 mm and a speed of 1.5 m/s.

The cutting depth was increased to 15 mm for the same speed 0.5 m/s (Figure 69), and it is still possible to differentiate between block C and block B, as the average of high peaks of block C has a value of 0.02455 approximately, and the highest peak is 0.0391, while the average of high peaks of block B is 0.01421 approximately and the highest peak is 0.0336, which are lower than those of block C. These averages are approximations and are calculated based on the ten highest peaks of each block.

An increase in the magnitude of FFT was observed when the cutting speed was increased, as the average of high peaks of block C increased from 0.01343 to 0.02455 and the highest peak increased from 0.0175 to 0.0391, as for block B, the average of the high peaks increased from 0.00794 to 0.01421 and the highest peak increased from 0.0121 to 0.0336.

The highest four MDFs for block C are 210.9, 231.4, 325.1, and 917.0, and the highest peak is the second at 210.9 Hz. The highest ten MDFs lie between 150-1150 Hz. As for the block B,

the Highest four MDFs are 234.4, 638.7, 1026.3, and 1092.8, and the highest peak is the first at 234.4 Hz. The highest ten MDFs lie between 20-1150 Hz.

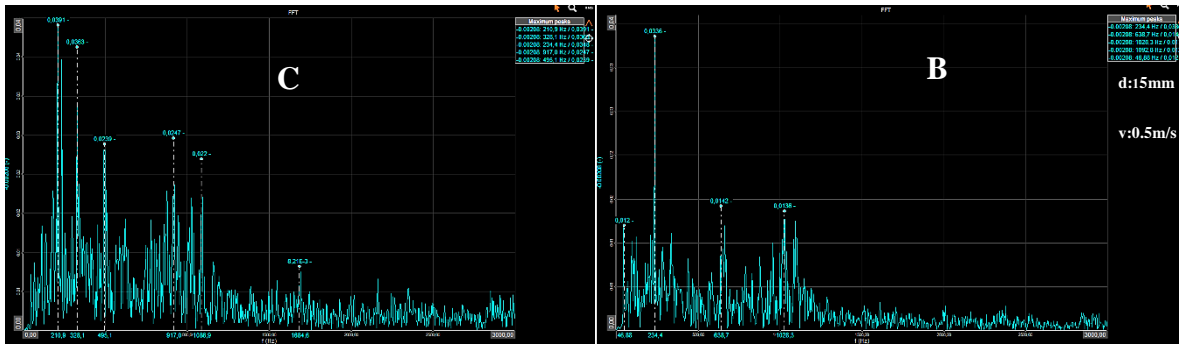


Figure 69. FFT of AE signal during cutting Block “CB” at a depth of 15 mm and a speed of 0.5 m/s.

The cutting speed was increased to 1.0 m/s for the same cutting depth (Figure 70), and it is still possible to differentiate between block C and block B, as the average of high peaks of block C has a value of 0.03746 approximately, and the highest peak is 0.0851, while the average of high peaks of block B is 0.02337 approximately and the highest peak is 0.0342, which are lower than those of block C. An increase in the magnitude of FFT was observed when the cutting speed was increased, as the average of high peaks of block C increased from 0.02455 to 0.03746 and the highest peak increased from 0.0391 to 0.0851, as for block B, the average of the high peaks increased from 0.01421 to 0.02337 and the highest peak increased from 0.0336 to 0.0342.

The highest four MDFs for block C are 328.1, 621.1, 673.8, and 949.2, and the highest peak is the first at 328.1 Hz. The highest ten MDFs lie between 150-1000 Hz. As for the block B, the Highest four MDFs are 304.7, 339.8, 644.5, and 1101.6, and the highest peak is the third at 641.5 Hz. The highest ten MDFs lie between 200-1150 Hz.

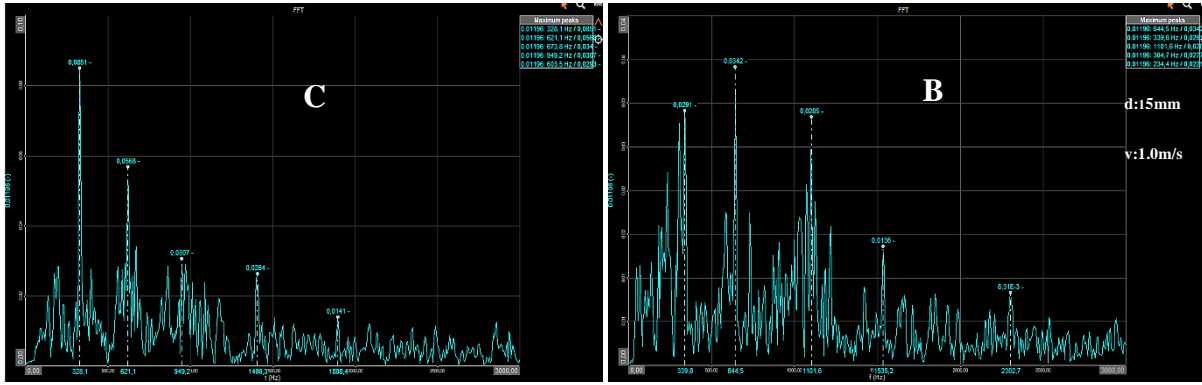


Figure 70. FFT of AE signal during cutting Block “CB” at a depth of 15 mm and a speed of 1.0 m/s.

The cutting speed was increased to 1.5 m/s for the same cutting depth (Figure 71), and it is still possible to differentiate between block C and block B, as the average of high peaks of block C has a value of 0.05258 approximately, and the highest peak is 0.0946, while the average of high peaks of block B is 0.04457 approximately and the highest peak is 0.0812, which are lower than those of block C.

An increase in the magnitude of FFT was observed when the cutting speed was increased, as the average of high peaks of block C increased from 0.03746 to 0.05258 and the highest peak increased from 0.0851 to 0.0946, as for block B, the average of the high peaks increased from 0.02337 to 0.04457 and the highest peak increased from 0.0342 to 0.0812.

The highest four MDFs for block C are 210.9, 316.4, 632.8, and 984.4, and the highest peak is the first at 210.9 Hz. The highest ten MDFs lie between 150-1150 Hz. As for the block B, the Highest four MDFs are 210.9, 328.1, 632.6, and 972.7, and the highest peak is the third at 632.6 Hz. The highest ten MDFs lie between 150-1250 Hz.

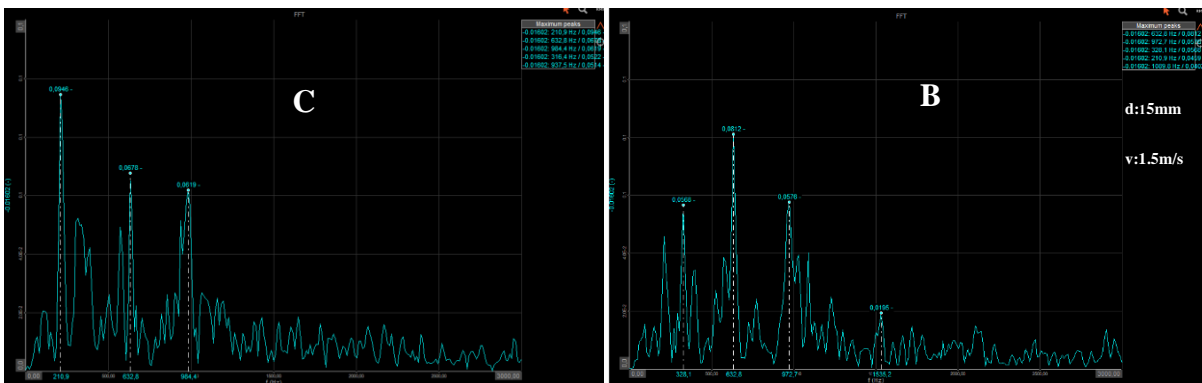


Figure 71. FFT of AE signal during cutting Block “CB” at a depth of 15 mm and a speed of 1.5 m/s.

The result of FFT analysis is that it is possible and with good accuracy and high resolution to differentiate between different rocks during cutting depending on the magnitude results of

FFT analysis of AE signals. But it is not possible to differentiate different rocks by analysis of MDFs, the location of the highest peak is always variable, sometimes close to 50 Hz, sometimes close to 100, 200, 500, 600, 700, 1000, or 1100 Hz. It hard to predict its location, but the location of the 10 MDFs is somewhat stable, lying between 20-1300 Hz for the majority of FFTs. Additionally, the highest MDF order change, sometimes it is the first, sometimes the second, the third, or the fourth. So, it is not possible to differentiate depending on the order of the highest peak.

(Table 6) summarize the results of the FFT analysis depending on the magnitude, showing the average of the highest ten peaks, the highest peak of each block and the location of the highest ten peaks. (Table 7) present the location of the highest four MDFs for each block: C and B, and it highlight the highest peak value and position in **Bold** font.

Table 6. Average peaks and maximum peaks in FFT analysis of AE signals recorded during cutting block CB.

| Depth (mm) | Speed (m/s) | Average of 10 highest peaks (C) | Maximum peak (C) | Average of 10 highest peaks (B) | Maximum peak (B) | Highest 10 peaks location in Hz (C) | Highest 10 peaks location in Hz (B) |
|------------|-------------|---------------------------------|------------------|---------------------------------|------------------|-------------------------------------|-------------------------------------|
| 2 | 0.5 | 0.00492 | 0.00915 | 0.00303 | 0.00472 | 100-1100 | 20-1100 |
| 2 | 1.0 | 0.01215 | 0.0191 | 0.0071 | 0.0113 | 100-1000 | 20-1300 |
| 2 | 1.5 | 0.01408 | 0.0231 | 0.00955 | 0.0141 | 200-1100 | 50-1150 |
| 5 | 0.5 | 0.01112 | 0.0169 | 0.00585 | 0.0105 | 20-1200 | 20-1050 |
| 5 | 1.0 | 0.0208 | 0.0316 | 0.0101 | 0.0169 | 300-1200 | 200-1200 |
| 5 | 1.5 | 0.0256 | 0.0518 | 0.0184 | 0.0445 | 200-2200 | 100-1000 |
| 10 | 0.5 | 0.01343 | 0.0175 | 0.00794 | 0.0121 | 200-1100 | 40-1100 |
| 10 | 1.0 | 0.01801 | 0.0233 | 0.01388 | 0.0197 | 50-1150 | 150-1150 |
| 10 | 1.5 | 0.02804 | 0.0506 | 0.01907 | 0.0394 | 20-1150 | 300-1100 |
| 15 | 0.5 | 0.02455 | 0.0391 | 0.01421 | 0.0336 | 150-1150 | 20-1150 |
| 15 | 1.0 | 0.03746 | 0.0851 | 0.02337 | 0.0342 | 150-1000 | 200-1150 |
| 15 | 1.5 | 0.05258 | 0.0946 | 0.04457 | 0.0812 | 150-1150 | 150-1250 |

Table 7. Highest four MDFs in FFT analysis of AE signals for block AC cutting.

| Depth (mm) | Speed (m/s) | Highest 4 MDFs (C) in Hz | | | | Highest 4 MDFs (B) in Hz | | | |
|---------------|----------------|--------------------------|-----------------|-----------------|-----------------|--------------------------|-----------------|-----------------|-----------------|
| | | 1 st | 2 nd | 3 rd | 4 th | 1 st | 2 nd | 3 rd | 4 th |
| 2 | 0.5 | 102.5 | 234.4 | 480.5 | 887.7 | 331.1 | 785.2 | 793.9 | 881.8 |
| 2 | 1.0 | 316.4 | 521.5 | 632.8 | 984.4 | 650.4 | 767.6 | 978.5 | 996.1 |
| 2 | 1.5 | 580.1 | 632.8 | 861.3 | 884.8 | 580.1 | 638.7 | 650.4 | 873.0 |
| 5 | 0.5 | 331.1 | 629.9 | 997.8 | 1092.8 | 45.88 | 272.5 | 334.0 | 1018.6 |
| 5 | 1.0 | 582.5 | 656.3 | 990.2 | 1066.4 | 345.7 | 638.7 | 1019.5 | 1113.3 |
| 5 | 1.5 | 527.3 | 679.7 | 937.5 | 1160.2 | 328.1 | 632.8 | 679.7 | 972.7 |
| 10 | 0.5 | 208.0 | 219.7 | 237.3 | 632.8 | 213.9 | 331.1 | 1013.7 | 1028.3 |
| 10 | 1.0 | 99.61 | 582.5 | 996.1 | 1084.0 | 234.4 | 638.7 | 1025.4 | 1101.8 |
| 10 | 1.5 | 328.1 | 691.4 | 925.8 | 984.4 | 46.88 | 632.8 | 668.0 | 972.7 |
| 15 | 0.5 | 210.9 | 231.4 | 325.1 | 917.0 | 234.4 | 638.7 | 1026.3 | 1092.8 |
| 15 | 1.0 | 328.1 | 621.1 | 673.8 | 949.2 | 304.7 | 339.8 | 644.5 | 1101.6 |
| 15 | 1.5 | 210.9 | 316.4 | 632.8 | 984.4 | 210.9 | 328.1 | 632.6 | 972.7 |

3.3 Analysis of “Moving Average” and “Interquartile Range”

Four cutting tests were selected for both blocks to be analyzed, and presented, different cutting factors were selected (different cutting speeds). The result is block C is higher in value than block A, because the high-strength block emits higher AE signals and the low-strength block emits lower AE signals.

3.3.1.1 Block AC

Two cutting tests were selected for block AC to be analyzed, and presented, different cutting speeds were selected. The result is that block C is higher in value than block A, because the high-strength block emits higher AE signals and the low-strength block emits lower AE signals.

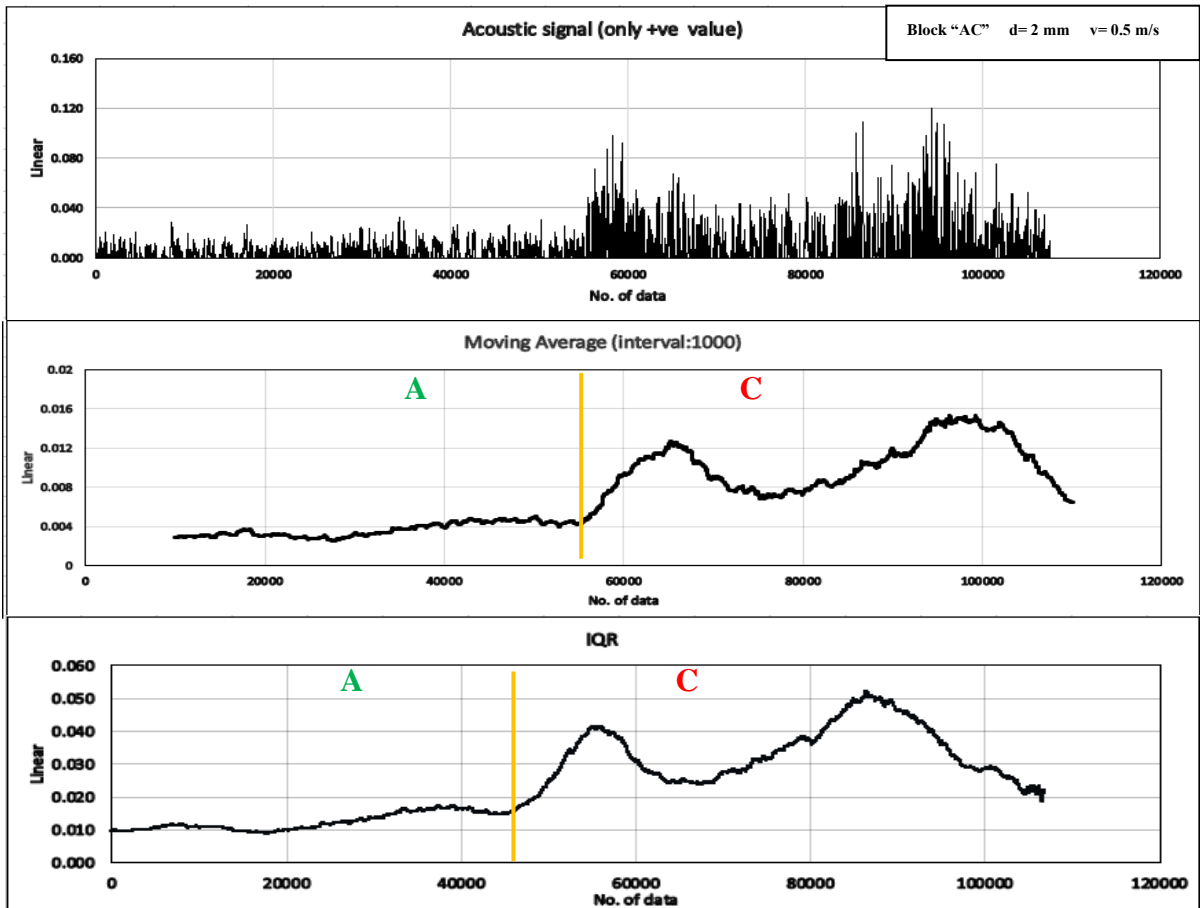


Figure 72 . AE signal positive values (top), Moving Average (middle) and Interquartile Range (bottom) during cutting Block "AC" at a depth of 2 mm and a speed of 0.5 m/s.

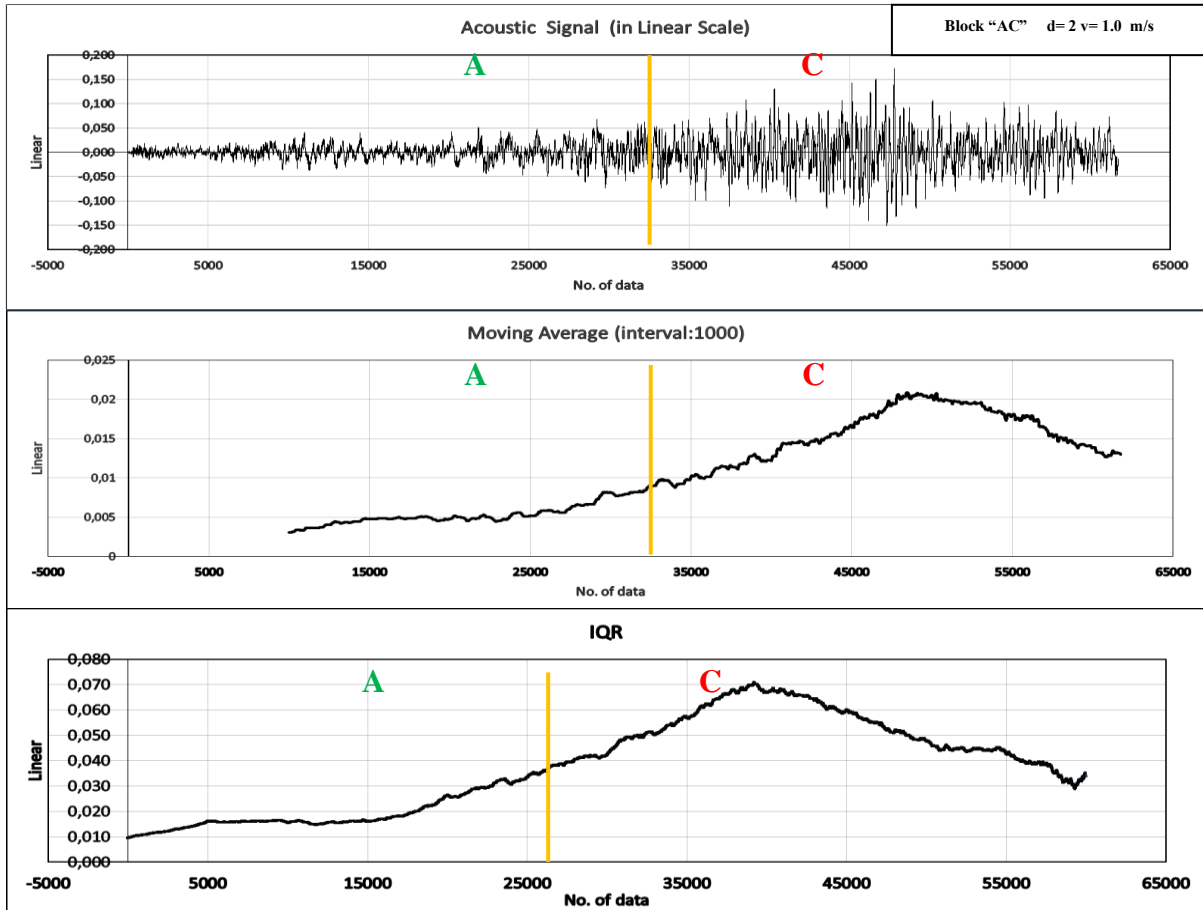


Figure 73. AE signal positive values (top), Moving Average (middle) and Interquartile Range (bottom) during cutting Block "AC" at a depth of 2 mm and a speed of 1.0 m/s.

3.3.1.2 Block CB

Two cutting tests were selected for block CB to be analyzed, and presented, different cutting speeds were selected. The result is that block C is higher in value than block A, because the high-strength block emits higher AE signals and the low-strength block emits lower AE signals.

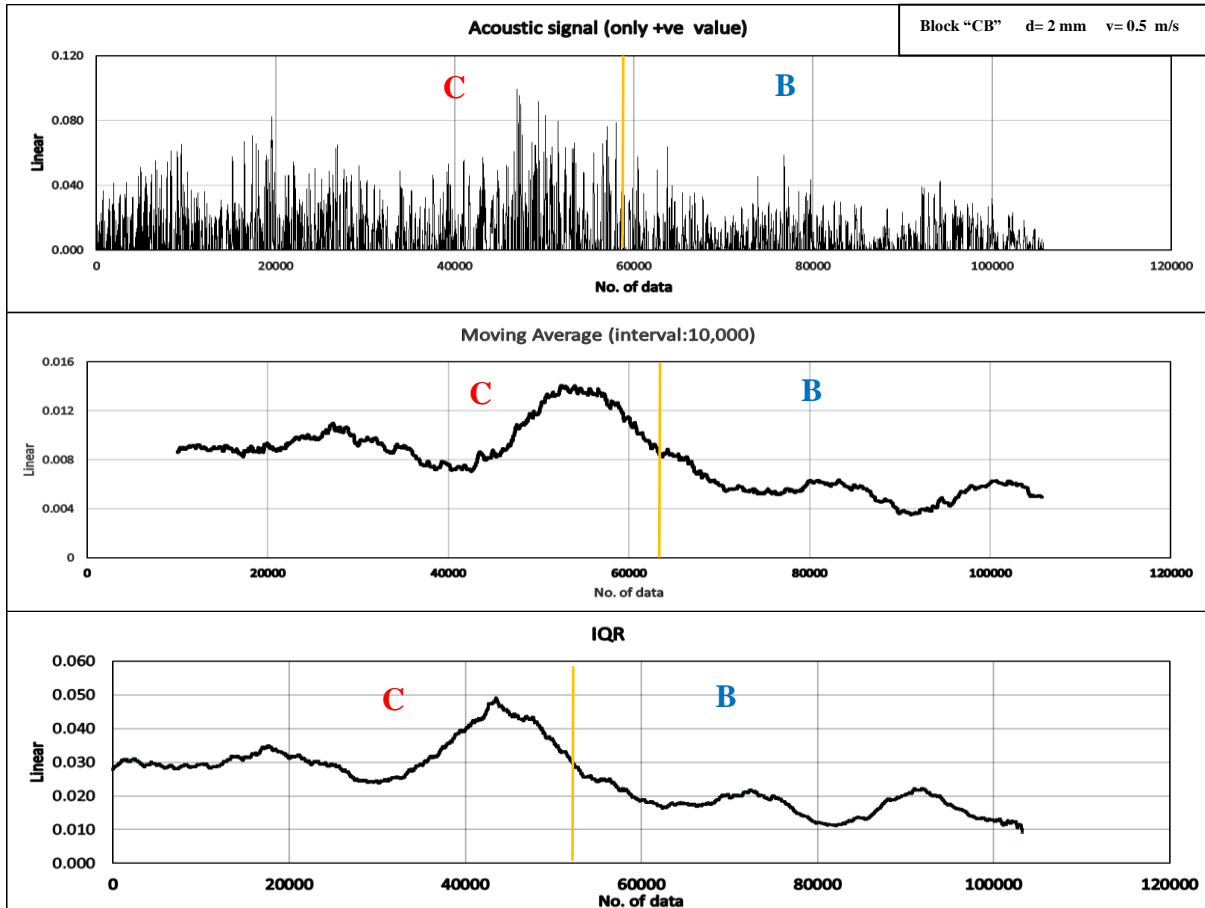


Figure 74. Positive values (top), Moving Average (middle) and Interquartile Range (bottom) of AE signal during cutting Block "CB" at a depth of 2 mm and a speed of 0.5 m/s.

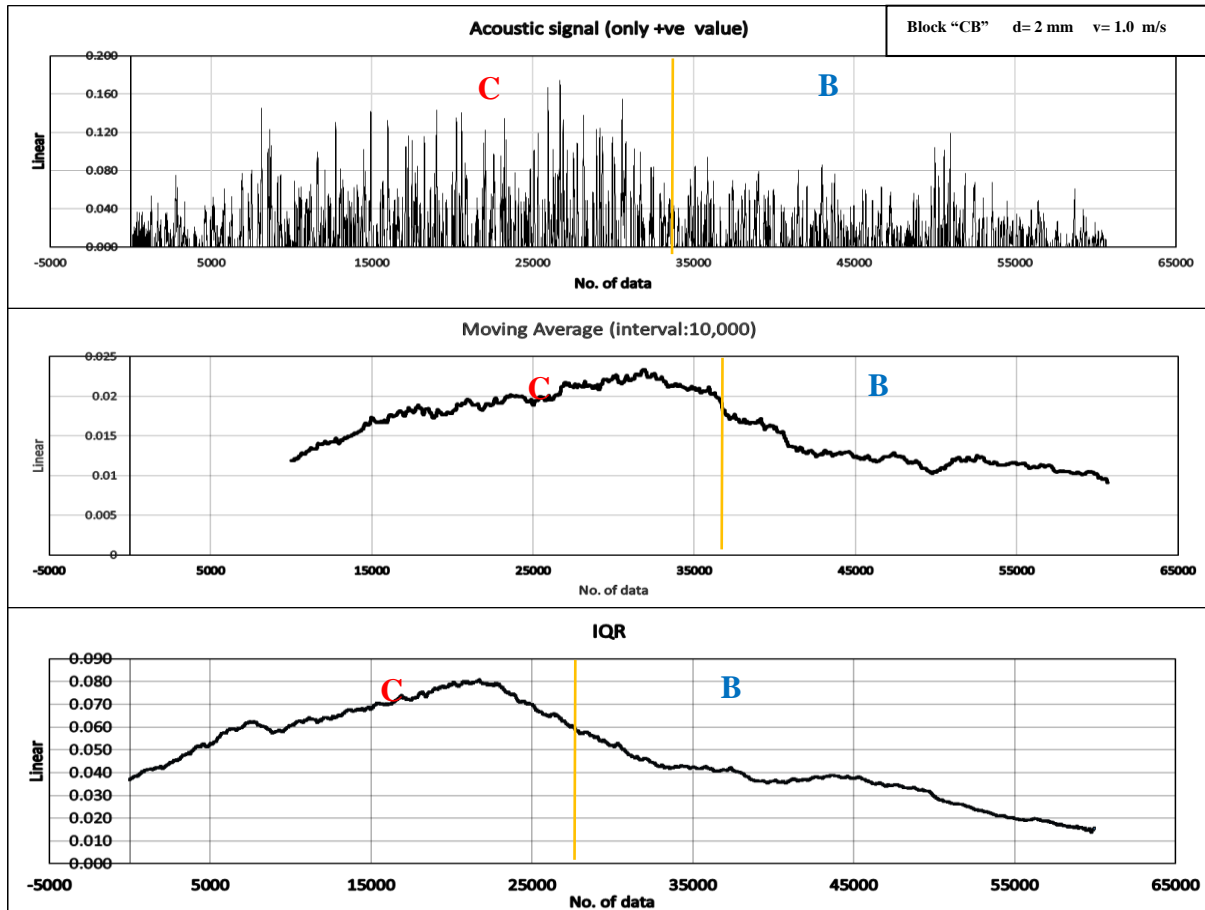
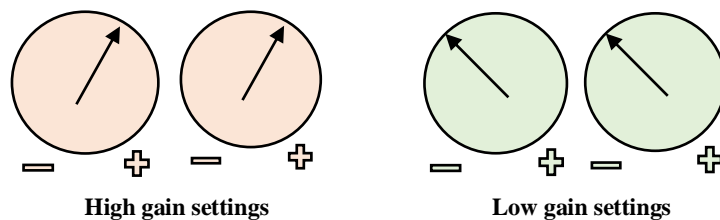


Figure 75. Positive values (top), Moving Average (middle) and Interquartile Range (bottom) of AE signal during cutting Block “CB” at a depth of 2 mm and a speed of 1.0 m/s.

3.4 Optimization of AE Signal Quality

3.4.1 Adjusting the Gain Level

In this section different gain settings (audio capture level) are compared under different cutting conditions: different cutting speed, different depths, to see how this affects the quality of the AE signal, in order to improve its quality.



In the previous section: Analyzing the AE signal, Low-gain settings were used (which had been explained earlier in the previous chapter), and it was possible to clearly see the difference between blocks of different strength (Figure 76). Moreover, when the cutting speed

or cutting depth was increased, the difference was evident on the AE signal, optically and numerically, where the intensity of AE increased as the values of the average peaks or maximum peaks increased, and there was also enough space to record higher AEs. Assuming there is a very strong rock or harsh condition, the recording device can pick up much louder sounds, thanks to the sufficient space left, as in most recordings only less than half of the possible capacity is used, and this proves that the use of Low gain settings is suitable, practical and efficient.

Looking at the AE signal recorded with high gain settings while cutting with a cutting depth of 5 mm and a cutting speed of 0.5 m/s (Figure 76), it can be seen that the quality of the AE signal is good, as the peaks have not yet reached the maximum capacity (highest sound that can be captured, =1 linear), and that means that there is no problem of clipping (the peaks reaching the maximum capacity). But the remaining area is very small, and assuming the presence of a much stronger rock, the peaks will reach the maximum possible sound capture capacity, and the clipping problem will appear, which will impair the quality of the recorded AE signal, and therefore many of the visible numbers will be incorrect.

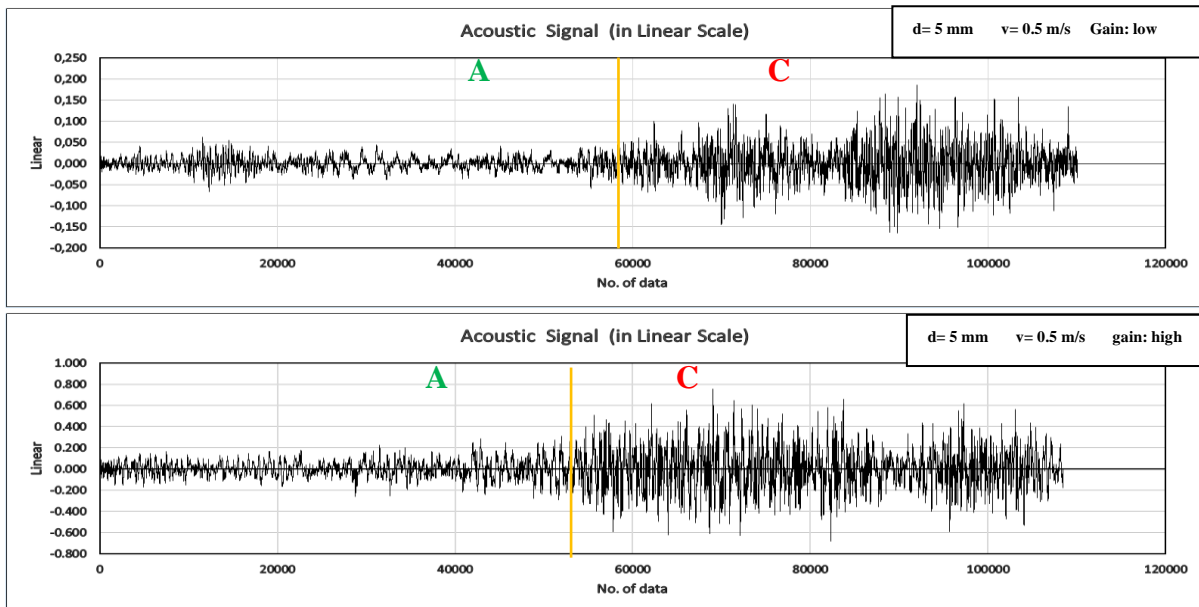


Figure 76. AE signal during cutting at a depth of 5 mm and a speed of 0.5 m/s, (a) Low gain settings (top), (b) High gain settings (bottom).

The cutting speed was increased from 0.5 m/s to 1.0 m/s for the same depth of cutting (Figure 77), and two clippings were observed on the high gain AE signal, as two of the peaks reached the maximum capacity (1 linear). Those two peaks have incorrect value, these numbers must be higher than 1 linear, but the device could not record the correct number because it has reached the maximum. This indicates that it is better to use low gain settings to give enough

space to pick up sounds for all types of rocks It has been shown previously that low settings are reliable to distinguish the difference even between weak rocks and those that have very low AE intensity.

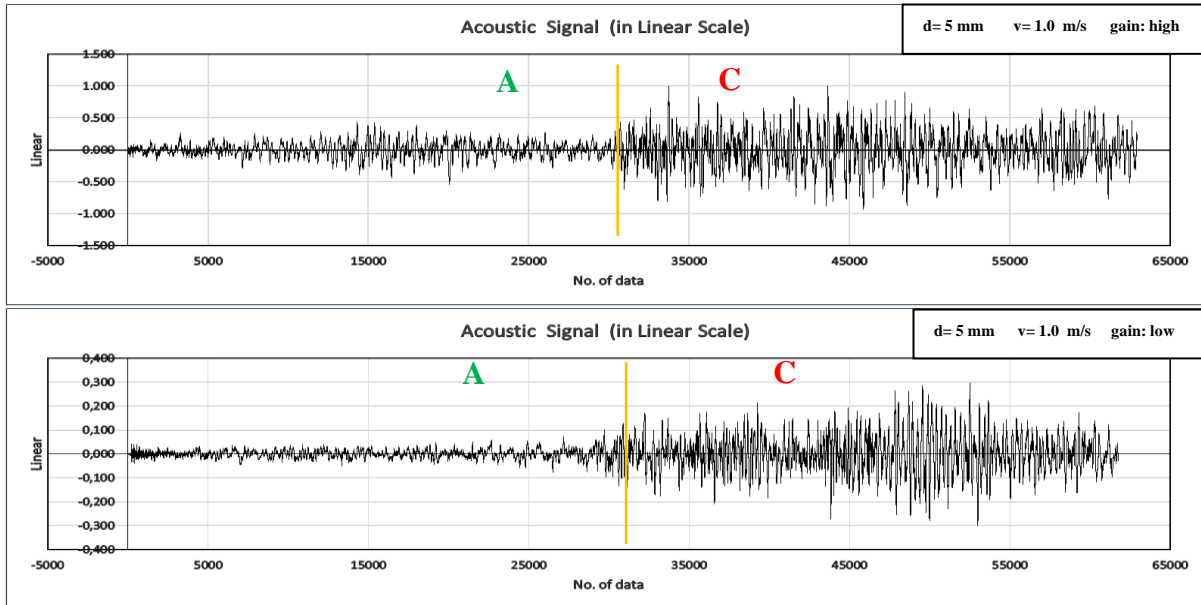


Figure 77. AE signal during cutting at a depth of 5 mm and a speed of 1.0 m/s, (a) Low gain settings (top), (b) High gain settings (bottom).

The cutting speed was increased to 1.5 m/s for the same cutting depth (Figure 78), and five clippings were noticed on the high gain AE signal, as five peaks reached the maximum capacity (1 linear), these peaks are more than 1 linear, but the audio recording device cannot pick up any higher sounds. This indicates that it is best to use low gain settings to give enough space to catch sounds for all types of strong and stronger rocks, and also it has been previously proven that low settings are reliable to differentiate even between weak rocks that have very low AE.

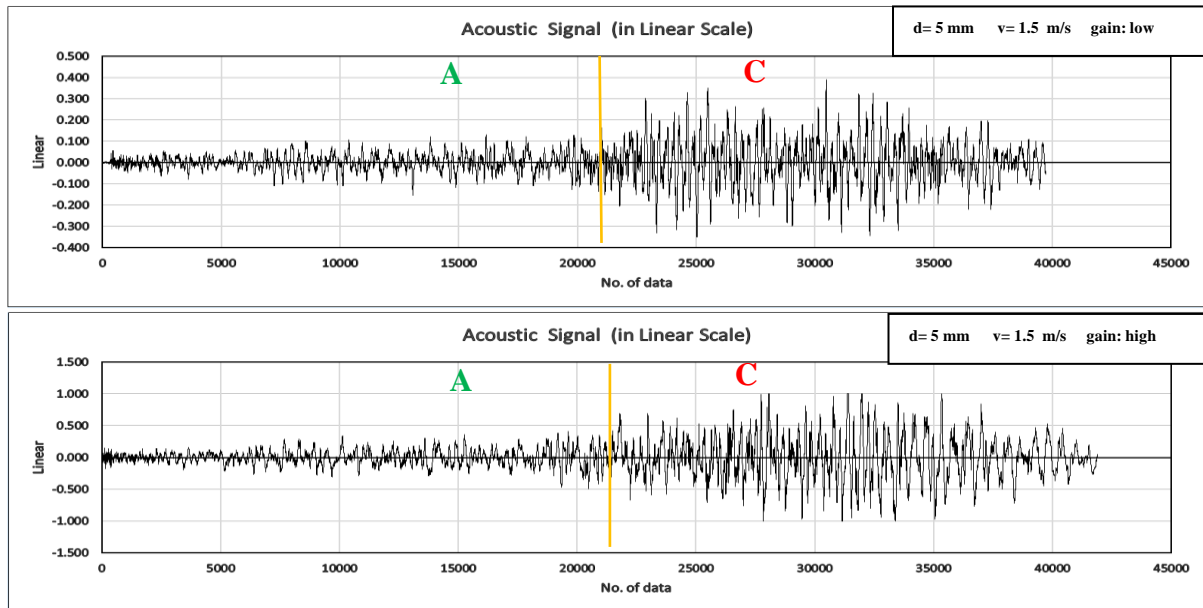


Figure 78 . AE signal during cutting at a depth of 5 mm and a speed of 1.5 m/s, (a) Low gain settings (top), (b) High gain settings (bottom).

The cutting depth was increased to 10 mm for a cutting speed of 0.5 m/s (Figure 79), and two clippings were observed for the high gain settings, as two peaks reached the maximum capacity (1 linear). The value of these two peaks are higher, but the device could not capture the correct value for exceeding the limit. This again indicates that it is best to use low gain settings to give enough space to record sounds for all types of strong and stronger rocks, and also it has been previously proven that low settings are reliable to distinguish the difference even between weak rocks that have very low AE.

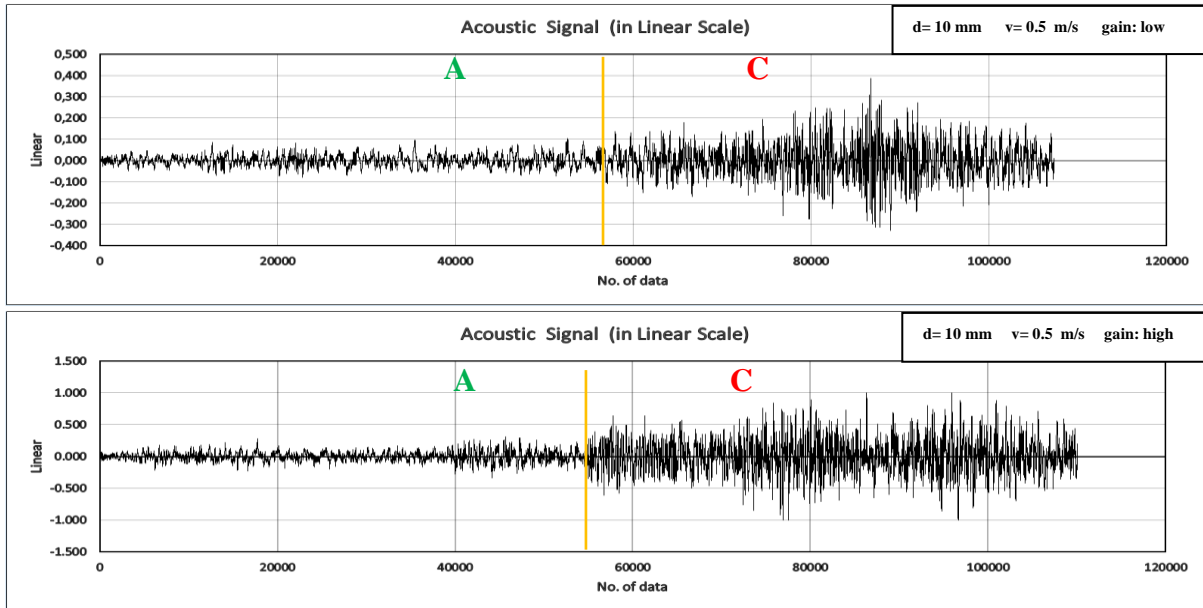


Figure 79. AE signal during cutting at a depth of 10 mm and a speed of 0.5 m/s, (a) Low gain settings (top), (b) High gain settings (bottom).

The cutting speed was increased to 1.0 m/s for the same cutting depth (Figure 80). Five clippings occurred, as five peaks reached the maximum capacity (1 linear). This is incorrect, these peaks are more than 1 linear, but the audio recording device cannot pick up the sound above the maximum capacity. This indicates once more that it is best to use low gain settings to give enough space to pick up sounds for all types of strong and stronger rocks, and also it has been previously proven that low settings are reliable to differentiate even between weak rocks that have very low AE.

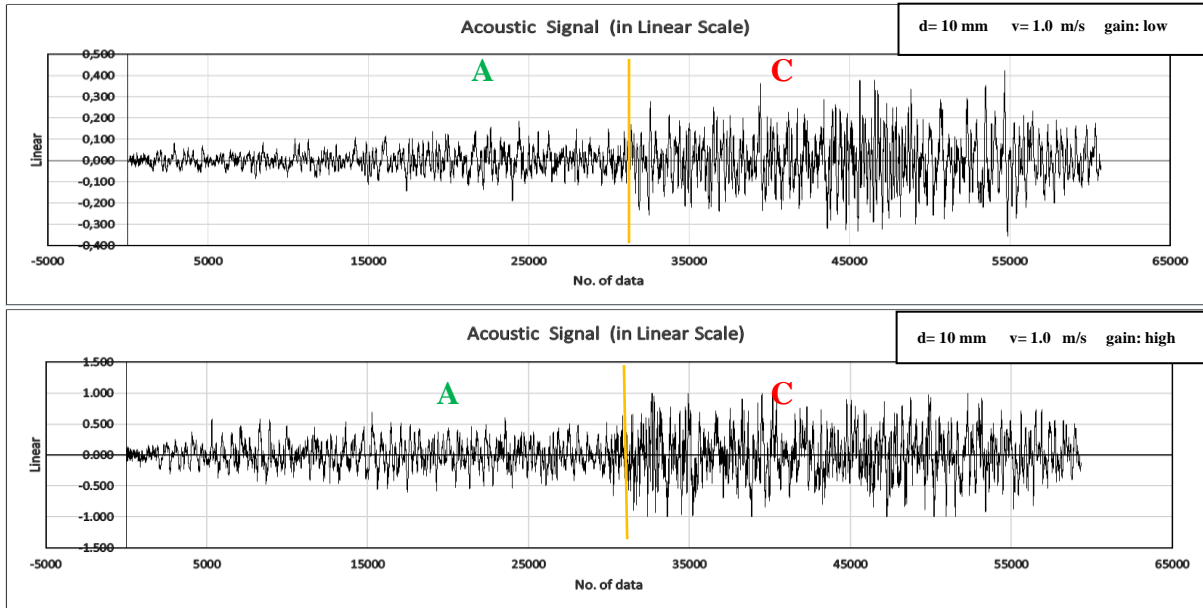


Figure 80. AE signal during cutting at a depth of 10 mm and a speed of 1.0 m/s, (a) Low gain settings (top), (b) High gain settings (bottom).

A table for comparing results between high and low gain settings is presented, showing the number of clipping occurrences for each one (Table 8).

Table 8. Number of clipping occurrences at high and low gain settings (comparison results).

| Cutting Depth (mm) | Cutting Speed (m/s) | No. of Clippings (high gain) | No. of Clippings (low gain) |
|--------------------|---------------------|------------------------------|-----------------------------|
| 5 | 0.5 | 0 | 0 |
| 5 | 1.0 | 2 | 0 |
| 5 | 1.5 | 5 | 0 |
| 10 | 0.5 | 2 | 0 |
| 10 | 1.0 | 5 | 0 |

3.4.2 Adjusting Proximity of The Cutting to The Microphone

AE signal of three cutting tests on block AC with different distances between the cutting position and the microphone (shown in the previous chapter) with a speed of 1.0 m/s and a cutting depth of 15 mm were analyzed in order to know the effect on the quality and intensity of the AE signals, and here the results are presented.

The first cutting was executed at a close distance to the microphone (Figure 81), and it was possible to differentiate between block A and block C, since the average peak value of block A is 0.123811346 and the maximum peak is 0.26577, while the average peak value of block C is 0.313801667 and the maximum peak is 0.58917, which are higher than those of block A.

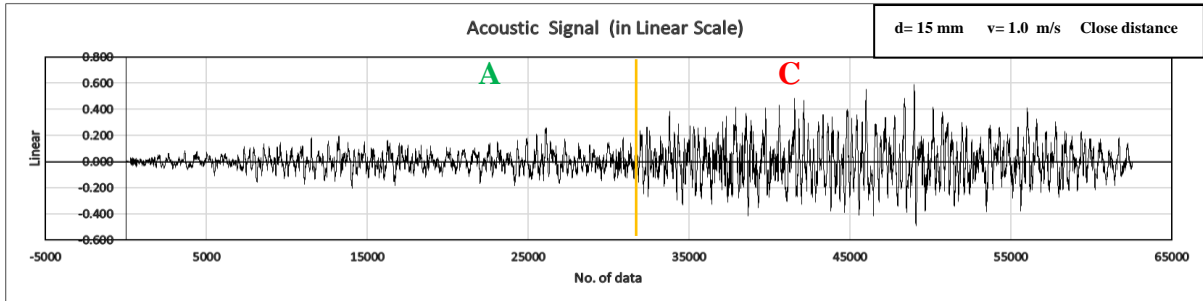


Figure 81. AE signal for cutting test of close distance from the microphone.

The distance between the cutting position and the microphone was increased to the middle position on the concrete block (Figure 82), and it remained possible to differentiate between block A and block C, since the average peak value of block A is 0.123811346 and the maximum peak is 0.26577, while the average peak value of block C is 0.313801667 and the maximum peak is 0.58917, which are higher than those of block A. It was also observed that the intensity of the AE signal decreased when the distance increased, as the value of the average peak of block A decreased from 0.123811346 to 0.088195192 and the maximum peak decreased from 0.26577 to 0.1531, and the same for block C, the value of the average peak of block C decreased from 0.313801667 to 0.289396458, and the maximum peak decreased from 0.58917 to 0.49483.

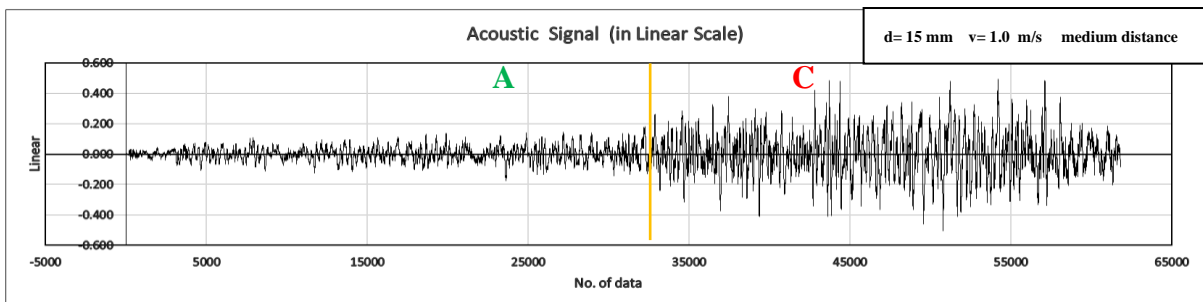


Figure 82. AE signal for cutting test of medium distance from the microphone.

The distance between the cutting position and the microphone was increased to the farthest position on the concrete block, (Figure 82), and it remained possible to differentiate between block A and block C, since the average peak value of block A is 0.109651538 and the maximum peak is 0.19366, while the average peak of block C is 0.264038125 and the

maximum peak is 0.45323, which are higher than those of block A. It was observed that the intensity of the AE signal decreased, comparing to the closest position from the microphone, as the value of the average peak of block A decreased from 0.123811346 to 0.109651538 and the maximum peak decreased from 0.26577 to 0.19366, and the same for block C, the value of the average peak of block C decreased from 0.313801667 to 0.264038125, and the maximum peak decreased from 0.58917 to 0.45323. But comparing to the middle distance from the microphone, the intensity of the AE signal of block A did not decrease, but it was decreased for block C, as the average peak of block A increased from 0.088195192 to 0.109651538 and the maximum peak increased from 0.1531 to 0.19366, but for block C, the value of the average peak of block C decreased from 0.289396458 to 0.264038125, and the maximum peak decreased from 0.49483 to 0.45323.

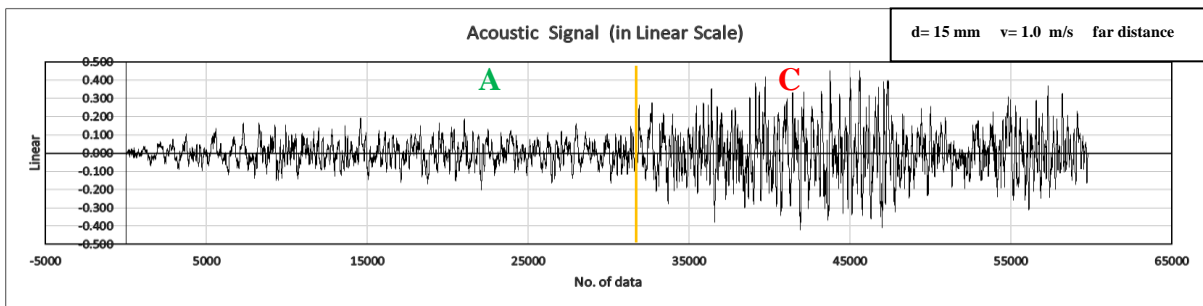


Figure 83. AE signal for cutting test of far distance from the microphone.

The conclusion of this test, that cutting at a very close distance from the microphone leads to a clear increase in the intensity of the AE, but cutting at a medium or far distance does not significantly affect the intensity of AE for the weak-strength concrete blocks (Block A), as the AE intensity was not weakened when the distance increased from the center position to the far position, but it affects the strong blocks (Block C), as the intensity of the AE decreased when the distance increased from the center position to the far position. But to prove this theory, further experiments must be done with different cutting parameters: different cutting depths, different cutting speeds, in which the distance between the microphone and the cutting position is changed.

Comparison results of cuttings position proximity to the microphone and their effect on the quality of the AE signal and on the average and maximum peaks values are shown in Table 9.

Table 9. Comparison results of microphone proximity to the cutting position, and the effect on AE signal intensity

| Proximity to microphone | Average peak (A) | Maximum peak (A) | Average peak (C) | Maximum peak (C) |
|--|-----------------------------|-----------------------------|-----------------------------|-----------------------------|
| close | 0.123811346 | 0.26577 | 0.313801667 | 0.58917 |
| Middle | 0.088195192 | 0.1531 | 0.289396458 | 0.49483 |
| Far | 0.109651538 | 0.19366 | 0.264038125 | 0.45323 |

4 Conclusion

Different rocks can be differentiated depending on the acoustic emission signal, as the AE intensity increases when cutting strong rocks, while the AE intensity decreases when cutting weak rocks. The AE intensity also increases with an increase in cutting depth or cutting speed. The distance of the microphone from the AE source (the rock cutting position) has a relatively small effect on the AE intensity, but this effect increases to a noticeable degree with close proximity to the microphone. So, the microphone should be installed at a medium distance from the rock cutting location. Adjusting the sensitivity of the gain level (sound capture level) to an appropriate level has an important role in distinguishing between different rocks, as the wrong setting leads to an incorrect AE signal, and it is not relied upon to differentiate between different rocks. The magnitude of MDFs in the FFT frequency spectrum of the AE signal increases when the depth or speed of the cut increases, as well as when the strength of the rock increases. Knowing the locations of the MDFs and the highest MDF in the FFT frequency spectrum of AE signal hasn't proved to be useful in differentiating between different rocks, as they didn't show reliable ordered results. Their locations were randomly variable, and their order was also randomly variable from one test to another. But knowing that the ten MDFs are mostly in the range from 20 to 1300 Hz, this may help in designing a rock differentiation interface based on the FFT frequency spectrum of the AE signal by calculating the average value of the ten highest MDFs within this range of frequencies. The analysis of the magnitudes of MDFs of the FFT frequency spectrum proved greater validity in differentiating between rocks of different strength than the analysis of the AE signal itself, as it always gave a clear difference without any error. It always gave a higher magnitude with the increase in the strength of the rock, the increase in the depth of cut, or the increase in the cutting speed.

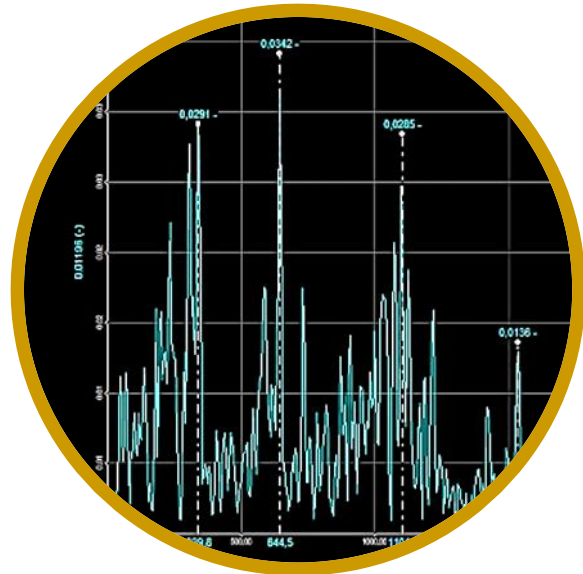
5 Future Recommendation

It is recommended to design a rock differentiation system based on the acoustic emission resulting from cutting the rock, for the installation on excavation machines. The interface shall display FFT frequency spectrum, the differentiation depends on the average magnitude of MDFs, the rang of frequencies to be included are those between 20 to 1300 Hz only (Figure 84). The reason for choosing the FFT frequency spectrum is that it is more accurate,

as each AE signal has a distinct frequency spectrum. This method is more accurate than relying on the AE signal itself, as it hasn't shown any error during analysis. The reason for choosing the mentioned frequency range, is that the distinctive frequencies (MDFs) at which the different rocks are differentiated lie between those values. The differentiation is done according to the difference in strength between the rocks, because the AE is also an indicator of the strength of the rock, as it is also an indicator of the cutting speed and cutting depth. All of these three parameters affect the value of the AE, and distinctively affect the magnitudes of MDFs in the FFT frequency spectrum. In this way it is possible to determine the strength of the rock, and thus

the possibility of cutting this rock, and whether this rock is the rock required for cutting or not (when desiring selective mining), and then choosing the right speed and depth of cutting: is it soft or hard rock? Shall we increase the cutting speed? Shall we increase the depth of cut?

The reason for choosing FFT over other methods to display the frequency spectrum, that the FFT is a very fast algorithm, which is very applicable and require less calculations than other methods.



FFT Average Magnitude

Depth / Speed

Rock Strength

Figure 84. AE differentiation system based on FFT frequency Spectrum

6 References

- Asadi, A., Abbasi, A. & Bagheri, A., 2017. *PREDICTION OF ROADHEADER BIT CONSUMPTION RATE IN COAL MINES USING ARTIFICIAL NEURAL NETWORKS*. Helsinki, Finland, s.n.
- Atlas Copco, 2007. *Mining Methods in Underground Mining*. 2 ed. Örebro, Sweden: Atlas Copco Rock Drills AB.
- Audacity , 2021. *Audacity Manual 3.04*. s.l.:Audacity.
- Bao, R., Zhang, L. & Yao, Q., 2011. Estimating the Peak Indentation Force of the Edge Chipping of Rocks Using Single Point-Attack Pick. *Rock Mech Rock Eng*, Volume 44, p. 339–347.
- Bartnitzki, T. & Vraetz, T., 2018. Acoustic fingerprint on rock cutting machinery. *Bergbau*, Issue 1, pp. 25-29.
- Bilgin, N., Copur, H. & Balci, C., 2014. *Mechanical Excavation in Mining and Civil Industries*. 1 ed. United Kingdom: Taylor & Francis.
- Bilgin, N. et al., 2006. Dominant rock properties affecting the performance of conical picks and the comparison of some experimental and theoretical results. *International Journal of Rock Mechanics and Mining Sciences*, 43(1), pp. 139-156.
- Bołoz, Ł., 2013. UNIQUE PROJECT OF SINGLE-CUTTING HEAD LONGWALL SHEARER USED FOR THIN COAL SEAMS EXPLOITATION. *Archives of Mining Sciences.*, 58(4), p. 1057–1070.
- Burrus, C. S., Frigo, M. & Johnson, S. G., 2012. *Fast Fourier Transforms*. Texas: Samuraj Media Limited.
- Cheluszka, P., 2019. *Experimental identification of the dynamic load of conical picks during the cutting process of transverse cutting heads of boom type roadheader.*. Athens, Greece, Saima Consult Ltd, pp. 167-176.
- Cheluszka, P., 2020. Optimization of the Cutting Process Parameters to Ensure High Efficiency of Drilling Tunnels and Use the Technical Potential of the Boom-Type Roadheader. *Energies*, Volume 13, p. 6597.

References

- Cooley, J. & Tukey, J., 1965. An algorithm for the machine calculation of complex Fourier series. *Mathematics of Computation*, Volume 19, pp. 297-301.
- Copur, H. et al., 2017. Effects of Different Cutting Patterns and Experimental Conditions on the Performance of a Conical Drag Tool. *Rock Mechanics and Rock Engineering* , pp. 1585-1609.
- Copur, H., Ozdemir, L. & Rostami, J., 1998. Roadheader applications in mining and tunneling. *Mining Engineering*, 50(3).
- Crosland, D., Mitra, R. & Hagan, P., 2009. *Changes in Acoustic Emissions when cutting different Rock Types*. Wollongong, Research Online: University of Wollongong, pp. 329-339.
- Deliac, E. P., 1993. Chapter 8: Theoretical and Practical Rules for Mechanical Rock Excavation. In: J. A. Hudson, ed. *Comprehensive Rock Engineering, Volume 4*. London, UK: Pergamon Press, pp. 177-227.
- Demou, S., Olson, R. & Wingquist, C. F., 1983. *Determination of Bit Forces Encountered in Hard Rock Cutting for Application to Continuous Miner Design*, USA: Bureau of Mines, USA.
- Deshmukh, S. et al., 2020. Roadheader – A comprehensive review. *Tunnelling and Underground Space Technology*, Volume 95, p. 103148.
- Dewangan , S. & Chattopadhyaya, S., 2016. Characterization of Wear Mechanisms in Distorted Conical Picks After Coal Cutting. *Rock Mechanics and Rock Engineering* , 49(1), p. 225–242 .
- Dewangan, S., Chattopadhyaya, S. & Hloch, S., 2015. Wear Assessment of Conical Pick used in Coal Cutting Operation. *Rock Mechanics and Rock Engineering*, 48(5), p. pages2129–2139.
- Dewangan, S. & Chattopadhyaya, S., 2016. Performance Analysis of Two Different Conical Picks Used in Linear Cutting Operation of Coal. *Arabian Journal for Science and Engineering* , 41(1), pp. 249-265.
- Dunbar, W. S., 2012. *2012 Americas School of Mines, Basics of Mining and Mineral Processing*. [Online]
Available at: <https://www.pwc.com/gx/en/mining/school-of-mines/2012/pwc-basics-of->

References

[mining-2-som-mining-methods.pdf](#)

[Accessed 12 2021].

Elliott, D. F., 1987. Chapter 7 - Fast Fourier Transforms. In: D. F. Elliott, ed. *Handbook of Digital Signal Processing*. Anaheim, California: Academic Press, Inc., pp. 527-631.

European Commission, 2018. *EIP on Raw Materials, Raw Materials Scoreboard 2018*, Luxembourg: Publications Office of the European Union.

Evans, I., 1984. A theory of the cutting force for point attack picks, Technical Note.. *International Journal of Mining Engineering*, Volume 2, pp. 63-71.

Fowell, R., 1993. Chapter 7: The Mechanics of Rock Cutting. In: J. A. Hudson, ed. *Comprehensive Rock Engineering: Principles, Practice, & Projects*. London: Pergamon Press, pp. 155-176.

Fowell, R. J., Hekimoglu, O. Z. & Altinoluk, S., 1987. *Drag Tools Employed on Shearer Drums and Roadheaders*. Ankara, s.n., pp. 529-550.

Goktan, R. M., 1990. Effect of cutter pick rake angle on the failure pattern of high-strength rocks. *Mining Science and Technology*, Volume 11, pp. 281-285.

Gollick, J. M., 1999. *Optimising roadheader performance based on laboratory and field work. PhD thesis, University of Nottingham.*, Nottingham: University of Nottingham.

Grafe, B., Shepel, T. & Drebenstedt, C., 2019. Innovations in Mechanical rock excavation at TU Bergakademie Freiberg. In: *Scientific and Practical Studies of Raw Material Issues*. s.l.:Taylor & Francis Group, London, pp. 34-45.

Hartman, H. L., 1992. *SME Mining Engineering Handbook*. 2 ed. Colorado: SME, Society for Mining, Metallurgy, and Exploration, Inc..

Harvey, M. C. & Audrey, F., 2000. *The Fundamentals of FFT-Based Signal Analysis and Measurement*. [Online]

Available at: https://www.sjsu.edu/people/burford.furman/docs/me120/FFT_tutorial_NI.pdf

[Accessed 1 12 2021].

Heckbert, .., 1995. *Fourier Transforms and the Fast Fourier Transform (FFT) Algorithm*.

[Online]

Available at: <http://www.cs.cmu.edu/afs/andrew/scs/cs/15->

References

463/2001/pub/www/notes/fourier/fourier.pdf

[Accessed 12 2021].

Heiniö, M., 1999. *Rock Excavation Handbook*. s.l.: Sandvik Tamrock Corp..

Hekimoglu, O. Z., 1995. The Radial Line Concept for Cutting Head Pick Lacing Arrangements. *Int. J. Rock Mech. Min. Sci. & Geomech.*, 32(4), pp. 301-311.

Heß, R., 2010. *DFT und FFT, Anwendung, Herleitung und Implementierung in C/C++*.

[Online]

Available at: <http://www.rrhess.de/pdf/Skript-FFT.pdf>

[Accessed 10 12 2021].

Hood, M. C. & Roxborough, F. F., 1992. Chapter 9.1: Rock Breakage Mechanical. In: H. L. Hartman, ed. *SME Mining Engineering Handbook*. Colorado: SME: Society Mining, Metallurgy, and Exploration, Inc., pp. 680-721.

Hurt, K. & MacAndrew, K., 1985. CUTTING EFFICIENCY AND LIFE OF ROCK-CUTTING PICKS. *Mining Science and Technology*, Volume 2, pp. 139-151 .

Hussein, E., 1996. *Mechanical Engineering: Course 7.2, Non-Destructive Testing, Chapter 6: Acoustic Emission*. [Online]

Available at: <https://canteach.candu.org/Content Library/20053107.pdf>

[Accessed 13 10 2021].

John F. Bryan, J., 1992. *Stratum boundary sensor for continuous excavators*. USA, Patent No. US5092657A.

Jung, S. J., Prisbrey, K. & Wu, G., 1994. Prediction of Rock Hardness and Drillability using Acoustic Emission Signatures during Indentation. *International Journal of Rock Mechanics and Mining Sciences & Geomechanics Abstracts*, 31(5), pp. 561-567.

Kargl, H., Gimpel, M. & Gerer, R., 2011. *Arrangement for Detecting the Load of a Chisel of Cutting Machines*. Austria, Patent No. WO2011116405.

Khair, A.-W., Reddy, N. & Quinn, M., 1989. Mechanisms of Coal Fragmentation by a Continuous Miner. *Mining Science and Technology*, Volume 8, pp. 189-214.

Krige, D., 1962. Effective Pay Limits for Selective Mining. *ournal of the South African Institute of Mining and Metallurgy*, pp. 345-363.

References

Liu, S. et al., 2021. Interrelationships between Acoustic Emission and Cutting Force in Rock Cutting. *Geofluids*, 2021 (1), pp. 1-12.

Li, X., 2020. A study on the influence of pick geometry on rock cutting based on full-scale cutting test and simulation. *Advances in Mechanical Engineering*, Volume 12, pp. (12) 1-13.

Luo, Y., 2014. *Highwall Mining Design Methodology, Safety and Suitability*, West Virginia: researchgate.net.

Marston, B., Mazlin, J. G. & Mazlin, D. J., 1997. *detecting a boundary between two layers of material*. AU, Patent No. WO1997018466.

Mezyk, A., Pawlak, M., Kania, J. & Klein, W., 2019. A new concept of vibration-control system in continuous miner machine. *Advances in Mechanical Engineering*, 11(1), p. 1–14.

Mohammadi, M., Hamidi, J., Rostami, J. & Goshtasbi, 2020. A Closer Look into Chip Shape/Size and Efficiency of Rock Cutting with a Simple Chisel Pick: A Laboratory Scale Investigation. *Rock Mechanics and Rock Engineering*, Volume 53, p. 1375–1392.

Moser, P., 2018. *Underground Mining 200.036 Sublevel Stopping and Open Stopping*. Leoben: MU Leoben.

Moser, P., Ladinig, T. & Wimmer, M., 2018. *underground mining 200.036*. Leoben: Montan Leoben University.

Oberst, U., 2007. The Fast Fourier Transform.. *SIAM Journal on Control and Optimization*, 46(2), pp. 496-540.

Orteu, J.-J., Catalina, J. C. & Devy, M., 1992. *Perception for a roadheader in automatic selective cutting operation*.. Nice, France, IEEE, pp. 626 - 632.

Oshana, R., 2006. 4 - Overview of Digital Signal Processing Algorithms. In: R. Oshana, ed. *SP Software Development Techniques for Embedded and Real-Time Systems*. Newnes: Elsevier Inc., pp. 59-121.

Prakash, A. et al., 2020. A methodology for designing cutting drum of surface miner to achieve production of desired chip size. *Sadhana*, Volume 45, p. 143.

Reid, D., Hainsworth, D., Ralston, J. & McPhee, R., 2006. Shearer Guidance: A Major Advance in Longwall Mining. In: A. H. P. E. T. T. S. Yuta S., ed. *Field and Service*

References

Robotics. Springer Tracts in Advanced Robotics, vol 24. s.l.:Springer, Berlin, Heidelberg, pp. 469-476.

Restner, U. & Plinnenger, R., 2015. *Rock Mechanical Aspects of Roadheader Excavation.* Salzburg, Austria, s.n.

Roberts, B. L., 1984. *The decibel Scale.* [Online]
Available at: <http://g2pc1.bu.edu/~roberts/py231/db3.pdf>
[Accessed 12 2021].

Roxborough, F., King, P. & Pedroncelli, E., 1981. Tests on the cutting performance of a continuous miner. *JOURNAL OF THE SOUTH AFRICAN INSTITUTE OF MINING AND METALLURGY*, Volume 81, pp. 9-25.

SFU, B. T. f. b. ". E., 1999. *SOUND INTENSITY.* [Online]
Available at: https://www.sfu.ca/sonic-studio-webdav/handbook/Sound_Intensity.html
[Accessed 12 2021].

Sifferlinger, N. A., 2018. *Mechanical Excavation.* Leoben: Montanuniversität Leoben.

Sifferlinger, N. A., Hartlieb, P. & Moser, P., 2017. The Importance of Research on Alternative and Hybrid Rock Extraction Methods. *BHM Berg- und Hüttenmännische Monatshefte*, 162(2), p. 58–66.

Steven, S., 1955. The Measurement of Loudness. *The Journal of the Acoustical Society of America*, 27(5), pp. 815-829..

Truax, B., 1984 . *Acoustic Communication.* 1 ed. Burnaby, British Columbia, Canada: Ablex Publishing Corporation .

UNSW, Wolfe, J., Hatsidimitris, G., Smith, J & UNSW, School of Physics, PHYSCLIPS, 1991. *dB: What is a decibel?.* [Online]
Available at: <https://www.animations.physics.unsw.edu.au/jw/dB.htm#logs>
[Accessed 25 11 2021].

Villaescusa, ., 1998. *Geotechnical design for dilution control in underground mining. Mine Planning and Equipment Selection..* [Online]
Available at:
https://www.researchgate.net/publication/237618005_Geotechnical_design_for_dilution_cont

rol in underground mining

[Accessed 12 2021].

Volk, H.-J., 2016. Wirtgen drives the development of surface mining. *Procedia Engineering*, 138(2016), p. 30 – 39.

Wang, X., Su, O., Wang, Q.-F. & Liang, Y.-P., 2017. Effect of cutting depth and line spacing on the cuttability behavior of sandstones by conical picks. *Arabian Journal of Geosciences*, Volume 10, pp. 525 (1-13).

Wang, X. et al., 2018. Dominant Cutting Parameters Affecting the Specific Energy of Selected Sandstones when Using Conical Picks and the Development of Empirical Prediction Models. *Rock Mechanics and Rock Engineering*, Volume 51, pp. 3111-3128.

Williams, E. & Hagan, P., 2006. *Observations on the Variation in Acoustic Emissioins with Changes in Rock Cutting Conditioins*. Wollongong, Research Online, University of Wollongong, pp. 93-103.

Yasar, S., 2020. A General Semi-Theoretical Model for Conical Picks. *Rock Mechanics and Rock Engineering*, Issue 53, pp. 2557-2579.

Yasar, S. & Yilmaz, A. O., 2017. Rock Cutting Tests with a Simple-Shaped Chisel Pick to Provide. *Rock Mech Rock Eng*, Volume 50, pp. 3261-3269.

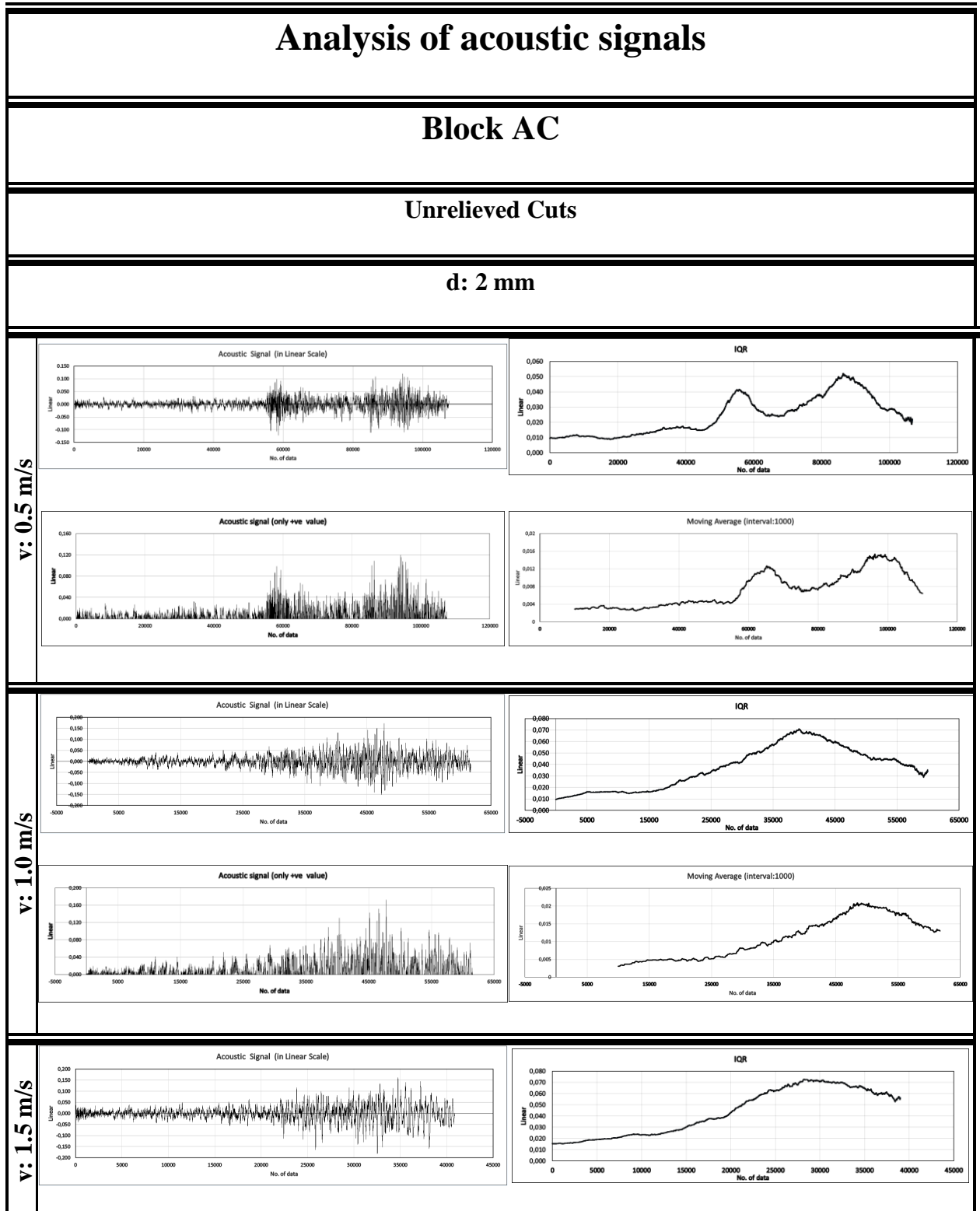
Yasar, S. & Yilmaz, A. O., 2018. Drag pick cutting tests: A comparison between experimental and theoretical resutls. *Journal of Rock Mechanics and Geotechnical Engineering*, 10(5), pp. 893-906.

Zhu, C., Huang, H. & Liu, H., 2014. *International Gear Conference 2014: On-line vibration monitoring and diagnosing of a multi-megawatt wind turbine gearbox*. Lyon, Chandos.

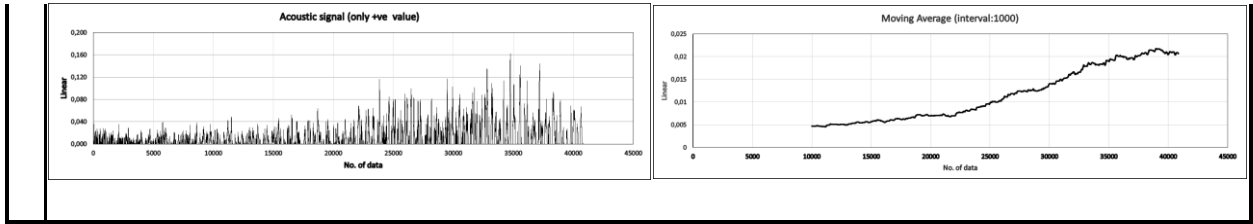
7 Appendices

7.1 Appendices AE Data

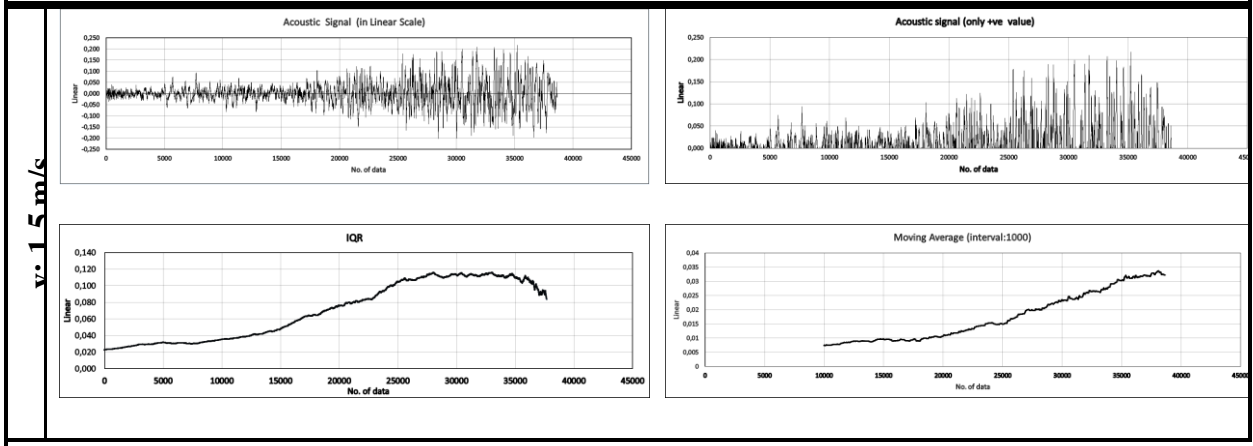
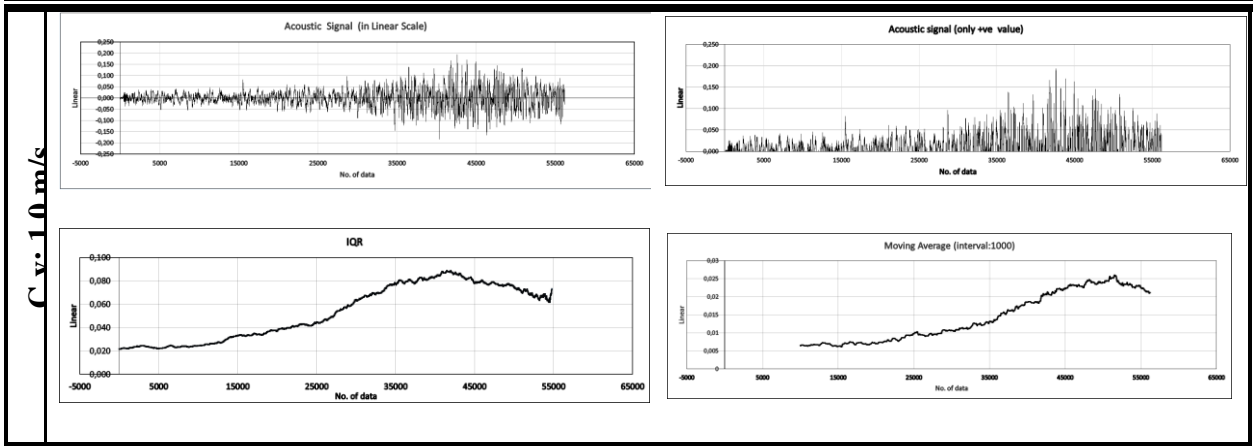
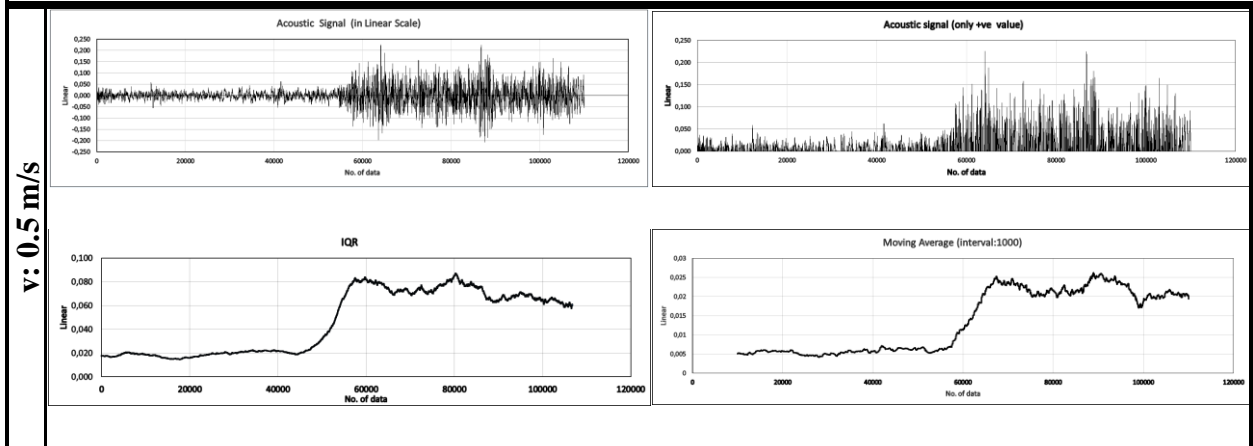
7.1.1 AE Signals Analysis



Appendices

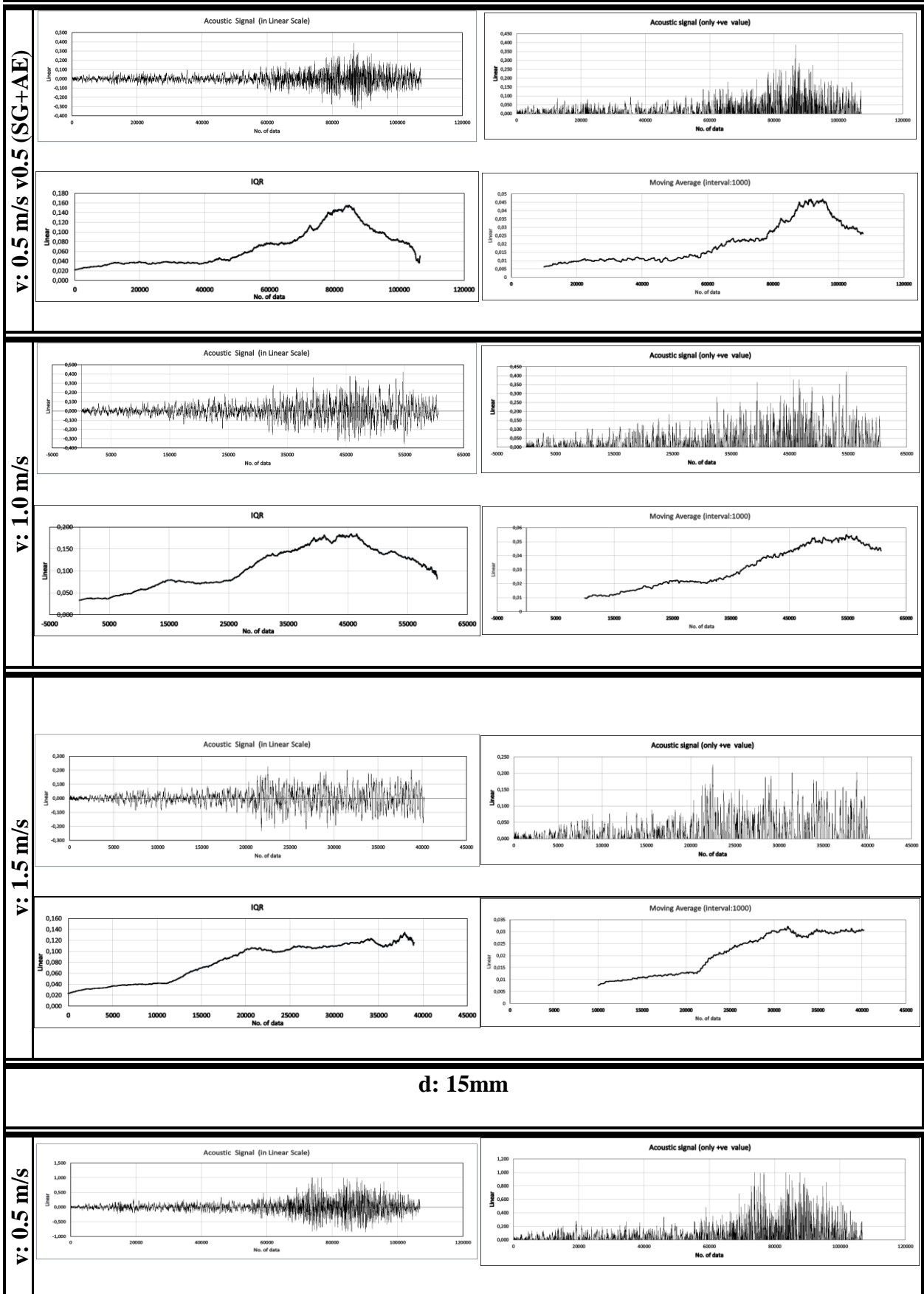


d: 5mm

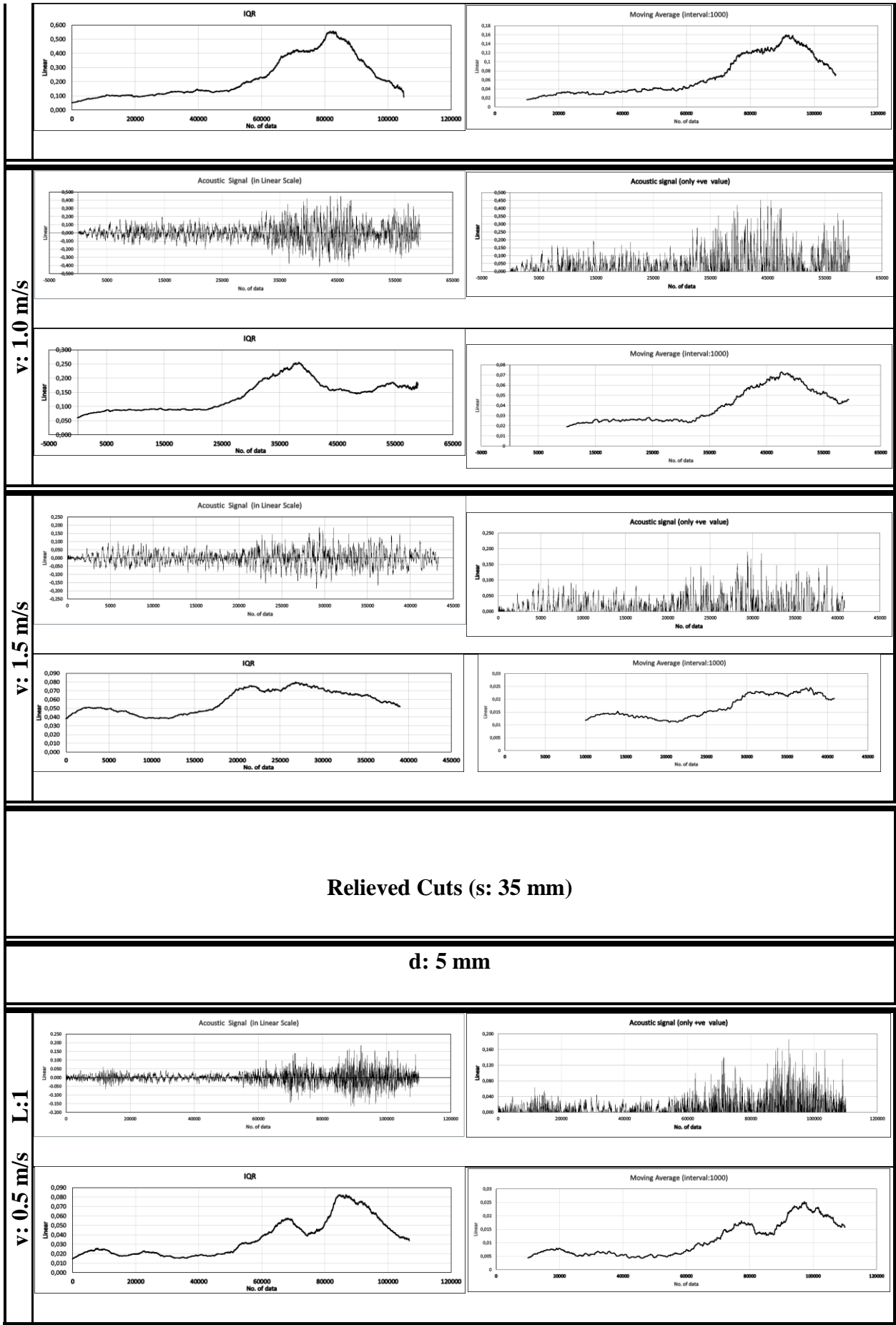


d: 10mm

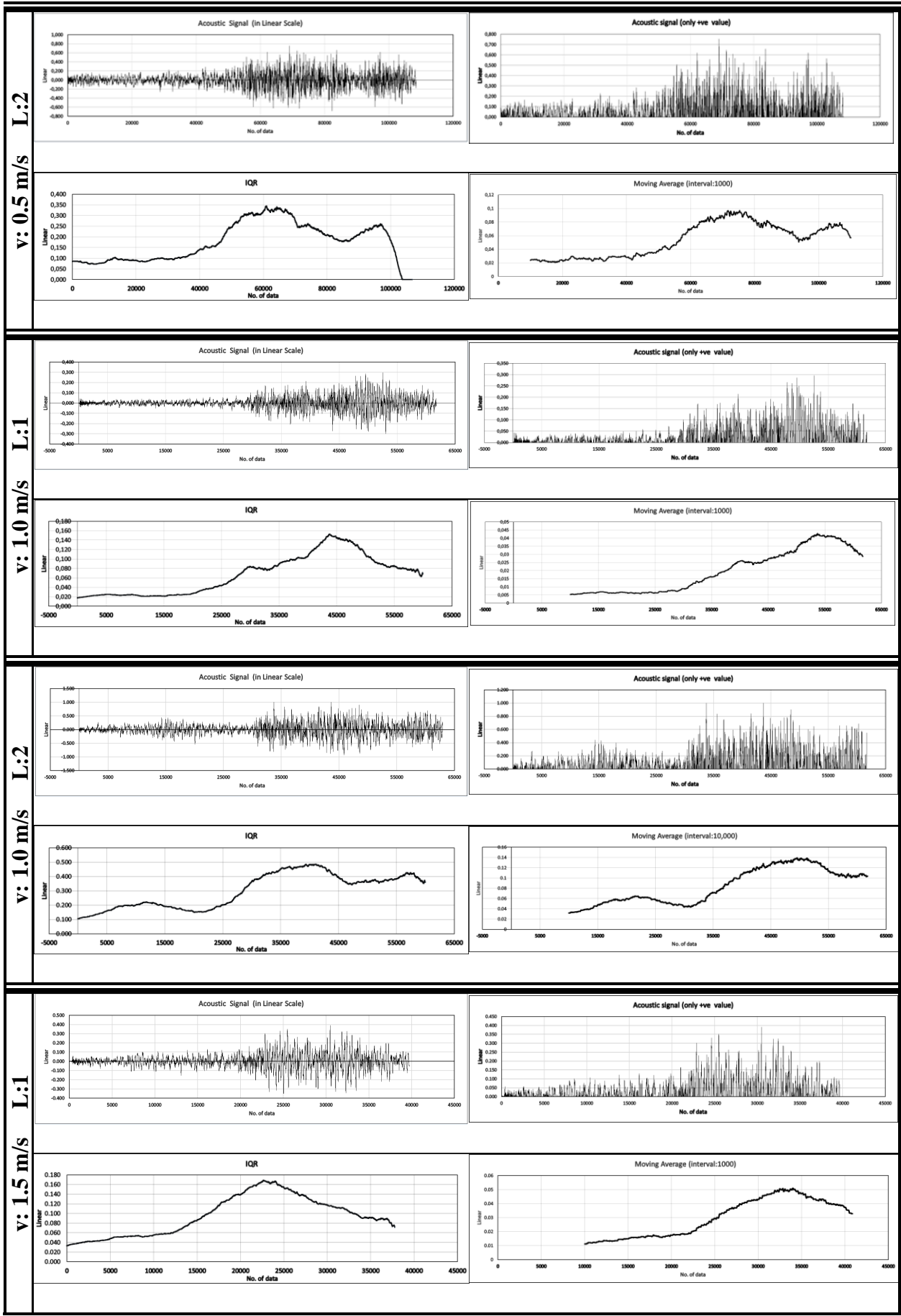
Appendices



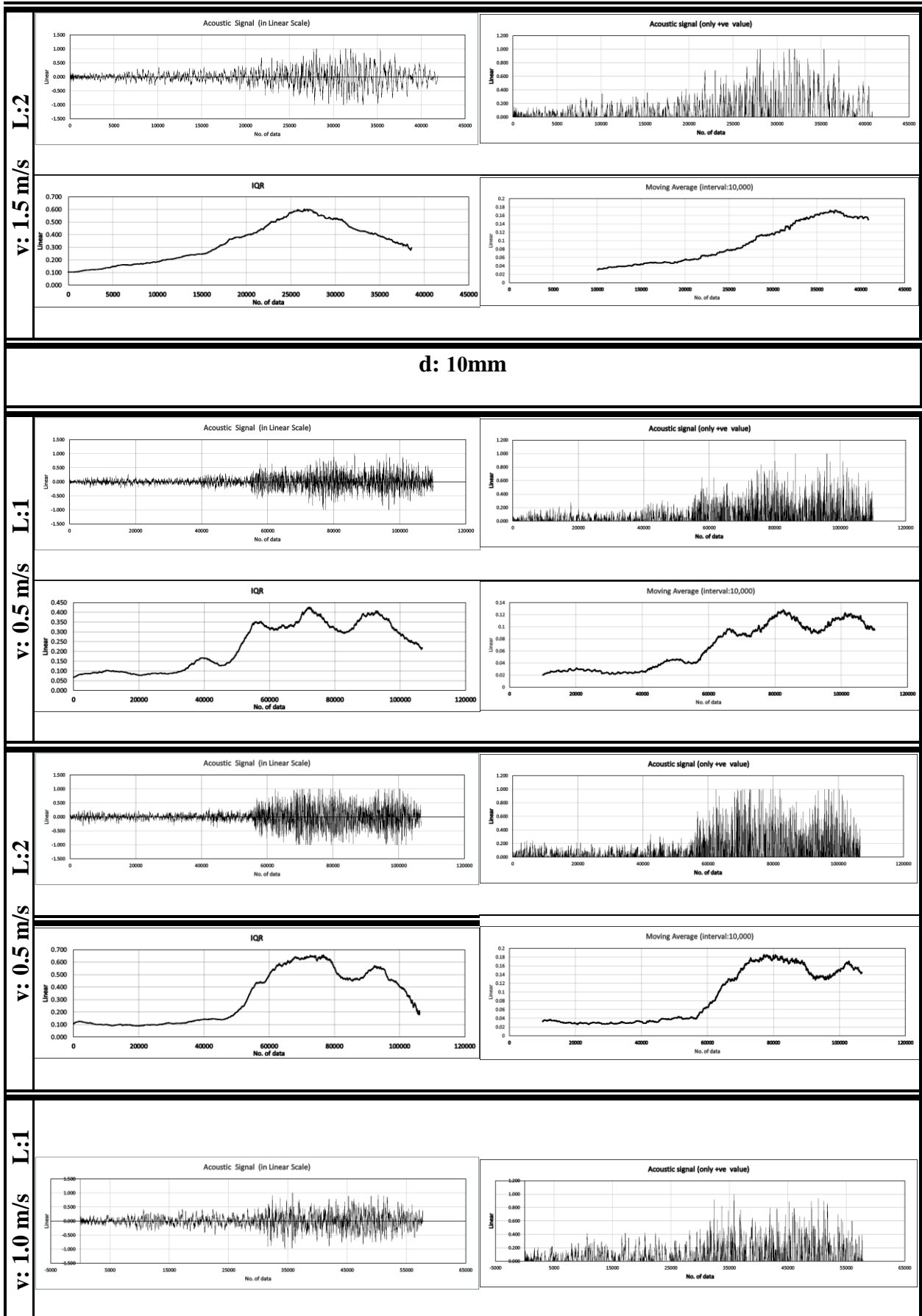
Appendices



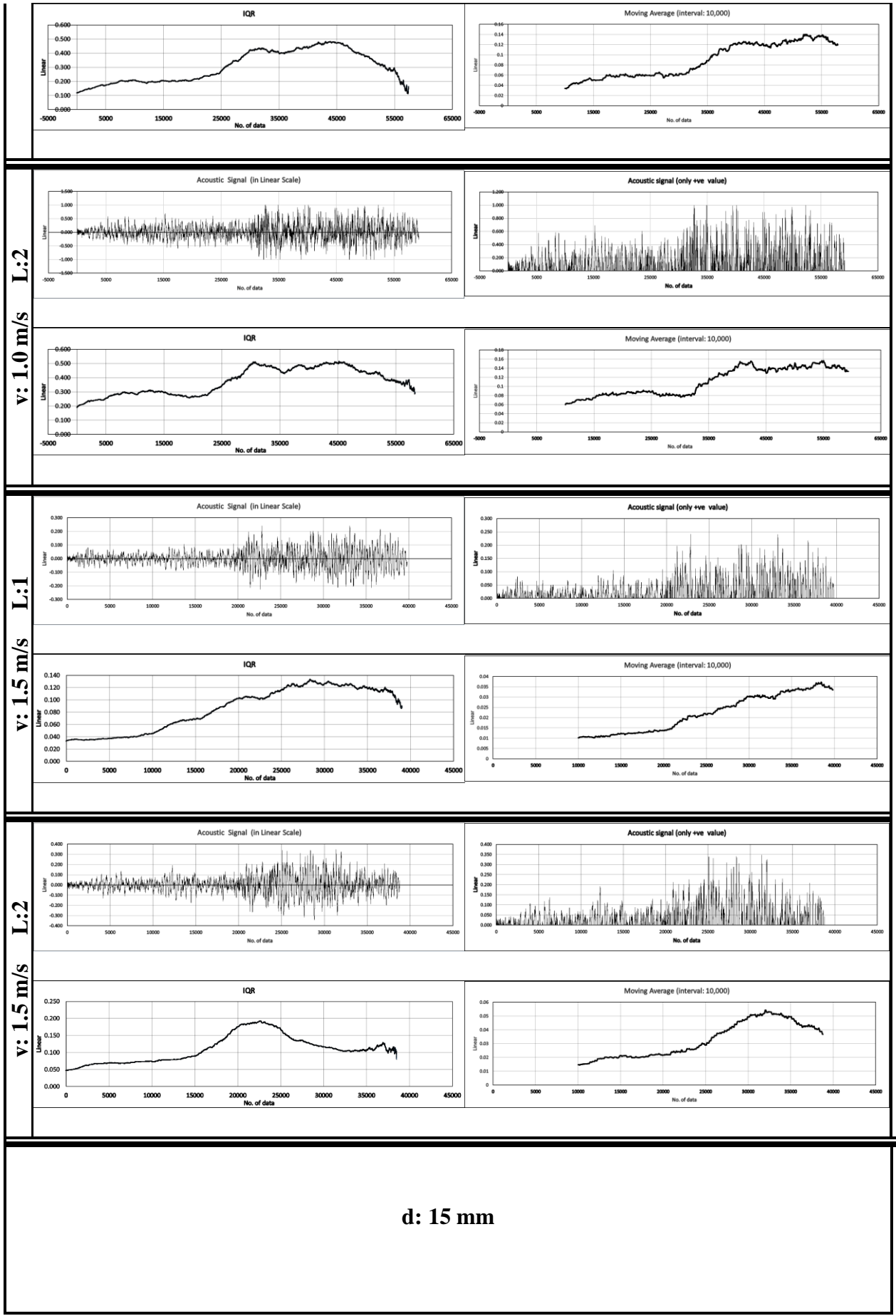
Appendices

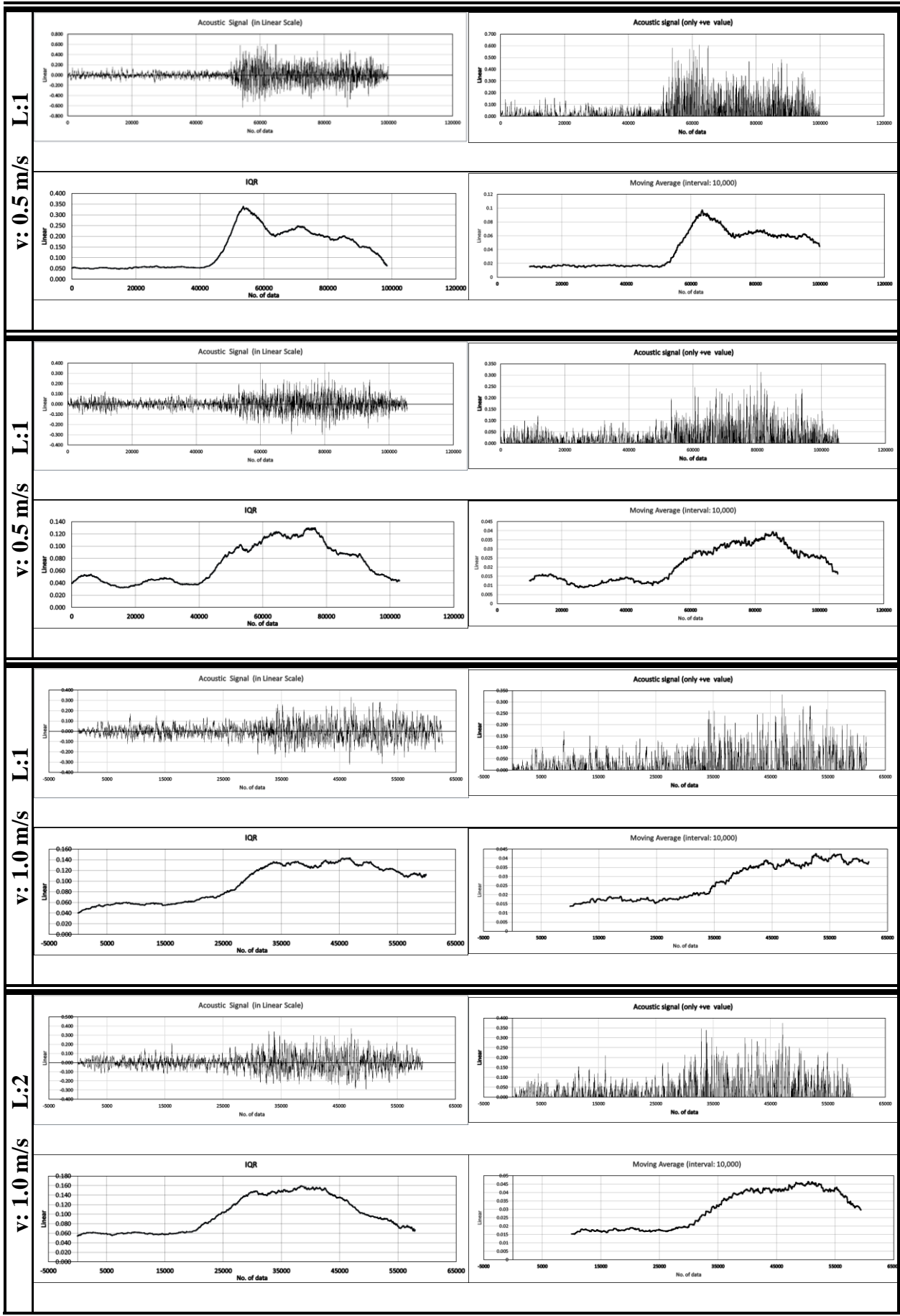


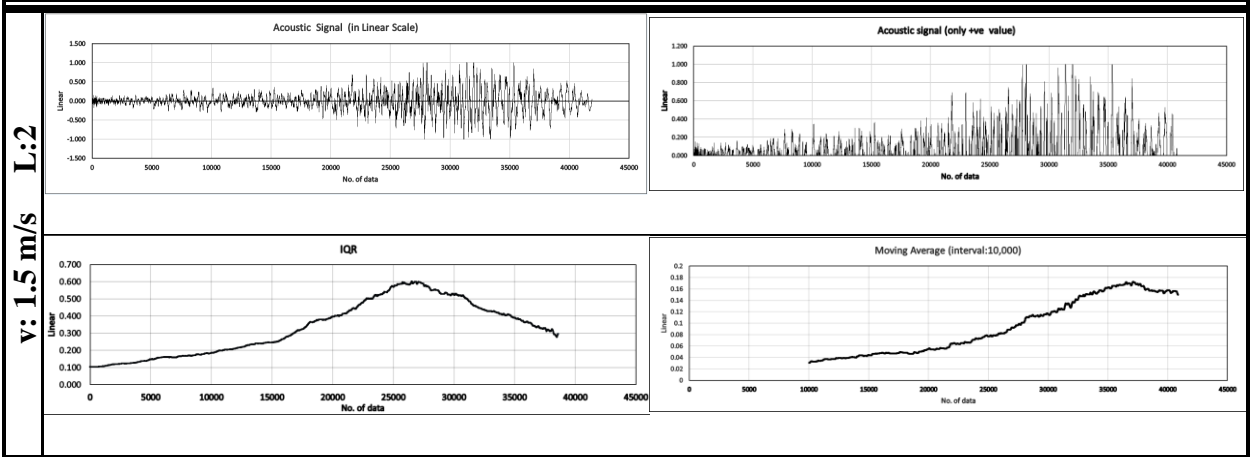
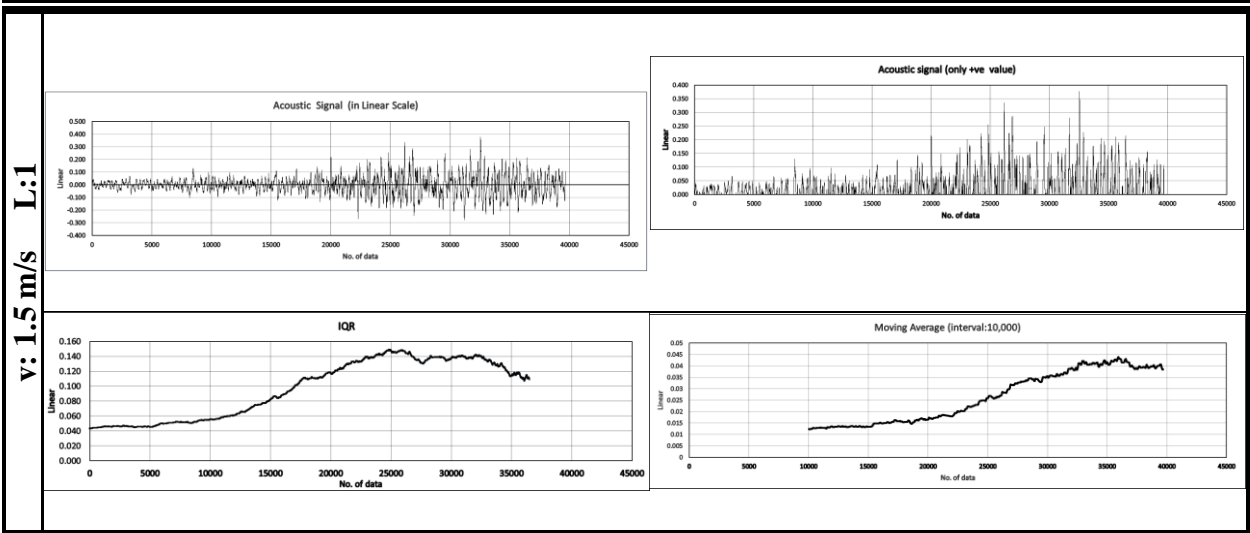
Appendices



Appendices



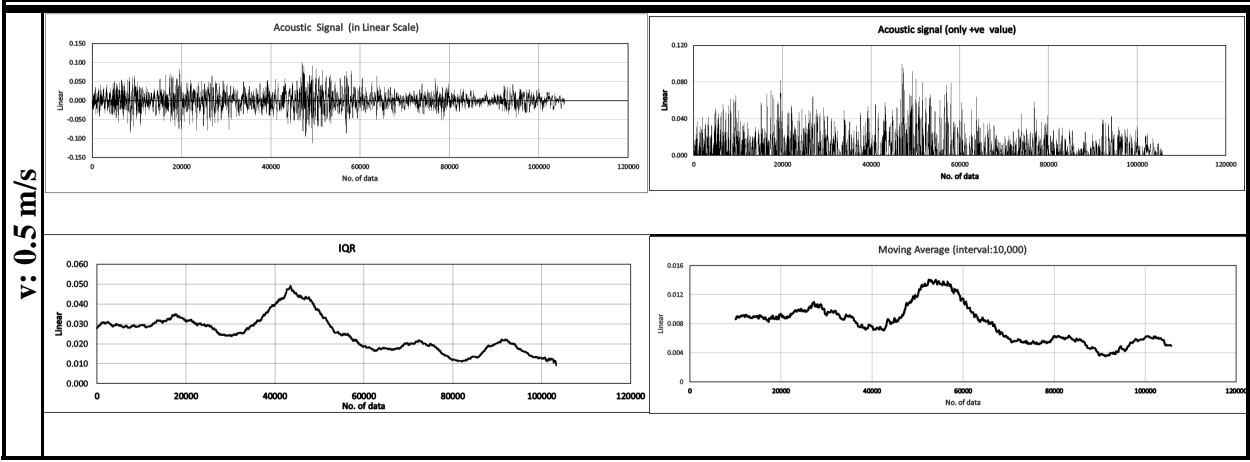




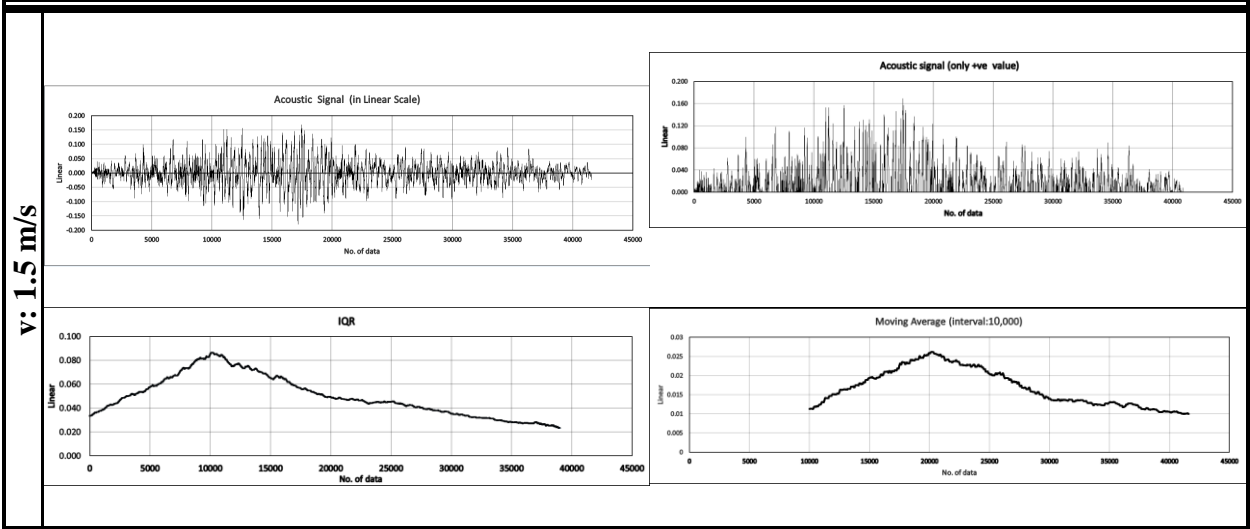
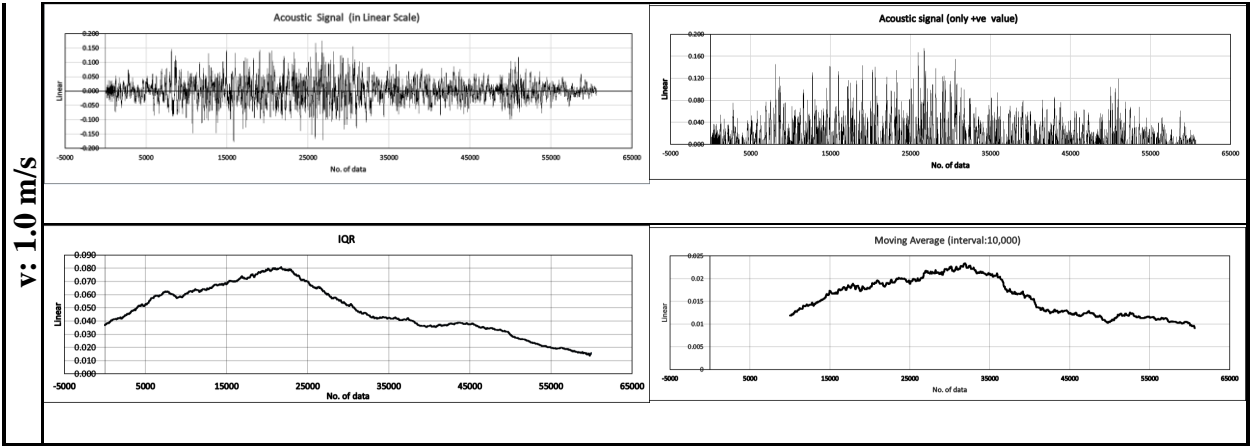
Block CB

Unrelieved

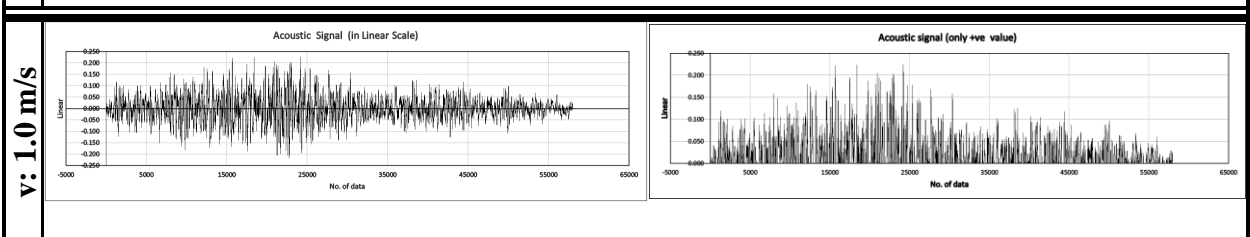
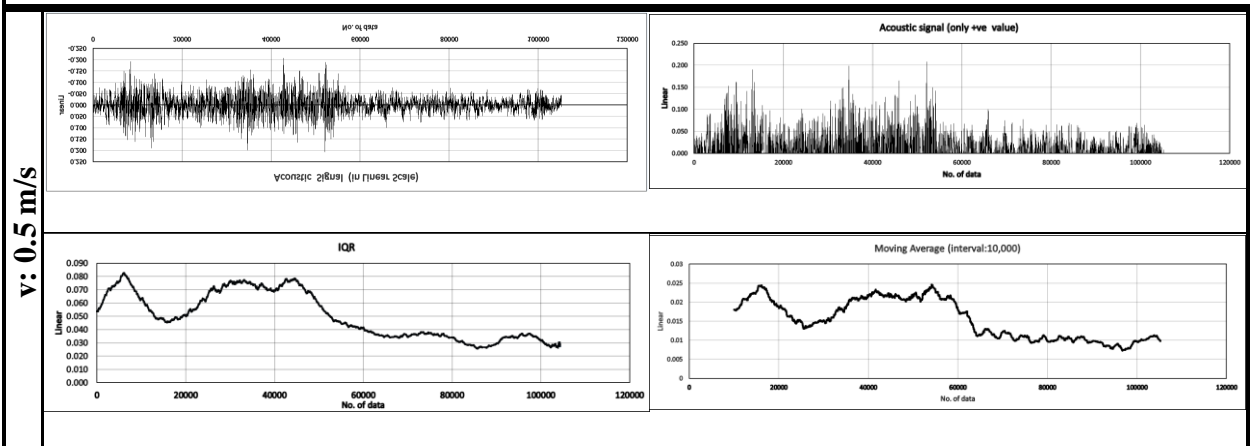
d: 2mm



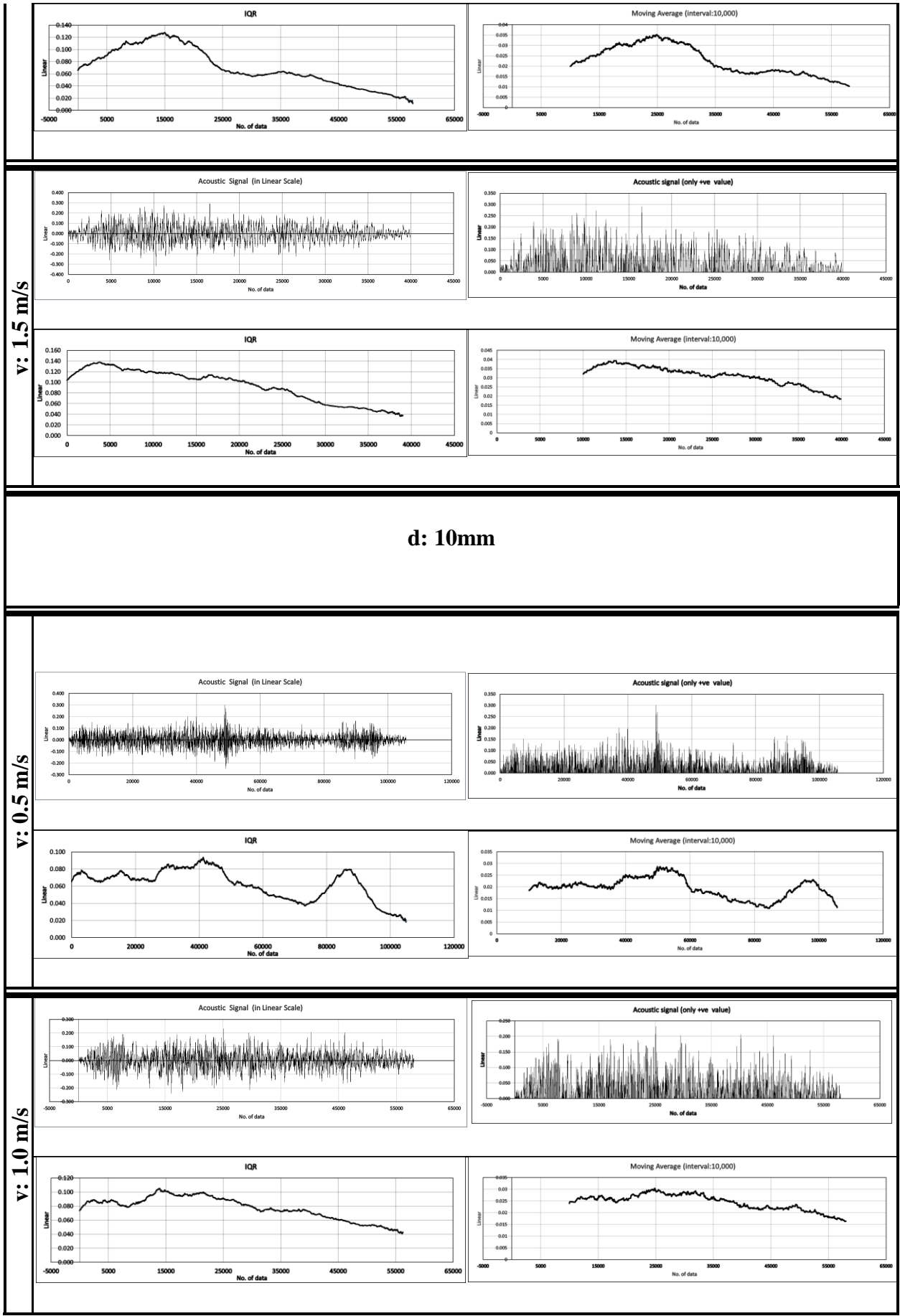
Appendices



d: 5mm

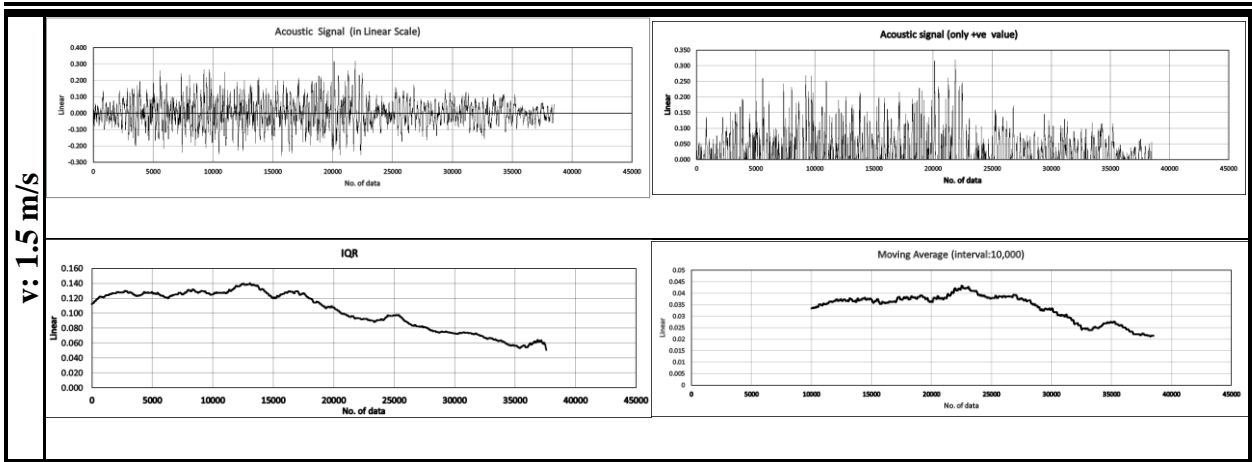


Appendices

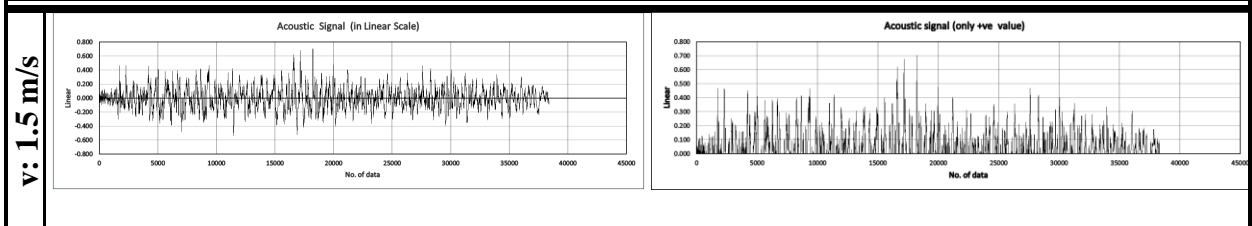
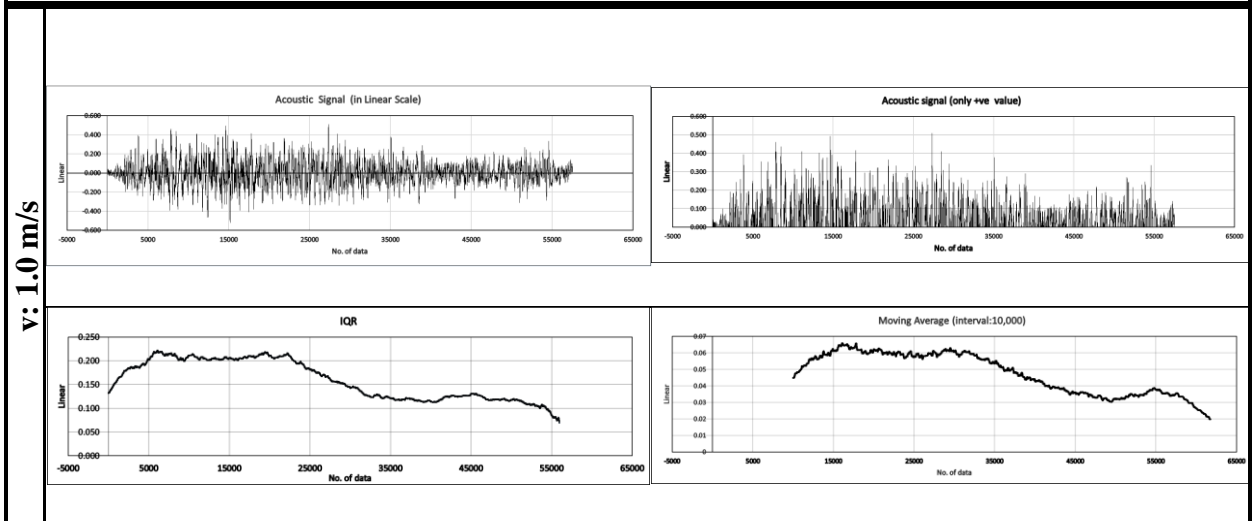
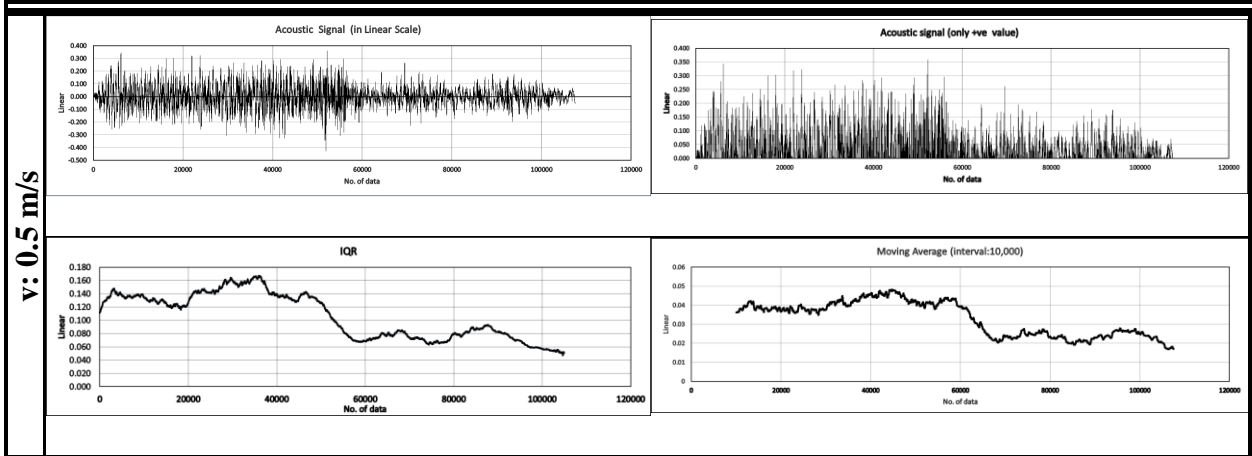


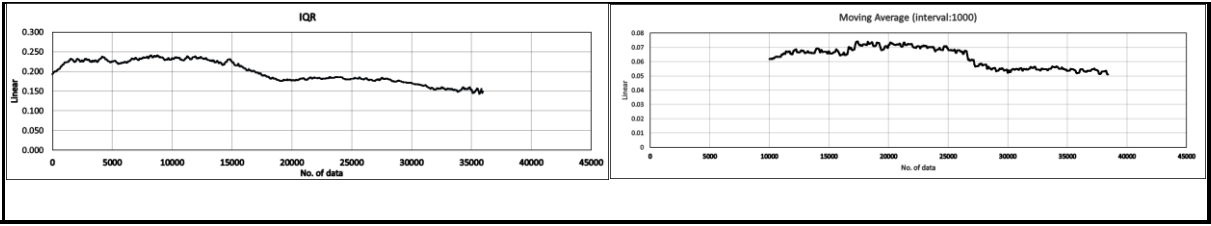
d: 10mm

Appendices



d: 15mm

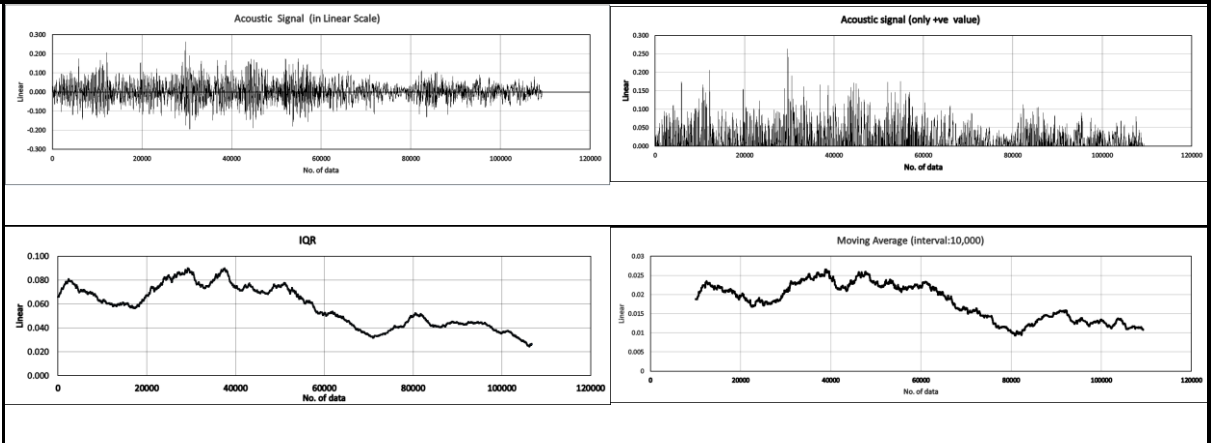




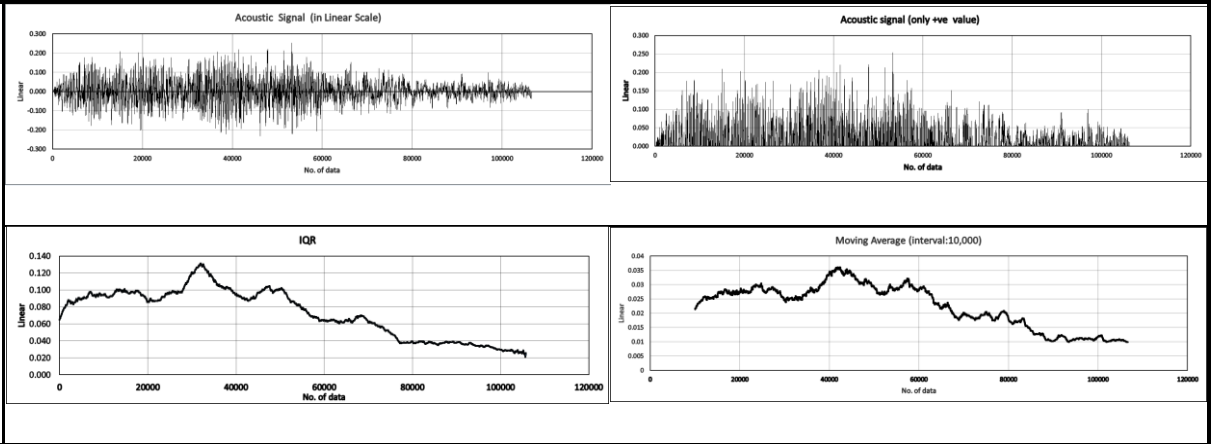
Relieved (s: 35mm)

d: 5mm

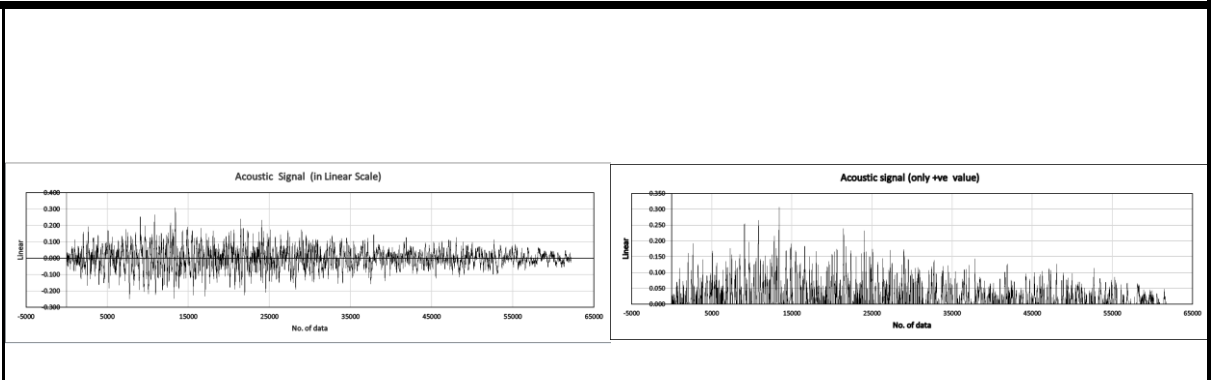
v: 0.5 m/s L:1



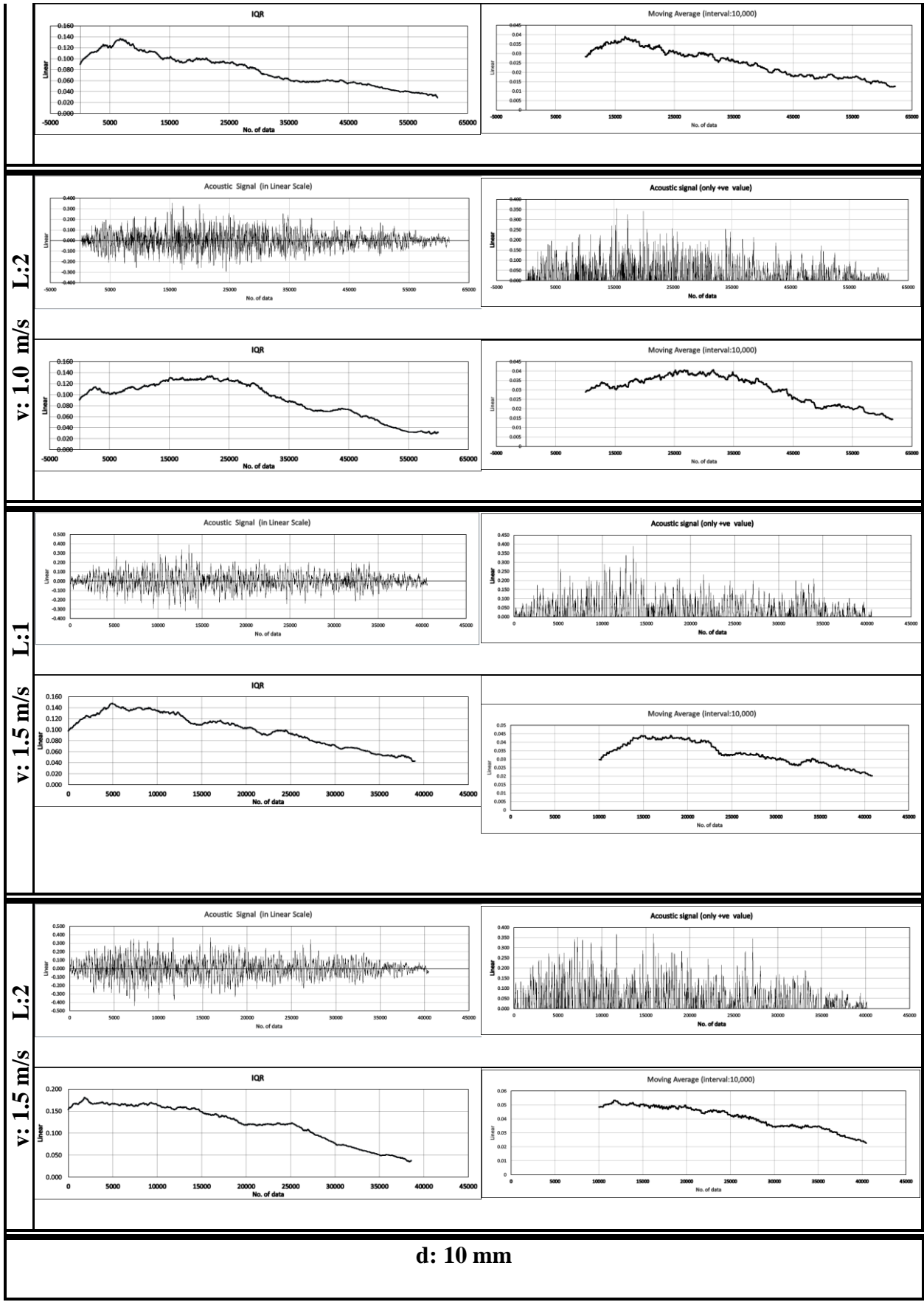
v: 0.5 m/s L:2

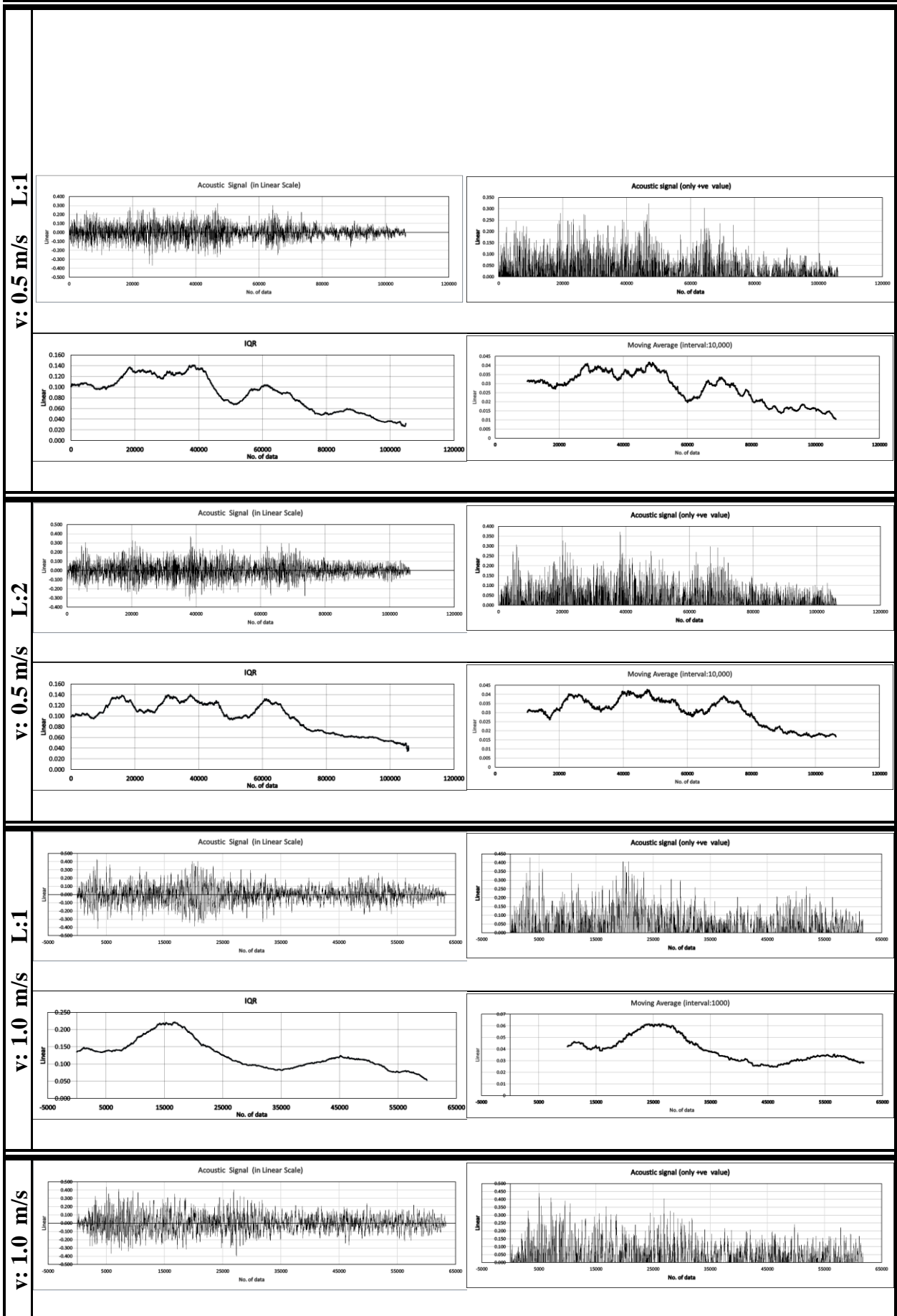


v: 1.0 m/s L:1

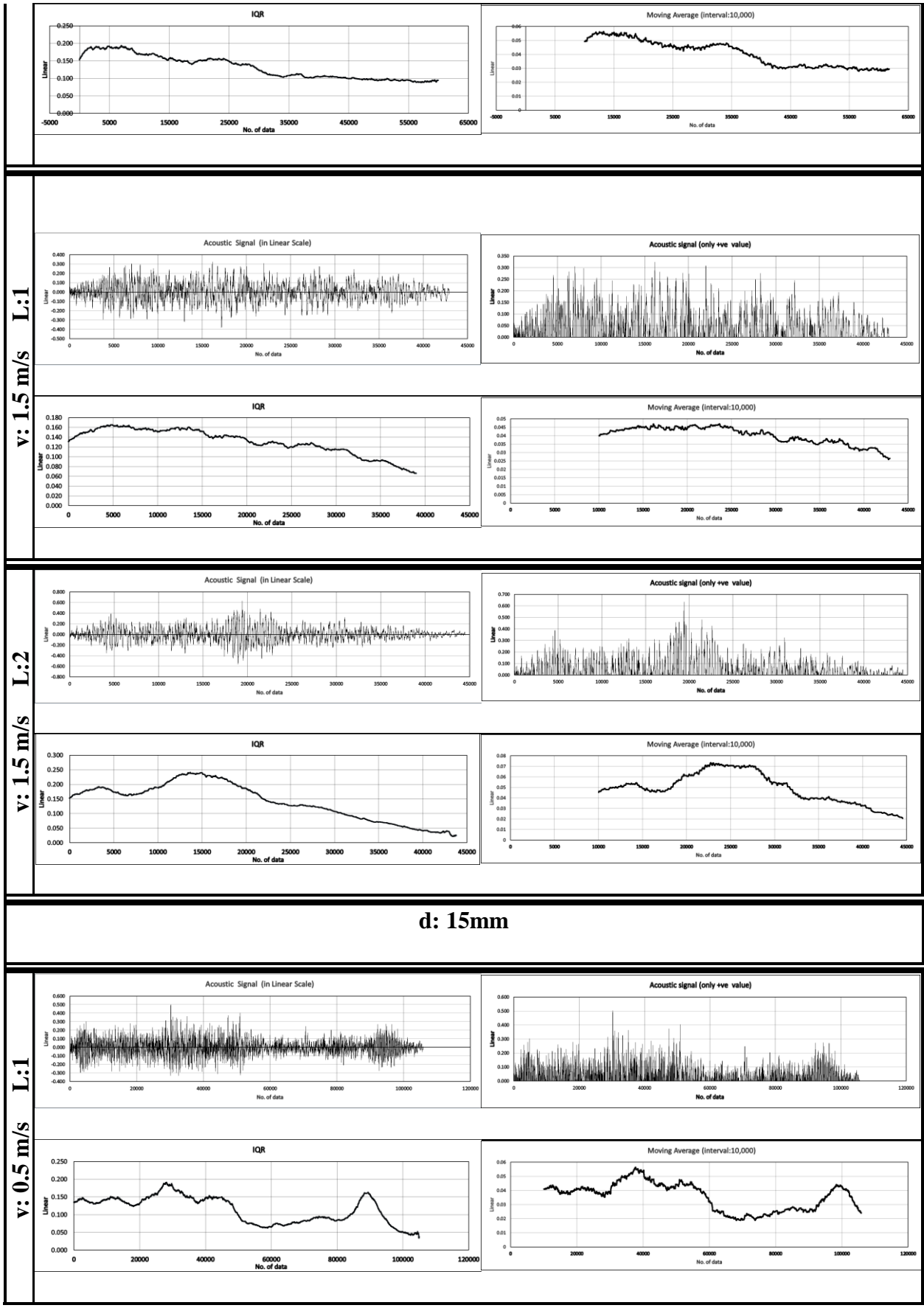


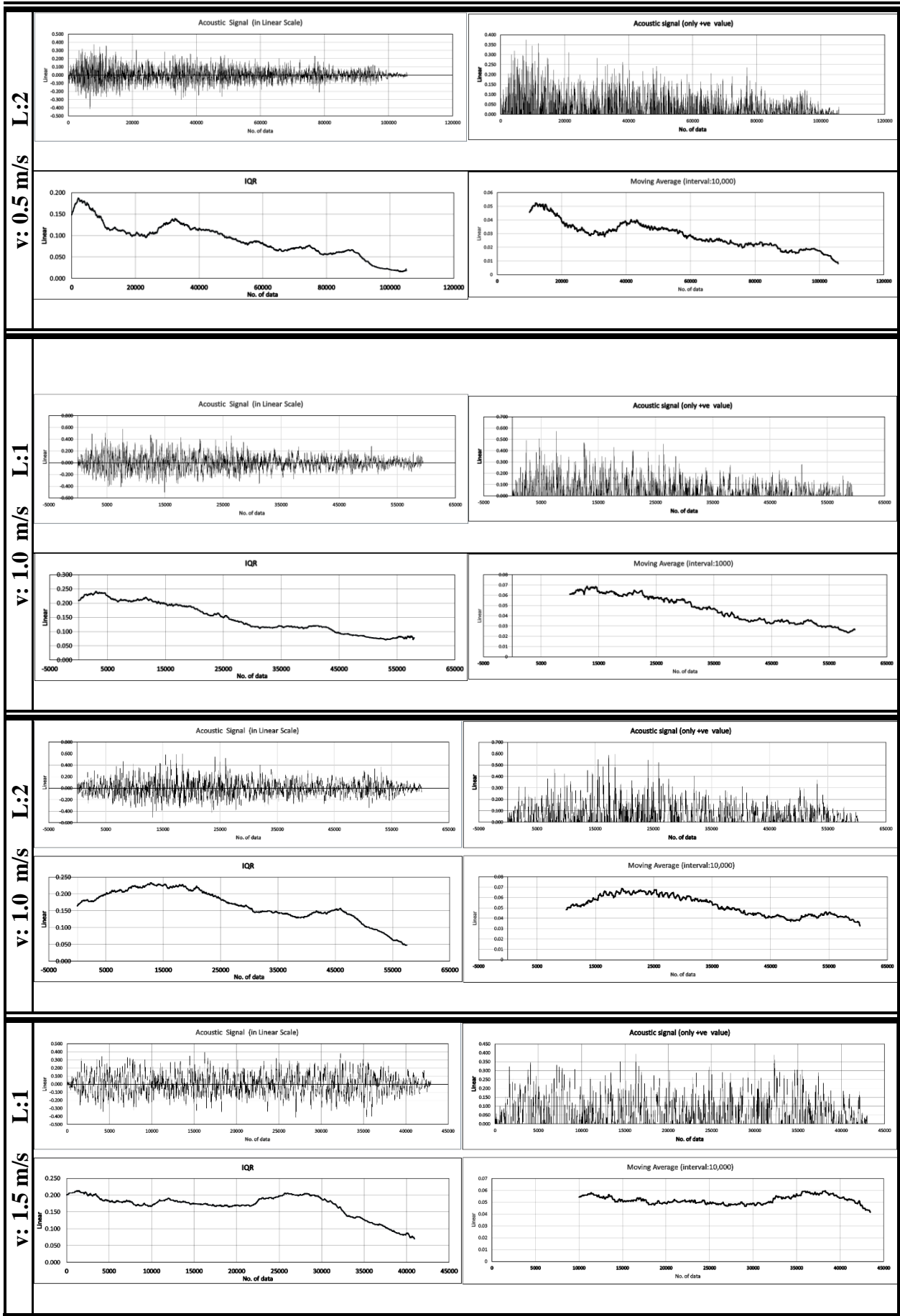
Appendices

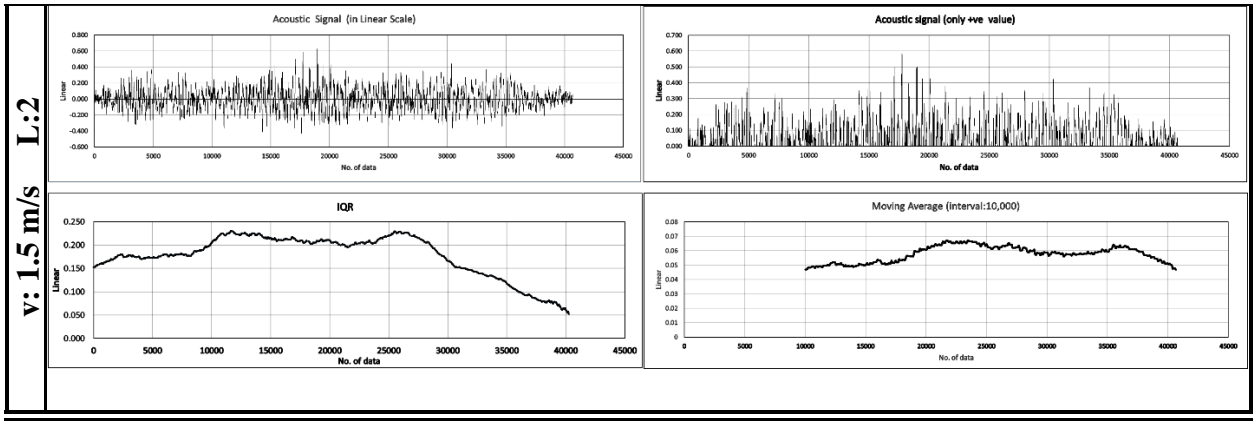




Appendices




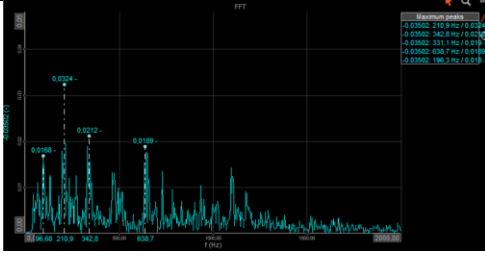
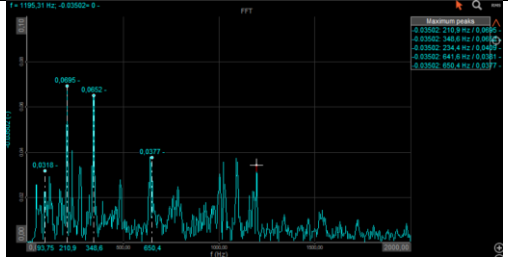

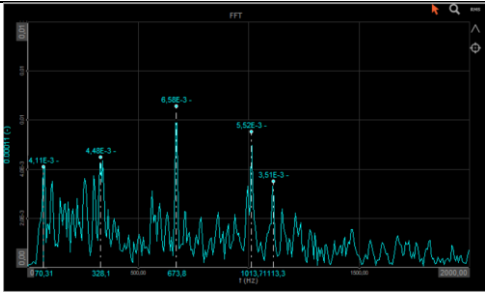
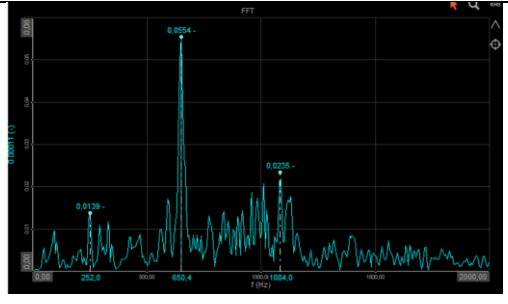

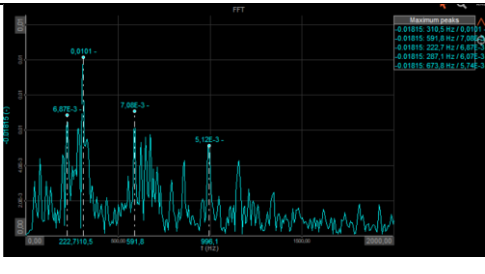
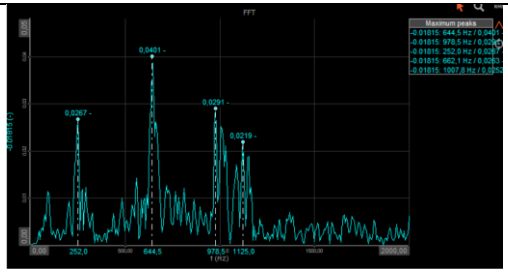

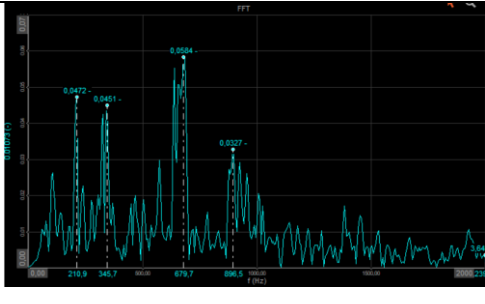
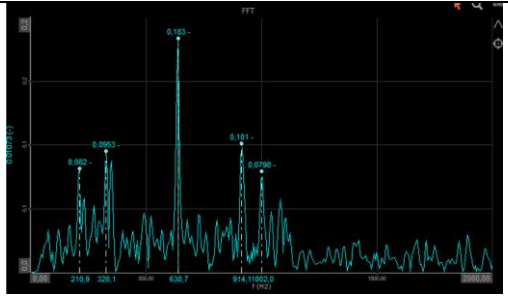

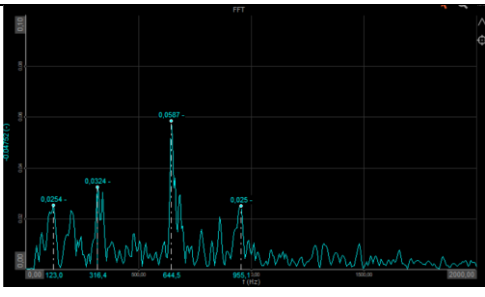
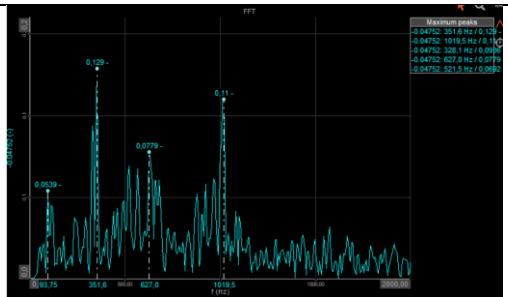

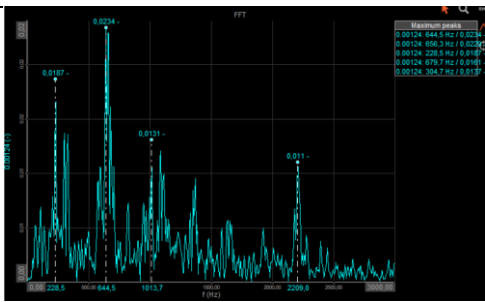
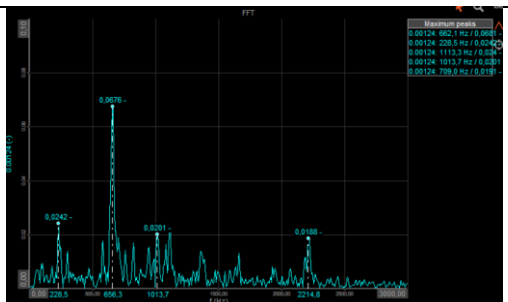




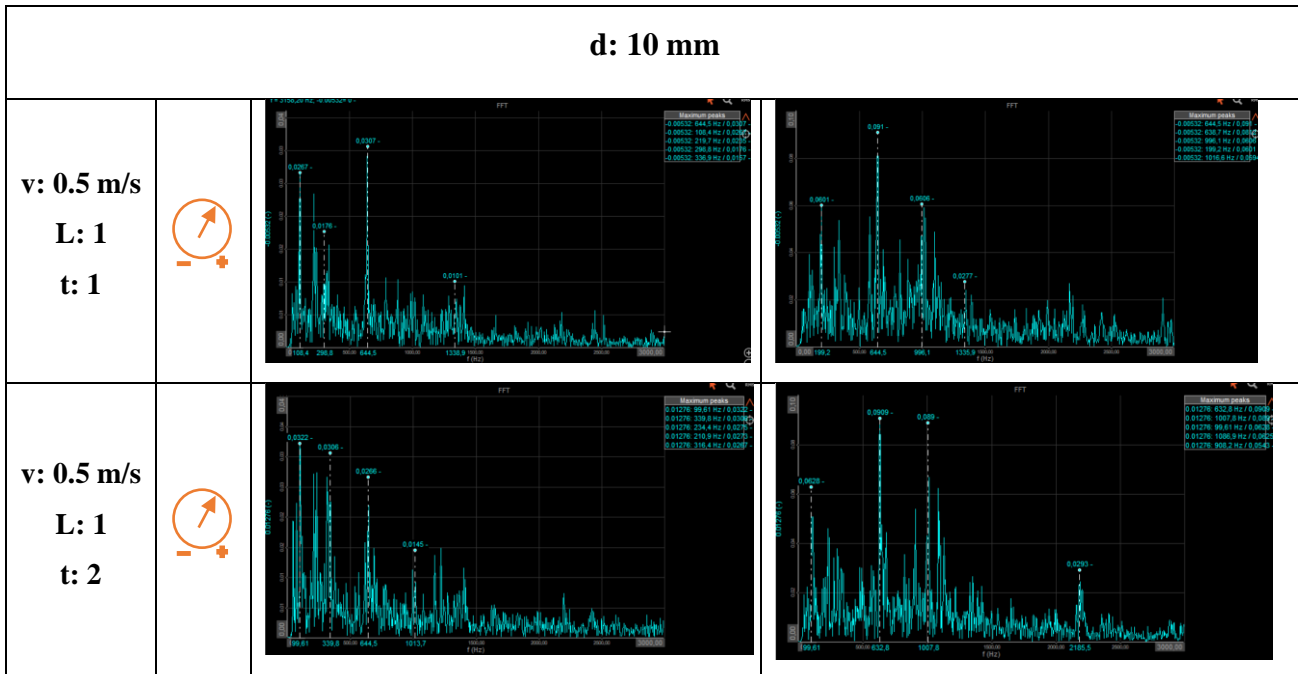
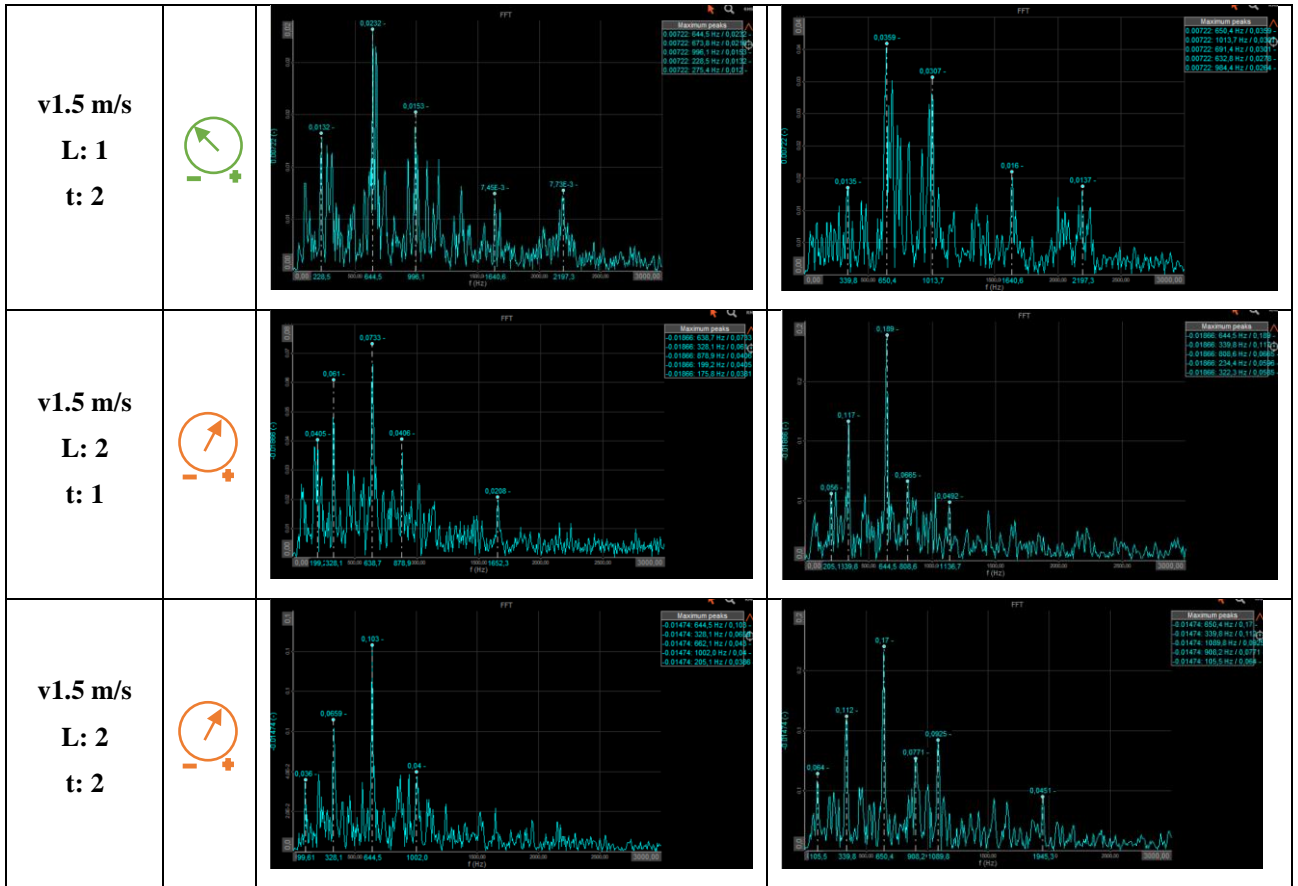
7.1.2 FFT Analysis of AE Signals

| FFT Analysis of AE Signals | | | |
|----------------------------|------|---------|---------|
| Block "AC" | | | |
| Relieved (s: 35mm) | | | |
| d: 5mm | | | |
| Name | gain | Block A | Block C |
| v: 0.5 m/s L: 1 t: 1 | | | |
| v: 0.5 m/s L: 1 t: 2 | | | |
| v: 0.5 m/s L: 2 t: 1 | | | |


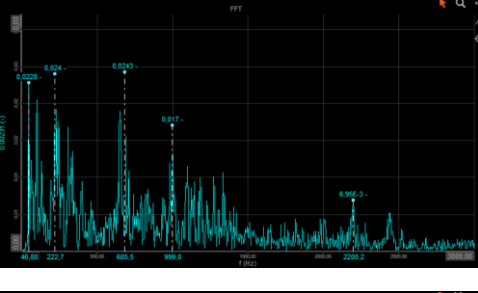
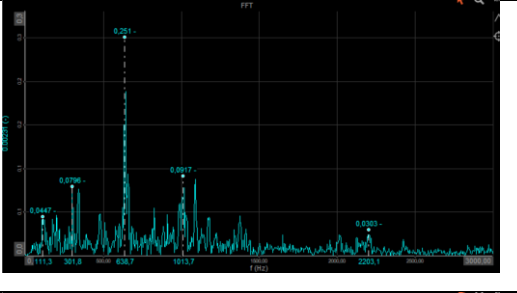

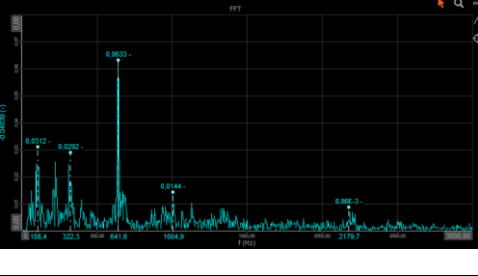
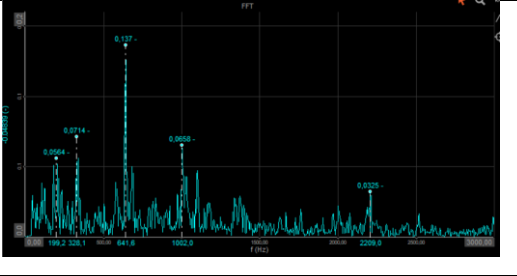

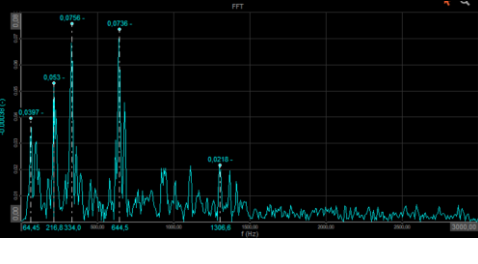
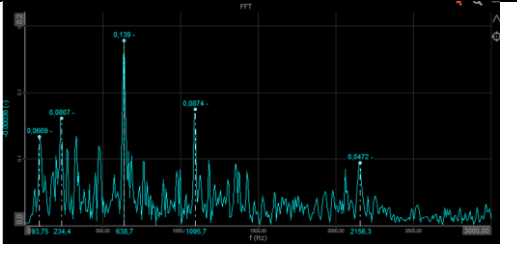

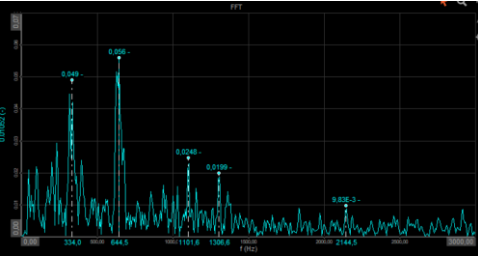
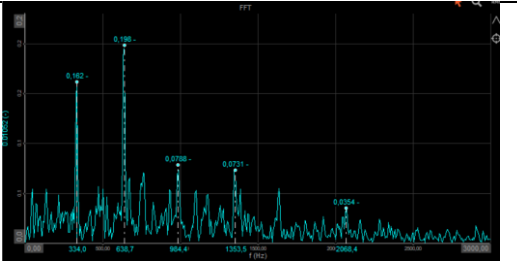

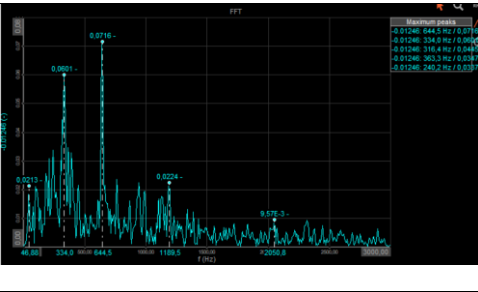
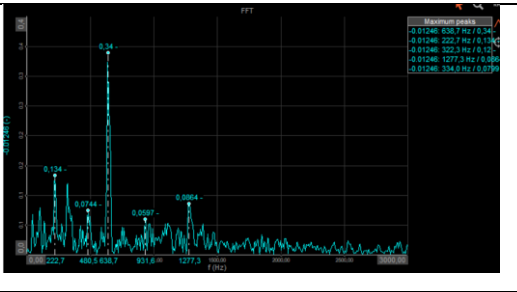

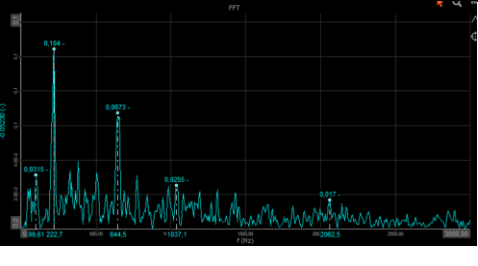
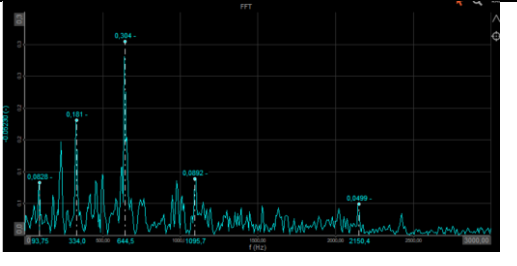
Appendices

| | | | |
|-------------------------------------|---|---|--|
| <p>v: 0.5 m/s L: 2 t: 2</p> |  |  |  |
| <p>v1.0 m/s L: 1 t: 1</p> |  |  |  |
| <p>v1.0 m/s L: 1 t: 2</p> |  |  |  |
| <p>v1.0 m/s L: 2 t: 1</p> |  |  |  |
| <p>v1.0 m/s L: 1 t: 2</p> |  |  |  |
| <p>v1.5 m/s L: 1 t: 1</p> |  |  |  |


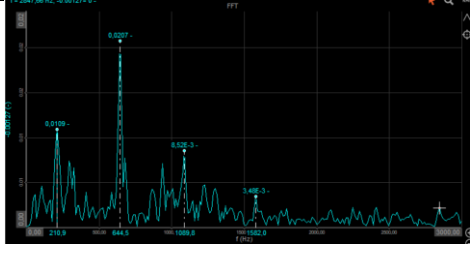
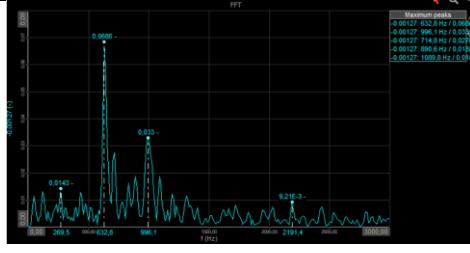

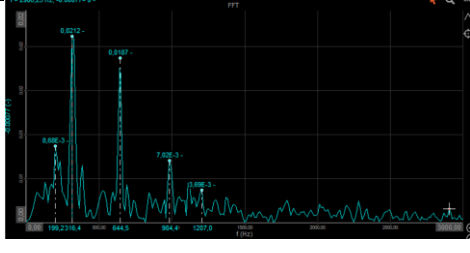
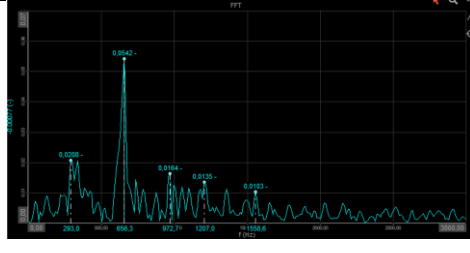

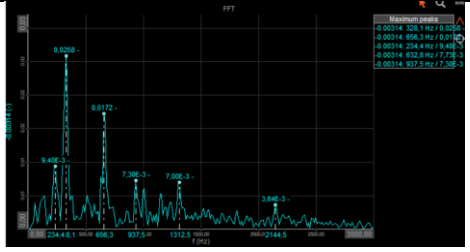
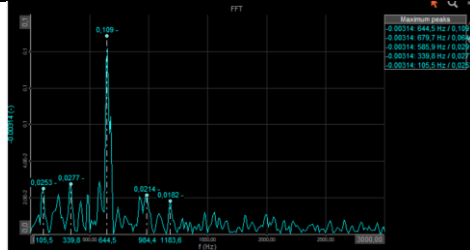

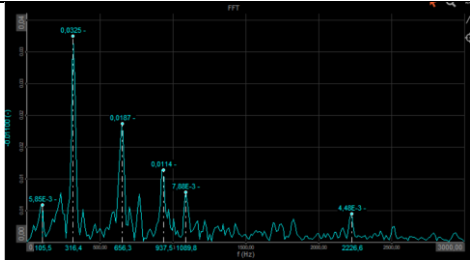
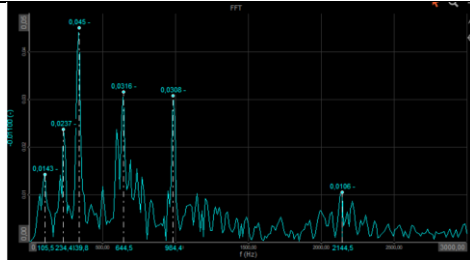

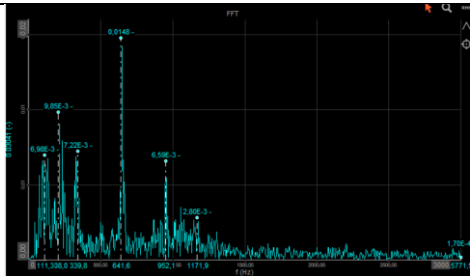
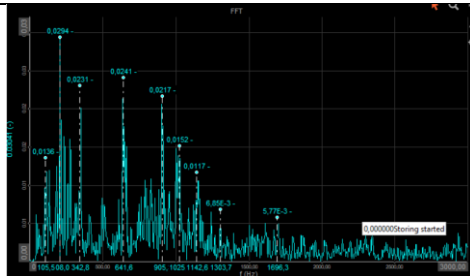

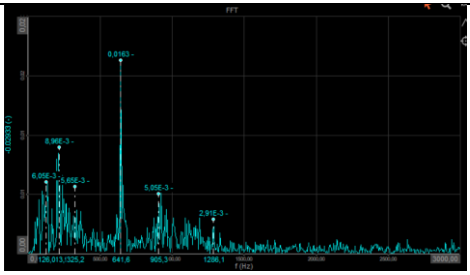
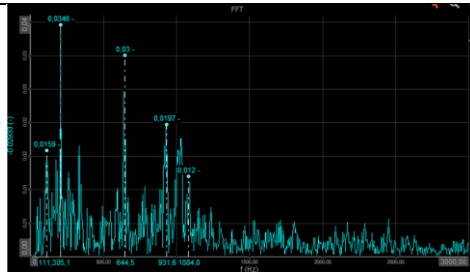
Appendices



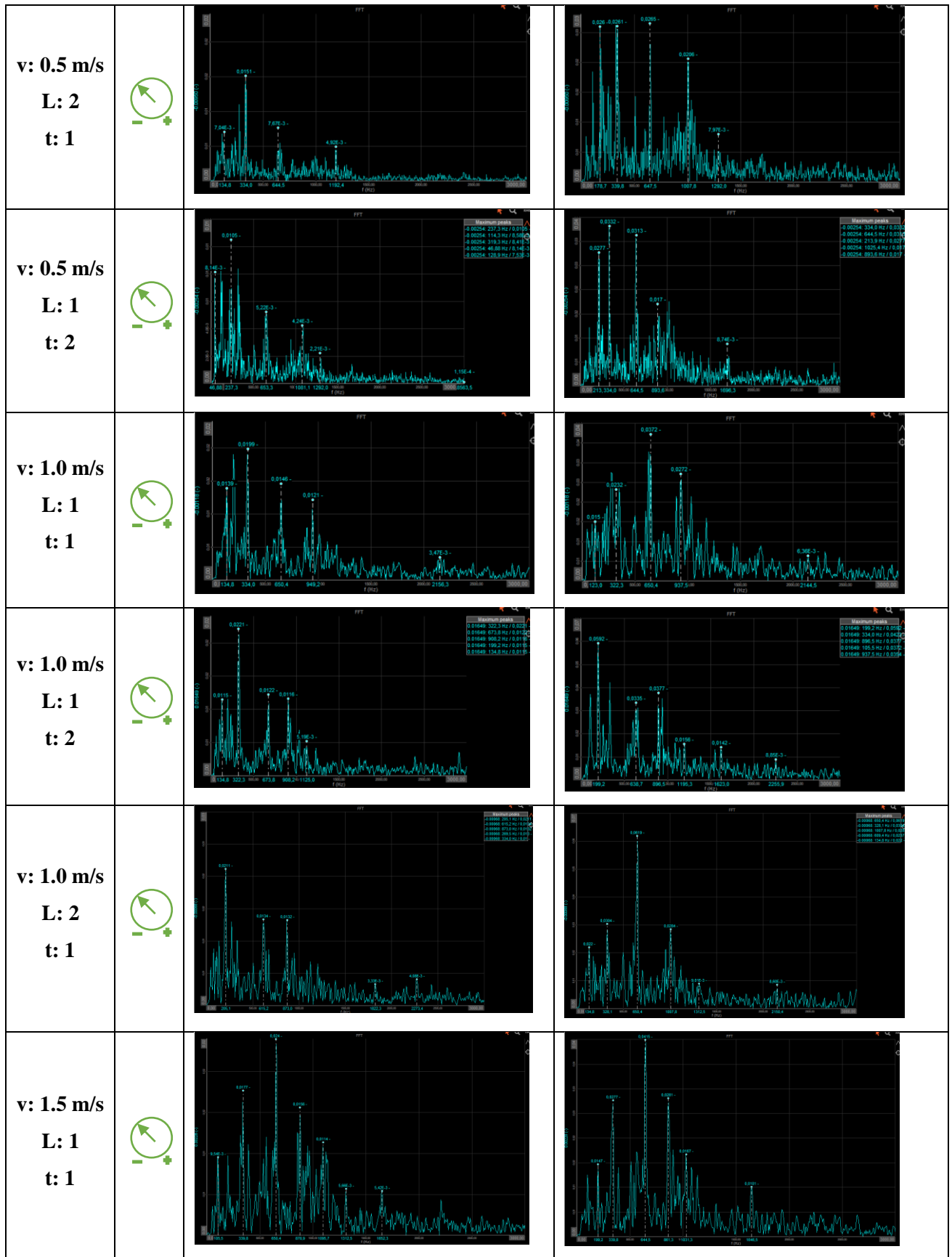
Appendices

| | | | |
|---|---|---|--|
| <p>v: 0.5 m/s L: 2 t: 1</p> |  |  |  |
| <p>v: 0.5 m/s L: 2 t: 2</p> |  |  |  |
| <p>v: 1.0 m/s L: 1 t: 1</p> |  |  |  |
| <p>v: 1.0 m/s L: 1 t: 2</p> |  |  |  |
| <p>v: 1.0 m/s L: 2 t: 3 close to mic</p> |  |  |  |
| <p>v: 1.0 m/s L: 2 t: 4 closer to mic</p> |  |  |  |

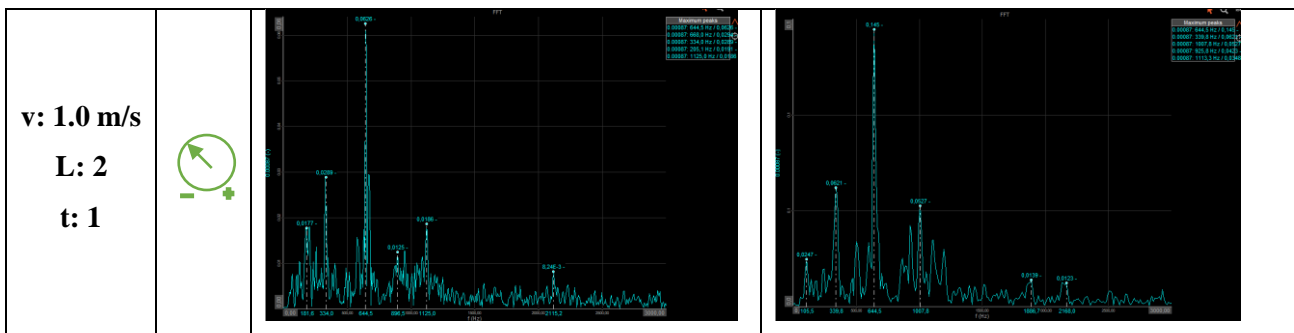
Appendices

| | | | |
|---|---|---|--|
| <p>v: 1.5 m/s L: 1 t: 1</p> |  |  |  |
| <p>v: 1.5 m/s L: 1 t: 2</p> |  |  |  |
| <p>v: 1.5 m/s L: 2 t: 3 close to mic.</p> |  |  |  |
| <p>v: 1.5 m/s L: 2 t: 4 closer to mic</p> |  |  |  |
| <p>d: 15 mm</p> | | | |
| <p>v: 0.5 m/s L: 1 t: 3</p> |  |  |  |
| <p>v: 0.5 m/s L: 1 t: 4</p> |  |  |  |

Appendices



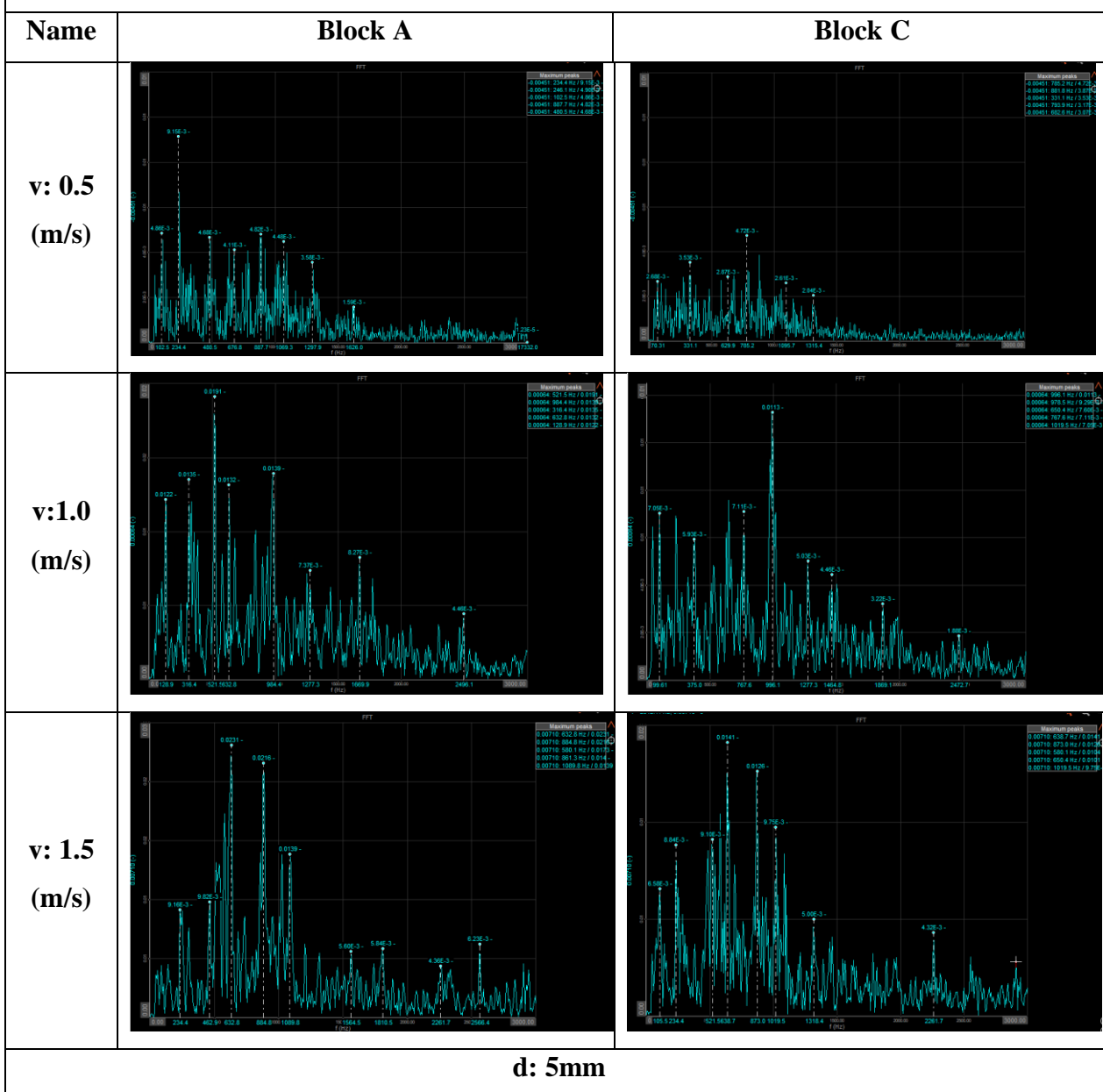
Appendices



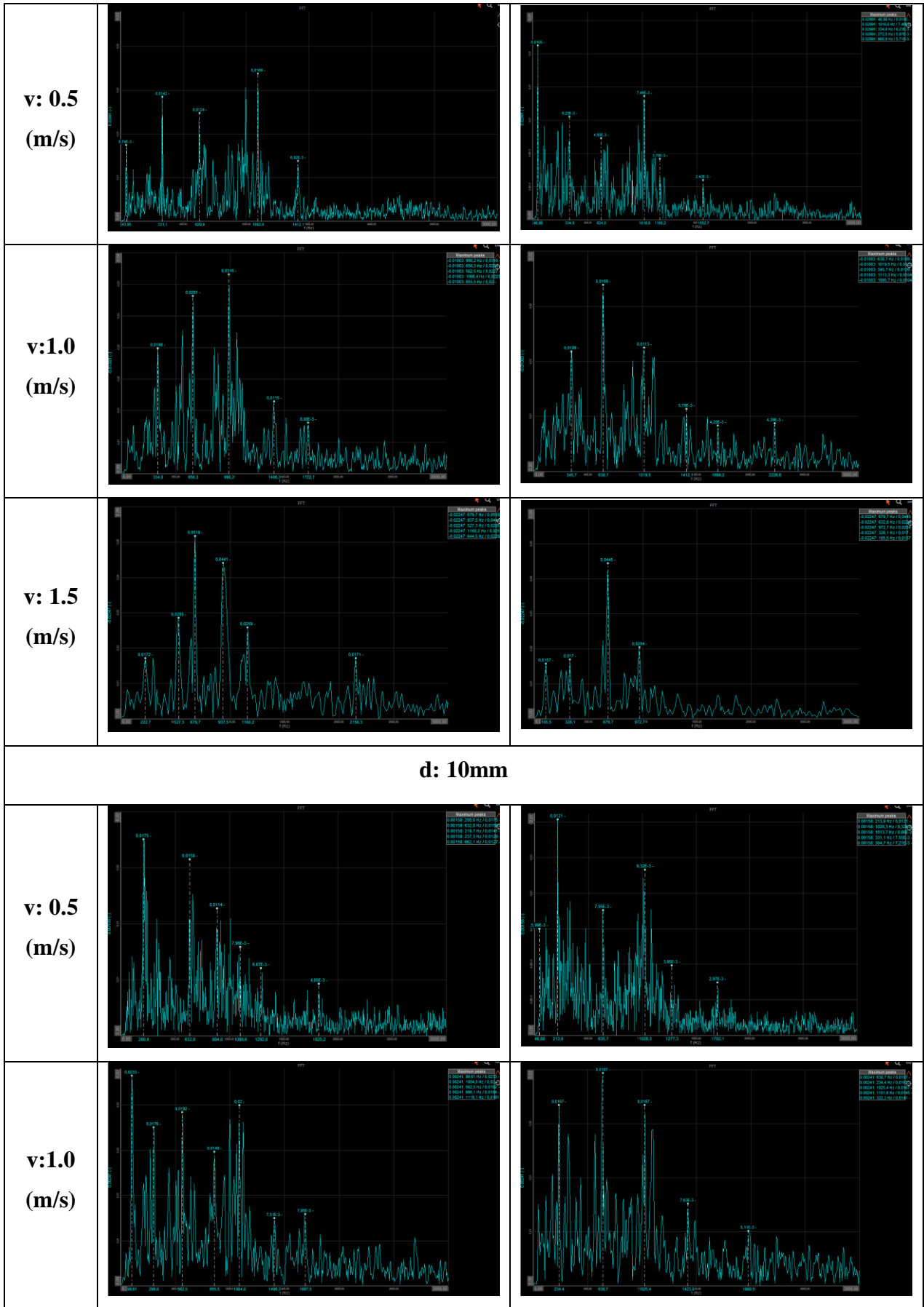
Block "CB"

Unrelieved

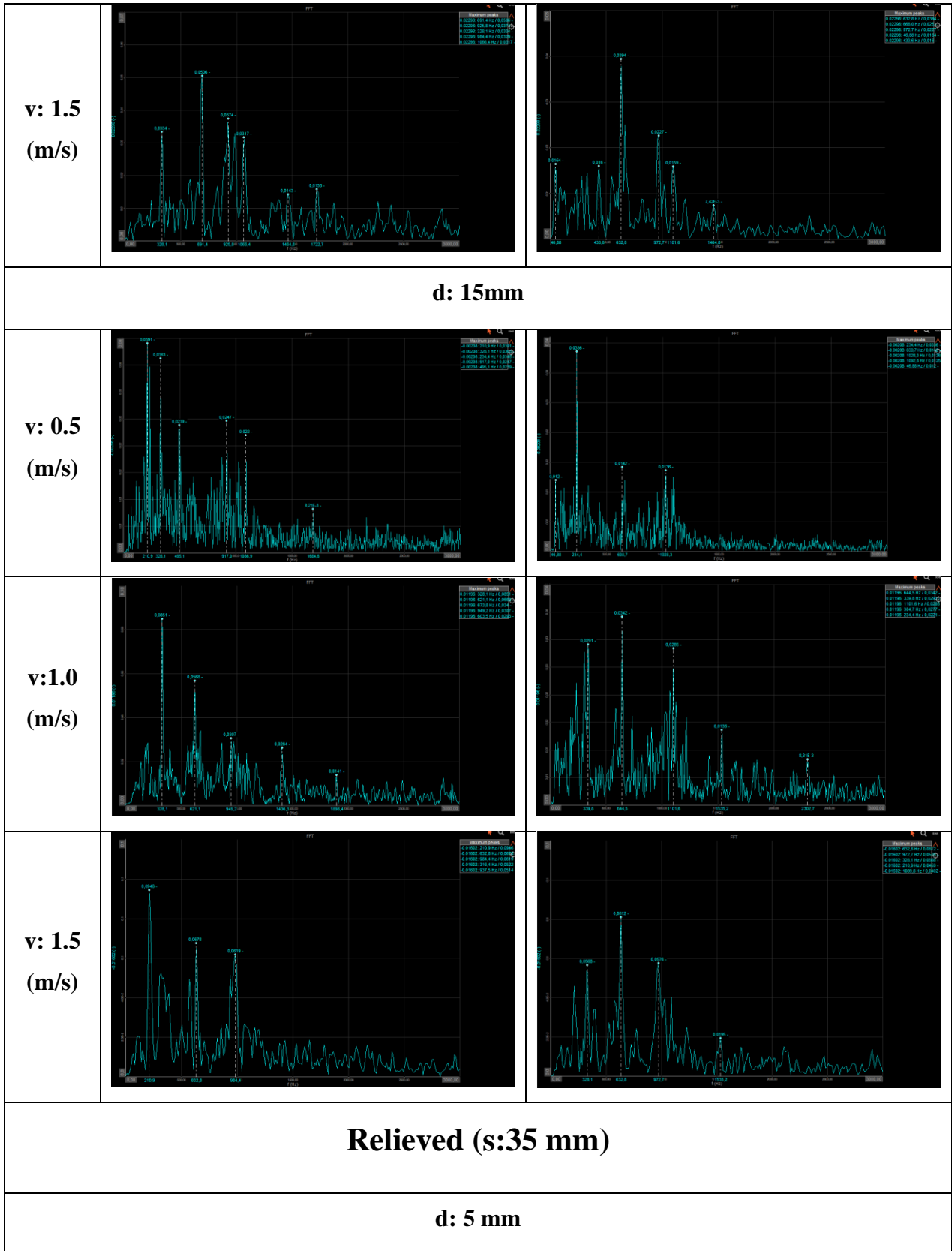
d: 2mm

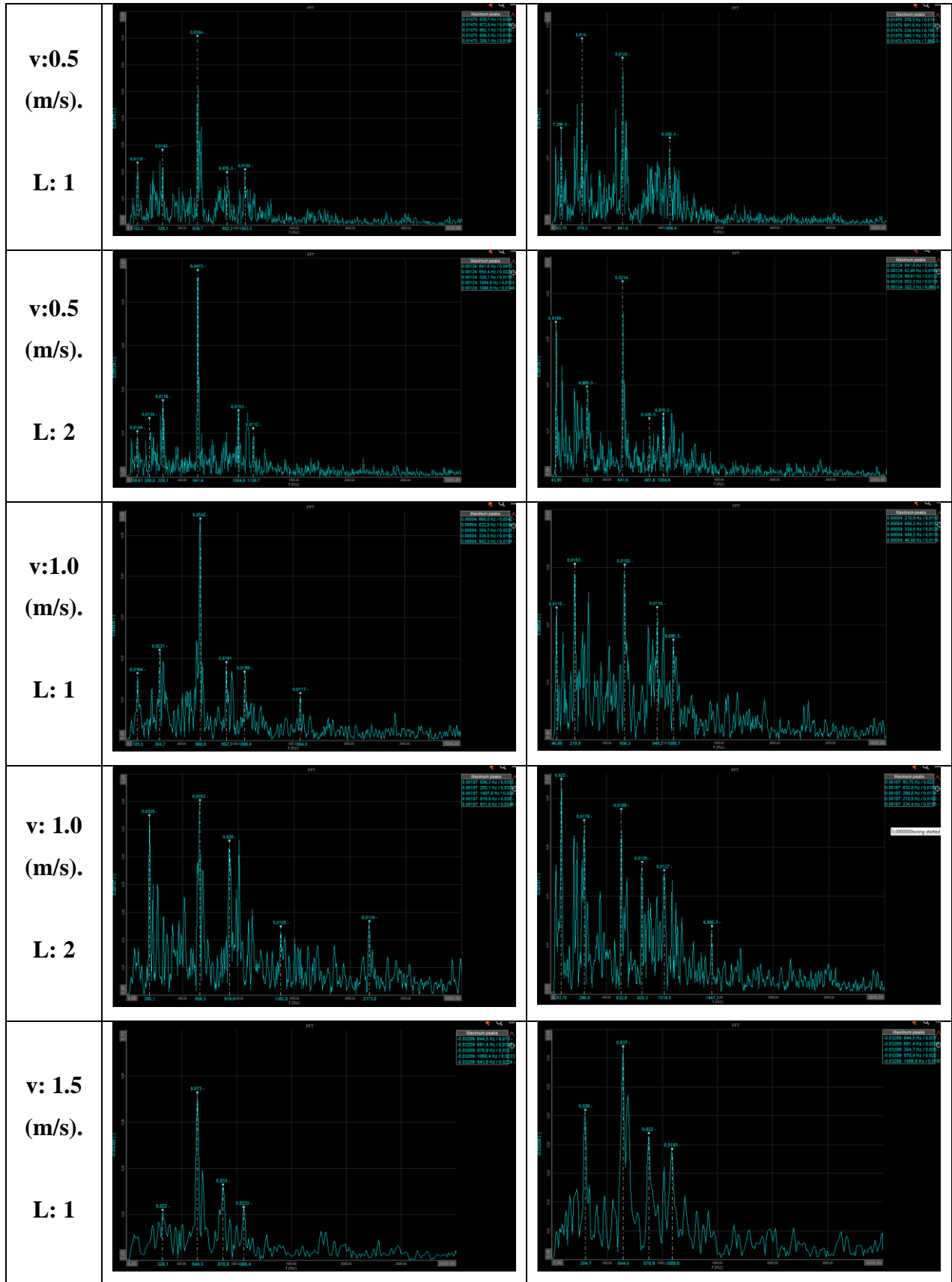


Appendices

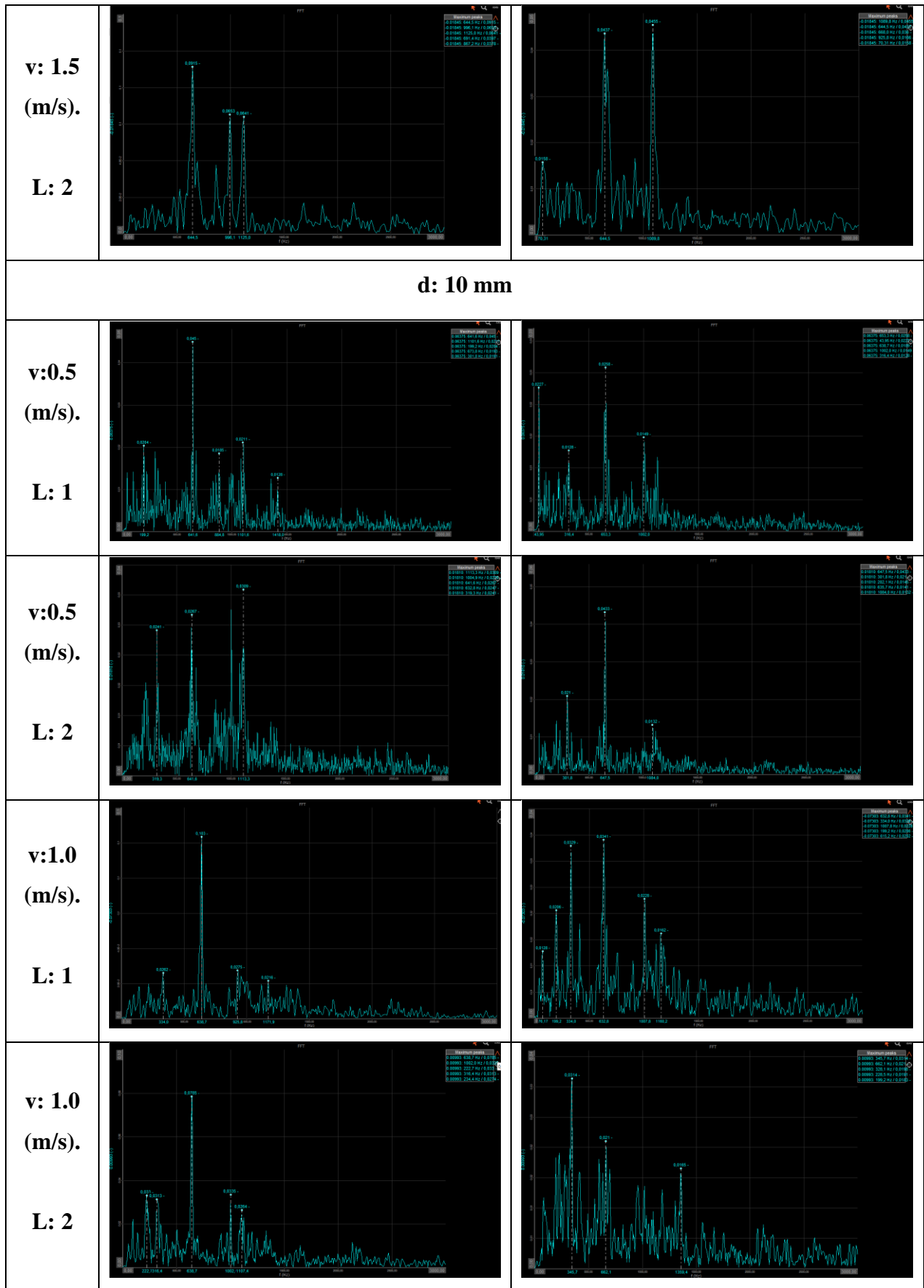


Appendices

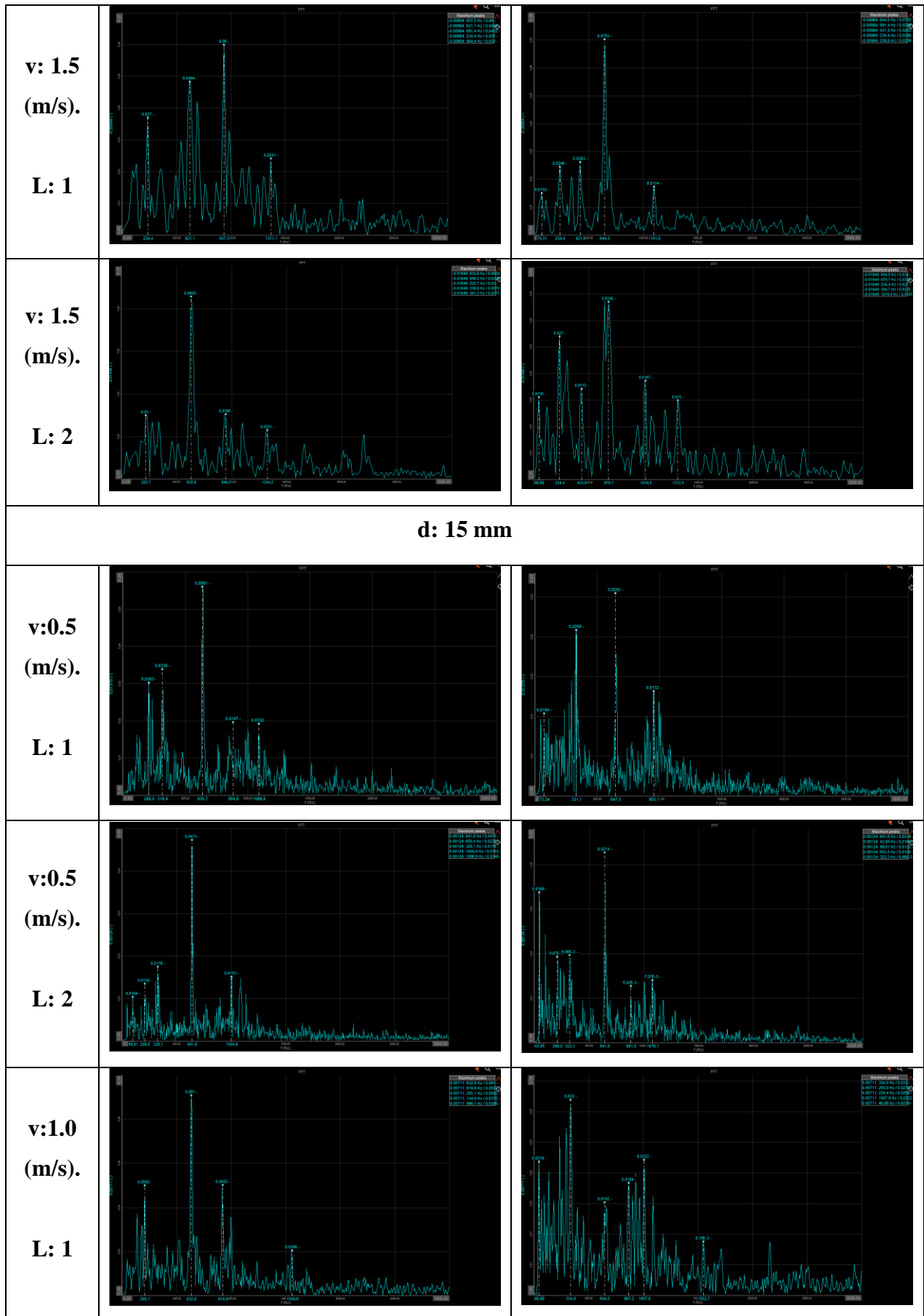


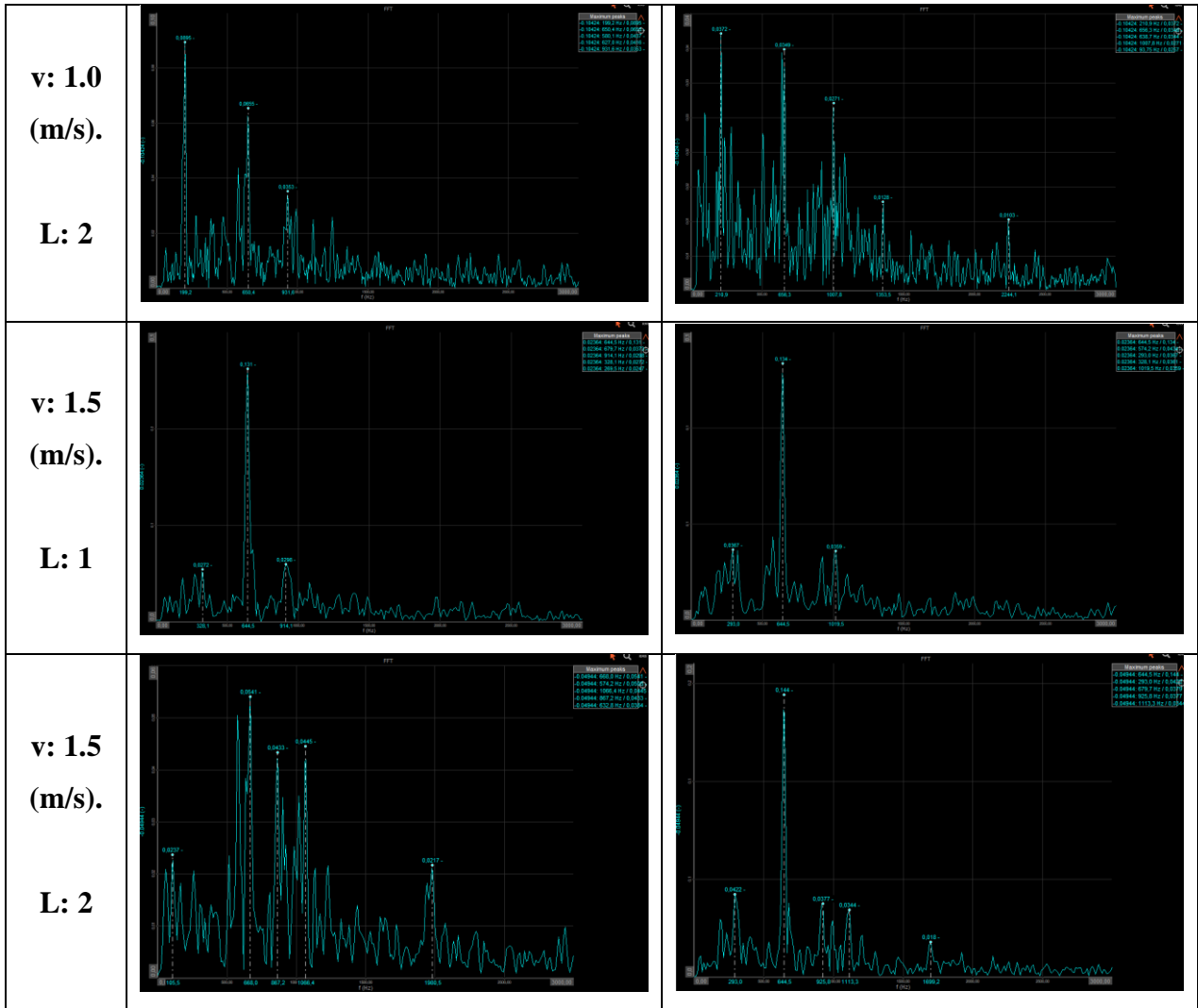


Appendices



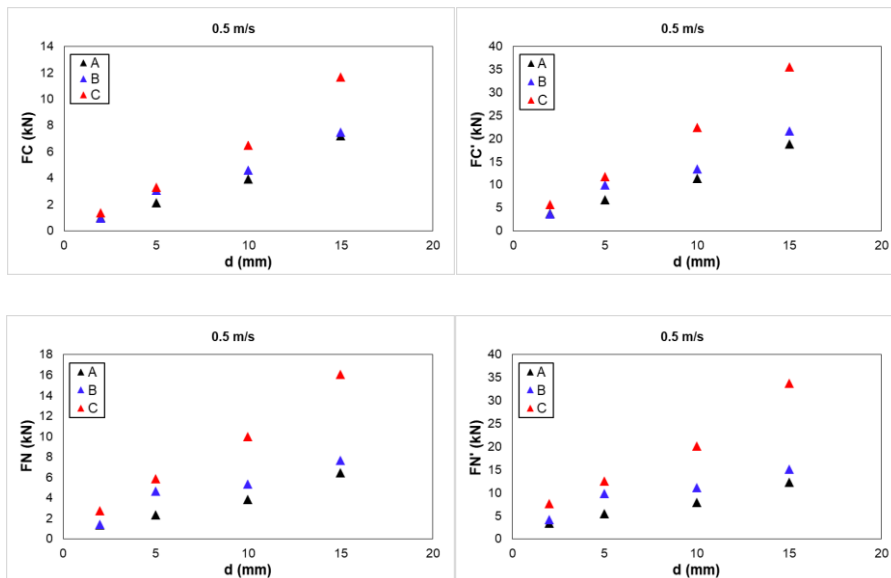
Appendices



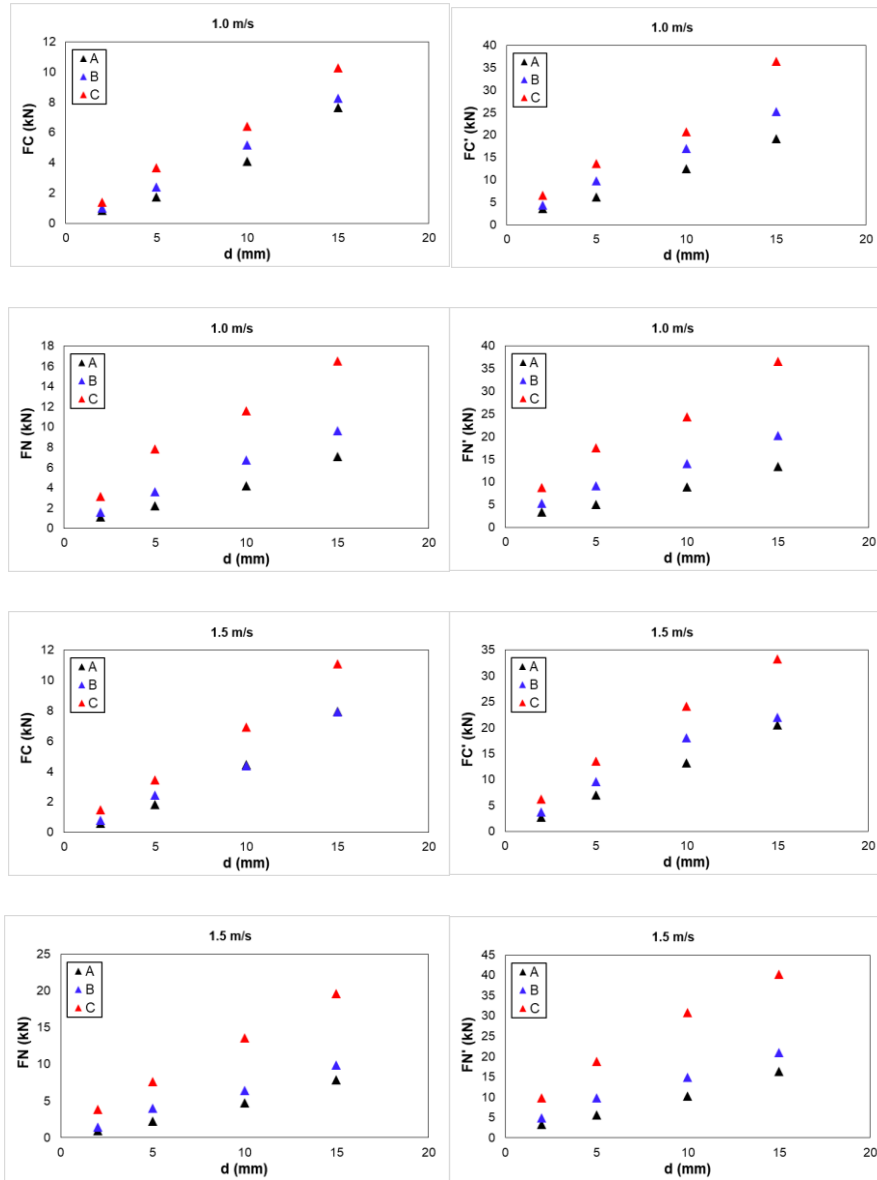


7.2 Appendices Force Data

7.2.1 Force Data Processing Graphs:



Appendices



7.2.2 Summary Force Data Relieved

| Material | d | v | s | L | FC | FC' | FC/d | FC'/d | FC'/FC | FN | FN' | FN'/FN | FN/FC |
|----------|----|-----|----|---|------|-------|------|-------|--------|------|-------|--------|-------|
| A | 5 | 0.5 | 35 | 1 | 2.03 | 5.94 | 0.41 | 1.19 | 2.93 | 2.30 | 5.01 | 2.19 | 1.14 |
| A | 5 | 1 | 35 | 1 | 2.02 | 6.68 | 0.40 | 1.34 | 3.30 | 2.48 | 5.59 | 2.25 | 1.23 |
| A | 5 | 1.5 | 35 | 1 | 1.67 | 6.56 | 0.33 | 1.31 | 3.94 | 2.40 | 5.94 | 2.47 | 1.44 |
| A | 5 | 0.5 | 35 | 2 | 2.81 | 8.44 | 0.56 | 1.69 | 3.00 | 2.75 | 5.84 | 2.12 | 0.98 |
| A | 5 | 1 | 35 | 2 | 2.77 | 10.24 | 0.55 | 2.05 | 3.72 | 3.00 | 7.11 | 2.38 | 1.08 |
| A | 5 | 1.5 | 35 | 2 | 2.52 | 8.08 | 0.50 | 1.62 | 3.21 | 2.92 | 6.73 | 2.31 | 1.16 |
| A | 10 | 0.5 | 35 | 1 | 4.01 | 10.94 | 0.40 | 1.09 | 2.77 | 3.61 | 7.52 | 2.10 | 0.92 |
| A | 10 | 1 | 35 | 1 | 3.70 | 10.60 | 0.37 | 1.06 | 2.89 | 3.94 | 8.24 | 2.10 | 1.07 |
| A | 10 | 1.5 | 35 | 1 | 4.05 | 12.27 | 0.41 | 1.23 | 3.06 | 4.72 | 10.14 | 2.15 | 1.16 |
| A | 10 | 0.5 | 35 | 2 | 4.51 | 12.09 | 0.45 | 1.21 | 2.69 | 4.35 | 8.13 | 1.88 | 0.96 |
| A | 10 | 1 | 35 | 2 | 4.35 | 12.68 | 0.44 | 1.27 | 2.93 | 4.58 | 9.44 | 2.07 | 1.06 |

Appendices

| | | | | | | | | | | | | | |
|---|----|-----|----|---|-------|-------|------|------|------|-------|-------|------|------|
| A | 10 | 1.5 | 35 | 2 | 5.00 | 13.28 | 0.50 | 1.33 | 2.67 | 5.51 | 11.53 | 2.11 | 1.10 |
| A | 15 | 0.5 | 35 | 1 | 5.57 | 16.06 | 0.37 | 1.07 | 2.88 | 5.12 | 10.75 | 2.11 | 0.92 |
| A | 15 | 1 | 35 | 1 | 5.38 | 15.73 | 0.36 | 1.05 | 2.92 | 5.03 | 10.60 | 2.11 | 0.94 |
| A | 15 | 1.5 | 35 | 1 | 5.47 | 14.92 | 0.36 | 0.99 | 2.74 | 5.49 | 11.71 | 2.14 | 1.00 |
| A | 15 | 0.5 | 35 | 2 | 6.42 | 17.09 | 0.43 | 1.14 | 2.68 | 5.73 | 10.93 | 1.91 | 0.89 |
| A | 15 | 1 | 35 | 2 | 6.55 | 20.91 | 0.44 | 1.39 | 3.28 | 4.85 | 11.32 | 2.39 | 0.76 |
| A | 15 | 1.5 | 35 | 2 | 6.90 | 22.30 | 0.46 | 1.49 | 3.30 | 6.02 | 13.73 | 2.34 | 0.87 |
| B | 5 | 0.5 | 35 | 1 | 2.74 | 9.23 | 0.55 | 1.85 | 3.36 | 3.82 | 8.17 | 2.14 | 1.40 |
| B | 5 | 1 | 35 | 1 | 2.51 | 8.52 | 0.50 | 1.70 | 3.40 | 3.58 | 7.94 | 2.23 | 1.42 |
| B | 5 | 1.5 | 35 | 1 | 2.70 | 10.14 | 0.54 | 2.03 | 3.78 | 4.88 | 11.41 | 2.34 | 1.81 |
| B | 5 | 0.5 | 35 | 2 | 3.70 | 12.19 | 0.74 | 2.44 | 3.31 | 5.51 | 11.91 | 2.23 | 1.43 |
| B | 5 | 1 | 35 | 2 | 3.19 | 11.75 | 0.64 | 2.35 | 3.71 | 4.44 | 9.66 | 2.19 | 1.39 |
| B | 5 | 1.5 | 35 | 2 | 3.17 | 11.38 | 0.63 | 2.28 | 3.58 | 5.16 | 10.85 | 2.13 | 1.63 |
| B | 10 | 0.5 | 35 | 1 | 4.76 | 16.70 | 0.48 | 1.67 | 3.51 | 5.86 | 12.75 | 2.18 | 1.23 |
| B | 10 | 1 | 35 | 1 | 4.66 | 15.17 | 0.47 | 1.52 | 3.27 | 6.53 | 13.89 | 2.13 | 1.40 |
| B | 10 | 1.5 | 35 | 1 | 4.51 | 14.70 | 0.45 | 1.47 | 3.27 | 6.88 | 14.93 | 2.17 | 1.52 |
| B | 10 | 0.5 | 35 | 2 | 5.52 | 17.16 | 0.55 | 1.72 | 3.11 | 6.75 | 13.50 | 2.00 | 1.22 |
| B | 10 | 1 | 35 | 2 | 4.57 | 14.89 | 0.46 | 1.49 | 3.25 | 6.14 | 13.00 | 2.12 | 1.34 |
| B | 10 | 1.5 | 35 | 2 | 4.70 | 15.17 | 0.47 | 1.52 | 3.22 | 6.93 | 14.70 | 2.12 | 1.47 |
| B | 15 | 0.5 | 35 | 1 | 6.53 | 19.69 | 0.44 | 1.31 | 3.03 | 7.71 | 16.29 | 2.11 | 1.18 |
| B | 15 | 1 | 35 | 1 | 6.12 | 20.75 | 0.41 | 1.38 | 3.43 | 7.62 | 16.30 | 2.14 | 1.24 |
| B | 15 | 1.5 | 35 | 1 | 6.65 | 24.70 | 0.44 | 1.65 | 3.73 | 9.31 | 20.66 | 2.25 | 1.40 |
| B | 15 | 0.5 | 35 | 2 | 6.94 | 19.33 | 0.46 | 1.29 | 2.80 | 8.09 | 15.77 | 1.96 | 1.17 |
| B | 15 | 1 | 35 | 2 | 6.42 | 20.79 | 0.43 | 1.39 | 3.31 | 8.31 | 16.81 | 2.06 | 1.30 |
| B | 15 | 1.5 | 35 | 2 | 7.16 | 22.93 | 0.48 | 1.53 | 3.24 | 10.16 | 22.21 | 2.22 | 1.41 |
| C | 5 | 0.5 | 35 | 1 | 3.75 | 14.06 | 0.75 | 2.81 | 3.74 | 6.85 | 13.89 | 2.03 | 1.82 |
| C | 5 | 1 | 35 | 1 | 3.62 | 13.13 | 0.72 | 2.63 | 3.63 | 7.89 | 17.27 | 2.20 | 2.18 |
| C | 5 | 1.5 | 35 | 1 | 3.29 | 12.82 | 0.66 | 2.56 | 3.95 | 7.99 | 18.82 | 2.37 | 2.44 |
| C | 5 | 0.5 | 35 | 2 | 4.92 | 17.19 | 0.98 | 3.44 | 3.51 | 8.06 | 16.46 | 2.05 | 1.63 |
| C | 5 | 1 | 35 | 2 | 4.34 | 16.48 | 0.87 | 3.30 | 3.80 | 8.32 | 19.39 | 2.33 | 1.91 |
| C | 5 | 1.5 | 35 | 2 | 4.15 | 15.72 | 0.83 | 3.14 | 3.79 | 8.44 | 21.04 | 2.50 | 2.04 |
| C | 10 | 0.5 | 35 | 1 | 6.77 | 24.17 | 0.68 | 2.42 | 3.57 | 10.58 | 21.59 | 2.04 | 1.57 |
| C | 10 | 1 | 35 | 1 | 6.31 | 19.95 | 0.63 | 1.99 | 3.18 | 11.70 | 24.75 | 2.13 | 1.85 |
| C | 10 | 1.5 | 35 | 1 | 5.96 | 20.92 | 0.60 | 2.09 | 3.53 | 12.55 | 27.42 | 2.20 | 2.11 |
| C | 10 | 0.5 | 35 | 2 | 7.24 | 25.66 | 0.72 | 2.57 | 3.58 | 11.14 | 23.17 | 2.08 | 1.54 |
| C | 10 | 1 | 35 | 2 | 6.91 | 22.38 | 0.69 | 2.24 | 3.26 | 13.22 | 27.36 | 2.08 | 1.91 |
| C | 10 | 1.5 | 35 | 2 | 6.54 | 22.04 | 0.65 | 2.20 | 3.40 | 12.93 | 29.49 | 2.29 | 1.98 |
| C | 15 | 0.5 | 35 | 1 | 8.90 | 29.77 | 0.59 | 1.98 | 3.36 | 12.86 | 27.40 | 2.13 | 1.45 |
| C | 15 | 1 | 35 | 1 | 8.70 | 33.21 | 0.58 | 2.21 | 3.85 | 14.17 | 32.60 | 2.31 | 1.63 |
| C | 15 | 1.5 | 35 | 1 | 7.97 | 27.31 | 0.53 | 1.82 | 3.44 | 14.38 | 32.57 | 2.27 | 1.81 |
| C | 15 | 0.5 | 35 | 2 | 10.37 | 33.34 | 0.69 | 2.22 | 3.27 | 14.59 | 30.52 | 2.11 | 1.41 |
| C | 15 | 1 | 35 | 2 | 9.53 | 35.06 | 0.64 | 2.34 | 3.72 | 14.69 | 32.66 | 2.24 | 1.56 |
| C | 15 | 1.5 | 35 | 2 | 9.73 | 31.96 | 0.65 | 2.13 | 3.34 | 17.47 | 37.95 | 2.19 | 1.80 |

7.2.3 Summary Force Data Unrelieved

| Material | d | v | FC | FC' | FC/d | FC'/d | FC'/FC | FN | FN' | FN'/FN | FN/FC |
|----------|----|-----|-------|-------|------|-------|--------|-------|-------|--------|-------|
| A | 2 | 0.5 | 1.02 | 3.72 | 0.51 | 1.86 | 3.65 | 1.38 | 3.44 | 2.49 | 1.35 |
| A | 5 | 0.5 | 2.11 | 6.72 | 0.42 | 1.34 | 3.18 | 2.38 | 5.54 | 2.33 | 1.12 |
| A | 10 | 0.5 | 3.94 | 11.40 | 0.39 | 1.14 | 2.90 | 3.85 | 7.98 | 2.08 | 0.98 |
| A | 15 | 0.5 | 7.23 | 18.85 | 0.48 | 1.26 | 2.60 | 6.44 | 12.25 | 1.90 | 0.89 |
| B | 2 | 0.5 | 0.98 | 3.63 | 0.49 | 1.81 | 3.70 | 1.45 | 4.19 | 2.89 | 1.48 |
| B | 5 | 0.5 | 3.06 | 9.99 | 0.61 | 2.00 | 3.25 | 4.65 | 9.91 | 2.14 | 1.46 |
| B | 10 | 0.5 | 4.61 | 13.45 | 0.46 | 1.35 | 2.92 | 5.36 | 11.09 | 2.07 | 1.16 |
| B | 15 | 0.5 | 7.48 | 21.60 | 0.50 | 1.44 | 2.88 | 7.67 | 15.19 | 1.98 | 1.03 |
| C | 2 | 0.5 | 1.39 | 5.74 | 0.69 | 2.87 | 4.20 | 2.73 | 7.63 | 2.86 | 1.98 |
| C | 5 | 0.5 | 3.31 | 11.80 | 0.66 | 2.36 | 3.55 | 5.88 | 12.50 | 2.13 | 1.77 |
| C | 10 | 0.5 | 6.49 | 22.44 | 0.65 | 2.24 | 3.47 | 9.99 | 20.20 | 2.02 | 1.54 |
| C | 15 | 0.5 | 11.67 | 35.60 | 0.78 | 2.37 | 3.06 | 16.05 | 33.75 | 2.12 | 1.37 |
| A | 2 | 1 | 0.84 | 3.57 | 0.42 | 1.78 | 4.29 | 1.14 | 3.43 | 3.10 | 1.34 |
| A | 5 | 1 | 1.76 | 6.25 | 0.35 | 1.25 | 3.58 | 2.19 | 5.03 | 2.31 | 1.25 |
| A | 10 | 1 | 4.10 | 12.53 | 0.41 | 1.25 | 3.05 | 4.19 | 8.91 | 2.14 | 1.02 |
| A | 15 | 1 | 7.63 | 19.16 | 0.51 | 1.28 | 2.52 | 7.09 | 13.42 | 1.90 | 0.93 |
| B | 2 | 1 | 1.00 | 4.44 | 0.50 | 2.22 | 4.44 | 1.59 | 5.34 | 3.35 | 1.58 |
| B | 5 | 1 | 2.40 | 9.82 | 0.48 | 1.96 | 4.09 | 3.59 | 9.19 | 2.57 | 1.50 |
| B | 10 | 1 | 5.18 | 16.95 | 0.52 | 1.70 | 3.29 | 6.72 | 14.07 | 2.09 | 1.30 |
| B | 15 | 1 | 8.27 | 25.22 | 0.55 | 1.68 | 3.08 | 9.63 | 20.28 | 2.12 | 1.17 |
| C | 2 | 1 | 1.41 | 6.54 | 0.70 | 3.27 | 4.86 | 3.16 | 8.74 | 2.93 | 2.25 |
| C | 5 | 1 | 3.65 | 13.63 | 0.73 | 2.73 | 3.74 | 7.85 | 17.59 | 2.25 | 2.15 |
| C | 10 | 1 | 6.42 | 20.73 | 0.64 | 2.07 | 3.26 | 11.60 | 24.43 | 2.11 | 1.81 |
| C | 15 | 1 | 10.28 | 36.40 | 0.69 | 2.43 | 3.54 | 16.50 | 36.56 | 2.24 | 1.62 |
| A | 2 | 1.5 | 0.59 | 2.74 | 0.29 | 1.37 | 4.67 | 0.97 | 3.31 | 3.35 | 1.67 |
| A | 5 | 1.5 | 1.84 | 7.05 | 0.37 | 1.41 | 3.83 | 2.24 | 5.62 | 2.52 | 1.21 |
| A | 10 | 1.5 | 4.47 | 13.18 | 0.45 | 1.32 | 2.96 | 4.77 | 10.29 | 2.16 | 1.07 |
| A | 15 | 1.5 | 7.97 | 20.51 | 0.53 | 1.37 | 2.59 | 7.84 | 16.37 | 2.10 | 0.98 |
| B | 2 | 1.5 | 0.81 | 3.80 | 0.41 | 1.90 | 4.75 | 1.46 | 4.94 | 3.38 | 1.66 |
| B | 5 | 1.5 | 2.45 | 9.62 | 0.49 | 1.92 | 3.96 | 4.00 | 9.89 | 2.50 | 1.63 |
| B | 10 | 1.5 | 4.37 | 18.06 | 0.44 | 1.81 | 4.02 | 6.43 | 14.94 | 2.31 | 1.47 |
| B | 15 | 1.5 | 7.95 | 22.00 | 0.53 | 1.47 | 2.76 | 9.88 | 20.93 | 2.12 | 1.24 |
| C | 2 | 1.5 | 1.47 | 6.28 | 0.73 | 3.14 | 4.32 | 3.89 | 9.90 | 2.56 | 2.69 |
| C | 5 | 1.5 | 3.44 | 13.60 | 0.69 | 2.72 | 3.99 | 7.62 | 18.79 | 2.48 | 2.21 |
| C | 10 | 1.5 | 6.94 | 24.13 | 0.69 | 2.41 | 3.54 | 13.57 | 30.80 | 2.28 | 1.95 |
| C | 15 | 1.5 | 11.11 | 33.31 | 0.74 | 2.22 | 2.94 | 19.64 | 40.26 | 2.05 | 1.78 |

7.2.4 Summary Concrete ‘A’

| CONCRETE ‘A’ summary: | | | | | | | | | | | | | | | |
|-----------------------|-----|---|-------|-------|-------------|--------------|-------------|-------------|-------------|-------------|-------------|-------------|-------------|--------------|-------------|
| Unrelieved Cuts | | | | | | | | | | | | | | | |
| z | v | s | Layer | Trial | FC | FC' | FC/d | FC'/d | FC'/FC | FN | FN' | FN'/FN | FN/FC | FS | FS' |
| 2 | 0.5 | - | - | 1 | 1.12 | 4.12 | 0.56 | 2.06 | 3.68 | 1.59 | 4.07 | 2.56 | 1.42 | 0.06 | 1.05 |
| 2 | 0.5 | - | - | 2 | 0.94 | 3.25 | 0.47 | 1.63 | 3.46 | 1.22 | 3.18 | 2.60 | 1.30 | 0 | 0.61 |
| 2 | 0.5 | - | - | 3 | 1.12 | 3.9 | 0.56 | 1.95 | 3.48 | 1.48 | 3.55 | 2.40 | 1.32 | -0.04 | 0.9 |
| 2 | 0.5 | - | - | 4 | 0.91 | 3.61 | 0.46 | 1.81 | 3.97 | 1.23 | 2.95 | 2.40 | 1.35 | 0.05 | 0.88 |
| Average: | | | | | 1.02 | 3.72 | 0.51 | 1.86 | 3.65 | 1.38 | 3.44 | 2.49 | 1.35 | 0.02 | 0.86 |
| 2 | 1 | - | - | 1 | 1.04 | 3.92 | 0.52 | 1.96 | 3.79 | 1.42 | 3.68 | 2.59 | 1.37 | 0.01 | 0.99 |
| 2 | 1 | - | - | 2 | 0.77 | 3.25 | 0.38 | 1.63 | 4.23 | 1.11 | 3.28 | 2.96 | 1.44 | 1.17 | 1.17 |
| 2 | 1 | - | - | 3 | 0.73 | 3.54 | 0.36 | 1.77 | 4.86 | 0.88 | 3.32 | 3.76 | 1.21 | 1.36 | 1.36 |
| Average: | | | | | 0.84 | 3.57 | 0.42 | 1.78 | 4.29 | 1.14 | 3.43 | 3.10 | 1.34 | 0.85 | 1.17 |
| 2 | 1.5 | - | - | 1 | 0.49 | 2.39 | 0.24 | 1.20 | 4.89 | 0.91 | 3.19 | 3.50 | 1.86 | -0.02 | 1.10 |
| 2 | 1.5 | - | - | 2 | 0.74 | 3.00 | 0.37 | 1.50 | 4.04 | 1.13 | 4.02 | 3.56 | 1.52 | 0.02 | 1.21 |
| 2 | 1.5 | - | - | 3 | 0.49 | 2.14 | 0.25 | 1.07 | 4.36 | 0.81 | 1.95 | 2.43 | 1.64 | -0.05 | 1.11 |
| 2 | 1.5 | - | - | 4 | 0.63 | 3.43 | 0.32 | 1.71 | 5.41 | 1.04 | 4.05 | 3.90 | 1.64 | -0.05 | 1.26 |
| Average: | | | | | 0.59 | 2.74 | 0.29 | 1.37 | 4.67 | 0.97 | 3.31 | 3.35 | 1.67 | -0.02 | 1.17 |
| 5 | 0.5 | - | - | 1 | 2.28 | 7.75 | 0.46 | 1.55 | 3.39 | 2.49 | 5.57 | 2.24 | 1.09 | -0.14 | 1.17 |
| 5 | 0.5 | - | - | 2 | 1.88 | 6.24 | 0.38 | 1.25 | 3.33 | 2.12 | 5.13 | 2.43 | 1.13 | 0.04 | 1.36 |
| 5 | 0.5 | - | - | 3 | 2.34 | 7.22 | 0.47 | 1.44 | 3.09 | 2.82 | 6.88 | 2.44 | 1.21 | 0.01 | 1.60 |
| 5 | 0.5 | - | - | 4 | 1.95 | 5.65 | 0.39 | 1.13 | 2.90 | 2.08 | 4.60 | 2.21 | 1.07 | -0.04 | 1.31 |
| Average: | | | | | 2.11 | 6.72 | 0.42 | 1.34 | 3.18 | 2.38 | 5.54 | 2.33 | 1.12 | -0.03 | 1.36 |
| 5 | 1 | - | - | 1 | 1.80 | 6.54 | 0.36 | 1.31 | 3.63 | 2.13 | 5.02 | 2.36 | 1.18 | -0.07 | 1.15 |
| 5 | 1 | - | - | 2 | 1.98 | 5.93 | 0.40 | 1.19 | 3.00 | 2.30 | 3.91 | 1.70 | 1.16 | 0.15 | 1.15 |
| 5 | 1 | - | - | 3 | 1.73 | 6.76 | 0.35 | 1.35 | 3.90 | 2.31 | 5.32 | 2.31 | 1.33 | 0.10 | 1.72 |
| 5 | 1 | - | - | 4 | 1.52 | 5.76 | 0.30 | 1.15 | 3.79 | 2.04 | 5.85 | 2.86 | 1.35 | -0.03 | 1.77 |
| Average: | | | | | 1.76 | 6.25 | 0.35 | 1.25 | 3.58 | 2.19 | 5.03 | 2.31 | 1.25 | 0.04 | 1.45 |
| 5 | 1.5 | - | - | 1 | 1.83 | 6.86 | 0.37 | 1.37 | 3.75 | 2.20 | 5.81 | 2.64 | 1.20 | -0.05 | 2.03 |
| 5 | 1.5 | - | - | 2 | 2.03 | 7.31 | 0.41 | 1.46 | 3.61 | 2.55 | 5.78 | 2.27 | 1.26 | 0.01 | 1.86 |
| 5 | 1.5 | - | - | 3 | 1.78 | 7.29 | 0.36 | 1.46 | 4.09 | 2.16 | 5.81 | 2.69 | 1.21 | 0.04 | 1.72 |
| 5 | 1.5 | - | - | 4 | 1.74 | 6.74 | 0.35 | 1.35 | 3.88 | 2.04 | 5.07 | 2.48 | 1.17 | -0.02 | 1.64 |
| Average: | | | | | 1.84 | 7.05 | 0.37 | 1.41 | 3.83 | 2.24 | 5.62 | 2.52 | 1.21 | 0.00 | 1.81 |
| 10 | 0.5 | - | - | 1 | 3.93 | 10.31 | 0.39 | 1.03 | 2.62 | 3.79 | 7.51 | 1.98 | 0.96 | -0.14 | 1.41 |
| 10 | 0.5 | - | - | 2 | 4.12 | 12.42 | 0.41 | 1.24 | 3.02 | 4.14 | 8.46 | 2.04 | 1.01 | 0.36 | 2.51 |
| 10 | 0.5 | - | - | 3 | 4.20 | 11.80 | 0.42 | 1.18 | 2.81 | 4.07 | 8.49 | 2.09 | 0.97 | -0.08 | 1.35 |
| 10 | 0.5 | - | - | 4 | 3.50 | 11.05 | 0.35 | 1.11 | 3.16 | 3.38 | 7.48 | 2.21 | 0.97 | -0.14 | 1.72 |
| Average: | | | | | 3.94 | 11.40 | 0.39 | 1.14 | 2.90 | 3.85 | 7.98 | 2.08 | 0.98 | 0.00 | 1.74 |
| 10 | 1 | - | - | 1 | 4.02 | 11.27 | 0.40 | 1.13 | 2.80 | 3.99 | 8.60 | 2.16 | 0.99 | 0.02 | 2.12 |
| 10 | 1 | - | - | 2 | 4.27 | 16.44 | 0.43 | 1.64 | 3.85 | 4.28 | 8.91 | 2.08 | 1.00 | -0.27 | 2.31 |
| 10 | 1 | - | - | 3 | 4.14 | 11.14 | 0.41 | 1.11 | 2.69 | 4.68 | 9.10 | 1.95 | 1.13 | 0.12 | 2.68 |
| 10 | 1 | - | - | 4 | 3.95 | 11.27 | 0.40 | 1.13 | 2.85 | 3.83 | 9.03 | 2.36 | 0.97 | -0.59 | 2.26 |
| Average: | | | | | 4.10 | 12.53 | 0.41 | 1.25 | 3.05 | 4.19 | 8.91 | 2.14 | 1.02 | -0.18 | 2.35 |
| 10 | 1.5 | - | - | 1 | 4.58 | 12.05 | 0.46 | 1.21 | 2.63 | 4.96 | 10.41 | 2.10 | 1.08 | 0.01 | 2.39 |

Appendices

| | | | | | | | | | | | | | | | |
|-----------------|-----|---|---|---|-------------|--------------|-------------|-------------|-------------|-------------|--------------|-------------|-------------|--------------|-------------|
| 10 | 1.5 | | - | 2 | 4.31 | 12.78 | 0.43 | 1.28 | 2.97 | 4.59 | 9.87 | 2.15 | 1.07 | 0.04 | 2.59 |
| 10 | 1.5 | - | - | 3 | 4.37 | 15.45 | 0.44 | 1.54 | 3.54 | 4.40 | 10.03 | 2.28 | 1.01 | -0.03 | 2.32 |
| 10 | 1.5 | - | - | 4 | 4.62 | 12.45 | 0.46 | 1.25 | 2.70 | 5.15 | 10.86 | 2.11 | 1.12 | 0.12 | 2.87 |
| Average: | | | | | 4.47 | 13.18 | 0.45 | 1.32 | 2.96 | 4.77 | 10.29 | 2.16 | 1.07 | 0.03 | 2.54 |
| 15 | 0.5 | - | - | 1 | 7.32 | 18.76 | 0.49 | 1.25 | 2.56 | 6.20 | 11.92 | 1.92 | 0.85 | -0.08 | 2.16 |
| 15 | 0.5 | - | - | 2 | 7.17 | 16.95 | 0.48 | 1.13 | 2.36 | 6.85 | 12.32 | 1.80 | 0.96 | 0.17 | 3.05 |
| 15 | 0.5 | - | - | 3 | 6.83 | 17.74 | 0.46 | 1.18 | 2.60 | 6.15 | 10.94 | 1.78 | 0.90 | -0.52 | 1.50 |
| 15 | 0.5 | - | - | 4 | 7.59 | 21.94 | 0.51 | 1.46 | 2.89 | 6.56 | 13.82 | 2.11 | 0.86 | -0.08 | 2.95 |
| Average: | | | | | 7.23 | 18.85 | 0.48 | 1.26 | 2.60 | 6.44 | 12.25 | 1.90 | 0.89 | -0.13 | 2.42 |
| 15 | 1 | - | - | 1 | 6.18 | 16.19 | 0.41 | 1.08 | 2.62 | 5.85 | 11.29 | 1.93 | 0.95 | 0.27 | 2.47 |
| 15 | 1 | - | - | 2 | 8.83 | 20.31 | 0.59 | 1.35 | 2.30 | 8.24 | 14.59 | 1.77 | 0.93 | 0.09 | 3.31 |
| 15 | 1 | - | - | 3 | 7.75 | 20.93 | 0.52 | 1.40 | 2.70 | 6.99 | 13.30 | 1.90 | 0.90 | 0.74 | 3.63 |
| 15 | 1 | - | - | 4 | 7.77 | 19.23 | 0.52 | 1.28 | 2.47 | 7.30 | 14.53 | 1.99 | 0.94 | -1.43 | 1.39 |
| Average: | | | | | 7.63 | 19.16 | 0.51 | 1.28 | 2.52 | 7.09 | 13.42 | 1.90 | 0.93 | -0.08 | 2.70 |
| 15 | 1.5 | - | - | 1 | 6.90 | 19.10 | 0.46 | 1.27 | 2.77 | 6.68 | 14.73 | 2.21 | 0.97 | -0.50 | 2.54 |
| 15 | 1.5 | | - | 2 | 9.04 | 21.92 | 0.60 | 1.46 | 2.42 | 9.00 | 18.01 | 2.00 | 0.99 | -0.42 | 3.86 |
| Average: | | | | | 7.97 | 20.51 | 0.53 | 1.37 | 2.59 | 7.84 | 16.37 | 2.10 | 0.98 | -0.46 | 3.20 |

| |
|----------------------|
| Relieved Cuts |
|----------------------|

| | | | | | | | | | | | | | | | |
|-----------------|-----|----|---|---|-------------|--------------|-------------|-------------|-------------|-------------|-------------|-------------|-------------|-------------|-------------|
| 5 | 0.5 | 35 | 1 | 1 | 1.85 | 5.56 | 0.37 | 1.11 | 3.00 | 2.12 | 5.07 | 2.39 | 1.14 | -0.05 | 0.91 |
| 5 | 0.5 | 35 | 1 | 2 | 2.25 | 6.46 | 0.45 | 1.29 | 2.88 | 2.53 | 5.17 | 2.05 | 1.13 | 0.08 | 1.32 |
| 5 | 0.5 | 35 | 1 | 3 | 2.25 | 6.46 | 0.45 | 1.29 | 2.88 | 2.53 | 5.17 | 2.05 | 1.13 | 0.08 | 1.32 |
| 5 | 0.5 | 35 | 1 | 4 | 1.87 | 5.15 | 0.37 | 1.03 | 2.76 | 2.01 | 4.66 | 2.32 | 1.08 | 0.20 | 1.41 |
| 5 | 0.5 | 35 | 1 | 5 | 1.92 | 6.04 | 0.38 | 1.21 | 3.14 | 2.32 | 4.97 | 2.14 | 1.21 | 0.01 | 1.06 |
| Average: | | | | | 2.03 | 5.94 | 0.41 | 1.19 | 2.93 | 2.30 | 5.01 | 2.19 | 1.14 | 0.07 | 1.20 |
| 5 | 0.5 | 35 | 2 | 1 | 2.85 | 8.55 | 0.57 | 1.71 | 3.00 | 2.79 | 5.93 | 2.12 | 0.98 | 0.16 | 2.13 |
| 5 | 0.5 | 35 | 2 | 2 | 2.58 | 7.97 | 0.52 | 1.59 | 3.09 | 2.82 | 6.06 | 2.15 | 1.09 | 0.23 | 1.64 |
| 5 | 0.5 | 35 | 2 | 3 | 2.92 | 8.73 | 0.58 | 1.75 | 2.99 | 2.53 | 5.63 | 2.23 | 0.86 | -0.06 | 1.29 |
| 5 | 0.5 | 35 | 2 | 4 | 2.90 | 8.51 | 0.58 | 1.70 | 2.93 | 2.88 | 5.73 | 1.99 | 0.99 | 0.24 | 1.35 |
| Average: | | | | | 2.81 | 8.44 | 0.56 | 1.69 | 3.00 | 2.75 | 5.84 | 2.12 | 0.98 | 0.14 | 1.60 |
| 5 | 1 | 35 | 1 | 1 | 1.89 | 5.93 | 0.38 | 1.19 | 3.13 | 2.42 | 5.07 | 2.10 | 1.28 | -0.11 | 1.23 |
| 5 | 1 | 35 | 1 | 2 | 2.03 | 6.61 | 0.41 | 1.32 | 3.26 | 2.47 | 5.99 | 2.43 | 1.22 | 0.14 | 1.92 |
| 5 | 1 | 35 | 1 | 3 | 2.00 | 7.15 | 0.40 | 1.43 | 3.58 | 2.56 | 5.84 | 2.28 | 1.28 | 0.17 | 1.72 |
| 5 | 1 | 35 | 1 | 4 | 2.11 | 6.74 | 0.42 | 1.35 | 3.20 | 2.42 | 5.64 | 2.33 | 1.15 | 0.13 | 2.13 |
| 5 | 1 | 35 | 1 | 5 | 2.08 | 6.96 | 0.42 | 1.39 | 3.34 | 2.53 | 5.41 | 2.14 | 1.22 | 0.25 | 2.02 |
| Average: | | | | | 2.02 | 6.68 | 0.40 | 1.34 | 3.30 | 2.48 | 5.59 | 2.25 | 1.23 | 0.12 | 1.80 |
| 5 | 1 | 35 | 2 | 1 | 2.73 | 10.06 | 0.55 | 2.01 | 3.69 | 2.70 | 6.34 | 2.35 | 0.99 | 0.08 | 2.20 |
| 5 | 1 | 35 | 2 | 2 | | | | | | | | | | | |
| 5 | 1 | 35 | 2 | 3 | 2.45 | 9.88 | 0.49 | 1.98 | 4.03 | 2.83 | 7.07 | 2.50 | 1.15 | 0.26 | 2.47 |
| 5 | 1 | 35 | 2 | 4 | 3.13 | 10.77 | 0.63 | 2.15 | 3.44 | 3.48 | 7.93 | 2.28 | 1.11 | 0.22 | 2.32 |
| Average: | | | | | 2.77 | 10.24 | 0.55 | 2.05 | 3.72 | 3.00 | 7.11 | 2.38 | 1.08 | 0.19 | 2.33 |
| 5 | 1.5 | 35 | 1 | 1 | 1.69 | 6.73 | 0.34 | 1.35 | 3.99 | 2.28 | 5.02 | 2.20 | 1.36 | -0.01 | 1.50 |

Appendices

| | | | | | | | | | | | | | | | |
|-----------------|-----|----|---|---|-------------|-------------|-------------|-------------|-------------|-------------|-------------|-------------|-------------|-------------|-------------|
| 5 | 1.5 | 35 | 1 | 2 | 1.78 | 7.10 | 0.36 | 1.42 | 4.00 | 2.44 | 5.35 | 2.19 | 1.37 | 0.08 | 1.95 |
| 5 | 1.5 | 35 | 1 | 3 | 1.58 | 7.16 | 0.32 | 1.43 | 4.54 | 2.19 | 6.11 | 2.79 | 1.39 | 0.21 | 1.92 |
| 5 | 1.5 | 35 | 1 | 4 | 1.55 | 6.04 | 0.31 | 1.21 | 3.90 | 2.46 | 6.55 | 2.66 | 1.59 | 0.16 | 1.92 |
| 5 | 1.5 | 35 | 1 | 5 | 1.77 | 5.75 | 0.35 | 1.15 | 3.25 | 2.63 | 6.67 | 2.53 | 1.49 | 0.05 | 1.81 |
| Average: | | | | | 1.67 | 6.56 | 0.33 | 1.31 | 3.94 | 2.40 | 5.94 | 2.47 | 1.44 | 0.10 | 1.82 |
| 5 | 1.5 | 35 | 2 | 1 | 2.66 | 8.21 | 0.53 | 1.64 | 3.08 | 3.15 | 6.92 | 2.19 | 1.18 | 0.21 | 2.22 |
| 5 | 1.5 | 35 | 2 | 2 | 2.69 | 8.46 | 0.54 | 1.69 | 3.15 | 2.94 | 6.77 | 2.30 | 1.10 | 0.39 | 2.30 |
| 5 | 1.5 | 35 | 2 | 3 | 2.40 | 7.38 | 0.48 | 1.48 | 3.07 | 2.86 | 6.43 | 2.25 | 1.19 | 0.12 | 2.31 |
| 5 | 1.5 | 35 | 2 | 4 | 2.34 | 8.27 | 0.47 | 1.65 | 3.54 | 2.72 | 6.81 | 2.51 | 1.16 | 0.10 | 1.77 |
| Average: | | | | | 2.52 | 8.08 | 0.50 | 1.62 | 3.21 | 2.92 | 6.73 | 2.31 | 1.16 | 0.21 | 2.15 |

| | | | | | | | | | | | | | | | |
|-----------------|-----|----|---|---|-------------|--------------|-------------|-------------|-------------|-------------|--------------|-------------|-------------|-------------|-------------|
| 10 | 0.5 | 35 | 1 | 1 | 3.60 | 9.92 | 0.36 | 0.99 | 2.76 | 3.76 | 7.39 | 1.97 | 1.04 | 0.50 | 2.33 |
| 10 | 0.5 | 35 | 1 | 2 | 4.47 | 12.03 | 0.45 | 1.20 | 2.69 | 4.22 | 7.89 | 1.87 | 0.94 | 0.56 | 3.08 |
| 10 | 0.5 | 35 | 1 | 3 | 3.43 | 11.02 | 0.34 | 1.10 | 3.21 | 3.44 | 7.67 | 2.23 | 1.00 | 0.12 | 2.24 |
| 10 | 0.5 | 35 | 1 | 4 | 3.54 | 10.16 | 0.35 | 1.02 | 2.87 | 3.36 | 7.59 | 2.26 | 0.95 | 0.59 | 2.86 |
| 10 | 0.5 | 35 | 1 | 5 | 5.00 | 11.55 | 0.50 | 1.16 | 2.31 | 3.25 | 7.04 | 2.16 | 0.65 | 0.46 | 2.60 |
| Average: | | | | | 4.01 | 10.94 | 0.40 | 1.09 | 2.77 | 3.61 | 7.52 | 2.10 | 0.92 | 0.45 | 2.62 |
| 10 | 0.5 | 35 | 2 | 1 | 4.63 | 12.04 | 0.46 | 1.20 | 2.60 | 4.54 | 8.21 | 1.81 | 0.98 | 0.05 | 1.63 |
| 10 | 0.5 | 35 | 2 | 2 | 4.44 | 12.39 | 0.44 | 1.24 | 2.79 | 3.96 | 7.50 | 1.90 | 0.89 | 0.65 | 3.25 |
| 10 | 0.5 | 35 | 2 | 3 | 3.92 | 11.03 | 0.39 | 1.10 | 2.81 | 3.79 | 7.43 | 1.96 | 0.97 | 0.70 | 3.03 |
| 10 | 0.5 | 35 | 2 | 4 | 5.02 | 12.91 | 0.50 | 1.29 | 2.57 | 5.10 | 9.39 | 1.84 | 1.02 | 0.57 | 3.13 |
| Average: | | | | | 4.51 | 12.09 | 0.45 | 1.21 | 2.69 | 4.35 | 8.13 | 1.88 | 0.96 | 0.50 | 2.76 |
| 10 | 1 | 35 | 1 | 1 | 3.13 | 10.84 | 0.31 | 1.08 | 3.46 | 3.39 | 7.73 | 2.28 | 1.08 | 0.59 | 2.73 |
| 10 | 1 | 35 | 1 | 2 | 3.79 | 10.14 | 0.38 | 1.01 | 2.68 | 3.66 | 7.92 | 2.16 | 0.97 | 0.78 | 3.38 |
| 10 | 1 | 35 | 1 | 3 | 3.60 | 10.66 | 0.36 | 1.07 | 2.96 | 4.20 | 8.22 | 1.96 | 1.17 | 0.75 | 3.70 |
| 10 | 1 | 35 | 1 | 4 | 4.10 | 11.32 | 0.41 | 1.13 | 2.76 | 4.44 | 8.79 | 1.98 | 1.08 | 0.92 | 4.30 |
| 10 | 1 | 35 | 1 | 5 | 3.86 | 10.06 | 0.39 | 1.01 | 2.60 | 4.02 | 8.52 | 2.12 | 1.04 | 0.42 | 2.78 |
| Average: | | | | | 3.70 | 10.60 | 0.37 | 1.06 | 2.89 | 3.94 | 8.24 | 2.10 | 1.07 | 0.69 | 3.38 |
| 10 | 1 | 35 | 2 | 1 | 5.48 | 14.82 | 0.55 | 1.48 | 2.70 | 5.60 | 10.61 | 1.89 | 1.02 | 0.43 | 3.30 |
| 10 | 1 | 35 | 2 | 2 | 3.64 | 10.75 | 0.36 | 1.08 | 2.95 | 3.69 | 7.79 | 2.11 | 1.01 | 0.50 | 3.26 |
| 10 | 1 | 35 | 2 | 3 | 3.71 | 11.52 | 0.37 | 1.15 | 3.11 | 4.46 | 9.45 | 2.12 | 1.20 | 0.54 | 3.04 |
| 10 | 1 | 35 | 2 | 4 | 4.59 | 13.62 | 0.46 | 1.36 | 2.97 | 4.58 | 9.92 | 2.16 | 1.00 | 0.69 | 3.89 |
| Average: | | | | | 4.35 | 12.68 | 0.44 | 1.27 | 2.93 | 4.58 | 9.44 | 2.07 | 1.06 | 0.54 | 3.37 |
| 10 | 1.5 | 35 | 1 | 1 | 4.07 | 12.42 | 0.41 | 1.24 | 3.05 | 4.73 | 10.45 | 2.21 | 1.16 | 0.34 | 3.11 |
| 10 | 1.5 | 35 | 1 | 2 | 3.54 | 13.54 | 0.35 | 1.35 | 3.82 | 4.00 | 9.00 | 2.25 | 1.13 | 0.71 | 3.68 |
| 10 | 1.5 | 35 | 1 | 3 | 4.13 | 11.52 | 0.41 | 1.15 | 2.79 | 4.78 | 9.69 | 2.02 | 1.16 | 0.42 | 3.29 |
| 10 | 1.5 | 35 | 1 | 4 | 4.48 | 12.45 | 0.45 | 1.25 | 2.78 | 5.08 | 10.59 | 2.08 | 1.13 | 0.69 | 3.99 |
| 10 | 1.5 | 35 | 1 | 5 | 4.02 | 11.43 | 0.40 | 1.14 | 2.84 | 4.98 | 10.98 | 2.20 | 1.24 | 0.65 | 5.06 |
| Average: | | | | | 4.05 | 12.27 | 0.41 | 1.23 | 3.06 | 4.72 | 10.14 | 2.15 | 1.16 | 0.56 | 3.82 |
| 10 | 1.5 | 35 | 2 | 1 | 5.67 | 13.50 | 0.57 | 1.35 | 2.38 | 6.37 | 12.12 | 1.90 | 1.12 | -0.05 | 2.34 |
| 10 | 1.5 | 35 | 2 | 2 | 5.33 | 14.53 | 0.53 | 1.45 | 2.73 | 5.77 | 12.09 | 2.09 | 1.08 | 0.68 | 4.53 |
| 10 | 1.5 | 35 | 2 | 3 | 4.42 | 12.47 | 0.44 | 1.25 | 2.82 | 4.53 | 10.52 | 2.32 | 1.03 | 0.63 | 4.69 |
| 10 | 1.5 | 35 | 2 | 4 | 4.58 | 12.63 | 0.46 | 1.26 | 2.76 | 5.36 | 11.38 | 2.12 | 1.17 | 0.61 | 3.98 |
| Average: | | | | | 5.00 | 13.28 | 0.50 | 1.33 | 2.67 | 5.51 | 11.53 | 2.11 | 1.10 | 0.47 | 3.89 |

Appendices

| | | | | | | | | | | | | | | | |
|-----------------|-----|----|---|---|-------------|--------------|-------------|-------------|-------------|-------------|--------------|-------------|-------------|-------------|-------------|
| 15 | 0.5 | 35 | 1 | 1 | 5.72 | 15.42 | 0.38 | 1.03 | 2.69 | 5.57 | 10.65 | 1.91 | 0.97 | 1.69 | 4.82 |
| 15 | 0.5 | 35 | 1 | 2 | 5.65 | 16.62 | 0.38 | 1.11 | 2.94 | 5.15 | 11.73 | 2.28 | 0.91 | 2.01 | 5.56 |
| 15 | 0.5 | 35 | 1 | 3 | 5.06 | 13.99 | 0.34 | 0.93 | 2.77 | 4.35 | 9.93 | 2.28 | 0.86 | 1.65 | 5.00 |
| 15 | 0.5 | 35 | 1 | 4 | 5.60 | 17.53 | 0.37 | 1.17 | 3.13 | 5.12 | 10.23 | 2.00 | 0.91 | 1.63 | 5.34 |
| 15 | 0.5 | 35 | 1 | 5 | 5.82 | 16.72 | 0.39 | 1.11 | 2.87 | 5.41 | 11.22 | 2.07 | 0.93 | 2.36 | 5.62 |
| Average: | | | | | 5.57 | 16.06 | 0.37 | 1.07 | 2.88 | 5.12 | 10.75 | 2.11 | 0.92 | 1.87 | 5.27 |
| 15 | 0.5 | 35 | 2 | 1 | 7.59 | 20.29 | 0.51 | 1.35 | 2.68 | 6.61 | 12.56 | 1.90 | 0.87 | -0.15 | 2.39 |
| 15 | 0.5 | 35 | 2 | 2 | 6.27 | 16.20 | 0.42 | 1.08 | 2.59 | 5.71 | 11.52 | 2.02 | 0.91 | 2.38 | 5.72 |
| 15 | 0.5 | 35 | 2 | 3 | 6.52 | 16.02 | 0.43 | 1.07 | 2.46 | 5.80 | 10.47 | 1.81 | 0.89 | 1.85 | 4.79 |
| 15 | 0.5 | 35 | 2 | 4 | 5.29 | 15.86 | 0.35 | 1.06 | 2.99 | 4.81 | 9.19 | 1.91 | 0.91 | 2.13 | 5.03 |
| Average: | | | | | 6.42 | 17.09 | 0.43 | 1.14 | 2.68 | 5.73 | 10.93 | 1.91 | 0.89 | 1.55 | 4.48 |
| 15 | 1 | 35 | 1 | 1 | 6.14 | 19.97 | 0.41 | 1.33 | 3.25 | 5.51 | 11.22 | 2.04 | 0.90 | 1.72 | 5.16 |
| 15 | 1 | 35 | 1 | 2 | 4.72 | 14.73 | 0.31 | 0.98 | 3.12 | 4.57 | 10.16 | 2.22 | 0.97 | 1.40 | 4.71 |
| 15 | 1 | 35 | 1 | 3 | 5.08 | 14.92 | 0.34 | 0.99 | 2.94 | 4.77 | 9.92 | 2.08 | 0.94 | 1.72 | 4.88 |
| 15 | 1 | 35 | 1 | 4 | 4.97 | 13.11 | 0.33 | 0.87 | 2.64 | 4.70 | 9.94 | 2.12 | 0.95 | 1.46 | 4.39 |
| 15 | 1 | 35 | 1 | 5 | 5.99 | 15.91 | 0.40 | 1.06 | 2.65 | 5.59 | 11.74 | 2.10 | 0.93 | 1.95 | 5.72 |
| Average: | | | | | 5.38 | 15.73 | 0.36 | 1.05 | 2.92 | 5.03 | 10.60 | 2.11 | 0.94 | 1.65 | 4.97 |
| 15 | 1 | 35 | 2 | 1 | 7.80 | 25.11 | 0.52 | 1.67 | 3.22 | 6.96 | 14.18 | 2.04 | 0.89 | 0.56 | 3.91 |
| 15 | 1 | 35 | 2 | 2 | 5.34 | 19.17 | 0.36 | 1.28 | 3.59 | 4.69 | 11.72 | 2.50 | 0.88 | 2.15 | 5.68 |
| 15 | 1 | 35 | 2 | 3 | 5.04 | 18.94 | 0.34 | 1.26 | 3.76 | 4.34 | 10.74 | 2.48 | 0.86 | 1.78 | 5.50 |
| 15 | 1 | 35 | 2 | 4 | 8.03 | 20.41 | 0.54 | 1.36 | 2.54 | 3.41 | 8.65 | 2.53 | 0.43 | 2.40 | 6.19 |
| Average: | | | | | 6.55 | 20.91 | 0.44 | 1.39 | 3.28 | 4.85 | 11.32 | 2.39 | 0.76 | 1.72 | 5.32 |
| 15 | 1.5 | 35 | 1 | 1 | 4.72 | 14.25 | 0.31 | 0.95 | 3.02 | 4.68 | 10.63 | 2.27 | 0.99 | 1.65 | 4.57 |
| 15 | 1.5 | 35 | 1 | 2 | 5.73 | 13.49 | 0.38 | 0.90 | 2.35 | 5.43 | 10.73 | 1.98 | 0.95 | 1.58 | 5.25 |
| 15 | 1.5 | 35 | 1 | 3 | 5.40 | 16.83 | 0.36 | 1.12 | 3.12 | 5.66 | 11.98 | 2.12 | 1.05 | 2.11 | 5.99 |
| 15 | 1.5 | 35 | 1 | 4 | 5.73 | 15.13 | 0.38 | 1.01 | 2.64 | 5.56 | 12.65 | 2.28 | 0.97 | 2.13 | 6.25 |
| 15 | 1.5 | 35 | 1 | 5 | 5.78 | 14.90 | 0.39 | 0.99 | 2.58 | 6.14 | 12.55 | 2.05 | 1.06 | 2.41 | 6.87 |
| Average: | | | | | 5.47 | 14.92 | 0.36 | 0.99 | 2.74 | 5.49 | 11.71 | 2.14 | 1.00 | 1.98 | 5.79 |
| 15 | 1.5 | 35 | 2 | 1 | 8.93 | 27.07 | 0.60 | 1.80 | 3.03 | 8.50 | 16.72 | 1.97 | 0.95 | 0.12 | 3.16 |
| 15 | 1.5 | 35 | 2 | 2 | 5.28 | 21.78 | 0.35 | 1.45 | 4.13 | 4.78 | 12.23 | 2.56 | 0.91 | 2.33 | 6.68 |
| 15 | 1.5 | 35 | 2 | 3 | 6.77 | 19.79 | 0.45 | 1.32 | 2.92 | 4.79 | 12.23 | 2.55 | 0.71 | 2.81 | 6.27 |
| 15 | 1.5 | 35 | 2 | 4 | 6.63 | 20.57 | 0.44 | 1.37 | 3.10 | 5.99 | 13.74 | 2.29 | 0.90 | 2.26 | 7.14 |
| Average: | | | | | 6.90 | 22.30 | 0.46 | 1.49 | 3.30 | 6.02 | 13.73 | 2.34 | 0.87 | 1.88 | 5.81 |

7.2.5 Summary Concrete 'B'

| Summary Block 'B' | | | | | | | | | | | | | | | |
|-------------------|-----|---|-------|-------|-------------|--------------|-------------|-------------|-------------|-------------|--------------|-------------|-------------|--------------|-------------|
| Unrelieved | | | | | | | | | | | | | | | |
| d | v | s | Layer | Trial | FC | FC' | FC/d | FC'/d | FC'/FC | FN | FN' | FN'/FN | FN/FC | FS | FS' |
| 2 | 0.5 | - | - | 1 | 0.90 | 3.24 | 0.45 | 1.62 | 3.61 | 1.33 | 4.04 | 3.03 | 1.49 | -0.11 | 1.02 |
| 2 | 0.5 | - | - | 2 | 1.07 | 4.20 | 0.53 | 2.10 | 3.93 | 1.62 | 4.82 | 2.97 | 1.52 | -0.05 | 0.99 |
| 2 | 0.5 | - | - | 3 | 0.97 | 3.44 | 0.49 | 1.72 | 3.54 | 1.39 | 3.70 | 2.66 | 1.43 | -0.05 | 1.11 |
| Average: | | | | | 0.98 | 3.63 | 0.49 | 1.81 | 3.70 | 1.45 | 4.19 | 2.89 | 1.48 | -0.07 | 1.04 |
| 2 | 1 | - | - | 1 | 1.04 | 4.06 | 0.52 | 2.03 | 3.89 | 1.69 | 5.96 | 3.53 | 1.62 | 0.15 | 1.84 |
| 2 | 1 | - | - | 2 | 0.97 | 4.83 | 0.48 | 2.41 | 4.99 | 1.49 | 4.71 | 3.16 | 1.54 | 0.16 | 1.62 |
| Average: | | | | | 1.00 | 4.44 | 0.50 | 2.22 | 4.44 | 1.59 | 5.34 | 3.35 | 1.58 | 0.16 | 1.73 |
| 2 | 1.5 | - | - | 1 | 0.93 | 3.50 | 0.47 | 1.75 | 3.75 | 1.45 | 4.35 | 2.99 | 1.56 | -0.07 | 1.49 |
| 2 | 1.5 | - | - | 2 | 0.71 | 3.29 | 0.36 | 1.64 | 4.63 | 1.19 | 4.32 | 3.62 | 1.68 | -0.01 | 1.04 |
| 2 | 1.5 | - | - | 3 | 0.79 | 4.62 | 0.39 | 2.31 | 5.86 | 1.37 | 4.96 | 3.62 | 1.74 | -0.06 | 1.58 |
| Average: | | | | | 0.81 | 3.80 | 0.41 | 1.90 | 4.75 | 1.46 | 4.94 | 3.38 | 1.66 | 0.05 | 1.55 |
| 5 | 0.5 | - | - | 1 | 2.35 | 7.40 | 0.47 | 1.48 | 3.15 | 3.00 | 6.49 | 2.17 | 1.28 | -0.18 | 1.64 |
| 5 | 0.5 | - | - | 2 | 2.41 | 7.96 | 0.48 | 1.59 | 3.30 | 3.29 | 7.11 | 2.16 | 1.37 | 0.05 | 1.78 |
| 5 | 0.5 | - | - | 3 | 4.41 | 14.61 | 0.88 | 2.92 | 3.31 | 7.65 | 16.12 | 2.11 | 1.73 | -0.61 | 2.65 |
| Average: | | | | | 3.06 | 9.99 | 0.61 | 2.00 | 3.25 | 4.65 | 9.91 | 2.14 | 1.46 | -0.25 | 2.02 |
| 5 | 1 | - | - | 1 | 2.42 | 10.45 | 0.48 | 2.09 | 4.32 | 3.54 | 9.13 | 2.58 | 1.46 | -0.13 | 3.15 |
| 5 | 1 | - | - | 2 | 2.49 | 10.41 | 0.50 | 2.08 | 4.18 | 3.94 | 9.74 | 2.47 | 1.58 | 0.03 | 2.82 |
| 5 | 1 | - | - | 3 | 2.28 | 8.59 | 0.46 | 1.72 | 3.77 | 3.29 | 8.71 | 2.64 | 1.44 | 0.18 | 2.52 |
| Average: | | | | | 2.40 | 9.82 | 0.48 | 1.96 | 4.09 | 3.59 | 9.19 | 2.57 | 1.50 | 0.03 | 2.83 |
| 5 | 1.5 | - | - | 1 | 2.54 | 10.63 | 0.51 | 2.13 | 4.19 | 4.66 | 11.07 | 2.38 | 1.83 | 0.23 | 3.33 |
| 5 | 1.5 | - | - | 2 | 2.08 | 8.88 | 0.42 | 1.78 | 4.27 | 3.18 | 8.82 | 2.77 | 1.53 | -0.32 | 2.61 |
| 5 | 1.5 | - | - | 3 | 2.74 | 9.35 | 0.55 | 1.87 | 3.41 | 4.14 | 9.78 | 2.36 | 1.51 | 0.16 | 2.89 |
| Average: | | | | | 2.45 | 9.62 | 0.49 | 1.92 | 3.96 | 4.00 | 9.89 | 2.50 | 1.63 | 0.02 | 2.94 |
| 10 | 0.5 | - | - | 1 | 4.58 | 13.21 | 0.46 | 1.32 | 2.88 | 5.56 | 11.93 | 2.15 | 1.21 | -0.23 | 2.96 |
| 10 | 0.5 | - | - | 2 | 4.44 | 13.09 | 0.44 | 1.31 | 2.95 | 5.15 | 10.30 | 2.00 | 1.16 | -0.22 | 1.66 |
| 10 | 0.5 | - | - | 3 | 4.82 | 14.05 | 0.48 | 1.41 | 2.91 | 5.38 | 11.04 | 2.05 | 1.12 | -0.50 | 2.07 |
| Average: | | | | | 4.61 | 13.45 | 0.46 | 1.35 | 2.92 | 5.36 | 11.09 | 2.07 | 1.16 | -0.32 | 2.23 |
| 10 | 1 | - | - | 1 | 5.25 | 15.24 | 0.53 | 1.52 | 2.90 | 6.58 | 14.81 | 2.25 | 1.25 | -0.16 | 3.00 |
| 10 | 1 | - | - | 2 | 4.85 | 19.04 | 0.49 | 1.90 | 3.92 | 6.41 | 12.62 | 1.97 | 1.32 | 0.17 | 4.36 |
| 10 | 1 | - | - | 3 | 5.43 | 16.57 | 0.54 | 1.66 | 3.05 | 7.19 | 14.77 | 2.05 | 1.33 | -0.27 | 4.21 |
| Average: | | | | | 5.18 | 16.95 | 0.52 | 1.70 | 3.29 | 6.72 | 14.07 | 2.09 | 1.30 | -0.09 | 3.86 |
| 10 | 1.5 | - | - | 1 | 3.62 | 9.95 | 0.36 | 0.99 | 2.74 | 5.13 | 11.27 | 2.20 | 1.41 | 0.25 | 2.89 |
| 10 | 1.5 | - | - | 2 | 4.73 | 20.30 | 0.47 | 2.03 | 4.29 | 6.71 | 15.76 | 2.35 | 1.42 | -0.23 | 3.48 |
| 10 | 1.5 | - | - | 3 | 4.76 | 23.93 | 0.48 | 2.39 | 5.03 | 7.45 | 17.81 | 2.39 | 1.57 | -0.32 | 2.87 |
| Average: | | | | | 4.37 | 18.06 | 0.44 | 1.81 | 4.02 | 6.43 | 14.94 | 2.31 | 1.47 | -0.10 | 3.08 |
| 15 | 0.5 | - | - | 1 | 7.15 | 18.50 | 0.48 | 1.23 | 2.59 | 7.90 | 14.81 | 1.87 | 1.10 | 0.41 | 4.09 |
| 15 | 0.5 | - | - | 2 | 7.59 | 21.33 | 0.51 | 1.42 | 2.81 | 7.56 | 14.26 | 1.89 | 1.00 | -0.14 | 3.41 |
| 15 | 0.5 | - | - | 3 | 7.69 | 24.97 | 0.51 | 1.66 | 3.25 | 7.57 | 16.51 | 2.18 | 0.98 | -0.25 | 2.58 |
| Average: | | | | | 7.48 | 21.60 | 0.50 | 1.44 | 2.88 | 7.67 | 15.19 | 1.98 | 1.03 | 0.01 | 3.36 |
| 15 | 1 | - | - | 1 | 7.07 | 24.43 | 0.47 | 1.63 | 3.46 | 8.34 | 19.09 | 2.29 | 1.18 | -0.34 | 3.50 |

Appendices

| | | | | | | | | | | | | | | | |
|-----------------|-----|---|---|---|-------------|--------------|-------------|-------------|-------------|-------------|--------------|-------------|-------------|--------------|-------------|
| 15 | 1 | - | - | 2 | 9.02 | 26.88 | 0.60 | 1.79 | 2.98 | 10.20 | 20.47 | 2.01 | 1.13 | -2.10 | 2.87 |
| 15 | 1 | - | - | 3 | 8.71 | 24.36 | 0.58 | 1.62 | 2.80 | 10.35 | 21.29 | 2.06 | 1.19 | -0.10 | 5.47 |
| Average: | | | | | 8.27 | 25.22 | 0.55 | 1.68 | 3.08 | 9.63 | 20.28 | 2.12 | 1.17 | -0.85 | 3.95 |
| 15 | 1.5 | - | - | 1 | 8.09 | 21.23 | 0.54 | 1.42 | 2.62 | 9.90 | 20.68 | 2.09 | 1.22 | 0.46 | 5.89 |
| 15 | 1.5 | | - | 2 | 8.13 | 24.96 | 0.54 | 1.66 | 3.07 | 9.93 | 19.72 | 1.99 | 1.22 | -0.07 | 4.28 |
| 15 | 1.5 | | - | 2 | 7.63 | 19.82 | 0.51 | 1.32 | 2.60 | 9.81 | 22.39 | 2.28 | 1.29 | -0.98 | 4.04 |
| Average: | | | | | 7.95 | 22.00 | 0.53 | 1.47 | 2.76 | 9.88 | 20.93 | 2.12 | 1.24 | -0.20 | 4.74 |

| | | | | | | | | | | | | | | | |
|----------------------|--|--|--|--|--|--|--|--|--|--|--|--|--|--|--|
| Relieved Cuts | | | | | | | | | | | | | | | |
|----------------------|--|--|--|--|--|--|--|--|--|--|--|--|--|--|--|

| | | | | | | | | | | | | | | | |
|-----------------|-----|----|---|---|-------------|--------------|-------------|-------------|-------------|-------------|--------------|-------------|-------------|--------------|-------------|
| 5 | 0.5 | 35 | 1 | 1 | 2.80 | 9.82 | 0.56 | 1.96 | 3.50 | 3.89 | 8.32 | 2.14 | 1.39 | 2.08 | 2.37 |
| 5 | 0.5 | 35 | 1 | 2 | 2.68 | 8.64 | 0.54 | 1.73 | 3.22 | 3.76 | 8.03 | 2.14 | 1.40 | 1.69 | 2.45 |
| 5 | 0.5 | 35 | 1 | 3 | | | | | | | | | | | |
| 5 | 0.5 | 35 | 1 | 4 | | | | | | | | | | | |
| 5 | 0.5 | 35 | 1 | 5 | | | | | | | | | | | |
| Average: | | | | | 2.74 | 9.23 | 0.55 | 1.85 | 3.36 | 3.82 | 8.17 | 2.14 | 1.40 | 1.89 | 2.41 |
| 5 | 0.5 | 35 | 2 | 1 | 3.42 | 9.90 | 0.68 | 1.98 | 2.89 | 4.47 | 9.69 | 2.17 | 1.30 | 0.07 | 2.60 |
| 5 | 0.5 | 35 | 2 | 2 | 2.99 | 10.62 | 0.60 | 2.12 | 3.56 | 4.06 | 10.28 | 2.53 | 1.36 | 0.26 | 2.79 |
| 5 | 0.5 | 35 | 2 | 3 | 2.98 | 10.39 | 0.60 | 2.08 | 3.48 | 3.80 | 8.51 | 2.24 | 1.27 | 0.28 | 3.08 |
| 5 | 0.5 | 35 | 2 | 4 | 5.39 | 17.84 | 1.08 | 3.57 | 3.31 | 9.71 | 19.15 | 1.97 | 1.80 | 0.02 | 4.85 |
| Average: | | | | | 3.70 | 12.19 | 0.74 | 2.44 | 3.31 | 5.51 | 11.91 | 2.23 | 1.43 | 0.16 | 3.33 |
| 5 | 1 | 35 | 1 | 1 | | | | | | | | | | | |
| 5 | 1 | 35 | 1 | 2 | 2.50 | 9.14 | 0.50 | 1.83 | 3.65 | 3.40 | 6.81 | 2.00 | 1.36 | -0.24 | 1.82 |
| 5 | 1 | 35 | 1 | 3 | 2.46 | 8.27 | 0.49 | 1.65 | 3.37 | 3.17 | 7.59 | 2.40 | 1.29 | 0.01 | 2.21 |
| 5 | 1 | 35 | 1 | 4 | 2.36 | 8.13 | 0.47 | 1.63 | 3.45 | 3.73 | 9.39 | 2.52 | 1.58 | 0.13 | 2.53 |
| 5 | 1 | 35 | 1 | 5 | 2.74 | 8.54 | 0.55 | 1.71 | 3.12 | 4.02 | 7.97 | 1.98 | 1.47 | 0.13 | 2.20 |
| Average: | | | | | 2.51 | 8.52 | 0.50 | 1.70 | 3.40 | 3.58 | 7.94 | 2.23 | 1.42 | 0.01 | 2.19 |
| 5 | 1 | 35 | 2 | 1 | 3.28 | 11.31 | 0.66 | 2.26 | 3.44 | 4.83 | 10.51 | 2.18 | 1.47 | -0.09 | 2.40 |
| 5 | 1 | 35 | 2 | 2 | 3.47 | 10.86 | 0.69 | 2.17 | 3.13 | 4.75 | 9.38 | 1.97 | 1.37 | 0.20 | 2.98 |
| 5 | 1 | 35 | 2 | 3 | 2.90 | 12.39 | 0.58 | 2.48 | 4.27 | 3.87 | 9.59 | 2.47 | 1.34 | 0.25 | 2.87 |
| 5 | 1 | 35 | 2 | 4 | 3.10 | 12.46 | 0.62 | 2.49 | 4.01 | 4.30 | 9.16 | 2.13 | 1.39 | 0.19 | 3.21 |
| Average: | | | | | 3.19 | 11.75 | 0.64 | 2.35 | 3.71 | 4.44 | 9.66 | 2.19 | 1.39 | 0.14 | 2.87 |
| 5 | 1.5 | 35 | 1 | 1 | 2.43 | 11.50 | 0.49 | 2.30 | 4.73 | 4.29 | 10.26 | 2.39 | 1.76 | -0.25 | 2.20 |
| 5 | 1.5 | 35 | 1 | 2 | 2.54 | 9.39 | 0.51 | 1.88 | 3.69 | 4.82 | 11.04 | 2.29 | 1.89 | 0.12 | 2.54 |
| 5 | 1.5 | 35 | 1 | 3 | 2.83 | 8.67 | 0.57 | 1.73 | 3.06 | 5.22 | 11.16 | 2.14 | 1.84 | -0.31 | 1.98 |
| 5 | 1.5 | 35 | 1 | 4 | 3.01 | 11.00 | 0.60 | 2.20 | 3.65 | 5.20 | 13.18 | 2.54 | 1.73 | -0.05 | 3.54 |
| 5 | 1.5 | 35 | 1 | 5 | | | | | | | | | | | |
| Average: | | | | | 2.70 | 10.14 | 0.54 | 2.03 | 3.78 | 4.88 | 11.41 | 2.34 | 1.81 | -0.13 | 2.56 |
| 5 | 1.5 | 35 | 2 | 1 | 2.56 | 10.06 | 0.51 | 2.01 | 3.94 | 4.08 | 10.36 | 2.54 | 1.60 | -0.37 | 2.01 |
| 5 | 1.5 | 35 | 2 | 2 | 2.83 | 9.21 | 0.57 | 1.84 | 3.26 | 4.88 | 9.72 | 1.99 | 1.73 | 0.02 | 2.36 |
| 5 | 1.5 | 35 | 2 | 3 | 3.80 | 15.03 | 0.76 | 3.01 | 3.96 | 6.40 | 12.66 | 1.98 | 1.69 | 0.44 | 3.52 |
| 5 | 1.5 | 35 | 2 | 4 | 3.52 | 11.21 | 0.70 | 2.24 | 3.18 | 5.28 | 10.68 | 2.02 | 1.50 | -0.21 | 1.70 |

Appendices

| | | | | | | | | | | | | | | |
|-----------------|--|--|--|-------------|--------------|-------------|-------------|-------------|-------------|--------------|-------------|-------------|--------------|-------------|
| Average: | | | | 3.17 | 11.38 | 0.63 | 2.28 | 3.58 | 5.16 | 10.85 | 2.13 | 1.63 | -0.03 | 2.40 |
|-----------------|--|--|--|-------------|--------------|-------------|-------------|-------------|-------------|--------------|-------------|-------------|--------------|-------------|

| | | | | | | | | | | | | | | | |
|-----------------|-----|----|---|---|-------------|--------------|-------------|-------------|-------------|-------------|--------------|-------------|-------------|-------------|-------------|
| 10 | 0.5 | 35 | 1 | 1 | 4.98 | 17.53 | 0.50 | 1.75 | 3.52 | 5.97 | 14.63 | 2.45 | 1.20 | 0.67 | 3.96 |
| 10 | 0.5 | 35 | 1 | 2 | 5.01 | 17.25 | 0.50 | 1.73 | 3.45 | 6.21 | 12.92 | 2.08 | 1.24 | 0.83 | 4.65 |
| 10 | 0.5 | 35 | 1 | 3 | 4.21 | 14.37 | 0.42 | 1.44 | 3.41 | 5.18 | 11.64 | 2.25 | 1.23 | 1.18 | 4.98 |
| 10 | 0.5 | 35 | 1 | 4 | 5.43 | 18.82 | 0.54 | 1.88 | 3.46 | 6.67 | 13.06 | 1.96 | 1.23 | 1.21 | 5.38 |
| 10 | 0.5 | 35 | 1 | 5 | 4.16 | 15.50 | 0.42 | 1.55 | 3.73 | 5.27 | 11.47 | 2.17 | 1.27 | 1.06 | 4.32 |
| Average: | | | | | 4.76 | 16.70 | 0.48 | 1.67 | 3.51 | 5.86 | 12.75 | 2.18 | 1.23 | 0.99 | 4.66 |
| 10 | 0.5 | 35 | 2 | 1 | 6.23 | 19.36 | 0.62 | 1.94 | 3.11 | 7.94 | 15.61 | 1.97 | 1.28 | 0.57 | 4.21 |
| 10 | 0.5 | 35 | 2 | 2 | 4.95 | 14.83 | 0.49 | 1.48 | 3.00 | 5.83 | 11.74 | 2.01 | 1.18 | 0.47 | 3.70 |
| 10 | 0.5 | 35 | 2 | 3 | 5.18 | 17.39 | 0.52 | 1.74 | 3.36 | 6.45 | 13.19 | 2.05 | 1.25 | 0.91 | 4.92 |
| 10 | 0.5 | 35 | 2 | 4 | 5.72 | 17.08 | 0.57 | 1.71 | 2.99 | 6.79 | 13.45 | 1.98 | 1.19 | 1.08 | 4.44 |
| Average: | | | | | 5.52 | 17.16 | 0.55 | 1.72 | 3.11 | 6.75 | 13.50 | 2.00 | 1.22 | 0.76 | 4.32 |
| 10 | 1 | 35 | 1 | 1 | 4.52 | 19.06 | 0.45 | 1.91 | 4.22 | 6.50 | 13.15 | 2.02 | 1.44 | 0.48 | 4.58 |
| 10 | 1 | 35 | 1 | 2 | 4.38 | 13.61 | 0.44 | 1.36 | 3.11 | 6.13 | 12.49 | 2.04 | 1.40 | 0.68 | 4.45 |
| 10 | 1 | 35 | 1 | 3 | 4.50 | 14.76 | 0.45 | 1.48 | 3.28 | 6.37 | 14.62 | 2.30 | 1.41 | 1.12 | 5.94 |
| 10 | 1 | 35 | 1 | 4 | 4.96 | 14.44 | 0.50 | 1.44 | 2.91 | 6.78 | 14.54 | 2.15 | 1.37 | 0.92 | 4.70 |
| 10 | 1 | 35 | 1 | 5 | 4.93 | 13.99 | 0.49 | 1.40 | 2.83 | 6.88 | 14.62 | 2.13 | 1.39 | 1.86 | 5.99 |
| Average: | | | | | 4.66 | 15.17 | 0.47 | 1.52 | 3.27 | 6.53 | 13.89 | 2.13 | 1.40 | 1.01 | 5.13 |
| 10 | 1 | 35 | 2 | 1 | 5.25 | 17.93 | 0.53 | 1.79 | 3.41 | 7.34 | 15.47 | 2.11 | 1.40 | 0.73 | 4.20 |
| 10 | 1 | 35 | 2 | 2 | 4.31 | 13.53 | 0.43 | 1.35 | 3.14 | 5.70 | 12.46 | 2.18 | 1.32 | 0.67 | 5.01 |
| 10 | 1 | 35 | 2 | 3 | 4.40 | 14.38 | 0.44 | 1.44 | 3.27 | 5.65 | 12.20 | 2.16 | 1.28 | 0.13 | 4.18 |
| 10 | 1 | 35 | 2 | 4 | 4.32 | 13.73 | 0.43 | 1.37 | 3.18 | 5.86 | 11.85 | 2.02 | 1.36 | 0.54 | 3.83 |
| Average: | | | | | 4.57 | 14.89 | 0.46 | 1.49 | 3.25 | 6.14 | 13.00 | 2.12 | 1.34 | 0.52 | 4.30 |
| 10 | 1.5 | 35 | 1 | 1 | 4.67 | 14.77 | 0.47 | 1.48 | 3.16 | 6.68 | 16.30 | 2.44 | 1.43 | -0.03 | 1.07 |
| 10 | 1.5 | 35 | 1 | 2 | 4.75 | 14.83 | 0.48 | 1.48 | 3.12 | 7.68 | 15.81 | 2.06 | 1.62 | 0.00 | 0.96 |
| 10 | 1.5 | 35 | 1 | 3 | 4.57 | 16.96 | 0.46 | 1.70 | 3.71 | 6.58 | 14.71 | 2.24 | 1.44 | -0.02 | 1.17 |
| 10 | 1.5 | 35 | 1 | 4 | 3.96 | 14.22 | 0.40 | 1.42 | 3.60 | 6.00 | 11.81 | 1.97 | 1.52 | 0.01 | 1.00 |
| 10 | 1.5 | 35 | 1 | 5 | 4.61 | 12.72 | 0.46 | 1.27 | 2.76 | 7.48 | 16.02 | 2.14 | 1.62 | 0.02 | 1.05 |
| Average: | | | | | 4.51 | 14.70 | 0.45 | 1.47 | 3.27 | 6.88 | 14.93 | 2.17 | 1.52 | 0.00 | 1.05 |
| 10 | 1.5 | 35 | 2 | 1 | 4.35 | 14.87 | 0.43 | 1.49 | 3.42 | 6.09 | 12.73 | 2.09 | 1.40 | 0.01 | 1.15 |
| 10 | 1.5 | 35 | 2 | 2 | 5.28 | 17.53 | 0.53 | 1.75 | 3.32 | 8.24 | 17.51 | 2.12 | 1.56 | -0.01 | 1.03 |
| 10 | 1.5 | 35 | 2 | 3 | 4.52 | 11.68 | 0.45 | 1.17 | 2.58 | 6.62 | 12.78 | 1.93 | 1.46 | 0.00 | 0.93 |
| 10 | 1.5 | 35 | 2 | 4 | 4.64 | 16.59 | 0.46 | 1.66 | 3.57 | 6.77 | 15.79 | 2.33 | 1.46 | 0.00 | 1.03 |
| Average: | | | | | 4.70 | 15.17 | 0.47 | 1.52 | 3.22 | 6.93 | 14.70 | 2.12 | 1.47 | 0.00 | 1.04 |

| | | | | | | | | | | | | | | | |
|-----------------|-----|----|---|---|-------------|--------------|-------------|-------------|-------------|-------------|--------------|-------------|-------------|-------------|-------------|
| 15 | 0.5 | 35 | 1 | 1 | 7.02 | 18.03 | 0.47 | 1.20 | 2.57 | 8.18 | 16.83 | 2.06 | 1.16 | 0.00 | 1.29 |
| 15 | 0.5 | 35 | 1 | 2 | 6.19 | 17.86 | 0.41 | 1.19 | 2.88 | 7.39 | 15.49 | 2.10 | 1.19 | 0.00 | 1.19 |
| 15 | 0.5 | 35 | 1 | 3 | 6.59 | 20.09 | 0.44 | 1.34 | 3.05 | 7.53 | 15.69 | 2.08 | 1.14 | 0.00 | 1.13 |
| 15 | 0.5 | 35 | 1 | 4 | 6.32 | 22.34 | 0.42 | 1.49 | 3.53 | 7.58 | 16.82 | 2.22 | 1.20 | -0.01 | 1.19 |
| 15 | 0.5 | 35 | 1 | 5 | 6.51 | 20.11 | 0.43 | 1.34 | 3.09 | 7.89 | 16.62 | 2.11 | 1.21 | -0.01 | 1.20 |
| Average: | | | | | 6.53 | 19.69 | 0.44 | 1.31 | 3.03 | 7.71 | 16.29 | 2.11 | 1.18 | 0.00 | 1.20 |
| 15 | 0.5 | 35 | 2 | 1 | 8.11 | 20.32 | 0.54 | 1.35 | 2.51 | 8.71 | 15.56 | 1.79 | 1.07 | 0.00 | 1.03 |
| 15 | 0.5 | 35 | 2 | 2 | 6.20 | 19.22 | 0.41 | 1.28 | 3.10 | 7.47 | 16.04 | 2.15 | 1.20 | -0.01 | 1.22 |
| 15 | 0.5 | 35 | 2 | 3 | 6.53 | 17.69 | 0.44 | 1.18 | 2.71 | 7.81 | 15.70 | 2.01 | 1.20 | 0.00 | 1.09 |

Appendices

| | | | | | | | | | | | | | | | |
|-----------------|-----|----|---|---|-------------|--------------|-------------|-------------|-------------|--------------|--------------|-------------|-------------|--------------|-------------|
| 15 | 0.5 | 35 | 2 | 4 | 6.92 | 20.08 | 0.46 | 1.34 | 2.90 | 8.38 | 15.78 | 1.88 | 1.21 | 0.00 | 1.15 |
| Average: | | | | | 6.94 | 19.33 | 0.46 | 1.29 | 2.80 | 8.09 | 15.77 | 1.96 | 1.17 | 0.00 | 1.12 |
| 15 | 1 | 35 | 1 | 1 | 6.52 | 17.74 | 0.43 | 1.18 | 2.72 | 8.15 | 17.86 | 2.19 | 1.25 | 0.00 | 1.10 |
| 15 | 1 | 35 | 1 | 2 | 6.50 | 19.02 | 0.43 | 1.27 | 2.92 | 8.18 | 16.47 | 2.01 | 1.26 | 0.03 | 1.12 |
| 15 | 1 | 35 | 1 | 3 | 5.95 | 21.38 | 0.40 | 1.43 | 3.59 | 7.58 | 15.03 | 1.98 | 1.27 | 0.00 | 1.08 |
| 15 | 1 | 35 | 1 | 4 | 5.47 | 23.76 | 0.36 | 1.58 | 4.34 | 6.72 | 14.26 | 2.12 | 1.23 | -0.03 | 1.03 |
| 15 | 1 | 35 | 1 | 5 | 6.17 | 21.87 | 0.41 | 1.46 | 3.55 | 7.49 | 17.86 | 2.38 | 1.21 | -0.01 | 1.01 |
| Average: | | | | | 6.12 | 20.75 | 0.41 | 1.38 | 3.43 | 7.62 | 16.30 | 2.14 | 1.24 | 0.00 | 1.07 |
| 15 | 1 | 35 | 2 | 1 | 9.97 | 28.98 | 0.66 | 1.93 | 2.91 | 12.63 | 24.09 | 1.91 | 1.27 | 0.02 | 1.12 |
| 15 | 1 | 35 | 2 | 2 | 5.78 | 20.74 | 0.39 | 1.38 | 3.59 | 7.52 | 14.71 | 1.96 | 1.30 | 0.01 | 1.04 |
| 15 | 1 | 35 | 2 | 3 | 4.75 | 17.81 | 0.32 | 1.19 | 3.75 | 6.41 | 15.23 | 2.38 | 1.35 | 0.00 | 1.06 |
| 15 | 1 | 35 | 2 | 4 | 5.18 | 15.64 | 0.35 | 1.04 | 3.02 | 6.66 | 13.22 | 1.98 | 1.29 | -0.01 | 1.04 |
| Average: | | | | | 6.42 | 20.79 | 0.43 | 1.39 | 3.31 | 8.31 | 16.81 | 2.06 | 1.30 | 0.01 | 1.07 |
| 15 | 1.5 | 35 | 1 | 1 | 6.32 | 24.65 | 0.42 | 1.64 | 3.90 | 9.72 | 21.06 | 2.17 | 1.54 | -0.02 | 1.03 |
| 15 | 1.5 | 35 | 1 | 2 | 6.11 | 25.94 | 0.41 | 1.73 | 4.25 | 7.43 | 19.85 | 2.67 | 1.22 | 0.00 | 1.00 |
| 15 | 1.5 | 35 | 1 | 3 | 7.24 | 25.79 | 0.48 | 1.72 | 3.56 | 10.89 | 22.60 | 2.08 | 1.50 | -0.03 | 1.01 |
| 15 | 1.5 | 35 | 1 | 4 | 6.78 | 22.70 | 0.45 | 1.51 | 3.35 | 9.82 | 19.06 | 1.94 | 1.45 | 0.00 | 1.03 |
| 15 | 1.5 | 35 | 1 | 5 | 6.80 | 24.43 | 0.45 | 1.63 | 3.59 | 8.69 | 20.70 | 2.38 | 1.28 | 0.00 | 1.10 |
| Average: | | | | | 6.65 | 24.70 | 0.44 | 1.65 | 3.73 | 9.31 | 20.66 | 2.25 | 1.40 | -0.01 | 1.03 |
| 15 | 1.5 | 35 | 2 | 1 | 10.10 | 30.61 | 0.67 | 2.04 | 3.03 | 14.96 | 30.27 | 2.02 | 1.48 | -0.01 | 1.11 |
| 15 | 1.5 | 35 | 2 | 2 | 5.67 | 20.37 | 0.38 | 1.36 | 3.59 | 7.78 | 19.67 | 2.53 | 1.37 | 0.00 | 1.07 |
| 15 | 1.5 | 35 | 2 | 3 | 6.09 | 19.26 | 0.41 | 1.28 | 3.16 | 8.60 | 18.21 | 2.12 | 1.41 | 0.00 | 1.00 |
| 15 | 1.5 | 35 | 2 | 4 | 6.80 | 21.46 | 0.45 | 1.43 | 3.15 | 9.28 | 20.68 | 2.23 | 1.36 | 0.00 | 1.03 |
| Average: | | | | | 7.16 | 22.93 | 0.48 | 1.53 | 3.24 | 10.16 | 22.21 | 2.22 | 1.41 | 0.00 | 1.05 |